Carrier-Carrier and Carrier-Phonon Scattering in Self-Assembled Quantum Dots

by Torben Roland Nielsen

University of Bremen 2005

Carrier-Carrier and Carrier-Phonon Scattering in Self-Assembled Quantum Dots

Vom Fachbereich für Physik und Elektrotechnik
der Universität Bremen

zur Erlangung des akademischen Grades
Doktor der Naturwissenschaften (Dr. rer. nat.)
genehmigte Dissertation

von
Torben Roland Nielsen
Candidatus Scientiarum (Cand. Scient.)

1. Gutachter: Prof. Dr. F. Jahnke
2. Gutachter: Prof. Dr. M. Kira

Eingereicht am: 02.08.2005
Tag des Promotionskolloqiums: 05.10.2005

There is more to the picture
than meets the eye

Abstract

In this work theoretical investigations of the carrier-carrier interaction and the carrier-phonon interaction in self-assembled quantum dots are presented. Based on the nonequilibrium Green's function technique, equations of motion are derived for the one-particle Green's function. To demonstrate our method we focus on lens-shaped quantum dots grown on top of a wetting layer, using typical InGaAs and InGaN material parameters.

For the carrier-carrier interaction, we study the scattering processes leading to carrier capture into and relaxation inside the quantum dots. The corresponding scattering rates are evaluated within the Boltzmann approximation under quasi-equilibrium conditions. For the InGaAs material system we find at elevated carrier densities in the wetting layer that Coulomb scattering provides processes with capture (relaxation) times typically faster than 10ps (1ps). For the InGaN material system the combined influence of the quantum-confined Stark effect and many-body renormalizations is furthermore taken into account. The charge separation induced by the built-in electrostatic field has important consequences on the capture and relaxation rates. It is shown that its main effect comes through the renormalization of the energies of the states involved in the collisions, and leads to an increase in the scattering efficency.

The carrier-phonon scattering is studied for the InGaAs material system. The interaction of carriers with longitudinal-optical (LO) phonons at the Boltzmann level predicts inefficient scattering (phonon bottleneck) when the transition energies of the quantum dot states do not match the LO-phonon energy. In contrast, we demonstrate that a quantum kinetic description of the carrier-phonon interaction supports experimental observed fast scattering processes.

Contents

Part I

Introduction

Chapter 1

Prologue

Advances made within the field of photonics have lead to the bold statement that the 21'st century should be referred to as the century of the photon [1.1, 1.2]. Behind this statement lies the fact that researchers around the world have learned to manipulate and engineer optical systems to a degree far better than ever before.

Roughly speaking this success can be divided into two categories. On one side scientists have learned to master Maxwell's equations in even more and more complicated materials and geometries and still be able to predict the electromagnetic properties and response of devices. On the other hand with the advent of the *laser*,[1] and its manifestation in different active media, be it atomic, molecular, or solid-state, a unique light source has emerged.

Two familiar examples are often put forward to show these new progresses in phononics and optoelectronics. The first prime example is optical data-storage. Two decades ago the CD player started to enter the market as a high-tech product, while today they are sold in supermarkets and are found in any household. A few years ago we have witnessed the breakthrough of the next generation in optical data-storage: the DVD player and recorder, where the amount of information which can be stored and read out optically on a DVD disk have raised about a factor of five compared to the CD media. The second prime example is the data-communication industry. Within the last decade progress in optical communication networks has made broadband internet connections available for everybody, even at a low cost for the end-consumer.

There are also other examples which shows how photonics have become or will become an integrated part of our everyday life. Welding or cutting with lasers is nowadays an important technology within many industries [1.2]. For example, for producing a shaver the company Phillips is using lasers in practical every step of the production. [1.3]. But also as sensors or detectors the field of photonics is breaking new ground [1.2]. Especially

[1] Acronym: light amplified by stimulated emission of radiation

regarding environmental issues, sensors are developed to optically monitor e.g. air pollution or to perform quality control of water supply systems [1.4]. Finally photonics is predicted to play a key role within display and illuminating technologies. For the latter, the trend goes toward develop LED[2] semiconductor alternatives to normal incandescent lamps which would be economically more favorable [1.5]. In first line white light is on the agenda, but natural light should also be possible by adding specific color LEDs to the white light and in this way to be able to mimic nature's own spectrum.

All of the above potential applications need some kind of light source. Depending on needs and wishes there are different solutions available. For example, molecular dye lasers, fiber lasers, semiconductor quantum-well lasers, and what is relevant for our work, semiconductor quantum-dot lasers.

The Quantum-Dot Laser

All laser devices need an active material, where the energy that is put into the system is transformed into light. That is to say, the active medium is like the heart of the entire photonic system. Without it, nothing else will work. In a quantum-dot laser, the quantum dots act as the active material. The current interest in the quantum-dot lasers both from Industry and Academics is due to the fact that it may out-perform the standard quantum-well laser on several issues.

First of all, quantum dots may in a first approximation be viewed as artificial atoms. A viewpoint which also reflects the historical evolution of the field of quantum dots. The bottom line is, that depending on how the quantum dots are grown, correspondingly different artificial atoms each with unique discrete transition energies are obtained. By the right choice of parameters, one can in principle construct a quantum dot with the desired emission wavelength needed for a laser. A second point is the threshold current needed to start the laser action. Compared to ordinary quantum-well lasers it should be lower [1.6, 1.7]. Finally, what is also very important for practical applications, the threshold current should have a weaker temperature dependence, preferably none [1.6, 1.7]. In this way expensive cooling mechanism may be saved, making the product cheaper.

If we return to the example of data-communication the hope is to develop a cheap quantum-dot laser working in the wavelength range 1.1-1.3 μm and 1.5 μm where standard optical glass fibers show minima in losses of the transmitted signal. If a quantum-dot laser may be designed to operate in this window, and if the threshold currents and temperature dependences turn out to be as optimal as expected, this would mean for the end-consumer a cheaper price per transfered Bit [1.8].

[2]Acronym: light emitting diode

However, to fully understand the gain mechanism in quantum-dot lasers and eventually to optimize it, a study of the basic carrier dynamics is needed. Only with the proper understanding of the fundamental carrier-carrier and carrier-phonon interaction will we be able to make progress.

Outline of the Thesis

The aim of this thesis is a theoretical analysis of the fundamental carrier-carrier interaction and carrier-phonon interaction in self-assembled quantum dots. Starting from a microscopic viewpoint we study the carrier-carrier and carrier-phonon scattering processes leading to carrier capture into and relaxation inside the quantum dots.

As in general the carriers in any device are found in a nonequilibrium state, the theory needs to be flexible enough the embrace such cases. The nonequilibrium Green's function technique turns out to be useful, and we will develop our theory along these lines.

If one does not have the patience to under take a full microscopic study of the carrier dynamics, one might go ahead and do some rate-equation models. Our calculated scattering rates may then by used as inputs or guidelines, to verify their range of validity.

The thesis has been divided into four parts. Here in the first part we give a short introduction to our topic, followed by a closer look at self-assembled quantum dots in the next chapter. In the second part of the thesis we present and develop the theoretical tools needed for describing the carrier-carrier and carrier-phonon interaction. The third part of the thesis contains the results. First we discuss the carrier-carrier scattering. Secondly, we turn to the carrier-phonon scattering. In both chapters we focus on the InGaAs material system, while carrier-carrier scattering for the InGaN material system is studied in a following chapter. The last part of the thesis contains a summary, along with other material appropriate for appendices.

References

[1.1] M. Klude, Ph.D. thesis, University of Bremen, Mensch & Buch Verlag, Berlin, 2002.

[1.2] R. Scharf, Physik Journal **3**, 114 (2004), Deutsche Physikalische Gesellschaft.

[1.3] Conference on Lasers and Electro-Optics (CLEO), San Francisco, USA, 2004, paper PTuA1.

[1.4] Conference on Lasers and Electro-Optics (CLEO), San Francisco, USA, 2004, paper PTuA2.

[1.5] "Semiconductor lightning enters the boardroom", Opto & Laser Europe, http://optics.org, August 2002.

[1.6] P. Bhattacharya, K. K. Kamath, J. Singh, D. Klotzkin, J. Philips, H.-T. Jiang, N. Chervela, T. B. Norris, T. Sosnowski, J. Laskar, and M. R. Murty, IEEE Transactions on Electron Devices **46**, 871 (1999).

[1.7] M. Grundmann, Physics E **5**, 167 (2000).

[1.8] "Quantum-dot pioneers target telecoms rebound", Opto & Laser Europe, http://optics.org, September 2002.

Chapter 2

Self-Assembled Quantum Dots and Scattering Processes

Quantum dots (QDs) are often defined as manmade mesoscopic or nanoscaled objects capable of confining electrons in all three spatial directions. The analogy to nature's atoms is therefore striking, and for this reason QDs are frequently referred to as artificial atoms.

Throughout this work we consider self-assembled QDs based on the Stranski-Krastanow growth mode [2.1, 2.2]. Two other major QD systems have also been established. Nanocrystal QDs and their potentials are shortly described in Ref. [2.3], while for QDs defined by lithography and etching techniques we refer to the review papers by Kowenhowen et al. [2.4] and Reimann et al. [2.5].

In Sec. 2.1 the Stranski-Krastanow growth mechanism leading to the formation of QDs is briefly reviewed. As our description of the scattering processes rely on the corresponding QD single-particle states we introduce these in Sec. 2.2 for lens-shaped QDs. Finally in Sec. 2.3 we shortly discuss the carrier-carrier and carrier-phonon scattering processes in such systems.

2.1 Stranski-Krastanow Growth Mode

The Stranski-Krastanow growth mode is by now state of the art, and has been applied and refined successfully to III-V material systems like InGaAs/GaAs, InP/GaInP, InGaN/GaN, GaN/AlN and IV-IV material systems GeSi/Si. Typical growth techniques are the heteroepitaxy methods like MBE[1] or MOVPE[2]. Stranski-Krastanow grown QDs are predominantly

[1] Acronym: molecular beam epitaxy.
[2] Acronym: metal-organic vapor phase epitaxy.

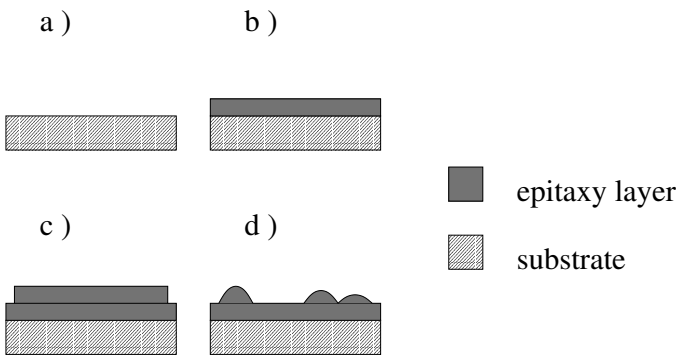

Figure 2.1: Schematic drawing of the Stranski-Krastanow growth mode. Light-gray corresponds to the substrate. Dark-gray corresponds to the deposited material, having a lager lattice constant and a smaller band-gap than the substrate. (Bulk values are implied).

studied within the field of photonics since they should be easier to integrate in optoelectronic devices, than e.g. QDs defined through lithography and etching techniques. Furthermore Stranski-Krastanow grown QDs have shown to be defect-free leading to high quality optical and electronic properties.

According to Seifert et al. [2.1] and Jacobi [2.2] the following picture of the Stranski-Krastanow growth mode has developed. The creation of QDs relies on two basic mechanisms. First, a material which we denote the epitaxy layer, is embedded in a surrounding barrier material having a larger band-gap. This leads to the confinement effect of electrons. The second effect is related to the morphology of the epitaxy layer. Just as in the case of a quantum well or a quantum wire, where the morphology of the embedded material determines the quasi-dimensionality of the system, so are the same principles at work for Stranski-Krastanow grown QDs. The Stranski-Krastanow growth mode is schematically shown in Fig. 2.1. Starting with a substrate, Fig. a), a single mono-layer is grown and one says the substrate has been wetted, Fig b). In the Stranski-Krastanow growth mode the epitaxy material has a larger lattice constant than the substrate, and following the epitaxy layer is grown under compressive strain. Adding more material to the substrate a metastable state of more mono-layers develops, Fig. c). At a certain critical thickness the epitaxy layer relaxes into a morphology of a thinner 2D wetting layer (WL) with small 3D islands on top which we denote QDs, Fig. d). Finally the QDs are overgrown with the material from the barrier or substrate, (not shown in figure), and one refers to these as buried QDs. It is important to understand that the transition from the metastable epitaxy layer into the WL-QD state is triggered by the system

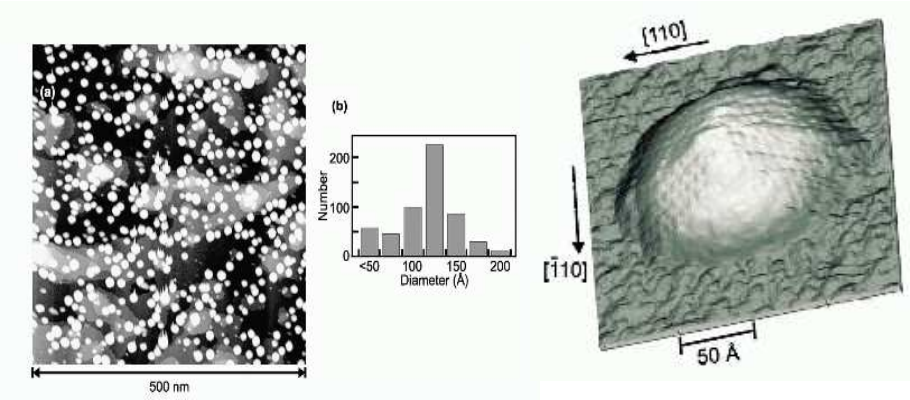

Figure 2.2: STM images of InAs QDs on GaAs (001), with a QD density of $1.9 \times 10^{11}\text{cm}^{-2}$. White spots correspond to QDs. Histogram shows the diameter distribution of QDs. From Ref. [2.2].

itself and not through external influence, hence the name self-organized or self-assembled QDs has developed. The intuitive picture, is that the build up of strain in the epitaxy layer reaches a point where it is more favorable to form QDs at the cost of higher surface energy, but the gain in a lower strain energy in WL drives the system towards this state. A detailed microscopic theoretical description of the Stranski-Krastanow transition is at present day not fully developed [2.2].

In Fig. 2.2 typically in-situ STM[3] images of uncapped InAs QDs grown on a GaAs (001) substrate are shown. First one should notice the random distribution of the QDs on the WL. Secondly, the QDs may be characterized as being lens-shaped. Thirdly the histogram shows that relative good control over the QD diameter be obtained. In the example shown here the QDs have a typical diameter of 12.5 nm, a height above the WL of 2.2 nm, and the thickness of the WL is typical a few mono layers.

Depending on growth conditions QDs can be manipulated in geometrical shape, diameter, and density. QDs have been reported to be formed as lenses, rings, disks, pyramids, or truncated pyramids [2.6, 2.7]. The most commonly investigated heterosystem is InGaAs. Throughout our work we focus on the InGaAs lens-shaped QDs. This is not at all a critical assumption for the work developed here, and can in principle be generalized to any other geometry and material system. However lots of experimental work exist for lens-shaped QDs.

[3]Acronym: scanning tunneling microscopy

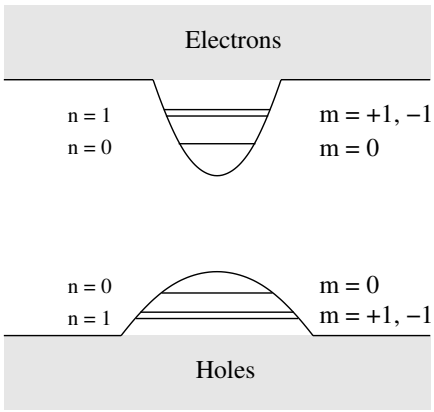

Figure 2.3: Schematic drawing of energy levels in the lens-shaped quantum-dot (QD) on wetting-layer (WL) system. The quasi-continuum of WL states (grey area) has larger interband transition energies than the discrete QD states labeled with the shell index n and the two-dimensional angular momentum m. The energetically degenerate states $m = \pm 1$ are visualized by two separated lines.

2.2 Single-Particle States

The starting point for a theoretical description of the QD carrier system are the non-interacting single-particle states. It is a complicated task on its own and beyond the scope of this thesis to compute from first principles these single-particle states for a given confinement situation that depends on the QD geometry, the strain profile and possible composition variations within the QD. Instead, we use a simplified model that reproduces the main features.

On the level of tight-binding and $\boldsymbol{k}\cdot\boldsymbol{p}$ models, zinc-blende QD structures have been studied in Refs. [2.8–2.13], while wurtzite QD structures have been addressed in Refs. [2.9, 2.10, 2.14, 2.15]. Our goals differ from these investigations in the respect that, for given single-particle states and energies, we calculate many-body energy renormalizations and scattering processes.

Lens-Shaped Quantum Dots

As mentioned above, we focus throughout the thesis on lens-shaped Stranski-Krastanow grown QDs. According to P. Hawrylak and co-workers [2.6, 2.7] the in-plane single-particle states of a lens-shaped QD can very well be described by those of a two-dimensional harmonic confinement potential. The authors found by comparisons using different levels of sophisticated models that the single-particle energy spectrum is equidistantly spaced, which is the first signature of a harmonic confinement potential. In Ref. [2.7] the authors

solved the 3D single-particle Schrödinger equation within the effective mass approximation using a confinement potential that is zero inside the QD and WL and equal to the band gap off-set otherwise. In this one band model the conduction and valence band are treated separately and all microscopic parameters like strain profile, and discontinuities in the effective mass are modeled by one effective mass. In one approach the authors solved the 3D Schrödinger equation by full 3D numerical diagonalization. This approach is however computationally very demanding. A faster method was implemented by using the so-called adiabatic approximation [2.7], in which the 3D Schrödinger equation is mapped onto a set of coupled 1D Schrödinger equations. Finally even using a fully 8-band $\boldsymbol{k}\cdot\boldsymbol{p}$ model showed according to the authors similar results [2.6]. Not only the energy spectrum is of interest, but also the single-particle wavefunctions are important. As shown by N. Baer [2.16] the single-particle in-plane wavefunctions agree very well with those for a two-dimensional harmonic oscillator.

Throughout this work we consider only the motion of carries in the quasi two-dimensional QD-WL system. Figure. 2.3 shows a schematic drawing of the energy spectrum for Stranski-Krastanow grown QDs with a two-dimensional harmonic oscillator confinement potential. For the sake of illustration this QD-WL system can, apart from spin degeneracy, confine three electrons and three holes in the QD, where the first excited state is double degenerated. According to Refs. [2.6, 2.7, 2.16] the in-plane wave-function for the QD ground state has a s-orbital character with angular momentum $m = 0$ and it is referred to as the s-shell, while the first excited state has a p-orbital character with angular momentum $m = \pm 1$ and it is referred to as the p-shell. The QD states are located energetically below the extended states of the WL which forms a quasi-continuum. The numerical results presented in Part III are based on the QD-WL model depicted in Fig. 2.3 with the parameters given in App. A and the harmonic oscillator states given in App. B.

Next to the theoretical model experimental findings strongly support the harmonic oscillator hypotheses. A recent work by Raymond et al. [2.17] shows photoluminensence spectra for lens-shaped QDs with equidistant spectrum, see Fig. 2.4. Other groups have found similar results, see e.g. Morris et al. [2.18].

2.3 Scattering Processes

From the single-particle states for the QD-WL system carrier-carrier and carrier-phonon scattering processes have been studied at various levels of sophistication and with different techniques. The basic question is, starting from e.g. the empty QD system, how can we get carries into the QD and what are the important mechanisms and scattering channels behind. Once

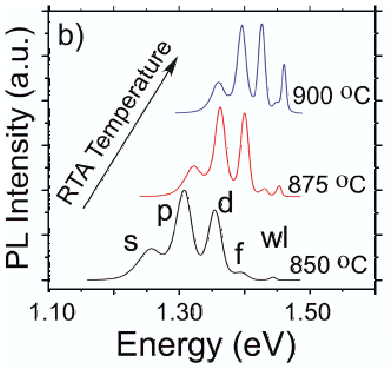

Figure 2.4: Photoluminensence measurement of InGaAs Stranski-Krastanow grow QDs. A clear shell structure with equidistant levels is observed. Notice how the width of each line is narrowed by using a higher post-grown annealing temperature. At the highest annealing temperature the peak spacing is 36 meV and FWHM of 15 meV, showing a highly homogeneity of the QD ensemble. The experiment was performed at 42 K. From Ref. [2.17].

the carriers are in the QD, how can they relax from energetically higher confined states to lower states. These questions we set out to answer in this thesis.

To illustrate the problem Fig. 2.5 shows the basic mechanisms in a typical photoluminensence experiment. Initially the system is in the ground state, i.e. no electors in the conduction band and no holes in the valence band are present. Carriers can then be injected into the WL either by electrical or optical pumping, or by the latter directly into the QDs. In general any creation of carriers in the system will lead to a nonequilibrium situation, which is thermalized by carrier-carrier and carrier-phonon scattering. For example, if the carriers are excited to the WL, the electrons and holes of the WL can then scatter among the WL carries themselves, or scatter directly to the energetically lower lying QD states. The latter we call a capture process. Once there are carriers in the QD they can relax downwards from higher to energetically lower lying QD states. This we call relaxation processes. Finally, the electrons and holes radiatively recombine and emit photons.

In Part III of the thesis, where we present the results, we will focus on the capture of carriers to the QD and relaxation inside the QD. The two basic interactions responsible for these scattering processes are the carrier-carrier interaction and the carrier-phonon interaction, and in Part II of the

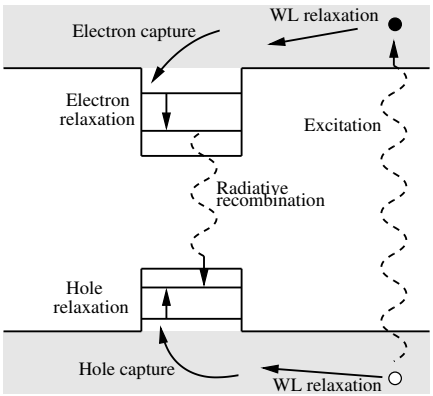

Figure 2.5: Schematic drawing of energy spectrum for Stranski-Krastanow grown QDs on a WL. The box corresponds to a confinement potential for the QDs with room for finite number of discreet states, while the gray area corresponds to the quasi-continuum of the WL. Different scattering processes are indicated by the arrows.

thesis we will develop a theory to describe both scattering mechanisms.

Carrier-Carrier Scattering

In Chap. 7 we study the carrier-carrier scattering processes for a InGaAs QD-WL system. For high carrier densities, carrier-carrier scattering can provide efficient transitions for electrons and holes from the delocalized WL states into the discrete localized QD states (carrier capture) as well as between the discrete QD states (carrier relaxation) [2.19, 2.20]. In previous references the transition rates have been calculated for processes where an electron or hole is scattered from the WL into the QD or between two QD states and the energy is transfered to another carrier in the WL. A detailed inspection of the kinetic equation for Coulomb scattering shows that these are only some of the possible processes. A relaxation process starting with two carriers in an excited QD state where one is scattered into the QD ground state and the other into the WL, studied in Ref. [2.21], is only one among other examples. The analysis in Ref. [2.19] has been simplified by assuming QD states of a three-dimensional infinite-barrier box. More realistic wave functions for this calculation have been used in Ref. [2.22] and the dependence of scattering rates on the QD geometry has been studied in Ref. [2.23].

The aim of Chap. 7 is to present a systematic study of the relative importance of various capture and relaxation processes due to carrier-carrier scattering. Previous investigations are expanded and clarified in the following directions: i) calculations are not restricted to Fermi's golden rule but include population effects, ii) both in- and out-scattering processes are

considered for the calculation of capture and relaxation times, iii) additional scattering processes and the role of Coulomb exchange contributions to the scattering integrals are examined, iv) properly orthogonalized states are systematically used and the influence of the wave function model on the scattering rates is analyzed, and v) a theoretical model of screening in the coupled QD-WL-system is provided.

In Chap. 9 we study the carrier-carrier scattering processes for a InGaN QD-WL system. Nitride based semiconductor systems are of current interest due to the unique potential they offer as short-wavelength light emitters and high-power/high-temperature electronics devices [2.24, 2.25]. However the question rises, to which extent previous results are modified by the peculiarities of this material system. Nitride-based heterostructures with a wurtzite crystal structure are known to have strong built-in fields due to spontaneous polarization and piezoelectric effects [2.26, 2.27], a pronounced mass anisotropy, and strongly non-parabolic hole energy dispersions [2.28]. The resulting modifications of the single-particle states directly influence the carrier scattering rates. On the other hand, the single-particle states are also influenced by Coulomb interaction effects. The corresponding renormalizations due to direct (Hartree) as well as exchange interaction and screening effects are usually neglected in the calculation of the scattering rates. In Chap. 9 we show that the discussed changes of the single-particle energies have a much stronger impact on the carrier scattering processes than modifications of the single-particle wave functions.

Carrier-Phonon Scattering

In Chap. 8 we study the carrier-phonon scattering processes for a InGaAs QD-WL system. For low carrier densities, where Coulomb scattering can be neglected, carrier-phonon interaction provides the dominant scattering channel. In QDs only phonons with small momenta can efficiently couple to the confined carriers [2.29]. Then interaction with longitudinal-acoustic (LA) phonons does not contribute for large transition energies and only quasi-monochromatic longitudinal-optical (LO) phonons need to be considered.

The simplest theoretical approach to electronic scattering processes is based on time-dependent perturbation theory. Fermi's golden rule for carrier transitions due to phonon emission or absorption contains a delta-function for strict energy conservation in terms of free-carrier energies of initial and final states and the phonon energy. When transition energies of localized QD states do not match the LO-phonon energy, efficient scattering is inhibited (leading to the prediction of a phonon bottleneck) and only higher-order processes, like a combination of LO and LA phonons [2.30, 2.31], weakly contribute. Attempts to broaden the delta-function "by hand" immediately change the results [2.31] which underlines that this point should be addressed

microscopically.

Within the microscopic theory developed in Part II of the thesis, we solve the kinetic equations for the capture process and relaxation processes, using the spectral properties of QD and WL polarons. For situations where, in terms of free-carrier energies, energy conserving scattering processes are not possible, the quantum-kinetic treatment provides efficient scattering rates.

References

[2.1] W. Seifert, N. Carlsson, M. Miller, M.-E. Pistol, L. Samuelson, and L. R. Wallenberg, Prog. Crystal Growth and Charact. **33**, 423 (1996).

[2.2] K. Jacobi, Prog. Surf. Sci. **71**, 185 (2003).

[2.3] V. I. Klimov, Los Alamos Science **28**, 214 (2003).

[2.4] L. P. Kouwenhoven, D. G. Austing, and S. Tarucha, Rep. Prog. Phys. **64**, 701 (2001).

[2.5] S. M. Reimann and M. Manninen, Rev. Mod. Phys. **74**, 1283 (2002).

[2.6] P. Hawrylak and M. Korkusiński, in *Topics in Applied Physics*, edited by P. Michler (Springer-Verlag, Heidelberg, 2003), Vol. 90, Chap. 2, pp. 25–92.

[2.7] A. Wojs, P. Hawrylak, S. Fafard, and L. Jack, Phys. Rev. B **54**, 5604 (1996).

[2.8] A. J. Williamson, L. W. Wang, and A. Zunger, Phys. Rev. B **62**, 12963 (2000).

[2.9] A. Bagga, P. K. Chattopadhyay, and S. Ghosh, Phys. Rev. B **68**, 155331 (2003).

[2.10] V. A. Fonoberov and A. A. Balandin, J. Appl. Phys. **94**, 7178 (2003).

[2.11] W. Sheng, S.-J. Cheng, and P. Hawrylak, Phys. Rev. B **71**, 035316 (2005).

[2.12] G. Bester and A. Zunger, Phys. Rev. B **71**, 045318 (2005).

[2.13] S. Schulz and G. Czycholl, arXiv:cond-mat/0507052, 2005.

[2.14] A. D. Andreev and E. P. O'Reilly, Phys. Rev. B **62**, 15851 (2000).

[2.15] A. Ranjan, G. Allen, C. Priester, and C. Delerue, Phys. Rev. B **68**, 115305 (2003).

[2.16] N. Baer, Optische Eigenschaften von Halbleiter-Quantenpunkten, Diplomarbeit, 2003, Universität Bremen, Fachberich Physik.

[2.17] S. Raymond, S. Studenikin, A. Sachrajda, Z. Wasilewski, S. J. Cheng, W. Schen, P. Hawrylak, A. Babinski, M. Potemski, G. Ortner, and M. Bayer, Phys. Rev. Lett. **92**, 187402 (2004).

[2.18] D. Morris, N. Perret, and S. Fafard, Appl. Phys. Lett. **75**, 3593 (1999).

[2.19] U. Bockelmann and T. Egeler, Phys. Rev. B **46**, 15574 (1992).

[2.20] A. V. Uskov, F. Adler, H. Schweizer, and M. H. Pilkuhn, J. Appl. Phys. **81**, 7895 (1997).

[2.21] R. Ferreira and G. Bastard, Appl. Phys. Lett. **74**, 2818 (1999).

[2.22] M. Brasken, M. Lindberg, and J. Tulkki, phys. stat. sol. (a) **167**, 427 (1997).

[2.23] I. Magnusdottir, S. Bischoff, A. V. Uskov, and J. Mørk, Phys. Rev. B **67**, 205326 (2003).

[2.24] I. Vurgaftman and J. R. Meyer, J. Appl. Phys. **94**, 3675 (2003).

[2.25] S. C. Jain, M. Willander, J. Narayan, and R. V. Overstraeten, J. Appl. Phys. **87**, 965 (2000).

[2.26] F. Bernardini, V. Fiorentini, and D. Vanderbilt, Phys. Rev. Lett. **79**, 3958 (1997).

[2.27] F. Bernardini and V. Fiorentini, Phys. Rev. B. **57**, R9427 (1998).

[2.28] S. L. Chuang and C. S. Chang, Phys. Rev. B **54**, 2491 (1996).

[2.29] T. Inoshita and H. Sakaki, Phys. Rev. B **56**, 4355 (1997).

[2.30] T. Inoshita and H. Sakaki, Phys. Rev. B **46**, 7260 (1992).

[2.31] H. Jiang and J. Singh, IEEE J. Quantum Electron **34**, 1188 (1998).

Part II

Theory

Chapter 3

Nonequilibrium Green's Functions

The basic object used to study the carrier dynamics of a semiconductor system is the one-particle density matrix. Given the one-particle density matrix one can then e.g. calculate the carrier distribution function or the microscopic polarization.

The first problem one faces is the so-called hierarchy problem, where the expectation value of the one-particle density operator via the carrier-carrier interaction couples to a two-particle expectation value, which further on couples to a three-particle expectation value, and so on. In the literature one often finds two approaches to tackle this problem. One where the infinite hierarchy problem is truncated at some n-particle expectation value followed by a factorization of the n-particle expectation into lower order expectation values. The second approach is the nonequilibrium Green's functions method, which is used throughout this thesis.

In this chapter we first review the hierarchy problem, after which the nonequilibrium Green's functions are introduced. We then proceed to derive the equation of motion for the Green's function, which is known as the Dyson equation. For a thorough introduction to nonequilibrium Green's functions we refer to Refs. [3.1–3.6], and unless otherwise stated this chapter is based on these references.

3.1 Introduction

The Hamiltonian for carriers in a semiconductor interacting with a classical external optical field reads

$$H = H_0 + H_{\rm d} + H_{\rm coul}.$$

Here H_0 describes the free motion of carriers in the semiconductor and contains the kinetic and potential energy, $H_{\rm d}$ is the dipole interaction between

carriers and the electric component of the optical field, while $H_{\rm coul}$ is the Coulomb interaction among the carriers themselves. The carrier-phonon interaction is treated in Chap. 6. For our purpose and to keep the introduction short we do not need to specify the form of the above three Hamiltonians at this point. Just note that the two first are single-particle operators, whereas the Coulomb Hamiltonian is a two-particle operator.

Then in second quantization the Hamiltonian reads

$$H = \sum_{ij} h^{(1)}_{ij} c^\dagger_i c_j + \frac{1}{2} \sum_{klmn} V^{(2)}_{klmn} c^\dagger_k c^\dagger_l c_m c_n$$

where $h^{(1)}_{ij}$ are the matrix-elements of the one-particle operator $h^{(1)} = h_0 + h_{\rm d}$, and $V^{(2)}_{klmn}$ the matrix elements of the two-particle Coulomb interaction operator. Here we have expanded H in the single-particle eigenbasis of the free Hamiltonian with $h_0(\boldsymbol{r})\varphi_i(\boldsymbol{r}) = \varepsilon_i \varphi_i(\boldsymbol{r})$, while $c^\dagger_i$ (c_i) correspondingly creates (annihilates) a carrier in state i. Formally we have

$$\begin{aligned} h^{(1)}_{ij} &= \langle i|h^{(1)}|j\rangle \\ &= \int {\rm d}\boldsymbol{r}\ \varphi^*_i(\boldsymbol{r}) h^{(1)}(\boldsymbol{r}) \varphi_j(\boldsymbol{r}), \\ V^{(2)}_{klmn} &= \langle kl|V^{(2)}|mn\rangle \\ &= \iint {\rm d}\boldsymbol{r}\, {\rm d}\boldsymbol{r}'\ \varphi_k(\boldsymbol{r})^* \varphi_l(\boldsymbol{r}')^* V^{(2)}(\boldsymbol{r},\boldsymbol{r}') \varphi_m(\boldsymbol{r}') \varphi_n(\boldsymbol{r}). \end{aligned}$$

Note that since the Coulomb potential is symmetric in the two space coordinates $V^{(2)}(\boldsymbol{r},\boldsymbol{r}') = V(|\boldsymbol{r}-\boldsymbol{r}'|)$ we obtain the identity $V_{klmn} = V_{lknm}$. Furthermore, since the Coulomb potential $V(\boldsymbol{r})$ is real we have the additional identity $V^*_{klmn} = V_{nmlk}$. For completeness let us mention that the Fermionic operators obey the anti-commutation relations

$$\begin{aligned} [c_i, c^\dagger_j]_+ &= \delta_{ij}, \\ [c_i, c_j]_+ &= [c^\dagger_i, c^\dagger_j]_+ = 0. \end{aligned}$$

In the Heisenberg picture equations of motion can be established for the creation and annihilation operators, and after some straightforward algebra we find

$$\begin{aligned} i\hbar \frac{d}{dt} c^\dagger_i &= [c^\dagger_i, H] = -\sum_l h^{(1)}_{li} c^\dagger_l + \sum_{lmn} V_{lmni} c^\dagger_l c^\dagger_m c_n, \\ i\hbar \frac{d}{dt} c_j &= [c_j, H] = \sum_l h^{(1)}_{jl} c_l - \sum_{lmn} V_{jlmn} c^\dagger_l c_m c_n, \end{aligned}$$

where we have used the symmetry property of the Coulomb matrix-element $\langle kl|V|mn\rangle = \langle lk|V|nm\rangle$.

The really interesting object to study is though the one-particle density matrix $\langle c_i^\dagger c_j \rangle$, where the symbol $\langle \cdots \rangle$ denotes the quantum-statistical expectation value.[1] Its diagonal elements give the carrier occupation probability $f_i = \langle c_i^\dagger c_i \rangle$, whereas the the off-diagonal elements yield the transition amplitudes $\Psi_{ij} = \langle c_i^\dagger c_j \rangle$ $(i \neq j)$ which can be driven (for dipole-allowed transition) by a coherent light field. The equation of motion for the one-particle density matrix reads

$$\begin{aligned} i\hbar \frac{d}{dt} \langle c_i^\dagger c_j \rangle &= -\sum_l \left(h_{li}^{(1)} \langle c_l^\dagger c_j \rangle - \langle c_i^\dagger c_l \rangle h_{jl}^{(1)} \right) \\ &\quad + \sum_{lmn} \left(V_{lmni} \langle c_l^\dagger c_m^\dagger c_n c_j \rangle - V_{jlmn} \langle c_i^\dagger c_l^\dagger c_m c_n \rangle \right), \end{aligned}$$

where we have used the product rule for differentiating $c_i^\dagger c_j$ and subsequently the equations of motion for $c_i^\dagger$ and c_j.

The differential equation for the one-particle density matrix highlights the so-called hierarchy problem where a low order correlation function couples to a higher order. For example, in the equation above the two-point correlation function $\langle c_i^\dagger c_j \rangle$ couples to a four-point correlation function $\langle c_i^\dagger c_k^\dagger c_l \, c_m \rangle$. The four-point correlation function on the other hand is connected to a six-point correlation function, as seen by differentiating $\langle c_i^\dagger c_k^\dagger c_l \, c_m \rangle$ with respect to time and using the equation of motion for creation and annihilation operators. Repeated application of this scheme leads to an infinite hierarchy of equations.

In order to solve the hierarchy problem one often relies on some kind of approximation scheme where the higher order correlation functions are decoupled into products of lower orders. The Hartree-Fock approximation is perhaps the most familiar example, where the four-point expectation value is decoupled into a linear combination of products of two-point expectation values. Applying this approximation to the equation of motion for the one-particle density matrix results in a generalized form of the Semiconductor Bloch Equations. But a systematic approximation beyond Hartree-Fock is not well established and different approximations can lead to different results [3.3].

There are however physical and practical reasons to consider terms beyond Hartree-Fock. Any coherence between carriers in a semiconductor does not live forever but is lost after a certain time scale. Among other things, due to the carrier-carrier interaction. This decoherence cannot be described within the Hartree-Fock approximation. Similarly, intraband relaxation of a nonequilibrium carrier distribution function f_i towards its quasi-equilibrium

[1] $\langle \cdots \rangle = \mathrm{Tr}\{\rho(t) \cdots\}$, but in the Heisenberg picture the quantum statistical operator is time independent and may be taken as $\rho(t = t_0) = \rho_0$. That is the ensemble expectation values are taken with respect to the initial state.

distribution function F_i cannot be deduced from the Hartree-Fock approximation and we need to go beyond in order to describe these phenomena. Correlations beyond the Hartree-Fock level, are e.g. also essential at low carrier densities, where biexcitonic effects become important (this regime is however not a subject of this thesis), or at elevated carrier densities where screening of the Coulomb interaction becomes important.

The Green's functions formalism offers a systematic way to overcome the hierarchy problem. Furthermore, as the name suggests, nonequilibrium Green's functions are designed to deal with situations where the system cannot be expected to be in equilibrium. As such nonequilibrium Green's functions have proven to be successful for the understanding of decoherence and carrier relaxation in semiconductors, as well as providing new insight into the carrier dynamics of semiconductors on a short femto- or pico-second time scale.

Thus to overcome the hierarchy problem we therefore set out the goal to derive an exact equation for the two-point correlation function also known as the one-particle Green's function. The resulting set of equations can in a schematic way be written as follows

$$\begin{aligned} G &= G_0 + G_0 \Sigma G, \\ \Sigma &= W \Gamma G, \\ W &= V + V P W, \\ P &= G \Gamma G, \\ \Gamma &= 1 + \frac{\delta \Sigma}{\delta G} G \Gamma G. \end{aligned}$$

Later within this chapter we define these symbols and derive this set of equations, but for now let us just focus on the structure. G is a one-particle correlation function and therefore it contains information about the single-particle properties of system, e.g., about the carrier occupation probability or about the spectral properties. G_0 is the solution in the limit of a vanishing self-energy Σ. W is the screened Coulomb potential, which is related to the bare Coulomb potential V and the polarization P. Finally Γ is the vertex function, formally it serves to close the system of equations (since $\delta\Sigma/\delta G$ may be determined by an iterative procedure).

Solving the above equation for G corresponds in some sense to solving the equation for the one-particle density matrix $\langle c_i^\dagger c_j \rangle$. In what follows we derive the set of equations given above, and only by going through the next two chapters we end up with a form which is more suitable for comparison with the equation of motion for the one-particle density matrix.

3.2 Keldysh Green's Functions

The first step towards the nonequilibrium Green's functions is a generalization of the one-particle density matrix to contain also temporal correlations. In terms of the Heisenberg field operators we are interested in the two-point correlation function

$$i\hbar G_{+-}(\boldsymbol{r}_1 t_1, \boldsymbol{r}_2 t_2) \;=\; \langle\, \Psi^\dagger(\boldsymbol{r}_2 t_2)\Psi(\boldsymbol{r}_1 t_1)\,\rangle$$

which describes the propagation of a hole from $\boldsymbol{r}_1 t_1$ to $\boldsymbol{r}_2 t_2$. Evaluated at equal times it reduces to the one-particle density matrix, while at equal space-time points it describes the particle density. For later reference we denote this correlation function as the *lesser* Green's function. Conversely

$$i\hbar G_{-+}(\boldsymbol{r}_1 t_1, \boldsymbol{r}_2 t_2) \;=\; \langle\, \Psi(\boldsymbol{r}_1 t_1)\Psi^\dagger(\boldsymbol{r}_2 t_2)\,\rangle$$

describes the propagation of a particle from $\boldsymbol{r}_2 t_2$ to $\boldsymbol{r}_1 t_1$, which is denoted the *greater* Green's function.

The equations of motion for the two propagators above are however not easy to deal with directly, and apart from also including temporal correlations we have not gained much compared to the density matrix approach given in the previous section. It has therefore been found easier to extend the family of Green's functions and introduce yet another two. The *chronological*

$$\begin{aligned} i\hbar G_{++}(\boldsymbol{r}_1 t_1, \boldsymbol{r}_2 t_2) &= \langle\, T\,\Psi(\boldsymbol{r}_1 t_1)\Psi^\dagger(\boldsymbol{r}_2 t_2)\,\rangle \\ &= \Theta(t_1 - t_2)\,\langle\,\Psi(\boldsymbol{r}_1 t_1)\Psi^\dagger(\boldsymbol{r}_2 t_2)\,\rangle \\ &\quad -\Theta(t_2 - t_1)\,\langle\,\Psi^\dagger(\boldsymbol{r}_2 t_2)\Psi(\boldsymbol{r}_1 t_1)\,\rangle, \end{aligned}$$

and the *anti-chronological*

$$\begin{aligned} -i\hbar G_{--}(\boldsymbol{r}_1 t_1, \boldsymbol{r}_2 t_2) &= \langle\, \widetilde{T}\,\Psi(\boldsymbol{r}_1 t_1)\Psi^\dagger(\boldsymbol{r}_2 t_2)\,\rangle \\ &= \Theta(t_1 - t_2)\,\langle\,\Psi^\dagger(\boldsymbol{r}_2 t_2)\Psi(\boldsymbol{r}_1 t_1)\,\rangle \\ &\quad -\Theta(t_2 - t_1)\,\langle\,\Psi(\boldsymbol{r}_1 t_1)\Psi^\dagger(\boldsymbol{r}_2 t_2)\,\rangle, \end{aligned}$$

where T and $\widetilde{T}$ are the time- and anti-time ordering operators. At first this might seem artificial, but is exactly one of the tricks that allow us to formally break the hierarchy problem. As will be clear later the four Green's functions can be put together in a so-called Keldysh 2×2 matrix which obey the (matrix) Dyson equation, from which one is lead to the same formal diagrammatic expansion known from equilibrium theory. In an equilibrium theory one needs however in principle only one Green's function, see e.g. Chap. 3 of Ref. [3.5] for a short summary.

The time-ordering operator T acts on all operators to the right and orders a set of operators in a time descending sequence from left to right

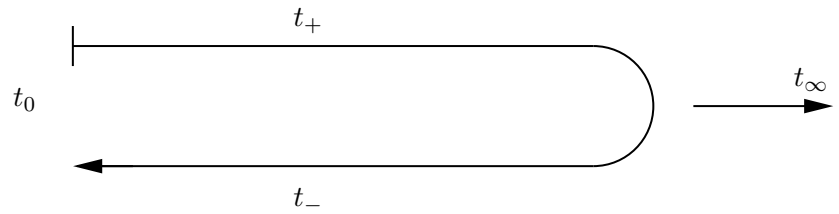

Figure 3.1: Keldysh time contour.

with the operator having the latest time to the far most left. "Late goes left" is useful to remember the action of T. The anti time-ordering operator $\widetilde{T}$ also acts on all operators to the right of it, and orders in the reverse order: early time operators to the left and then with increasing time argument to the right. Every time two fermionic operators are interchanged there is a minus sign being picked up.

As mentioned above the four introduced correlation functions can formally be combined into a single 2×2 matrix, if we assign to each time argument a so-called Keldysh index $b = \pm$. The one-particle Keldysh Green's function matrix is then defined as

$$G(\underline{1}, \underline{2}) \;=\; \frac{-i}{\hbar} b_2 \langle T_c \Psi(\underline{1}) \Psi^\dagger(\underline{2}) \rangle, \tag{3.1}$$

where T_c is the Keldysh time-ordering operator and the field operators are in the Heisenberg picture. Furthermore, we have introduced a compact notation $\underline{1} = \{\boldsymbol{r}_1, t_1, b_1\}$. The Keldysh time-ordering operator T_c orders operators with Keldysh-index $b = -$ to the left and Keldysh-index $b = +$ to the right. Every time two fermionic field operators are flipped to produce the right time sequence a minus sign is being picked up. With this rule, we easily obtain G_{+-} and G_{-+} given above. If both operators come with the same Keldysh index, they are by T_c ordered chronologically as the T and anti-chronologically as $\widetilde{T}$ for the $++$ and $--$ combinations, respectively, and we find G_{++} and G_{--}. In this way the combined introduction of the Keldysh indices and time-ordering operator is a compact way of keeping track of the four correlation functions.

The Keldysh time may be visualized by the Keldysh time contour depicted in Fig. 3.1. The real time axis is split into two, where times on the upper t_+ branch is to be interpreted as being earlier than times on the lower t_- branch. Thus we see that the above defined Green's functions are "chronological" time-ordered on the Keldysh contour, which is the basic requirement for using methods like Wick's theorem and the Feynman diagram technique.

To keep the notation compact the idea is now to derive a closed set of equations of motion for the Keldysh Green's function. Later we "unfold"

the Keldysh matrix and find the equation of motion for each of its elements. As a final step we expand the field operators in a basis and at the end result can be compared to the equation of motion for the density matrix given in Sec. 3.1.

3.3 Equation of Motion

The Hamiltonian for carriers in a semiconductor interacting with a classical external electric field was introduced in Sec. 3.1, and its real space representation expressed in terms of field operators reads [2]

$$\begin{aligned} H &= \int \mathrm{d}\boldsymbol{r}\; \Psi^\dagger(\boldsymbol{r}t)\big[h(\boldsymbol{r}t) + e\phi_{\mathrm{ext}}(\boldsymbol{r}t)\big]\Psi(\boldsymbol{r}t) \\ &\quad + \frac{e^2}{2}\iint \mathrm{d}\boldsymbol{r}\;\mathrm{d}\boldsymbol{r}'\;\Psi^\dagger(\boldsymbol{r}t)\Psi^\dagger(\boldsymbol{r}'t)V(\boldsymbol{r}-\boldsymbol{r}')\Psi(\boldsymbol{r}'t)\Psi(\boldsymbol{r}t), \end{aligned} \tag{3.2}$$

where $h(\boldsymbol{r}t)$ is the one-particle Hamiltonian

$$h(\boldsymbol{r}t) = -\frac{\hbar^2}{2m}\nabla^2 + eU(\boldsymbol{r}) + \boldsymbol{d}\cdot\boldsymbol{E}(\boldsymbol{r}t), \tag{3.3}$$

with kinetic energy, potential energy of the ionic lattice, and the light-matter interaction in the dipole approximation respectively. For details concerning the dipole interaction see Refs. [3.7, 3.8]. Furthermore we have added an arbitrary external time-dependent potential $\phi_{\mathrm{ext}}(\boldsymbol{r}t)$, which is set equal to zero at the end. Its role will be clear in a while. Finally, the bare Coulomb potential reads $V(\boldsymbol{r}) = 1/(4\pi\varepsilon_0|\boldsymbol{r}|)$. For completeness we notice that the fermion field operators obey the anti-commutation relations

$$\Big[\;\Psi(\boldsymbol{r}t),\Psi^\dagger(\boldsymbol{r}'t)\Big]_+ = \delta(\boldsymbol{r}-\boldsymbol{r}'), \tag{3.4}$$

$$\Big[\Psi^\dagger(\boldsymbol{r}t),\Psi^\dagger(\boldsymbol{r}'t)\Big]_+ = \big[\Psi(\boldsymbol{r}t),\Psi(\boldsymbol{r}'t)\big]_+ = 0. \tag{3.5}$$

The equation of motion for the Green's function can now be derived by using the Heisenberg equation of motion and the result is

$$\begin{aligned} i\hbar\frac{\partial}{\partial\, t_1}G(\underline{1},\underline{2}) &= \frac{i}{\hbar}b_2\langle T_c\left[H,\Psi(\underline{1})\right]\Psi^\dagger(\underline{2})\rangle \\ &\quad + \delta_{b_1b_2}\delta(t_1-t_2)\langle\Psi(\underline{1})\Psi^\dagger(\underline{2}) + \Psi^\dagger(\underline{2})\Psi(\underline{1})\rangle. \end{aligned} \tag{3.6}$$

The first term is as expected from the equation of motion $-i\hbar\dot{A} = [H, A]$, whereas the second term is related to the derivative of the Heaviside step-

[2] The spin index has been included tacitly in the coordinate argument.

function $\Theta(t)$

$$\begin{aligned}\frac{\partial}{\partial t_1}\Theta(t_1-t_2) &= \delta(t_1-t_2),\\ \frac{\partial}{\partial t_1}\Theta(t_2-t_1) &= -\delta(t_1-t_2).\end{aligned}$$

Using the anti-commutation relations the second line of Eq. (3.6) reduces to

$$\delta(\underline{1},\underline{2}) = \delta_{b_1 b_2}\delta(t_1-t_2)\delta(\boldsymbol{r}_1-\boldsymbol{r}_2), \tag{3.7}$$

and in a similar manner we introduce a compact notation for the Coulomb potential and integrals

$$V(\underline{1},\underline{2}) = V(\boldsymbol{r}_1-\boldsymbol{r}_2)\delta(t_1-t_2)\delta_{b_1 b_2}, \tag{3.8}$$

$$\int \mathrm{d}\,\underline{1} = \sum_{b_1}\iint \mathrm{d}\boldsymbol{r}_1\,\mathrm{d}t_1. \tag{3.9}$$

Finally using the commutation relations the equation of motion for the Green's function can be expressed as

$$\begin{aligned}i\hbar\frac{\partial}{\partial t_1}G(\underline{1},\underline{2}) &= \delta(\underline{1},\underline{2}) + \big[h(\underline{1}) + e\phi_{\mathrm{ext}}(\underline{1})\big]G(\underline{1},\underline{2})\\ &\quad - \frac{i}{\hbar}b_2\, e^2\int \mathrm{d}\underline{3}\; V(\underline{1}^+,\underline{3})\langle T_c\Psi^\dagger(\underline{3}^+)\Psi(\underline{3})\Psi(\underline{1})\Psi^\dagger(\underline{2})\rangle.\end{aligned} \tag{3.10}$$

Here $\underline{1}^+$ indicates a shift of the time argument t_1 as follows $t_1 \to t_1 + b_1\epsilon$ (where $\epsilon \to 0_+$). This is to ensure the correct ordering of operators with equal times. Furthermore, for the single-particle Hamiltonian we have $h(1,+) = h(1,-) = h(1)$ being equal on both branches, while the arbitrary potential is principle allowed to be different on the two branches $\phi_{\mathrm{ext}}(1,+) \neq \phi_{\mathrm{ext}}(1,-)$.

At this level the hierarchy problem is still explicitly present. The one-particle Green's function is coupled to a higher order two-particle correlation function. Formally we can now bypass this problem by introducing the functional derivative of the Green's function G with respect to the external potential ϕ_{ext}, and thus expressing the two-particle correlation function by means of the functional derivative. This is the basic trick! The idea behind is to transform the one-particle Green's function into a *generating* functional for higher correlation functions. ϕ_{ext} is the argument of this functional and therefore it is left arbitrary and even free from the physical restrictions of having the same value on both branches. At the end one should perform the "physical limit" setting $\phi_{\mathrm{ext}} \to 0$ [3.1, 3.4]. In terms of response theory the variational or functional derivative of $G(\underline{1},\underline{2})$ with respect to the external potential $\phi_{\mathrm{ext}}(\underline{3})$ gives the functional change in $G(\underline{1},\underline{2})$, $\delta G(\underline{1},\underline{2})$, due to a functional change in $\phi_{\mathrm{ext}}(\underline{3})$ at $\underline{3}$.

Then as shown in appendix 3.A

$$\frac{\delta\, G(\underline{1},\underline{2})}{\delta\, \phi_{\rm ext}(\underline{3})} = -\, b_2 b_3 \frac{e}{\hbar^2} \langle T_c \Psi^\dagger(\underline{3}^+)\Psi(\underline{3})\Psi(\underline{1})\Psi^\dagger(\underline{2})\rangle + e G(\underline{1},\underline{2}) G(\underline{3},\underline{3}^+), \tag{3.11}$$

and in this way we obtain

$$i\hbar \frac{\partial}{\partial\, t_1} G(\underline{1},\underline{2}) = \delta(\underline{1},\underline{2}) + [h(\underline{1}) + e\phi_{\rm eff}(\underline{1})]\, G(\underline{1},\underline{2}) + i\hbar e b_1 \int \mathrm{d}\underline{3}\; V(\underline{1}^+,\underline{3}) \frac{\delta\, G(\underline{1},\underline{2})}{\delta\, \phi_{\rm ext}(\underline{3})}, \tag{3.12}$$

where

$$\phi_{\rm eff}(\underline{1}) \;=\; \phi_{\rm ext}(\underline{1}) - i\hbar e b_1 \int \mathrm{d}\underline{3}\; V(\underline{1},\underline{3}) G(\underline{3},\underline{3}^+). \tag{3.13}$$

Since $-i\hbar e b_3 G(\underline{3},\underline{3}^+)$ describes a charge density the last term of the effective potential can be shown to equal the Hartree-potential, see Refs. [3.3, 3.4].

At this point we have formally replaced the two-particle correlation function in Eq. (3.10) by a functional derivative. The idea is now that by successive use of the functional derivative technique we end up with a closed set of equations which is formally exact for the one-particle Green's function. In the next chapter we therefore introduce the one-particle self-energy Σ, the screened Coulomb potential W, and the polarization propagator P. To close the set of equation we introduce the vertex function Γ.

3.4 Dyson's Equation

Assuming that the Green's function $G(\underline{1},\underline{2})$ has a unique inverse $G^{-1}(\underline{1},\underline{2})$ defined through

$$\int \mathrm{d}\underline{3}\; G^{-1}(\underline{1},\underline{3})\; G(\underline{3},\underline{2}) = \int \mathrm{d}\underline{3}\; G(\underline{1},\underline{3})\; G^{-1}(\underline{3},\underline{2}) \;=\; \delta(\underline{1},\underline{2}), \tag{3.14}$$

we obtain in this way the trivial identity

$$G(\underline{1},\underline{2}) = \iint \mathrm{d}\underline{4}\; \mathrm{d}\underline{5}\; G(\underline{1},\underline{4})\, G^{-1}(\underline{4},\underline{5})\, G(\underline{5},\underline{2}). \tag{3.15}$$

According to DuBois, see Ref. [3.6] p. 508, this assumption is equivalent to restricting the times t_1 and t_2 of the Green's function to an interval later than the initial time t_0 of the statistical operator $\rho(t_0)$ such that all initial

correlations have decayed. See also Binder and Koch [3.4] p. 343 and p. 346 for further discussions.

Taking the functional derivative of $G(\underline{1},\underline{2})$ with respect to $\phi_{\text{ext}}(\underline{3})$ and using the product rule yields

$$\frac{\delta\, G(\underline{1},\underline{2})}{\delta\, \phi_{\text{ext}}(\underline{3})} \;=\; -\iint \mathrm{d}\underline{4}\;\mathrm{d}\underline{5}\; G(\underline{1},\underline{4})\,\frac{\delta\, G^{-1}(\underline{4},\underline{5})}{\delta\, \phi_{\text{ext}}(\underline{3})}\, G(\underline{5},\underline{2}). \tag{3.16}$$

By plugging this result into the equation of motion for $G(\underline{1},\underline{2})$ we can now introduce the one-particle self-energy $\Sigma(\underline{1},\underline{2})$, and as such we can formally decouple the hierarchy problem. Following, the last line of Eq. (3.12) may be written as

$$i\hbar e b_1 \int \mathrm{d}\,\underline{3} V(\underline{1}^+,\underline{3})\frac{\delta\, G(\underline{1},\underline{2})}{\delta\, \phi_{\text{ext}}(\underline{3})} = \int \mathrm{d}\,\underline{5}\;\Sigma(\underline{1},\underline{5})\, G(\underline{5},\underline{2}), \tag{3.17}$$

where we have introduced the self-energy

$$\Sigma(\underline{1},\underline{2}) \;\equiv\; -i\hbar e b_1 \iint \mathrm{d}\underline{3}\;\mathrm{d}\underline{4}\; V(\underline{1}^+,\underline{3}) G(\underline{1},\underline{4})\,\frac{\delta\, G^{-1}(\underline{4},\underline{2})}{\delta\, \phi_{\text{ext}}(\underline{3})}. \tag{3.18}$$

The equation of motion for the Green's function can then be cast into the form

$$\left[i\hbar\frac{\partial}{\partial\, t_1} - h(\underline{1}) - e\phi_{\text{eff}}(\underline{1})\right] G(\underline{1},\underline{2}) \\ - \int \mathrm{d}\,\underline{3}\;\Sigma(\underline{1},\underline{3}) G(\underline{3},\underline{2}) \;=\; \delta(\underline{1},\underline{2}), \tag{3.19}$$

which is known as the Dyson equation. The hierarchy problem has now formally been eliminated. The original term with the four-point expectation value has however only been reformulated in terms of the self-energy and the Green's function. For practical purposes however one often has to resolve to some kind of approximation for the self-energy.

Equivalent Representation of the Dyson Equation

The solution to the Dyson equation with the self-energy set equal to zero is denoted G_0

$$\left[i\hbar\frac{\partial}{\partial\, t_1} - h(\underline{1}) - e\phi_{\text{eff}}(\underline{1})\right] G_0(\underline{1},\underline{2}) \;=\; \delta(\underline{1},\underline{2}). \tag{3.20}$$

This implies

$$G_0^{-1}(\underline{1},\underline{2}) \;=\; \left[i\hbar\frac{\partial}{\partial\, t_1} - h(\underline{1}) - e\phi_{\text{eff}}(\underline{1})\right]\delta(\underline{1},\underline{2}), \tag{3.21}$$

since the identity $\int \mathrm{d}\underline{3}\; G_0^{-1}(\underline{1},\underline{3})G_0(\underline{3},\underline{2}) = \delta(\underline{1},\underline{2})$ then yields Eq. (3.20).

An equivalent representation of the Dyson equation can thus be written in an integral form

$$\int \mathrm{d}\,\underline{3}\;\left[G_0^{-1}(\underline{1},\underline{3}) - \Sigma(\underline{1},\underline{3})\right] G(\underline{3},\underline{2}) \quad = \quad \delta(\underline{1},\underline{2}). \tag{3.22}$$

Applying now G_0 from left, integrating out inner arguments, and rearranging terms yields

$$G(\underline{1},\underline{2}) \quad = \quad G_0(\underline{1},\underline{2}) + \iint \mathrm{d}\underline{3}\,\mathrm{d}\underline{4}\; G_0(\underline{1},\underline{3})\,\Sigma(\underline{3},\underline{4})\,G(\underline{4},\underline{2}). \tag{3.23}$$

3.5 Auxiliary Equations

By successive use of the chain rule we can now derive a set of auxiliary equations which are needed to solve the Dyson equation. We therefore introduce three new functions, the screened Coulomb interaction W, the vertex function Γ, and the polarization propagator P.

Using the chain rule allow us to rewrite the self-energy as

$$\Sigma(\underline{1},\underline{2}) = -i\hbar e b_1 \iiint \mathrm{d}\underline{3}\,\mathrm{d}\underline{4}\,\mathrm{d}\underline{5}\; V(\underline{1},\underline{3}^+)G(\underline{3},\underline{4})\frac{\delta\, G^{-1}(\underline{1},\underline{2})}{\delta\,\phi_{\mathrm{eff}}(\underline{5})}\frac{\delta\,\phi_{\mathrm{eff}}(\underline{5})}{\delta\,\phi_{\mathrm{ext}}(\underline{3})}. \tag{3.24}$$

Introducing the screened Coulomb potential W and the vertex Γ given by

$$W(\underline{1},\underline{2}) = \int \mathrm{d}\,\underline{3}\; V(\underline{2},\underline{3})\frac{\delta\,\phi_{\mathrm{eff}}(\underline{1})}{\delta\,\phi_{\mathrm{ext}}(\underline{3})}, \tag{3.25}$$

$$\Gamma(\underline{1},\underline{2},\underline{3}) = \frac{\delta\, G^{-1}(\underline{1},\underline{2})}{\delta\,\phi_{\mathrm{eff}}(\underline{3})}, \tag{3.26}$$

the self-energy reads in its final form

$$\Sigma(\underline{1},\underline{2}) = \; -i\hbar e b_1 \iint \mathrm{d}\underline{3}\,\mathrm{d}\underline{4}\; W(\underline{3},\underline{1}^+)G(\underline{1},\underline{4})\Gamma(\underline{4},\underline{2},\underline{3}). \tag{3.27}$$

Continuing now to the screened Coulomb potential we need to evaluate

$$\begin{aligned}\frac{\delta\,\phi_{\mathrm{eff}}(\underline{1})}{\delta\,\phi_{\mathrm{ext}}(\underline{3})} &= \delta(\underline{1},\underline{3}) - i\hbar e b_1 \int \mathrm{d}\,\underline{2}\; V(\underline{1},\underline{2})\frac{\delta\, G(\underline{2},\underline{2}^+)}{\delta\,\phi_{\mathrm{ext}}(\underline{3})} \\ &= \delta(\underline{1},\underline{3}) - i\hbar e b_1 \iint \mathrm{d}\underline{2}\,\mathrm{d}\underline{4}\; V(\underline{1},\underline{2})\frac{\delta\, G(\underline{2},\underline{2}^+)}{\delta\,\phi_{\mathrm{eff}}(\underline{4})}\frac{\delta\,\phi_{\mathrm{eff}}(\underline{4})}{\delta\,\phi_{\mathrm{ext}}(\underline{3})},\end{aligned} \tag{3.28}$$

so that

$$\begin{aligned} W(\underline{1},\underline{2}) &= V(\underline{2},\underline{1}) \\ &\quad - i\hbar e b_1 \iiint \mathrm{d}\underline{3}\,\mathrm{d}\underline{5}\,\mathrm{d}\underline{4}\; V(\underline{2},\underline{3})V(\underline{1},\underline{5})\frac{\delta\, G(\underline{5},\underline{5}^+)}{\delta\,\phi_{\mathrm{eff}}(\underline{4})}\frac{\delta\,\phi_{\mathrm{eff}}(\underline{4})}{\delta\,\phi_{\mathrm{ext}}(\underline{3})} \\ &= V(\underline{2},\underline{1}) - i\hbar e b_1 \iint \mathrm{d}\underline{5}\mathrm{d}\,\underline{4}\; V(\underline{1},\underline{5})\frac{\delta\, G(\underline{5},\underline{5}^+)}{\delta\,\phi_{\mathrm{eff}}(\underline{4})} W(\underline{4},\underline{2}). \end{aligned} \tag{3.29}$$

As the last function we introduce the polarization propagator

$$\begin{aligned} P(\underline{1},\underline{2}) &= -i\hbar e b_1 \frac{\delta\, G(\underline{1},\underline{1}^+)}{\delta\,\phi_{\mathrm{eff}}(\underline{2})} \\ &= i\hbar e b_1 \iint \mathrm{d}\underline{3}\,\mathrm{d}\underline{4}\; G(\underline{1},\underline{3})\frac{\delta\, G^{-1}(\underline{3},\underline{4})}{\delta\,\phi_{\mathrm{eff}}(\underline{2})} G(\underline{4},\underline{1}^+), \end{aligned} \tag{3.30}$$

which in terms of the vertex function reads

$$P(\underline{1},\underline{2}) = i\hbar e b_1 \iint \mathrm{d}\underline{3}\,\mathrm{d}\underline{4}\; G(\underline{1},\underline{3})\Gamma(\underline{3},\underline{4},\underline{2})G(\underline{4},\underline{1}^+). \tag{3.31}$$

Thus using the polarization propagator the screened Coulomb potential obeys a Dyson-like equation

$$W(\underline{1},\underline{2}) = V(\underline{2},\underline{1}) + \iint \mathrm{d}\underline{3}\,\mathrm{d}\underline{4}\; V(\underline{1},\underline{3})P(\underline{3},\underline{4})W(\underline{4},\underline{2}). \tag{3.32}$$

To close the set of equations we must evaluate the vertex function. As a first step the inverse Green's function can easily be read off from the Dyson equation

$$G^{-1}(\underline{1},\underline{2}) = \left[i\hbar\frac{\partial}{\partial\, t_1} - h(\underline{1}) - e\phi_{\mathrm{eff}}(\underline{1})\right]\delta(\underline{1}-\underline{2}) - \Sigma(\underline{1},\underline{2}). \tag{3.33}$$

Then taking the functional derivative with respect to the effective potential yields

$$\begin{aligned} \Gamma(\underline{1},\underline{2},\underline{3}) &= \frac{\delta\, G^{-1}(\underline{1},\underline{2})}{\delta\,\phi_{\mathrm{eff}}(\underline{3})} \\ &= -e\delta(\underline{1},\underline{3})\,\delta(\underline{1},\underline{2}) - \frac{\delta\,\Sigma(\underline{1},\underline{2})}{\delta\,\phi_{\mathrm{eff}}(\underline{3})} \\ &= -e\delta(\underline{1},\underline{3})\,\delta(\underline{1},\underline{2}) - \iint \mathrm{d}\underline{4}\,\mathrm{d}\underline{5}\;\frac{\delta\,\Sigma(\underline{1},\underline{2})}{\delta\, G(\underline{4},\underline{5})}\frac{\delta\, G(\underline{4},\underline{5})}{\delta\,\phi_{\mathrm{eff}}(\underline{3})} \\ &= -e\delta(\underline{1},\underline{3})\,\delta(\underline{1},\underline{2}) \\ &\quad + \iint \mathrm{d}\underline{4}\,\mathrm{d}\underline{5}\;\frac{\delta\,\Sigma(\underline{1},\underline{2})}{\delta\, G(\underline{4},\underline{5})}\iint \mathrm{d}\underline{6}\,\mathrm{d}\underline{7}\; G(\underline{4},\underline{6})\frac{\delta\, G^{-1}(\underline{6},\underline{7})}{\delta\,\phi_{\mathrm{eff}}(\underline{3})} G(\underline{7},\underline{5}). \end{aligned} \tag{3.34}$$

Finally we have

$$\Gamma(\underline{1},\underline{2},\underline{3}) = -e\delta(\underline{1},\underline{3})\,\delta(\underline{1},\underline{2}) + \iiiint \mathrm{d}\underline{4}\,\mathrm{d}\underline{5}\,\mathrm{d}\underline{6}\,\mathrm{d}\underline{7}\,\frac{\delta\,\Sigma(\underline{1},\underline{2})}{\delta\,G(\underline{4},\underline{5})} G(\underline{4},\underline{6})G(\underline{7},\underline{5})\Gamma(\underline{6},\underline{7},\underline{3}). \tag{3.35}$$

Fundamental Set of Equations

Equations (3.23), (3.27), (3.32), (3.31), and (3.35) constitute the fundamental set of equations already given in section 3.1. Another popular visualization of the fundamental system of equation is given by the Feynman diagrams, see e.g. Refs. [3.2, 3.6]. The diagrammatic approach is however not used in the work presented here.

The fundamental set of equations shows how the hierarchy problem can be by-passed in a self-consistent way. As mentioned before one often has to rely on some kind of approximation for the self-energy, but by the iterative structure of the Dyson equation these selected diagrams (interactions) are then repeated to infinite order. That is, the selected diagrams are then treated exactly, in a non-perturbative way. The remaining challenge for the Green's function technique is to choose the right class of diagrams for a given physical problem. Here one frequently has to rely on previous experience.

3.A Functional Derivative

In this appendix we sketch how the four-point correlation function introduced in Eq. (3.10), i.e. $\left\langle T_c\Psi^\dagger(\underline{3}^+)\Psi(\underline{3})\Psi(\underline{1})\Psi^\dagger(\underline{2})\right\rangle$, can be expressed in terms of the two-point correlation function, i.e. our Green's function $G(\underline{1},\underline{2})$, and by functional derivative of the Green's function with respect to the external potential ϕ_{ext}. For details see Refs. [3.3, 3.4]. It is advantageous for this purpose to use the interaction representation with respect to the external Hamiltonian H_{ext}

$$H = H_0 + H_{\mathrm{d}} + H_{\mathrm{coul}} + H_{\mathrm{ext}},$$

where

$$H_{\mathrm{ext}} = \int \mathrm{d}\boldsymbol{r}\ \Psi^\dagger(\boldsymbol{r}t)e\phi_{\mathrm{ext}}(\boldsymbol{r}t)\Psi(\boldsymbol{r}t),$$

see Eq. (3.2).

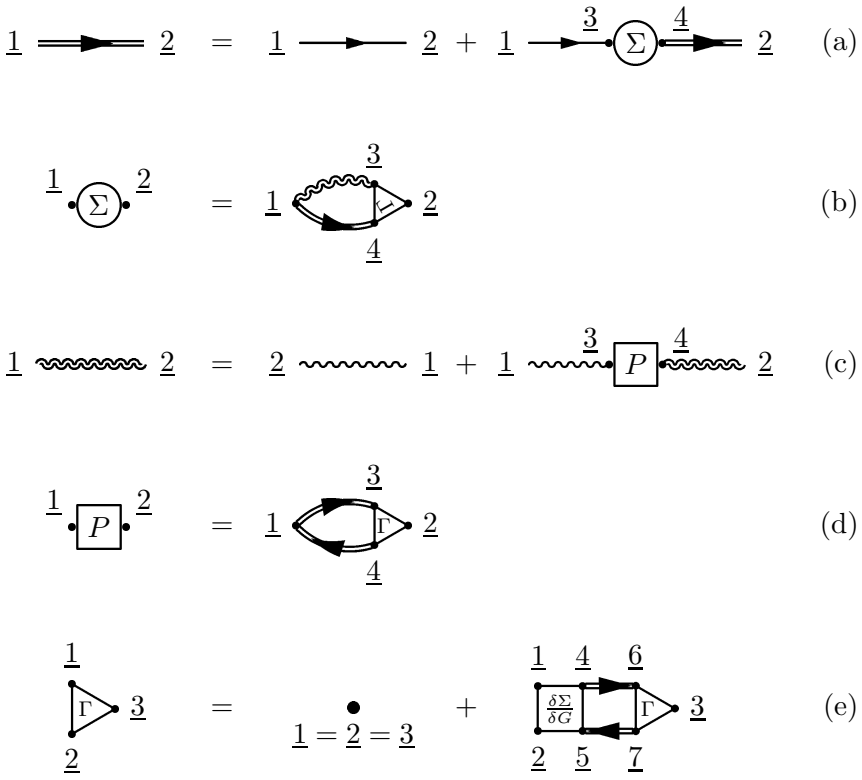

Figure 3.2: Diagamatic representation of the fundamental set of equations. The double solid line corresponds to the full Green's function $G(\underline{1},\underline{2})$ while the single solid line represents the free one $G_0(\underline{1},\underline{2})$. Similar, the screened (bare) Coulomb interaction is given by the double (single) wavy line. Integration over all inner arguments is implicitly understood. Depicted in
(a): Dyson equation for the electron propagator, see Eq. (3.23),
(b): Self-energy, see Eq. (3.27),
(c): Dyson equation for the screened Coulomb potential , see Eq. (3.32),
(d): Polarization function, see Eq. (3.31),
(e): Vertex function, see Eq. (3.35).

Operators in the Heisenberg- and interaction-picture are related through[3]

$$\Psi(\boldsymbol{r},t) \;=\; S(t_0,t)\hat{\Psi}(\boldsymbol{r},t)S(t,t_0), \tag{3.A.1}$$

where S is the time evolution operator given in the Interaction-picture by

$$S(t,t_0) \;=\; T\,\exp\left(-\frac{i}{\hbar}\int_{t_0}^{t}\mathrm{d}t_3\,\hat{H}_{\mathrm{ext}}(t_3)\right), \tag{3.A.2}$$

$$S(t_0,t) \;=\; \widetilde{T}\,\exp\left(-\frac{i}{\hbar}\int_{t}^{t_0}\mathrm{d}t_3\,\hat{H}_{\mathrm{ext}}(t_3)\right), \tag{3.A.3}$$

where $t > t_0$. Notice that $\hat{H}_{\mathrm{ext}}$ in the equation above is the external Hamiltonian given in the interaction picture. The time evolution operator obeys the identities

$$\begin{aligned} S(t_1,t_2) \;&=\; S^{-1}(t_2,t_1) \;=\; S^{\dagger}(t_2,t_1),\\ S(t_1,t_2) \;&=\; S(t_1,t_3)S(t_3,t_2), \end{aligned}$$

of which the latter is known as the semi-group property while the first shows that S is an unitary operator.

The expectation value of an operator depending on one time only takes then in the interaction picture the from

$$\langle O(t)\rangle \;=\; \langle S(t_0,t)\hat{O}(t)S(t,t_0)\rangle.$$

Reading from right the expectation value looks look like a time evolution from the remote past t_0 to the time t where the measurement is performed with $\hat{O}(t)$ and then a time evolution back in time to t_0. Such a history of events have we already encountered in Fig. 3.1.

The presence of both $S(t_0,t)$ and $S(t,t_0)$ implies a mixed time-order sequence, of chronological and anti-chronological and in-between the operator $\hat{O}(t)$. This mixed time ordering is the natural sequence of operators in the Green's function theory. In equilibrium situations the backward time evolution is mapped into a forward one using the adiabatic theorem [3.9, 3.10]. This is not possible in genuinely nonequilibrium problems. However, as we saw earlier in this chapter we may formally obtain a "chronological" time ordered sequence with the introduction of the Keldysh time, and this is why nonequilibrium Green's functions are naturally defined in terms of Keldysh-time arguments.

To eliminate the two-particle correlation function of Eq. (3.10) we introduce a *generating* functional $\mathcal{G}$ which by functional derivative gives the

[3]Operators in the interaction picture are labeled $\hat{\Psi}$ while while operators without are in the Heisenberg picture.

desired four-point correlation function. Following Binder and Koch [3.4] we use as generating functional the Keldysh Green's function in the interaction picture

$$
\begin{aligned}
i\hbar\mathcal{G}_{++}(1,2) &= \frac{1}{\langle S_{\mathcal{C}}\rangle}\left\langle S_{-}^{\dagger}\left[TS_{+}\hat{\Psi}(1)\ \hat{\Psi}^{\dagger}(2)\right]\right\rangle, && \text{(3.A.4)}\\
i\hbar\mathcal{G}_{+-}(1,2) &= \frac{1}{\langle S_{\mathcal{C}}\rangle}\left\langle \left[\widetilde{T}S_{-}^{\dagger}\hat{\Psi}^{\dagger}(2)\right]\left[TS_{+}\hat{\Psi}(1)\ \right]\right\rangle, && \text{(3.A.5)}\\
i\hbar\mathcal{G}_{-+}(1,2) &= \frac{1}{\langle S_{\mathcal{C}}\rangle}\left\langle \left[\widetilde{T}S_{-}^{\dagger}\hat{\Psi}(1)\ \right]\left[TS_{+}\hat{\Psi}^{\dagger}(2)\right]\right\rangle, && \text{(3.A.6)}\\
-i\hbar\mathcal{G}_{--}(1,2) &= \frac{1}{\langle S_{\mathcal{C}}\rangle}\left\langle \left[\widetilde{T}S_{-}^{\dagger}\hat{\Psi}(1)\ \hat{\Psi}^{\dagger}(2)\right]S_{+}\right\rangle. && \text{(3.A.7)}
\end{aligned}
$$

The four Green's functions may be unified in a Keldysh matrix

$$
\mathcal{G}(\underline{1},\underline{2}) = \frac{-i}{\hbar}b_2\frac{\langle T_{\mathcal{C}}S_{\mathcal{C}}\hat{\Psi}(\underline{1})\ \hat{\Psi}^{\dagger}(\underline{2})\rangle}{\langle S_{\mathcal{C}}\rangle}, \qquad \text{(3.A.8)}
$$

where

$$
\begin{aligned}
S_{\mathcal{C}} &= S_{-}^{\dagger}S_{+}, && \text{(3.A.9)}\\
S_{+} &= T\ \exp\left(-\frac{i}{\hbar}\int_{-\infty}^{\infty}\mathrm{d}t\,\hat{H}_{\mathrm{ext}}^{+}(t)\right), && \text{(3.A.10)}\\
S_{-}^{\dagger} &= \widetilde{T}\ \exp\left(+\frac{i}{\hbar}\int_{-\infty}^{\infty}\mathrm{d}t\,\hat{H}_{\mathrm{ext}}^{-}(t)\right). && \text{(3.A.11)}
\end{aligned}
$$

Furthermore we have pushed the initial time to the remote past, formally $t_0 = -\infty$. The S_+ operator evolves the system forward in time on the upper (chronological) branch with the operator $\hat{H}_{\mathrm{ext}}^{+}$, while the $S_-^{\dagger}$ operator evolves the system forward in time on the lower (anti-chronological) branch with the operator $\hat{H}_{\mathrm{ext}}^{-}$. Thus formally we have assumed that we can distinguish between the evolution on the upper and lower branch by using two *different* time evolution operators. At the end of the calculation we should perform the limit $\phi_{ext} \to 0$ and we obtain the usual Green's function $\mathcal{G}(\underline{1},\underline{2}) \to G(\underline{1},\underline{2})$.

We can now finally return to evaluating the functional derivative of the Green's function with respect to the external potential. At first we need the functional derivative of the time evolution operator

$$
\begin{aligned}
\frac{\delta S_{+}}{\delta\,\phi_{\mathrm{ext}}(3+)} &= -\frac{ie}{\hbar}\,T\,\left[S_{+}\ \hat{\Psi}^{\dagger}(3)\hat{\Psi}(3)\right], && \text{(3.A.12)}\\
\frac{\delta S_{-}^{\dagger}}{\delta\,\phi_{\mathrm{ext}}(3-)} &= \frac{ie}{\hbar}\,\widetilde{T}\,\left[S_{-}^{\dagger}\ \hat{\Psi}^{\dagger}(3)\hat{\Psi}(3)\right], && \text{(3.A.13)}
\end{aligned}
$$

which can be combined into

$$\frac{\delta S_c}{\delta\,\phi_{\rm ext}(\underline{3})} \;=\; -b_3\frac{ie}{\hbar}\,T_c\,\left[S_c\;\hat{\Psi}^\dagger(\underline{3}^+)\hat{\Psi}\;(\underline{3})\right]. \tag{3.A.14}$$

By using the product rule we then find

$$\begin{aligned}\frac{\delta\,\mathcal{G}(\underline{1},\underline{2})}{\delta\,\phi_{ext}(\underline{3})} &= -\frac{i}{\hbar}b_2\frac{\delta}{\delta\,\phi_{ext}(\underline{3})}\frac{\langle T_cS_c\hat{\Psi}(\underline{1})\hat{\Psi}^\dagger(\underline{2})\rangle}{\langle S_c\rangle}\\ &= -\frac{i}{\hbar}b_2\frac{1}{\langle S_c\rangle}\left\langle\frac{\delta S_c}{\delta\,\phi_{ext}(\underline{3})}\hat{\Psi}(\underline{1})\hat{\Psi}^\dagger(\underline{2})\right\rangle\\ &\quad-\frac{i}{\hbar}b_2\langle T_cS_c\hat{\Psi}(\underline{1})\hat{\Psi}^\dagger(\underline{2})\rangle\frac{-1}{\langle S_c\rangle^2}\frac{\delta\langle S_c\rangle}{\delta\,\phi_{ext}(\underline{3})}\end{aligned} \tag{3.A.15}$$

And finally by inserting previous results we get

$$\begin{aligned}\frac{\delta\,\mathcal{G}(\underline{1},\underline{2})}{\delta\,\phi_{ext}(\underline{3})} =& -b_2b_3\frac{e}{\hbar^2}\langle T_c\hat{\Psi}^\dagger(\underline{3}^+)\hat{\Psi}(\underline{3})\hat{\Psi}(\underline{1})\hat{\Psi}^\dagger(\underline{2})\rangle\frac{1}{\langle S_-^\dagger S_+\rangle}\\ &+e\mathcal{G}(\underline{1},\underline{2})\mathcal{G}(\underline{3},\underline{3}^+).\end{aligned} \tag{3.A.16}$$

In the limit $\phi_{ext}\to 0$ we reproduce Eq. (3.11).

References

[3.1] F. Jahnke, *Many-Body Theory* (Lecture notes, University of Bremen, 2003).

[3.2] P. Gartner, *Many-Body Theory Vol. I & II* (Lecture notes, University of Bremen, 2002).

[3.3] W. Schäfer and M. Wegener, in *Semiconductor Optics and Transport Phenomena* (Springer, Berlin Heidelberg, 2002), Chap. 10.

[3.4] R. Binder and S. W. Koch, Prog. Quant. Electr. **19**, 307 (1995).

[3.5] H. Haug and A.-P. Jauho, *Quantum Kinetics in Transport and Optics of Semiconductors* (Springer, Berlin Heidelberg, 1996).

[3.6] D. F. DuBois, in *Lectures in Theoretical Physics*, edited by W. E. B. et al. (Gordon and Breach, New York, 1967), Vol. 9 C, Chap. Nonequilibrium quantum statistical mechanics of plasmas and radiation, pp. 469–620.

[3.7] C. Cohen-Tannoudji, J. Dupont-Roc, and G. Grynberg, *Photons & Atoms* (Wiley, New York, 1989).

[3.8] G. Khitrova, H. M. Gibbs, F. Jahnke, M. Kira, and S. W. Koch, Rev. Mod. Phys. **71**, 1591 (1999).

[3.9] A. L. Fetter and J. D. Walecka, *Quantum Theory of Many-Particle Systems* (McGraw-Hill Book Company, New York, 1971).

[3.10] G. Mahan, *Many-Particle Physics* (Plenum, New York, 1990).

Chapter 4

Kadanoff-Baym Equations

4.1 Breaking the Keldysh Contour

As shown in Chap. 3 the Dyson equation for the one-particle nonequilibrium Keldysh Green's function reads

$$\int \mathrm{d}\underline{3}\left[G_0^{-1}(\underline{1},\underline{3}) - \Sigma(\underline{1},\underline{3})\right] G(\underline{3},\underline{2}) \quad = \quad \delta(\underline{1},\underline{2}). \tag{4.1}$$

With respect to the Keldysh indices ($\pm$) the Green's functions have the matrix structure

$$G(\underline{1},\underline{2}) \;=\; \begin{pmatrix} G_{++}(1,2) & G_{+-}(1,2) \\ G_{-+}(1,2) & G_{--}(1,2) \end{pmatrix} \;\equiv\; \begin{pmatrix} G(1,2) & G^{<}(1,2) \\ G^{>}(1,2) & \widetilde{G}(1,2) \end{pmatrix}, \tag{4.2}$$

which for the Dyson equation translates into solving a set of four equations. This is done in a two step procedure. First unfold the Keldysh contour by fixing the outer indices of the Dyson equation $\underline{1}$ and $\underline{2}$ to the upper (+) or lower (-) branch of the Keldysh contour. Second, the integral over the time contour integral is performed according to

$$\int \mathrm{d}\underline{t} \quad = \quad \sum_b \int_{-\infty}^{\infty} \mathrm{d}t_b \quad , \tag{4.3}$$

where b is the Keldysh branch index ($\pm$). Notice that on both branches the integral runs from $-\infty$ to $+\infty$, and not as indicated by Fig. 3.1. This is related to the definition of the Green's functions where the second branch index b_2 has been included in the definition. Thus for the four different combinations of $\underline{t}_1$ and $\underline{t}_2$ on the Keldysh contour the Dyson equation $\int \mathrm{d}\underline{3}\, F(\underline{1},\underline{3})G(\underline{3},\underline{2}) = \delta(\underline{1},\underline{2})$ with $F(\underline{1},\underline{3}) = G_0^{-1}(\underline{1},\underline{3}) - \Sigma(\underline{1},\underline{3})$ is unfolded

to

$$\int \mathrm{d}3\,[F_{++}(1,3)G_{++}(3,2) + F_{+-}(1,3)G_{-+}(3,2)] = \delta(1,2), \quad (4.4a)$$

$$\int \mathrm{d}3\,[F_{++}(1,3)G_{+-}(3,2) + F_{+-}(1,3)G_{--}(3,2)] = 0, \quad (4.4b)$$

$$\int \mathrm{d}3\,[F_{-+}(1,3)G_{++}(3,2) + F_{--}(1,3)G_{-+}(3,2)] = 0, \quad (4.4c)$$

$$\int \mathrm{d}3\,[F_{-+}(1,3)G_{+-}(3,2) + F_{--}(1,3)G_{--}(3,2)] = \delta(1,2). \quad (4.4d)$$

At this point all objects are time ordered in a specific way on a single time axis running from $-\infty$ to $+\infty$, and the Keldysh contour is no longer necessary. For later reference we notice that the four elements of the Keldysh Green's function matrix are in the literature known as: $G_{++} = G$ the chronological, $G_{--} = \widetilde{G}$ the anti-chronological, $G_{+-} = G^{<}$ the lesser, and $G_{-+} = G^{>}$ the greater Green's function, respectively. Due to linear relations and symmetry properties the four Green's functions are not independent and instead of solving the above four equations it is sufficient to solve only two.

4.2 Relations between Green's Functions

From the definition of G follow the linear relations[1]

$$G_{++}(1,2) + G_{+-}(1,2) = G_{--}(1,2) + G_{-+}(1,2) \quad (4.5a)$$

$$= \frac{1}{i\hbar}\Theta(t_1 - t_2)\left\langle \left[\Psi(1), \Psi^\dagger(2)\right]_+ \right\rangle \quad (4.5b)$$

$$= \Theta(t_1 - t_2)\,[G_{-+}(1,2) + G_{+-}(1,2)] \quad (4.5c)$$

$$\equiv G^r(1,2), \quad (4.5d)$$

and

$$G_{++}(1,2) - G_{-+}(1,2) = G_{--}(1,2) - G_{+-}(1,2) \quad (4.6a)$$

$$= -\frac{1}{i\hbar}\Theta(t_2 - t_1)\left\langle \left[\Psi(1), \Psi^\dagger(2)\right]_+ \right\rangle \quad (4.6b)$$

$$= -\Theta(t_2 - t_1)\,[G_{-+}(1,2) + G_{+-}(1,2)] \quad (4.6c)$$

$$\equiv G^a(1,2). \quad (4.6d)$$

Here we have defined two new functions with the symmetry properties

$$[G^r(1,2)]^* = G^a(2,1), \quad (4.7)$$

[1] The form of the linear relations depends on the definition of the Green's function and as such one can find different results in the literature reflecting the sign arbitrariness in the definition of $G(\underline{1},\underline{2})$. The b) equations are however the same in all representations.

and for completeness we add also

$$\left[G^{\gtrless}(1,2)\right]^* \;=\; -G^{\gtrless}(2,1). \tag{4.8}$$

In Chap. 5 and Chap. 6 we shall see that the *retarded* and *advanced* Green's functions $G^{r,a}$ are related to the spectral properties of the system.

From the definition of the self-energy Σ one can also obtain the same kind of linear relations as above (for details see Ref. [4.1])

$$\Sigma_{++}(1,2) + \Sigma_{+-}(1,2) \;=\; \Sigma_{--}(1,2) + \Sigma_{-+}(1,2), \tag{4.9a}$$
$$\Sigma_{++}(1,2) - \Sigma_{-+}(1,2) \;=\; \Sigma_{--}(1,2) - \Sigma_{+-}(1,2). \tag{4.9b}$$

As seen from Eq. (3.35) the lowest order contribution to the vertex function Γ is proportional to the product of two delta-functions and thus the lowest order contribution to the self-energy becomes instantaneous in time, since the bare Coulomb potential V is instantaneous is time. That is, the self-energy can have a non-retarded or non-advanced contribution, depending on only one time. Denoting the instantaneous self-energy by Σ^δ

$$\Sigma^\delta(\underline{1},\underline{2}) \;=\; i\hbar e^2 b_1 V(\underline{1}^+,\underline{2})G(\underline{1},\underline{2}), \tag{4.10}$$

which can be shown to be the Fock-term from the Hartree-Fock approximation, see Refs. [4.1, 4.2]. The instantaneous self-energy has the properties $\Sigma^\delta_{++}(1,2) = \Sigma^\delta_{--}(1,2)$ and $\Sigma^\delta_{+-}(1,2) = \Sigma^\delta_{-+}(1,2) = 0$.

According to Danielewicz [4.3] the retarded and advanced self-energies have to be generalized compared to Eqs. (4.5c) and (4.6c), to take this instantaneous part into account as follows

$$\Sigma^r(1,2) \;=\; \Sigma^\delta(1,2) + \Theta(t_1 - t_2)\left[\Sigma_{+-}(1,2) + \Sigma_{-+}(1,2)\right], \tag{4.11a}$$
$$\Sigma^a(1,2) \;=\; \Sigma^\delta(1,2) - \Theta(t_2 - t_1)\left[\Sigma_{+-}(1,2) + \Sigma_{-+}(1,2)\right]. \tag{4.11b}$$

This allows us later to construct an equation of motion for the Green's function which consist of two parts, one related to an effective one-particle Hartree-Fock Hamiltonian and a second part with correlations beyond the Hartree-Fock approximation.

Finally, for the screened interaction W and the polarization P the same linear relations can also be proven (for details see Refs. [4.1, 4.2]). To summarize we obtain for all elements $C = \{G, \Sigma, W, P\}$

$$C_{++}(1,2) \;+\; C_{+-}(1,2) \;=\; C_{--}(1,2) \;+\; C_{-+}(1,2), \tag{4.12a}$$
$$C_{++}(1,2) \;-\; C_{-+}(1,2) \;=\; C_{--}(1,2) \;-\; C_{+-}(1,2)\,. \tag{4.12b}$$

4.3 Kadanoff-Baym Equations

By appropriate linear combinations of the unfolded Dyson equations above and successive introduction of $G^{r,a}$ we finally arrive at a fundamental set of equations. For example by adding Eqs.(4.4a) and (4.4b) we obtain an equation for the retarded Green's function G^r, while Eq.(4.4b) can be restated as an equation for the propagator $G^<$ in terms of retarded and advanced functions. We obtain

$$\int \mathrm{d}3 \quad \left[G_0^{-1}(1,3) - \Sigma^r(1,3)\right] G^r(3,2) = \delta(1-2), \tag{4.13a}$$

$$\int \mathrm{d}3 \, \left\{ \left[G_0^{-1}(1,3) - \Sigma^r(1,3)\right] G^<(3,2) - \Sigma^<(1,3) G^a(3,2) \right\} = 0, \tag{4.13b}$$

which are known as the 1st Kadanoff-Baym equations. One should notice the coupling of the spectral functions $G^{r,a}$ to the propagator $G^<$.

Langreth-Wilkins Theorems

The unfolded Dyson equations have a structure like $C = \int \mathrm{d}\underline{t}\; AB$, where we have only explicitly written the temporal integrals whereas all other integrals and sums are implicitly understood by the matrix structure of the equation. As an example consider Eq.(4.4b) which can be cast in the form

$$C^<(t_1,t_2) = \int \mathrm{d}\underline{t}_3 \; A(t_1,\underline{t}_3) B(\underline{t}_3,t_2)$$

and then by the 1st Kadanoff-Baym equation Eq.(4.13b) re-written as

$$C^<(t_1,t_2) = \int_{-\infty}^{\infty} \mathrm{d}t_3 \; A^r(t_1,t_3)B^<(t_3,t_2) + A^<(t_1,t_3)B^a(t_3,t_2).$$

Using a shorthand notation with integration implicitly understood we then have

$$C = A\; B, \tag{4.14}$$

$$C^{\lessgtr} = A^r B^{\lessgtr} + A^{\lessgtr} B^a, \tag{4.15}$$

$$C^{r,a} = A^{r,a} B^{r,a}, \tag{4.16}$$

where the results for greater, retarded, and advanced function follow by similar considerations (for a detailed proof see Refs. [4.1, 4.4, 4.5]). The relations stated here are known as the Langreth-Wilkins Theorems.

4.4 Two-Time Formalism

The Green's functions introduced in Chap. 3 are two-time correlation functions of one-particle expectation values. By allowing for two time arguments we could write down a compact form of the (Keldysh) Dyson equation, but after being unfolded at the cost of many auxillary functions which all depend on two time arguments as shown in the 1st Kadanoff-Baym equations. This approch should be contrasted to the single-time equation of motion for the density matrix $\langle c_i^\dagger c_j \rangle$ introduced in Chap. 3, where its real-space representation reads

$$\begin{aligned} i\hbar\frac{\partial}{\partial t}\langle\Psi^\dagger(\boldsymbol{r}_1 t)\Psi(\boldsymbol{r}_2 t)\rangle &= [h(\boldsymbol{r}_2) - h(\boldsymbol{r}_1)]\,\langle\Psi^\dagger(\boldsymbol{r}_1 t)\Psi(\boldsymbol{r}_2 t)\rangle \\ &+ \int \mathrm{d}\boldsymbol{r}_3 \big\{ V(\boldsymbol{r}_2 - \boldsymbol{r}_3)\langle\Psi^\dagger(\boldsymbol{r}_1 t)\Psi^\dagger(\boldsymbol{r}_3 t)\Psi(\boldsymbol{r}_3 t)\Psi(\boldsymbol{r}_2 t)\rangle \\ &- V(\boldsymbol{r}_1 - \boldsymbol{r}_3)\langle\Psi^\dagger(\boldsymbol{r}_1 t)\Psi^\dagger(\boldsymbol{r}_3 t)\Psi(\boldsymbol{r}_3 t)\Psi(\boldsymbol{r}_2 t)\rangle \big\}. \end{aligned} \tag{4.17}$$

Solving the above equation corresponds to asking how does $G^<(1,2)$ change on the time-diagonal

$$\frac{\partial}{\partial t}G^<(t,t) \;=\; \left[\frac{\partial}{\partial t_1}G^<(t_1,t_2) + \frac{\partial}{\partial t_2}G^<(t_1,t_2)\right]_{t_1=t_2=t}.$$

Let us therefore now consider changes in the Green's functions with respect to the second time argument t_2.

The iterative structure of the Dyson equation, written here in a shorthand notation, suggests

$$\begin{aligned} G &= G_0 + G_0\Sigma\, G_0 + G_0\Sigma\, G_0\Sigma\, G_0 + \cdots \\ &= G_0 + G\Sigma\, G_0, \end{aligned}$$

where in going to the second line we have re-grouped the right hand side. Applying G_0^{-1} from the right, and re-arranging terms yields

$$\int \mathrm{d}\underline{3}\; G(\underline{1},\underline{3})\left(G_0^{-1}(\underline{3},\underline{2}) - \Sigma(\underline{3},\underline{2})\right) \;=\; \delta(\underline{1},\underline{2}), \tag{4.18}$$

where

$$\int \mathrm{d}\underline{3}\; G(\underline{1},\underline{3})G_0^{-1}(\underline{3},\underline{2}) = \left(-i\hbar\frac{\partial}{\partial t_2} - h(\underline{2}) - e\phi_{\mathrm{eff}}(\underline{2})\right) G(\underline{1},\underline{2}). \tag{4.19}$$

The change of sign in-front of the time derivative with respect to t_2 compared to the time derivative with respect to t_1 is due to the fact that we are now

taking the derivative of the field operator $\Psi^\dagger$ and not Ψ. In this notation there is a difference, whether G_0^{-1} is acting from the left or the right, compare with Eq. (3.21)

Then using the procedure presented previously in Sec. 4.1 and Sec. 4.3 we obtain,

$$\int \mathrm{d}3 \quad G^a(1,3)\left[G_0^{-1}(3,2) - \Sigma^a(3,2)\right] = \delta(1-2), \tag{4.20a}$$

$$\int \mathrm{d}3 \left\{G^<(1,3)\left[G_0^{-1}(3,2) - \Sigma^a(3,2)\right] - G^r(1,3)\Sigma^<(3,2)\right\} = 0, \tag{4.20b}$$

which are known as the 2nd Kadanoff-Baym equations. See Ref. [4.1] for more details.

Kinetic Equations

From the two Dyson equations

$$\begin{aligned}\int \mathrm{d}\underline{3}\ \left(G_0^{-1}(\underline{1},\underline{3}) - \Sigma(\underline{1},\underline{3})\right) G(\underline{3},\underline{2}) &= \delta(\underline{1},\underline{2}),\\ \int \mathrm{d}\underline{3}\ G(\underline{1},\underline{3})\left(G_0^{-1}(\underline{3},\underline{2}) - \Sigma(\underline{3},\underline{2})\right) &= \delta(\underline{1},\underline{2}),\end{aligned}$$

we can either build the sum or the difference

$$\begin{aligned}&\left[i\hbar\left(\frac{\partial}{\partial t_1} \mp \frac{\partial}{\partial t_2}\right) - \left[h(\underline{1}) + e\phi_{\text{eff}}(\underline{1})\right] \mp \left[h(\underline{2}) + e\phi_{\text{eff}}(\underline{2})\right]\right] G(\underline{1},\underline{2})\\ &\quad - \int \mathrm{d}\underline{3}\left\{\Sigma(\underline{1},\underline{3})G(\underline{3},\underline{2}) \pm G(\underline{1},\underline{3})\Sigma(\underline{3},\underline{2})\right\} = (1 \pm 1)\,\delta(\underline{1},\underline{2}),\end{aligned} \tag{4.21}$$

where we have used the properties of the inverse Green's function G_0^{-1}. By the Langreth-Wilkins theorems we can unfold the Keldysh contour and cast the equations into the form

$$\begin{aligned}&\left[i\hbar\left(\frac{\partial}{\partial t_1} \mp \frac{\partial}{\partial t_2}\right) - \left[h(1) + e\phi_{\text{eff}}(1)\right] \mp \left[h(2) + e\phi_{\text{eff}}(2)\right]\right] G^r(1,2)\\ &\quad - \int \mathrm{d}3\left\{\Sigma^r(1,3)G^r(3,2) \pm G^r(1,3)\Sigma^r(3,2)\right\} = (1 \pm 1)\,\delta(1,2)\end{aligned} \tag{4.22}$$

$$\begin{aligned}&\left[i\hbar\left(\frac{\partial}{\partial t_1} \mp \frac{\partial}{\partial t_2}\right) - \left[h(1) + e\phi_{\text{eff}}(1)\right] \mp \left[h(2) + e\phi_{\text{eff}}(2)\right]\right] G^<(1,2)\\ &\quad - \int \mathrm{d}3\left\{\Sigma^r(1,3)G^<(3,2) + \Sigma^<(1,3)G^a(3,2)\right\}\\ &\quad \mp \int \mathrm{d}3\left\{G^r(1,3)\Sigma^<(3,2) + G^<(1,3)\Sigma^a(3,2)\right\} = 0\end{aligned} \tag{4.23}$$

which are known as the *kinetic equations*. Using the symmetry relations Eqs. (4.7) and (4.8), the kinetic equations constitute a closed set of equations which can propagate the system anywhere around in the two-time plane (t_1, t_2), see Fig. 4.1. Furthermore, since except for trivial cases the self-energy is expressed terms of the Green's functions and the screened Coulomb interaction, the kinetic equations show that one has to solve both the spectral (G^r) and dynamical ($G^<$) properties simultaneously.

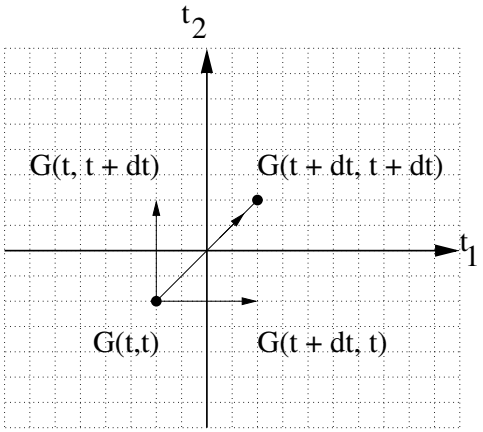

Figure 4.1: Schematic drawing of the two-time plane (t_1, t_2). Use 1nd and 2nd Kadanoff-Baym equations to evolve the Green's functions along the t_1 and t_2 time axis, respectively. The kinetic equations with the sum of the two time derivatives evolve the Green's functions parallel to the time diagonal.

As already mentioned we would like to evolve the lesser Green's functions on the time diagonal in order to make contact with the temporal behavior of the carrier occupation probabilities or the transition amplitudes. As also mentioned we do not expect any correlation to exist forever, and as such it is sufficient to look at temporal correlations "close" to the time diagonal. For these reasons it is advantageous to introduce new time variables. Some popular choices are

$$t_r = t_1 - t_2, \tag{4.24a}$$

$$t = t_1, \tag{4.24b}$$

$$\frac{\partial}{\partial t_1} = \frac{\partial}{\partial t} + \frac{\partial}{\partial t_r}, \tag{4.24c}$$

$$\frac{\partial}{\partial t_2} = -\frac{\partial}{\partial t_r} \tag{4.24d}$$

or

$$
\begin{aligned}
t_r &= t_1 - t_2, && \text{(4.25a)}\\
t &= \frac{t_1 + t_2}{2}, && \text{(4.25b)}\\
\frac{\partial}{\partial t_1} &= \frac{1}{2}\frac{\partial}{\partial t} + \frac{\partial}{\partial t_r}, && \text{(4.25c)}\\
\frac{\partial}{\partial t_2} &= \frac{1}{2}\frac{\partial}{\partial t} - \frac{\partial}{\partial t_r}. && \text{(4.25d)}
\end{aligned}
$$

In the latter case t may be interpreted as a center of mass time and t_r as the relative time.

In practice however, solving the kinetic equations as described above is not an easy task. Keeping track of the whole two-time plane solution is time and memory exhausting even with todays supercomputers. Instead, one has to rely on approximation schemes.

For the lesser Green's function $G^<(t_1, t_2)$ one often uses the generalized Kadanoff-Baym ansatz to map the temporal correlations back onto the time-diagonal, while for the retarded Green's function $G^r(t_1, t_2)$ one often assumes some spectral properties of the system (in the simplest case those of the free non-interacting system).

4.5 Generalized Kadanoff-Baym Ansatz

In this section we shortly show how one can bypass the two-time problem of relating the lesser Green's function outside the time-diagonal to its diagonal components. State of the art is the so-called generalized Kadanoff-Baym ansatz (GKBA). As shown in Refs. [4.5, 4.6], the lesser Green's function obeys the identity

$$
\begin{aligned}
G^<(t_1,t_2) = i\hbar \left[G^r(t_1,t_2)G^<(t_2,t_2) - G^<(t_1,t_1)G^a(t_1,t_2)\right]\\
+ \Theta(t_1 - t_2)\int_{t_2}^{t_1} \mathrm{d}t_3 \int_{-\infty}^{t_2} \mathrm{d}t_4\\
\times G^r(t_1,t_3)\left[\Sigma^r(t_3,t_4)G^<(t_4,t_2) + \Sigma^<(t_3,t_4)G^a(t_4,t_2)\right]\\
+ \Theta(t_2 - t_1)\int_{t_1}^{t_2} \mathrm{d}t_3 \int_{-\infty}^{t_1} \mathrm{d}t_4\\
\times \left[G^<(t_1,t_4)\Sigma^a(t_4,t_3) + G^r(t_1,t_4)\Sigma^<(t_4,t_3)\right] G^a(t_3,t_2). \quad \text{(4.26)}
\end{aligned}
$$

A similar equality holds for the greater Green's function, only replace $<$ with $>$. To keep the notation clear we have only written the temporal integrals while all other integrals and sums are implicitly understood by the matrix structure of the equation. The above result shows that the lesser Green's function at any given point in the two-time plane (t_1, t_2) may be constructed

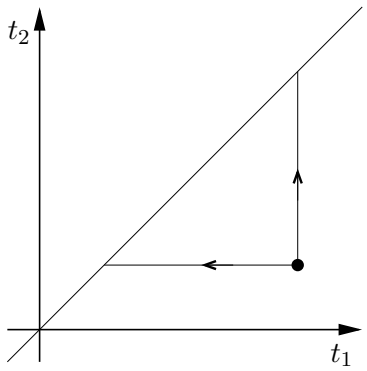

Figure 4.2: Consider a point in the two-time plane with $t_1 > t_2$ for $G^<(t_1, t_2)$. Using the GKBA the propagator is now brought back to the time-diagonal at $t_1 = t_2$ with the horizontal projection.

by an iterative procedure from the lesser Green's function given on the time diagonal (weighted by the spectral function). Using only the first term of the RHS in Eq. (4.26) corresponds to the GKBA. Conversely the identity may serve as a check for the GKBA. Let us for completeness mention that the original idea was given by Lipavský et al. [4.7] and latter revisited in Refs. [4.8, 4.9].

The advantages of the GKBA may not be fully appreciated yet, as we still have to determine the two-time spectral functions $G^{r,a}(t_1, t_2)$. For the spectral functions $G^{r,a}(t_1, t_2)$ further approximations are possible even in nonequilibrium situations. In this way one often uses simplified models for the spectral functions, like using those for the non-interacting system. Or one may try two solve the equations for $G^{r,a}(t_1, t_2)$ using rather simplified assumptions. At the end we somehow supply a solution for the spectral functions, and then by the GKBA the kinetic equations for the propagators may be mapped onto one single time argument.

The GKBA may be said to exhibit maximum retardation, since the two-time propagator is always brought back to the diagonal at the earliest time. The case for $t_1 > t_2$, is depicted in Fig. 4.2 with the horizontal projection. Keeping in mind that the two-time propagator enters the kinetic equation (4.23) under a time integral, the GKBA amounts to summing up contributions from the past starting with the earliest time in which as the equal time propagator $G^<(t, t)$ is different from zero. The GKBA with maximum retardation, should be contrasted to Markov approximation where one brings $G^<(t_1, t_2)$ to the diagonal for the latest time, see Fig. 4.2 with the vertical projection. In this case the time integral in the kinetic equation involves only the spectral function, the history of the propagtors is neglected and enter the equation at the latest time.

Validity of GKBA

The GKBA becomes exact in the absence of interaction or if the interaction is treated at the Hartree-Fock level, i.e. in the cases of one-particle Hamiltonians, see Refs. [4.2, 4.6] for details. In general the GKBA is an approximation, expected to hold better for low strengths of the interaction.

The range of validity of the GKBA is an open question and an ongoing research topic. In case of doubt one has two choices to test the approximation. Either evaluate the first iteration to $G^<(t_1, t_2)$ and check if the corrections are significant. Or one can always start the full machinery and undertake a two-time calculation.

In the case of electron-phonon coupling, P. Gartner et al. [4.10] have studied the validity of the GKBA. For the Fröhlich interaction they found good agreement between the GKBA and a two-time calculation in the weak interaction regime ($\alpha \ll 1$) while in the intermediate regime ($\alpha \approx 1$) the two approaches yield different results.

References

[4.1] R. Binder and S. W. Koch, Prog. Quant. Electr. **19**, 307 (1995).

[4.2] W. Schäfer and M. Wegener, *Semiconductor Optics and Transport Phenomena* (Springer, Berlin Heidelberg, 2002), chap. 10.

[4.3] P. Danielewicz, Ann. Phys. **152**, 239 (1984).

[4.4] P. Gartner, *Many-Body Theory Vol. I & II* (Lecture notes, University of Bremen, 2002).

[4.5] H. Haug and A.-P. Jauho, *Quantum Kinetics in Transport and Optics of Semiconductors* (Springer, Berlin Heidelberg, 1996).

[4.6] F. Jahnke, *Many-Body Theory* (Lecture notes, University of Bremen, 2003).

[4.7] P. Lipavský, V. Špička, and B. Velický, Phys. Rev. B **34**, 6933 (1986).

[4.8] V. Špička and P. Lipavský, Phys. Rev. Lett. **73**, 3439 (1994).

[4.9] V. Špička and P. Lipavský, Phys. Rev. B **52**, 14615 (1995).

[4.10] P. Gartner, L. Bányai, and H. Haug, Phys. Rev. B **60**, 14234 (1999).

Chapter 5

Theory of Coulomb Scattering

In this chapter the kinetic equations of Chap. 4 are re-written in the basis of the field operators. The resulting equation of motion for the Green's function can then finally be compared to the equation of motion for the density matrix $\langle c_i^\dagger c_j \rangle$ already introduced in Chap. 3. At the Hartree-Fock level both methods give the same result. The correlations beyond Hartree-Fock are in the Green's function formalism described by the so-called scattering terms. The aim of this chapter is to evaluate these scattering terms for the carrier Coulomb interaction.

Even though the Dyson equation is formally exact for the one-particle Green's function, one still has to provide a solution scheme at some point. Correspondingly one has to provide an approximation for the self-energy. In the work presented here we use the *Second Order Born Approximation*, and consider all Coulomb scattering processes up to quadratic order in the screened Coulomb potential. Within this approximation for the scattering terms we can finally derive the Boltzmann scattering terms for the carrier-carrier scattering. This result forms the starting point for the discussion of carrier-carrier scattering in self-assembled quantum dots of Chaps. 7 and 9.

5.1 Expansion of Field Operators

In second quantization the field operators are expanded in a single-particle basis

$$\Psi(\boldsymbol{r},t) = \sum_\nu \varphi_\nu(\boldsymbol{r}) c_\nu(t), \qquad \Psi^\dagger(\boldsymbol{r},t) = \sum_\nu \varphi_\nu^*(\boldsymbol{r}) c_\nu^\dagger(t), \tag{5.1}$$

where $\Psi(\boldsymbol{r},t)$ annihilates a particle at space-time point $(\boldsymbol{r},t)$ while c_ν annihilates a particle in state ν. The corresponding creation operators are given by $\Psi^\dagger$ and $c_\nu^\dagger$. The expansion coefficients $\varphi_\nu(\boldsymbol{r})$ form a complete set and are

the eigenstates of some single-particle Hamiltonian h_0 appropriate for the problem at hand

$$h_0(\boldsymbol{r})\phi_\nu(\boldsymbol{r}) \;=\; \varepsilon_\nu\varphi_\nu(\boldsymbol{r}). \tag{5.2}$$

It then follows straightforwardly that the Green's function can be expressed as

$$G(\underline{1},\underline{2}) \;= G(\boldsymbol{r}_1\underline{t}_1,\boldsymbol{r}_2\underline{t}_2) = \sum_{\nu_1\nu_2}\varphi_{\nu_1}(\boldsymbol{r}_1)G_{\nu_1\,\nu_2}(\underline{t}_1\underline{t}_2)\varphi^*_{\nu_2}(\boldsymbol{r}_2), \tag{5.3}$$

and for the self-energy $\Sigma(\underline{1},\underline{2})$ we apply an analogous expansion. Each matrix-element is given by the projection onto the two states ν_1 and ν_2 as follows, e.g., for the self-energy

$$\Sigma_{\nu_1\,\nu_2}(\underline{t}_1,\underline{t}_2) \;=\; \iint \mathrm{d}\boldsymbol{r}_1\,\mathrm{d}\boldsymbol{r}_2\;\varphi^*_{\nu_1}(\boldsymbol{r}_1)\,\Sigma(\underline{1},\underline{2})\,\varphi_{\nu_2}(\boldsymbol{r}_2). \tag{5.4}$$

For a bulk semiconductor the combined index would be $\nu = \{\lambda, s, \boldsymbol{k}\}$ with λ the band index, s the spin, and $\boldsymbol{k}$ the 3D momentum. The eigenfunctions would be those of an electron moving in a periodic lattice and given by the Bloch wavefunctions. For a quantum-dot wetting-layer system, the combined index reads $\nu = \{\lambda, s, \sigma, l\}$. As before λ is the band index, s is the spin, while σ is the z-confinement sub-band quantum number, and l is the in-plane quantum number, either a two-dimensional momentum or a discrete index specifying a localized state. (See Chap. 7 for further details.) To keep the presentation short we use in following the combined index ν.

5.2 Equation of Motion

Having introduced the expansion for the Green's function and the self-energy the kinetic equations of Chap. 4 can now be expressed in this basis. In general we find terms of the structure

$$C(1,2) = \int \mathrm{d}3\; A(1,3)B(3,2),$$

which transform to

$$C_{\nu_1\nu_2}(t_1,t_2) = \sum_{\nu_3}\int \mathrm{d}t_3\; A_{\nu_1\,\nu_3}(t_1,t_3)B_{\nu_3\,\nu_2}(t_3,t_2),$$

when projected onto eigenstates ν_1 and ν_2.

For the lesser Green's function we then obtain

$$\begin{aligned} &i\hbar\left[\frac{\partial}{\partial t_1} \mp \frac{\partial}{\partial t_2}\right] G^<_{\nu_1\,\nu_2}(t_1,t_2) \\ &- \sum_{\nu_3}\Big(\hat{h}_{\nu_1\,\nu_3}(t_1)G^<_{\nu_3\,\nu_2}(t_1,t_2) \pm G^<_{\nu_1\,\nu_3}(t_1,t_2)\hat{h}_{\nu_3\,\nu_2}(t_2)\Big) \\ &= S^\mp_{\nu_1\,\nu_2}(t_1,t_2), \end{aligned} \tag{5.5}$$

where

$$S^{\mp}_{\nu_1\,\nu_2}(t_1,t_2) = \sum_{\nu_3}\int \mathrm{d}t_3 \Big\{ \Sigma^{r}_{\nu_1\,\nu_3}(t_1,t_3)G^{<}_{\nu_3\,\nu_2}(t_3,t_2) + \Sigma^{<}_{\nu_1\,\nu_3}(t_1,t_3)G^{a}_{\nu_3\,\nu_2}(t_3,t_2) \pm \left[G^{r}_{\nu_1\,\nu_3}(t_1,t_3)\Sigma^{<}_{\nu_3\,\nu_2}(t_3,t_2) + G^{<}_{\nu_1\,\nu_3}(t_1,t_3)\Sigma^{a}_{\nu_3\,\nu_2}(t_3,t_2)\right]\Big\}. \tag{5.6}$$

Notice that the time integrals drop out for the single-particle operators on the left hand side of Eq. (5.5), since the corresponding inverse Green's function $G_0^{-1}(\underline{1},\underline{2})$ contains the delta-function in time. Furthermore we have added the effective potential to the single-particle Hamiltonian, i.e., $\hat{h} = h^{(1)} + \phi_{\mathrm{eff}}$.

For completeness let us mention that given the procedure above, a similar equation can be obtained for the retarded Green's function G^r.

The (Generalized) Semiconductor Bloch Equations

The carrier occupation probability and the transition amplitude are given by

$$i\hbar G^{<}_{\nu_1\,\nu_1}(tt) = f_{\nu_1}(t) \qquad \text{carrier occupation probability ,} \tag{5.7}$$

$$i\hbar G^{<}_{\nu_1\,\nu_2}(tt) = \Psi_{\nu_1\nu_2}(t) \qquad \text{transition amplitude } \nu_1 \neq \nu_2. \tag{5.8}$$

Notice that $\Psi_{\nu_1\nu_2}$ corresponds to the transition amplitude between any two different states, while $P^{\mathrm{cv}}_{\nu} = i\hbar G^{<}_{\nu_c\,\nu_v}$ would be the more familiar form of the diagonal interband conduction-band valence-band polarization. Sometimes $\Psi_{\nu_1\,\nu_2}(tt)$ is also referred to as the coherence between state ν_1 and ν_2 [5.1, 5.2].

To extract information such as the carrier occupation probability or the transition amplitude from the Green's function $G^{<}_{\nu_1\nu_2}(t_1,t_2)$ one should propagate the Green's function along the time diagonal $t_1 = t_2 = t$. Then as shown in Chap. 4 it is useful to introduce a change of the time arguments. We use the first convention setting $t = t_1$ and $t_r = t_1 - t_2$, which conversely implies $t_2 = t - t_r$. Furthermore we set $G(t_1,t_2) = \tilde{G}(t, t-t_r)$, and in order to stay on the time diagonal we should set the relative time equal to zero $\tilde{G}(t,t-t_r)|_{t_r=0}$. In the following we drop the tilde to keep the notation simple. Then by taking the sum of the two time derivatives with respect to t_1 and t_2 Eq. (5.5) reads

$$i\hbar\frac{\partial}{\partial t}G^{<}_{\nu_1\,\nu_2}(tt) - \sum_{\nu_3}\left[\hat{h}_{\nu_1\,\nu_3}(t)G^{<}_{\nu_3\,\nu_2}(tt) - G^{<}_{\nu_1\,\nu_3}(tt)\hat{h}_{\nu_3\,\nu_2}(t)\right] = S^{+}_{\nu_1\,\nu_2}(tt). \tag{5.9}$$

The above equation has the matrix structure

$$i\hbar\frac{\partial}{\partial t}G^{<} \; - \; \left[\hat{h}, G^{<}\right]_{-} \;\; = \;\; S^{+}. \tag{5.10}$$

The Hartree potential of the effective potential ϕ_{eff} can be combined with the Fock potential from the instantaneous part of the retarded and advanced self energy Σ^{δ}, (see Eqs. (4.11a) and (4.11b)). Considering furthermore the splitting of the single particle Hamiltonian into its free part and the dipole interaction the effective one-particle Hamiltonian reads

$$h_{\text{eff}} \;\; = \;\; \hat{h} + \Sigma^{\delta} \;\; = \;\; h_0 + h_{\text{d}} + \Sigma^{\text{HF}}, \tag{5.11}$$

where $\Sigma^{\text{HF}} = \Sigma^{\text{H}} + \Sigma^{\text{F}}$. The commutator $[h_{\text{eff}}, G^{<}]_{-}$ is ultimately what gives rise to the Hartree-Fock renormalized one-particle energy and generalized Rabi-frequency. The right hand side of Eq. (5.10) is often referred to as the scattering- or correlation-terms.

Hence by multiplying Eq. (5.9) with $i\hbar$ we find for the transition amplitude and carrier occupation probability the well known generalized *semiconductor Bloch equations* [1]

$$\begin{aligned} i\hbar\frac{\partial}{\partial t}\Psi_{\nu_1\,\nu_2}(t) \;\; &- \;\; \left[\widetilde{\varepsilon}_{\nu_1}(t) - \widetilde{\varepsilon}_{\nu_2}(t)\right]\Psi_{\nu_1\,\nu_2}(t) - \left[f_{\nu_2}(t) - f_{\nu_1}(t)\right]\Omega_{\nu_1\,\nu_2}(t) \\ &- \;\; \sum_{\nu_3 \neq \nu_1,\nu_2} \left[\Omega_{\nu_1\,\nu_3}(t)\Psi_{\nu_3\,\nu_2}(t) - \Psi_{\nu_1\,\nu_3}(t)\Omega_{\nu_3\,\nu_2}(t)\right] \\ &= \;\; i\hbar S_{\nu_1\,\nu_2}(tt), \end{aligned} \tag{5.12}$$

$$\begin{aligned} i\hbar\frac{\partial}{\partial t}f_{\nu_1}(t) \;\; &- \;\; \sum_{\nu_3 \neq \nu_1} \left[\Omega_{\nu_1\,\nu_3}(t)\Psi_{\nu_3\,\nu_1}(t) - \Psi_{\nu_1\,\nu_3}(t)\Omega_{\nu_3\,\nu_1}(t)\right] \\ &= \;\; i\hbar S_{\nu_1\,\nu_1}(tt), \end{aligned} \tag{5.13}$$

where

$$\widetilde{\varepsilon}_{\nu}(t) = \varepsilon_{\nu} + \Sigma^{\text{HF}}_{\nu\,\nu}(t) + h^{\text{d}}_{\nu\,\nu}(t), \quad \Omega_{\nu_1\,\nu_2}(t) = h^{\text{d}}_{\nu_1\,\nu_2}(t) + \Sigma^{\text{HF}}_{\nu_1\,\nu_2}(t), \tag{5.14}$$

are the renormalized one-particle energy and the generalized Rabi frequency,

[1] By the semiconductor Block equations one typically uses only the direct interband transitions amplitude, e.g. $\Psi_{\nu_1\,\nu_2}(t) = \Psi_{\nu_1\,\nu_2}(t)\cdot\delta(\nu_1'\nu_2')\cdot[1-\delta(\lambda_1'\lambda_2')]$, where ν' represents all quantum numbers other than the band index λ'.

respectively. The Hartree-Fock elements[2] are given by

$$\Sigma^{\mathrm{HF}}_{\nu_1\,\nu_2}(t) = i\hbar e^2 \sum_{\nu_3\nu_4} \left[V_{\nu_1\nu_4\nu_3\nu_2} - V_{\nu_1\nu_4\nu_2\nu_3}\right] G^<_{\nu_3\,\nu_4}(tt), \tag{5.15}$$

where the first part is the Hartree ("direct") term and the second part the Fock ("exchange") term, see Eqs. (3.13) and (4.10).

The scattering terms now have the structure

$$\begin{aligned} &S_{\nu_1\,\nu_2}(tt) = \\ &\sum_{\nu_3} \int_{-\infty}^{t} \mathrm{d}t_3 \Big\{ \quad \Sigma^>_{\nu_1\,\nu_3}(t,t_3) G^<_{\nu_3\,\nu_2}(t_3,t) - \Sigma^<_{\nu_1\,\nu_3}(t,t_3) G^>_{\nu_3\,\nu_2}(t_3,t) \\ &\qquad\qquad - G^>_{\nu_1\,\nu_3}(t,t_3)\Sigma^<_{\nu_3\,\nu_2}(t_3,t) + G^<_{\nu_1\,\nu_3}(t,t_3)\Sigma^>_{\nu_3\,\nu_2}(t_3,t)\Big\}, \end{aligned} \tag{5.16}$$

where we have used the identities

$$\begin{aligned} \Sigma^r_{\nu_1\,\nu_2}(t_1,t_2) &= \Sigma^\delta_{\nu_1\,\nu_2}(t_1,t_2) \\ &\quad +\Theta(t_1-t_2)\left[\Sigma^>_{\nu_1\,\nu_2}(t_1,t_2) + \Sigma^<_{\nu_1\,\nu_2}(t_1,t_2)\right], \quad (5.17) \\ \Sigma^a_{\nu_1\,\nu_2}(t_1,t_2) &= \Sigma^\delta_{\nu_1\,\nu_2}(t_1,t_2) \\ &\quad -\Theta(t_1-t_2)\left[\Sigma^>_{\nu_1\,\nu_2}(t_1,t_2) + \Sigma^<_{\nu_1\,\nu_2}(t_1,t_2)\right], \quad (5.18) \end{aligned}$$

$$\begin{aligned} G^r_{\nu_1\,\nu_2}(t_1,t_2) &= \Theta(t_1-t_2)\left[G^>_{\nu_1\,\nu_2}(t_1,t_2) + G^<_{\nu_1\,\nu_2}(t_1,t_2)\right], \quad (5.19) \\ G^a_{\nu_1\,\nu_2}(t_1,t_2) &= -\Theta(t_2-t_1)\left[G^>_{\nu_1\,\nu_2}(t_1,t_2) + G^<_{\nu_1\,\nu_2}(t_1,t_2)\right], \quad (5.20) \end{aligned}$$

to split off the instantaneous part of the self-energy Σ^δ and to express the remaining terms of the scattering integral in terms of lesser and greater functions.

By neglecting the scattering terms $S_{\nu_1\,\nu_2}(tt)$ the generalized semiconductor Bloch equations equal the equation of motion for the density matrix within the Hartree-Fock approximation. Reversely, the correlations beyond the Hartree-Fock level are given by the scattering terms.

The inclusion of the scattering terms presents however a threefold problem. First, the propagation of the Green's function on the time diagonal is by the time integral coupled to two-time Green's functions off the time diagonal. In principle one would then also need to propagate the off-diagonal

[2]Notice: $\widetilde{\varepsilon}_\nu(t) = \varepsilon_\nu + \Sigma^{\mathrm{HF}}_{\nu\,\nu}(t)$ could look like a complex energy renormalization since Coulomb-matrix elements and polarization are in general complex. If this is true it would indicate a decay of the polarization. But one can show that $\left[\Sigma^{\mathrm{HF}}_{\nu_1\,\nu_2}\right]^* = \Sigma^{\mathrm{HF}}_{\nu_2\,\nu_1}$ and its diagonal elements are real.

Green's functions in time. Second, since one has to integrate over the history of the Green's functions one has to keep track of the past for all Green's functions. In this way one may speak about memory effects. Third, one has to specify a given approximation for the self-energy. We now turn to this last issue. The dicussion of the first two problems follows afterwards.

5.3 Second Order Born Approximation

In the work presented here we use the so-called Second Order Born Approximation (SBA) and consider all Coulomb scattering processes up to quadratic order in the screened Coulomb potential. This is basically a classification of the scattering processes (diagrams) which are used for the self-energy. As we recall from Eq. (3.27) the self-energy is related to the screened Coulomb potential and the vertex function; formally written as $\Sigma = WG\Gamma$. At first we therefore investigate the screened Coulomb potential and turn later to the vertex function. Finally we give the full Coulomb self-energy within the SBA.

The Screened Coulomb Interaction

The Dyson equation for the screened Coulomb potential reads in compact notation

$$W = V + VPW, \tag{5.21}$$

where integrals and sums are implied by the matrix structure of the equation. For the lesser part we obtain by successive use of the Langreth-Wilkins Theorem

$$\begin{aligned} W^< &= V^< + VP^rW^< + VP^<W^a + V^<P^aW^a \\ &= VP^rW^< + VP^<W^a, \end{aligned} \tag{5.22}$$

since $V^< = 0$ by the definition of $V(\underline{1},\underline{2})$, see Eq. (3.8). For the retarded part we find

$$W^r = V + VP^rW^r. \tag{5.23}$$

By multiplying Eq. (5.23) with the inverse potential V^{-1} from the left and using $[W^r]^{-1}W^r = 1$ we obtain $[W^r]^{-1} = V^{-1} - P^r$. In this way one obtains after a small calculation

$$[W^r]^{-1}W^< = P^<W^a, \tag{5.24}$$

and finally by multiplying from the left with W^r

$$W^< = W^rP^<W^a. \tag{5.25}$$

Similarly we have

$$W^{>} = W^r P^{>} W^a. \tag{5.26}$$

Vertex Function

As we recall from Chap. 3 the vertex function reads

$$\Gamma(\underline{1},\underline{2},\underline{3}) = -e\delta(\underline{1}-\underline{2})\,\delta(\underline{1}-\underline{3}) + \iiiint \mathrm{d}\underline{4}\,\mathrm{d}\underline{5}\,\mathrm{d}\underline{6}\,\mathrm{d}\underline{7}\,\frac{\delta\,\Sigma(\underline{1},\underline{2})}{\delta\,G(\underline{4},\underline{5})} G(\underline{4},\underline{6})G(\underline{7},\underline{5})\Gamma(\underline{6},\underline{7},\underline{3}).$$

The first term on the right hand side can be considered as the 0^{th} iteration to the vertex function, while the second term proportional to $\delta\Sigma/\delta G$ describes the *vertex corrections*. The simplest starting point of any theory is to neglect the vertex corrections to Γ, and is known as the Random Phase Approximation (RPA).

Thus within the RPA we find

$$\Gamma^{\mathrm{RPA}}(\underline{1},\underline{2},\underline{3}) = -e\delta(\underline{1}-\underline{2})\,\delta(\underline{1}-\underline{3}), \tag{5.27}$$

$$\Sigma^{\mathrm{RPA}}(\underline{1},\underline{2}) = +i\hbar e^2 b_1 W(\underline{2},\underline{1})G(\underline{1},\underline{2}), \tag{5.28}$$

$$P^{\mathrm{RPA}}(\underline{1},\underline{2}) = -i\hbar e^2 b_1 G(\underline{1},\underline{2})G(\underline{2},\underline{1}). \tag{5.29}$$

The first correction to the vertex function can be computed by the screened ladder approximation [5.3]. Here the functional derivative of the full self-energy in the vertex corrections is approximated by the RPA result

$$\frac{\delta\,\Sigma(\underline{1},\underline{2})}{\delta G(\underline{4},\underline{5})} \simeq \frac{\delta\,\Sigma^{\mathrm{RPA}}(\underline{1},\underline{2})}{\delta G(\underline{4},\underline{5})} = \quad i\hbar e^2 b_1 W(\underline{2},\underline{1})\,\delta(\underline{1},\underline{4})\,\delta(\underline{2},\underline{5}). \tag{5.30}$$

Then the first vertex correction to Γ yields by *one* iteration

$$\Gamma^{\mathrm{Vertex}}_{\mathrm{first}}(\underline{1},\underline{2},\underline{3}) = -ei\hbar e^2 b_1 W(\underline{2},\underline{1})\,G(\underline{1},\underline{3})\,G(\underline{3},\underline{2}). \tag{5.31}$$

As will be clear later, the RPA vertex result leads to the direct scattering term within SBA, while the first vertex correction in Σ leads to the exchange scattering term.

RPA Self-Energy and Polarization Propagator

Unfolding the Keldysh time arguments we find for the RPA self-energy

$$\Sigma^{\gtrless}(1,2) \;=\; \Sigma_{\mp\pm}(1,2) \;=\; \quad i\hbar e^2 b_1 W^{\lessgtr}(2,1)\,G^{\gtrless}(1,2), \tag{5.32}$$

and for the RPA polarization propagator

$$P^{\lessgtr}(1,2) \;=\; P_{\pm\mp}(1,2) \;=\; -i\hbar e^2 b_1 G^{\lessgtr}(1,2)G^{\gtrless}(2,1). \tag{5.33}$$

Putting all results together we obtain[3]

$$\Sigma^{\gtrless}_{\mathrm{RPA}}(1,2) = (i\hbar)^2(e^2)^2 \times \iint \mathrm{d}3\,\mathrm{d}4 \left[W^r(2,3)G^{\lessgtr}(3,4)G^{\gtrless}(4,3)W^a(4,1)\right] G^{\gtrless}(1,2). \tag{5.34}$$

Thus within the RPA we find that the greater/lesser self-energy is quadratic in the screened Coulomb potential. The retarded screened Coulomb potential is obtained from solving Eq. (5.23), which we shall return to in detail in Sec. 7.C.

Coulomb Vertex Contributions to the Self-Energy

For the first vertex correction we find the self-energy

$$\Sigma(\underline{1},\underline{2}) = (i\hbar)^2(e^2)^2 b_1 \times \iint \mathrm{d}\underline{3}\,\mathrm{d}\underline{4}\; b_4\, W(\underline{3},\underline{1})G(\underline{1},\underline{4})W(\underline{2},\underline{4})G(\underline{4},\underline{3})G(\underline{3},\underline{2}). \tag{5.35}$$

By using the same procedure as in Chap. 4 we can unfold the Keldysh indices on the contour. In this way e.g. $\Sigma_{+-}(1,2)$ will have the structure of the equation above, only the right hand side will be repeated four times corresponding to the different combinations of the Keldysh indices b_3 and b_4. Using the identities

$$W^r = W_{++} - W_{-+} \quad = W_{--} - W_{+-}\,, \tag{5.36}$$

$$W^a = W_{++} + W_{+-} \quad = W_{--} + W_{-+}\,, \tag{5.37}$$

and noting that $W^{\lessgtr}$ goes at least with the screened Coulomb interaction to second order, see Eq. (5.25), only one single combination of the Keldysh indices remains to second order in the screened Coulomb potential (while all other combinations are of higher order). Finally to second order in the screened Coulomb potential we obtain for the greater/lesser self-energy

$$\Sigma^{\gtrless}_{\mathrm{Vertex}}(1,2) = -(i\hbar)^2(e^2)^2 \times \iint \mathrm{d}3\,\mathrm{d}4\; W^a(3,1)G^{\gtrless}(1,4)W^r(2,4)G^{\lessgtr}(4,3)G^{\gtrless}(3,2). \tag{5.38}$$

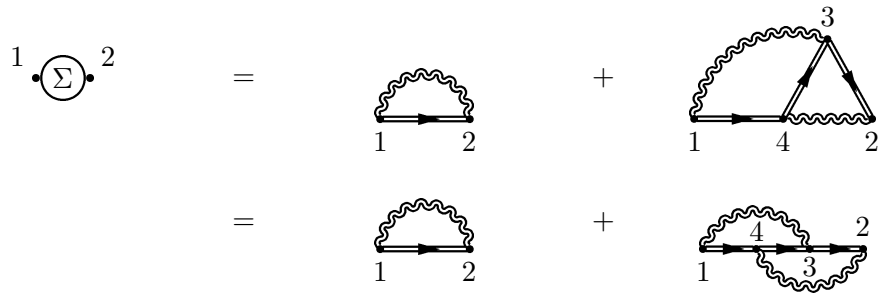

Figure 5.1: The self-energy within the second order Born approximation.

SBA Self-Energy

Within the Second Order Born Approximation the self-energy with both the direct and the exchange terms, diagramaticly depicted in Fig. 5.1, reads when projected onto the states ν_1 and ν_2

$$\begin{aligned}\Sigma^{\gtrless}_{\nu_1\,\nu_2}(t_1t_2) &= (i\hbar)^2(e^2)^2\sum_{\alpha\beta}\sum_{\gamma\delta}\sum_{\epsilon\mu}\iint \mathrm{d}t_3\,\mathrm{d}t_4 \\ &\times\big\{W^r_{\mu\delta\alpha\nu_2}(t_2,t_3)W^a_{\beta\nu_1\epsilon\gamma}(t_4,t_1)G^{\lessgtr}_{\alpha\,\beta}(t_3t_4)G^{\gtrless}_{\gamma\,\delta}(t_4t_3)G^{\gtrless}_{\epsilon\,\mu}(t_1t_2) \\ &- \;W^r_{\mu\beta\gamma\nu_2}(t_2,t_4)W^a_{\delta\nu_1\alpha\epsilon}(t_3,t_1)G^{\gtrless}_{\alpha\,\beta}(t_1t_4)G^{\lessgtr}_{\gamma\,\delta}(t_4t_3)G^{\gtrless}_{\epsilon\,\mu}(t_3t_2)\big\},\end{aligned} \tag{5.39}$$

with the screened Coulomb matrix elements

$$W_{\alpha\beta\gamma\delta}(t',t'') = \iint \mathrm{d}\boldsymbol{r}'\,\mathrm{d}\boldsymbol{r}''\phi^*_\alpha(\boldsymbol{r}')\phi^*_\beta(\boldsymbol{r}'')W(\boldsymbol{r}'t',\boldsymbol{r}''t'')\phi_\gamma(\boldsymbol{r}'')\phi_\delta(\boldsymbol{r}'). \tag{5.40}$$

For the screened Coulomb potential we assume $W(\boldsymbol{r}'t,\boldsymbol{r}''t) = W(\boldsymbol{r}''t,\boldsymbol{r}'t)$, which results in the same symmetry relations as for the bare Coulomb matrix elements and thus $W_{1234}(t,t) = W_{2134}(t,t) = W^*_{4321}(t,t)$.

For practical purposes the equation for the SBA self-energy is however not very useful. First, the twofold time integral is numerical very challenging in terms of central processing unit (CPU) time and in terms of random access memory (ram) needed to perform these integrals (since each element of the RHS of Eq. (5.39) must be saved for any combination its two times). Second, keeping track of all elements of the Green's function $G^{\gtrless}_{\nu_1\,\nu_2}(t_1t_2)$ is unnecessary in most cases. For example, in order to describe changes of an incoherent carrier distribution due to carrier-carrier scattering it may be sufficient to keep only the diagonal elements of the Green's function, since e.g. by Eq. (5.7) the lesser Grenn's function describes the single particle carrier occupation probabilities. Or, in cases where the carrier distribution

[3]The product of the Keldysh band indices equals minus one ($b_\mp \cdot b_\pm = -1$).

is generated by a coherent optical excitation tuned around the band gap energy, the changes of the carrier distribution is now also coupled to the interband transition amplitudes $P^{\rm cv}_{\nu}$ between valence band and conduction band, whereas intra-band transition amplitudes $P^{\rm bb}_{\nu\nu'}$ (b=c,v and $\nu \neq \nu'$) may still be neglected. For these reasons we apply some further approximations.

5.4 Simplifying Approximations and Intraband Scattering

The kinetic equation for the time changes of the carrier occupation probabilities has the structure

$$i\hbar\frac{\partial}{\partial t}f_{\nu_1}(t) \;=\; i\hbar\frac{\partial}{\partial t}f_{\nu_1}(t)\Big|_{\rm HF} \;+\; i\hbar S_{\nu_1\,\nu_1}(tt), \tag{5.41}$$

where the first term on the right hand side corresponds to changes due to the effective Hartree-Fock one-particle Hamiltonian and the second term is the scattering term.

In this section we investigate the scattering term $i\hbar S_{\nu_1\,\nu_1}(tt)$. The general form of the scattering term is given in Eq. (5.13), and contains carrier as well as polarization scattering. In the following we consider only changes in the carrier distribution due to carrier-carrier scattering, i.e., only intraband scattering processes are considered. As discussed above this is sufficient in the incoherent limit. With the proper approximations for the scattering term we then re-cover the Boltzmann scattering integral for the carrier Coulomb interaction, which constitutes the backbone of Chap. 7.

(Instantaneous) Carrier-Carrier Scattering

The contributions to the scattering term $i\hbar S_{\nu_1\,\nu_1}(tt)$ contaning only the single particle carrier-carrier scattering processes are obtained from Eq. (5.13) by keeping only the diagonal elements of the propagators $G^{\gtrless}_{\nu_1\,\nu_2} = G^{\gtrless}_{\nu_1\,\nu_1}\delta_{\nu_1\nu_2}$. By applying the GKBA the two-time propagators diagonal in the quantum index ν are then related to the carrier occupation probabilities f_{ν}. In this way we obtain for the scattering term

$$\begin{aligned} &S_{\nu_1\,\nu_1}(tt) = \\ &\int_{-\infty}^{t}{\rm d}t_3\,\Big\{\quad \Sigma^{>}_{\nu_1\,\nu_1}(t,t_3)G^{<}_{\nu_1\,\nu_1}(t_3,t) - \Sigma^{<}_{\nu_1\,\nu_1}(t,t_3)G^{>}_{\nu_1\,\nu_1}(t_3,t) \\ &\qquad\qquad - G^{>}_{\nu_1\,\nu_1}(t,t_3)\Sigma^{<}_{\nu_1\,\nu_1}(t_3,t) + G^{<}_{\nu_1\,\nu_1}(t,t_3)\Sigma^{>}_{\nu_1\,\nu_1}(t_3,t)\Big\}, \end{aligned} \tag{5.42}$$

where

$$\Sigma^{\gtrless}_{\nu_1\,\nu_1}(t_1,t_2) = (i\hbar)^2(e^2)^2\sum_{\alpha\gamma\epsilon}$$
$$\times\left\{W^r_{\epsilon\gamma\alpha\nu_1}(t_2,t_2)\,W^a_{\alpha\nu_1\epsilon\gamma}(t_1,t_1)\,G^{\lessgtr}_{\alpha\,\alpha}(t_2,t_1)\,G^{\gtrless}_{\gamma\,\gamma}(t_1,t_2)\,G^{\gtrless}_{\epsilon\,\epsilon}(t_1,t_2)\right.$$
$$\left.-\;\;W^r_{\epsilon\alpha\gamma\nu_1}(t_2,t_2)\,W^a_{\gamma\nu_1\alpha\epsilon}(t_1,t_1)\,G^{\gtrless}_{\alpha\,\alpha}(t_1,t_2)\,G^{\lessgtr}_{\gamma\,\gamma}(t_2,t_1)\,G^{\gtrless}_{\epsilon\,\epsilon}(t_1,t_2)\right\}. \quad (5.43)$$

In the above equation for the self-energy we have furthermore applied the approximation of an instantaneous screened Coulomb potential

$$W^{r,a}_{1234}(t',t'') \;\;=\;\; W_{1234}(t')\;\delta(t'-t''). \quad (5.44)$$

This simplifies the equations, and corresponds to neglecting dynamical screening effects and the build up of screening. See Haug and Jauho [5.4] and Schäfer and Wegener [5.5] for details about build up of screening.

By using the symmetry relations for the Green's functions, see Eq. (4.8) and those for the screened Coulomb matrix elements one can show for the above given self-energy

$$\begin{aligned}\Sigma^{>}_{\nu_1\,\nu_1}(t,t_3)G^{<}_{\nu_1\,\nu_1}(t_3,t) &= \left[G^{<}_{\nu_1\,\nu_1}(t,t_3)\Sigma^{>}_{\nu_1\,\nu_1}(t_3,t)\right]^*\\ \Sigma^{<}_{\nu_1\,\nu_1}(t,t_3)G^{>}_{\nu_1\,\nu_1}(t_3,t) &= \left[G^{>}_{\nu_1\,\nu_1}(t,t_3)\Sigma^{<}_{\nu_1\,\nu_1}(t_3,t)\right]^*,\end{aligned}$$

and thus we obtain

$$S_{\nu_1\,\nu_1}(tt) =$$
$$2\mathrm{Re}\int_{-\infty}^{t}\mathrm{d}t_3\;\Sigma^{>}_{\nu_1\,\nu_1}(t,t_3)G^{<}_{\nu_1\,\nu_1}(t_3,t) - \Sigma^{<}_{\nu_1\,\nu_1}(t,t_3)G^{>}_{\nu_1\,\nu_1}(t_3,t). \quad (5.45)$$

Generalized Kadanoff-Baym Ansatz

At this point the scattering terms are still functions of two time arguments. To map the propagators back onto the time-diagonal we now employ the generalized Kadanoff-Baym ansatz (GKBA). With this approximation the complexity of the equations can be reduced, and we need only to worry about the single time propagators. For $t > t_3$ we find by the matrix form of

the GKBA from Chap. 4

$$\boxed{t > t_3:} \qquad \begin{aligned} G^{\gtrless}_{\nu\,\nu}(t,t_3) &= i\hbar G^{r}_{\nu\,\nu}(t,t_3) G^{\gtrless}_{\nu\,\nu}(t_3,t_3) \\ &= G^{r}_{\nu\,\nu}(t,t_3) \begin{cases} 1-f_\nu(t_3) \\ f_\nu(t_3) \end{cases} \end{aligned} \tag{5.46}$$

$$\boxed{t > t_3:} \qquad \begin{aligned} G^{\gtrless}_{\nu\,\nu}(t_3,t) &= -i\hbar G^{\gtrless}_{\nu\,\nu}(t_3,t_3) G^{a}_{\nu\,\nu}(t_3,t) \\ &= -G^{a}_{\nu\,\nu}(t_3,t) \begin{cases} 1-f_\nu(t_3) \\ f_\nu(t_3)\,, \end{cases} \end{aligned} \tag{5.47}$$

where we have kept only the diagonal elements, in order to stay diagonal in the quantum index ν for the propagators $G^{\gtrless}_{\nu\nu}$ as discussed above. This allows us to write the scattering terms as

$$\begin{aligned} \Sigma^{>}_{\nu_1\,\nu_1}(t,t_3) G^{<}_{\nu_1\,\nu_1}(t_3,t) = -\hbar^2 (e^2)^2 \sum_{\alpha\gamma\epsilon} \\ \times W^{a}_{\nu_1\alpha\gamma\epsilon}(t) \big[W^{r*}_{\nu_1\alpha\gamma\epsilon}(t_3) - W^{r*}_{\nu_1\alpha\epsilon\gamma}(t_3) \big] \\ \times G^{a}_{\alpha\,\alpha}(t_3,t)\, f_\alpha(t_3)\;\; G^{r}_{\gamma\,\gamma}(t,t_3) \big[1-f_\gamma(t_3)\big] \\ \times G^{r}_{\epsilon\,\epsilon}(t,t_3) \big[1-f_\epsilon(t_3)\big]\;\; G^{a}_{\nu_1\,\nu_1}(t_3,t)\, f_{\nu_1}(t_3), \end{aligned} \tag{5.48}$$

while the result for $\Sigma^{<}G^{>}$ can be obtained by the same trivial substitutions and one obtains the same structure as above, only replace $f \to (1-f)$.

Free Spectral Functions

The remaining challenge for the scattering terms is to determine the spectral properties. Proceeding along the lines of the derivation leading to the Boltzmann equation we therefore impose the simplest approximation for $G^{r,a}$, and use the free spectral functions. Then the retarded and advanced Green's functions are given by

$$G^{r}_{\nu_1\,\nu_2}(t_1,t_2) = -\frac{i}{\hbar}\Theta(t_1-t_2) e^{-\frac{i}{\hbar}(\varepsilon_{\nu_1} t_1 - \varepsilon_{\nu_2} t_2)} \delta_{\nu_1\nu_2}, \tag{5.49}$$

$$G^{a}_{\nu_2\,\nu_1}(t_2,t_1) = \frac{i}{\hbar}\Theta(t_1-t_2) e^{\frac{i}{\hbar}(\varepsilon_{\nu_1} t_1 - \varepsilon_{\nu_2} t_2)} \delta_{\nu_1\nu_2}. \tag{5.50}$$

The underlying assumption is that the time evolution of the creation and annihilation operators is determined by the free Hamiltonian h_0, i.e. we have $c_\nu(t) = \exp(-i\varepsilon_\nu t/\hbar) c_\nu$ and $c^\dagger_\nu(t) = \exp(+i\varepsilon_\nu t/\hbar) c^\dagger_\nu$. Then by the linear dependencies, e.g., $i\hbar G^r = \Theta(t_1-t_2)[G_{-+} + G_{+-}]$, the above relation can

be proven. The results may also be verified directly as a solution of the 1st and 2nd Kadanoff-Baym equations with the additional constrains of setting the self-energy, the dipole interaction and the effective potentials equal to zero.

In this way we obtain

$$\begin{aligned} S_{\nu_1\,\nu_1}(tt) = -(\hbar e^2)^2 2\mathrm{Re}\int_{-\infty}^{t} \mathrm{d}t_3 \sum_{\alpha\gamma\epsilon} W_{\nu_1\alpha\gamma\epsilon}(t)\left[W^*_{\nu_1\alpha\gamma\epsilon}(t_3) - W^*_{\nu_1\alpha\epsilon\gamma}(t_3)\right] \\ \times \frac{1}{\hbar^4}\exp\left\{\frac{i}{\hbar}(\varepsilon_\alpha - \varepsilon_\gamma - \varepsilon_\epsilon + \varepsilon_{\nu_1})[t-t_3]\right\} \\ \times \left\{f_\alpha(t_3)\left[1-f_\epsilon(t_3)\right]\left[1-f_\gamma(t_3)\right]f_{\nu_1}(t_3) - (f\to 1-f)\right\}. \quad (5.51) \end{aligned}$$

Notice that the scattering terms are now only dependent on the single time propagator, e.g. $i\hbar G^<(t,t) = f_\nu(t)$ by (5.7), and all references to two time arguments have disappeared.

Using the free spectral functions, or any other model for the spectral function, implies a simplification of the kinetic equations. The original coupled set of equations for spectral functions and propagators has been decoupled, and a solution for the retarded and advanced Green's functions has been assumed.

What the energies are concerned, one is back to the level of perturbation theory. Improvements of this picture have been discussed e.g. by Manzke et al. [5.6] in the context of polarization scattering. As long as the single-particle energies are only slightly shifted and broadened, a simple quasiparticle approximation or even the use of the free carrier spectral functions might be possible. Examples for strong (quasiparticle) renormalization are given in Chap. 8.

Markov Approximation

The final step towards the Boltzmann scattering integral for carrier Coulomb interaction is to impose the so-called Markov approximation. Loosely stated, it neglects memory and retardation effects for the propagators $G^{\lessgtr}(tt)$ and the screened Coulomb potentials $W^{r,a}(t)$. In the scattering terms they may therefore be evaluated at the upper limit of the time integral. The time integral is thus restriced to concern only the spectral functions, in this case the exponential functions, and we end up with a term like

$$\lim_{\gamma\to 0}\mathrm{Re}\int_{-\infty}^{t_1}\mathrm{d}t_2 e^{\frac{i\varepsilon-\gamma}{\hbar}(t_1-t_2)} \;=\; \pi\hbar\delta(\varepsilon), \quad (5.52)$$

where we have included a damping factor γ to insure sound results at the remote past. The result shows the delta-function for energy conservation.

Thus, for the scattering rates the end result is

$$\begin{aligned} S_{\nu_1}(t_1) = -\frac{2\pi}{\hbar}(e^2)^2 \sum_{\nu_2\nu_3\nu_4} & \delta(\varepsilon_{\nu_1} - \varepsilon_{\nu_2} + \varepsilon_{\nu_3} - \varepsilon_{\nu_4}) \\ & \times W_{\nu_1\nu_3\nu_4\nu_2}(t_1) \left[W^*_{\nu_1\nu_3\nu_4\nu_2}(t_1) - W^*_{\nu_1\nu_3\nu_2\nu_4}(t_1)\right] \\ & \times \left\{f_{\nu_1}(t_1)\left[1 - f_{\nu_2}(t_1)\right] f_{\nu_3}(t_1)\left[1 - f_{\nu_4}(t_1)\right] - (f \to 1-f)\right\}. \end{aligned} \quad (5.53)$$

The delta-function in the first line expresses energy conservation, the second line describes the direct and exchange Coulomb scattering, while the third line describes the out- and in-scattering channels. This Boltzmann scattering integral for the carrier Coulomb interaction provides the very basic foundation for the discussion of carrier-carrier scattering in self-assembled quantum-dots presented in Chap. 7.

Electron-Hole Picture

As often done in semiconductor physics it is more advantageous for computational reasons and for the sake of discussion to switch to the electron-hole picture. In Chap. 7 where we study the carrier-carrier scattering we will take the same approch. Thus, transforming to the electron-hole picture Eq. (5.53) retains its structure. To see this remember the following from going from the cv-picture to the eh-picture. The occupation probability and energy for an electron in the conduction band remains unchanged, when going from conduction band to electron picture. The occupation probability of finding an electron in the valence band in state v equals the probability of not finding a hole in the same state. In addition, the hole energy changes sign. Thus,

$$\begin{aligned} f_{\mathrm{c}} &= f_{\mathrm{e}}, & \varepsilon_{\mathrm{c}} &= \quad \varepsilon_{\mathrm{e}}, \\ f_{\mathrm{v}} &= 1 - f_{\mathrm{h}}, & \varepsilon_{\mathrm{v}} &= -\varepsilon_{\mathrm{h}}. \end{aligned}$$

The field operators for electrons in the conduction band are still given by Eq. (5.1) while the field operators for the holes in the valence band are related to electron valence field operator through

$$\Psi_{\mathrm{v}}(\boldsymbol{r},t) = \sum_{\alpha} \varphi^{\mathrm{v}}_{\alpha}(\boldsymbol{r})\mathrm{v}_{\alpha}(t) \quad = \quad \sum_{\alpha} \varphi^{\mathrm{h}*}_{\alpha}(\boldsymbol{r})\mathrm{h}^{\dagger}_{\alpha}(t) = \Psi^{\dagger}_{\mathrm{h}}(\boldsymbol{r},t),$$

where v_α annihilates an electron in the valence band in state α, which is equivalent to creating a hole in the valence band in state α, done by $\mathrm{h}^\dagger_\alpha$. A similar expression is valid for $\Psi^\dagger_{\mathrm{v}}(\boldsymbol{r},t)$. Compared to Eq. (5.1) the expansion coefficients for the hole field operates are now complex conjugated. For the coulomb matrix elements we thus find e.g. the identity $W^{\mathrm{cvvc}}_{1234} = W^{\mathrm{ehhe}}_{1324}$. Thus, using these rules it is easy to show the Eq. (5.53) has the same form in the electron-hole picture.

References

[5.1] C. Cohen-Tannoudji, J. Dupont-Roc, and G. Grynberg, *Atom-Photon Interaction* (Wiley, New York, 1998).

[5.2] R. Binder and S. W. Koch, Prog. Quant. Electr. **19**, 307 (1995).

[5.3] F. Jahnke, Many-Body Theory, 2003, lecture notes.

[5.4] H. Haug and A.-P. Jauho, *Quantum Kinetics in Transport and Optics of Semiconductors* (Springer, Berlin Heidelberg, 1996).

[5.5] W. Schäfer and M. Wegner, in *Semiconductor Optics and Transport Phenomena* (Springer, Berlin Heidelberg, 2002), Chap. 10.

[5.6] G. Manzke and K. Henneberger, phys. stat. sol. (b) **234**, 233 (2002).

Chapter 6

Theory of Carrier-Phonon Interaction

In the previous chapters we described the motion of carriers in a rigid periodic ionic-lattice that makes up the semiconductor. However, in general the ions will move around the equilibrium positions of the crystal lattice, and accordingly the carriers will respond to these fluctuations of the ionic charge densities.

The theory developed so far needs therefore to be extended to include the interaction of carriers with lattice vibrations. In this chapter we review the consequences of the carrier response to the fluctuations of the ionic charge densities, formulating the theory along the lines of the previous chapters. It is well-known that this effect is best described by phonons and the carrier-phonon interaction. We find that our previous results can be reused, provided we add the so-called phonon-induced interaction to the screened Coulomb potential.

The phonon-subsystem is modeled as a bath or reservoir in thermal equilibrium. In this approach we therefore neglect influence of the carriers on the phonon subsystem. It is a model of describing the dissipation of energy between the carrier subsystem and the vibrational subsystem. This corresponds to the assumption that the crystal is kept at a constant temperature.

In Secs. 6.1 and 6.2 we briefly summerize some of the fundamental properties of the carrier-phonon interaction. For a thorough introduction to the carrier-phonon interaction the reader should consult Refs. [6.1–6.6]. Equations of motion for the carrier interaction with longitudinal-optical phonons are the following derived in Secs. 6.3 -6.5. The results obtained in this chapter form the basis for the studies of the carrier-phonon interaction in the quantum-dot wetting-layer system presented in Chap. 8.

6.1 Hamiltonian

The general Hamiltonian describing the Coulomb interaction between electrons and ions that make up the semiconductor has the following form

$$H = H_{\rm el} + H_{\rm n} + H_{\rm ext}, \tag{6.1}$$

with the electronic part given by

$$\begin{aligned} H_{\rm el} &= \int {\rm d}\boldsymbol{r}\ \Psi(\boldsymbol{r}t)^\dagger\ h(\boldsymbol{r}t)\ \Psi(\boldsymbol{r}t) \\ &+ \iint {\rm d}\boldsymbol{r}\,{\rm d}\boldsymbol{r}'\ \Psi(\boldsymbol{r}t)^\dagger\ \Psi(\boldsymbol{r}'t)^\dagger\ V(\boldsymbol{r}-\boldsymbol{r}')\ \Psi(\boldsymbol{r}'t)\ \Psi(\boldsymbol{r}t). \end{aligned} \tag{6.2}$$

As in Chap. 3 the single particle electron Hamiltonian reads

$$h(\boldsymbol{r}t) = -\frac{\hbar^2}{2m}\nabla^2 + eU(\boldsymbol{r},\,\{\boldsymbol{R}(\boldsymbol{L},\boldsymbol{\kappa})\}) + \boldsymbol{d}\cdot\boldsymbol{E}(\boldsymbol{r}t), \tag{6.3}$$

where the ionic lattice potential U is now no longer frozen but depends on the actual instantaneous positions of all the ions. In this notation we have $\boldsymbol{R}(\boldsymbol{L},\boldsymbol{\kappa}) = \boldsymbol{L}+\boldsymbol{\kappa}+\boldsymbol{u}(\boldsymbol{L}\boldsymbol{\kappa})$, where $\boldsymbol{L}$ is the equilibrium lattice vector, $\boldsymbol{\kappa}$ the basis vector within the unit cell and $\boldsymbol{u}(\boldsymbol{L}\boldsymbol{\kappa})$ the actual lattice displacement.

The ions are described by the Hamiltonian $H_{\rm n}$

$$\begin{aligned} H_{\rm n} &= \sum_{\boldsymbol{L}\,\boldsymbol{\kappa}\,\alpha} -\frac{\hbar^2}{2M_{\boldsymbol{\kappa}}}\frac{\partial^2}{\partial[u_\alpha(\boldsymbol{L}\boldsymbol{\kappa})]^2} \\ &+ \sum_{\boldsymbol{L}\boldsymbol{\kappa}\ \boldsymbol{L}'\boldsymbol{\kappa}'} \iint {\rm d}\boldsymbol{r}\,{\rm d}\boldsymbol{r}'\ \rho_{\boldsymbol{\kappa}}(\boldsymbol{r}-\boldsymbol{R}(\boldsymbol{L},\boldsymbol{\kappa}))V(\boldsymbol{r}-\boldsymbol{r}')\ \rho_{\boldsymbol{\kappa}'}(\boldsymbol{r}'-\boldsymbol{R}(\boldsymbol{L}',\boldsymbol{\kappa}')). \end{aligned} \tag{6.4}$$

The first part represents the kinetic energy, where α denotes the Cartesian component. The second term corresponds to the Coulomb interaction among the ions themselves. The charge density of the ionic cores $\hat{\rho}_{\rm n}(\boldsymbol{r})$ is given as a sum of local charge densities $\rho_{\boldsymbol{\kappa}}(\boldsymbol{r}-\boldsymbol{R}(\boldsymbol{L},\boldsymbol{\kappa}))$.

Finally, proceeding along the method outlined in Chap. 3 we have included coupling to external sources for the electrons and ions as follows

$$H_{\rm ext}(t) = \int {\rm d}\boldsymbol{r}\,\Big\{\big[\hat{\rho}_{\rm el}(\boldsymbol{r})+\hat{\rho}_{\rm n}(\boldsymbol{r})\big]\phi_{\rm ext}(\boldsymbol{r}t) + \hat{\rho}_{\rm n}(\boldsymbol{r})J(\boldsymbol{r}t)\Big\}, \tag{6.5}$$

where the electronic density is given by $\hat{\rho}_{\rm el}(\boldsymbol{r}) = -e\Psi^\dagger(\boldsymbol{r})\Psi(\boldsymbol{r})$. The two first terms are more or less as expected, while the ionic coupling to the external source $J(\boldsymbol{r}t)$ is a mathematical trick used in connection with the functional derivative technique. For details see [6.1]. As previously, the external sources are set to zero at the end of the derivation.

Fundamental set of equations

By repeating the steps of Chap. 3 leading to the fundamental set of equations depicted in Fig. 3.2, we find that we can formally reuse the results provided that we replace the effective potential $\phi_{\rm eff}$ of Chap. 3 by the sum of the external and the electronic Hartree-potentials as follows

$$\phi_{\rm eff}(\underline{1}) \;\rightarrow\; V_{\rm eff}(\underline{1}), \tag{6.6}$$

$$V_{\rm eff}(\underline{1}) \;=\; \phi_{\rm ext}(\underline{1}) + \int \mathrm{d}\underline{3}\; v(\underline{1}-\underline{3})\;\{\langle\hat{\rho}_{\rm el}(\underline{3})\rangle + \langle\hat{\rho}_{\rm n}(\underline{3})\rangle\}\,. \tag{6.7}$$

This corresponds to the total electrostatic potential seen by the carriers.

The auxiliary functions needed for the Dyson equation, the self-energy, effective screened interaction, vertex-function, and the electronic polarization are then introduced in the same way as in Chap. 3 and the end result is as follows [6.1, 6.2],

$$G(\underline{1},\underline{2}) \;=\; G_0(\underline{1},\underline{2}) + \iint \mathrm{d}\underline{3}\,\mathrm{d}\underline{4}\; G_0(\underline{1},\underline{3})\,\Sigma(\underline{3},\underline{4})G(\underline{4},\underline{2}), \tag{6.8}$$

$$\Sigma(\underline{1},\underline{2}) \;=\; -i\hbar b_1 \iint \mathrm{d}\underline{3}\,\mathrm{d}\underline{4}\; W_{\rm eff}(\underline{3},\underline{1})\,G(\underline{1},\underline{4})\Gamma(\underline{4},\underline{2},\underline{3}), \tag{6.9}$$

$$W_{\rm eff}(\underline{1},\underline{2}) \;=\; \int \mathrm{d}\underline{3}\; v(\underline{2}-\underline{3})\,\frac{\delta V_{\rm eff}(\underline{1})}{\delta\phi_{\rm ext}(\underline{3})}, \tag{6.10}$$

$$\Gamma(\underline{1},\underline{2},\underline{3}) \;=\; \frac{\delta G^{-1}(\underline{1},\underline{2})}{\delta V_{\rm eff}(\underline{3})}, \tag{6.11}$$

$$P(\underline{1},\underline{2}) \;=\; \frac{\delta\langle\hat{\rho}_{\rm el}(\underline{1})\rangle}{\delta V_{\rm eff}(\underline{2})}. \tag{6.12}$$

Proceeding along the lines of Chap. 3 we now have to evaluate the effective screened interaction $W_{\rm eff}$ and the electronic polarization P. For the latter, one often performs the so-called adiabatic approximation where the derivative $\delta\hat{\rho}_{\rm el}/\delta V_{\rm eff}$ is replaced by the purely electronic expression which has already been used in Chap. 3, see Eq. 3.30. That is, the phononic influence on the electronic polarization P is neglected. To proceed further one has to evaluate the effective screened interaction which amounts to evaluate the derivative $\delta V_{\rm eff}/\delta\phi_{\rm ext}$. After a lengthy calculation (Schäfer et al. [6.1, 6.2]) one obtains within the adiabatic approximation that the effective screened interaction may be written as,

$$W_{\rm eff}(\underline{1},\underline{2}) \;=\; W(\underline{1},\underline{2}) + W_{\rm ph}(\underline{1},\underline{2}). \tag{6.13}$$

For the first term on the RHS we recover the screened Coulomb interaction W, while the second term is denoted the phonon induced interaction [6.1, 6.2]. Thus, in this description the carrier-phonon interaction appears as an additional term to the screened Coulomb potential, describing

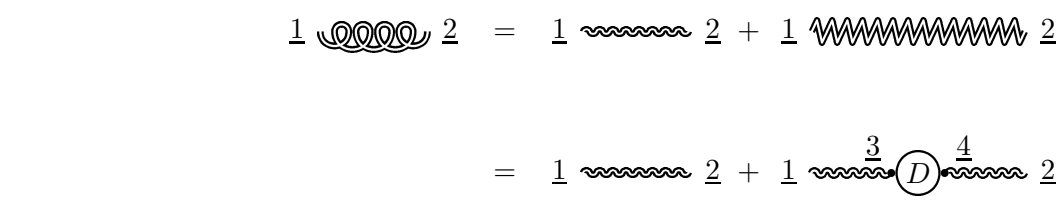

Figure 6.1: Diagrammatic representation of the effective electron-electron interaction. The double curly line corresponds to the total screened interaction $W_{\text{eff}}(\underline{1},\underline{2})$, the double wavy line the screened electronic Coulomb interaction $W(\underline{1},\underline{2})$, the double zigzag line corresponds to the phonon interaction $W_{\text{ph}}(\underline{1},\underline{2})$, and finally D denotes the phonon-propagator.

screening due to the motion of the nuclei [6.6]. The remaining equations keep their structure, i.e. the set of equations retain their form as shown diagrammatically in Fig. 3.2.

The phonon-induced interaction is given by

$$W_{\text{ph}}(\underline{1},\underline{2}) = \iint \mathrm{d}\underline{3}\,\mathrm{d}\underline{4}\; W(\underline{1},\underline{3})D(\underline{3},\underline{4})W(\underline{4},\underline{2}), \tag{6.14}$$

$$D(\underline{1},\underline{2}) = -\frac{i}{\hbar}\langle T_c \Delta\hat{\rho}_{\text{n}}(\underline{1})\Delta\hat{\rho}_{\text{n}}(\underline{2})\rangle = \frac{\delta\langle\hat{\rho}_{\text{n}}(\underline{1})\rangle}{\delta J(\underline{2})}, \tag{6.15}$$

and is diagrammatic depicted in Fig. 6.1. Here $\Delta\hat{\rho} = \hat{\rho} - \langle\hat{\rho}\rangle$ is the deviation operator, and D is the *density-density* correlation function of the ions. For the rigid lattice the ions are fixed at their equilibrium positions and hence $D = 0$. We are then left with the usual Coulomb interaction. If $D \neq 0$ the ions move around their equilibrium position and the electrons respond to these fluctuations. The interaction is best described by phonons.

6.2 Phonon Green's Function

The only new objects that need to be evaluated are the density-density correlation function of the ions and the phonon-induced interaction. In order to proceed one therefore usually performs the so-called harmonic approximation [6.1–6.4].

The ion density is Taylor expanded around the equilibrium position of the ions up to first order in the lattice displacements $u_\alpha(\boldsymbol{L\kappa})$

$$\hat{\rho}_{\text{n}}(\boldsymbol{r},t) = \sum_{\boldsymbol{L\kappa}} \rho_{\boldsymbol{\kappa}}(\boldsymbol{r}-\boldsymbol{L}-\boldsymbol{\kappa}) + \sum_{\boldsymbol{L\kappa}\alpha} \nabla_\alpha \rho_{\boldsymbol{\kappa}}(\boldsymbol{r}-\boldsymbol{L}-\boldsymbol{\kappa}) u_\alpha(\boldsymbol{L\kappa},t).$$

In this way we may write the density-density correlation function of the ions as follows

$$D(\boldsymbol{r}t;\boldsymbol{r}'t') = \sum_{\boldsymbol{L}\boldsymbol{\kappa}\alpha\ \boldsymbol{L}'\boldsymbol{\kappa}'\beta} \nabla_\alpha \rho_{\boldsymbol{\kappa}}(\boldsymbol{r}-\boldsymbol{L}-\boldsymbol{\kappa}) D_{\alpha\beta}(\boldsymbol{L}\boldsymbol{\kappa},\boldsymbol{L}'\boldsymbol{\kappa}';t,t') \nabla_\beta \rho_{\boldsymbol{\kappa}'}(\boldsymbol{r}'-\boldsymbol{L}'-\boldsymbol{\kappa}'),$$

where

$$D_{\alpha\beta}(\boldsymbol{L}\boldsymbol{\kappa},\boldsymbol{L}'\boldsymbol{\kappa}';\underline{t},\underline{t}') \;=\; -\frac{i}{\hbar}\left\langle\, T_C\, u_\alpha(\boldsymbol{L}\boldsymbol{\kappa},\underline{t})\, u_\beta(\boldsymbol{L}'\boldsymbol{\kappa}',\underline{t}')\,\right\rangle,$$

is the phonon Green's function.

From this equation we see, that the density-density correlation function depends on the displacement vectors $\boldsymbol{u}$. The next step is to evaluate and solve the equation of motion for the displacement vectors $\boldsymbol{u}$. Once we have the $\boldsymbol{u}$'s they may be used to determine the phonon Green's function which together with the screened Coulomb potential gives the phonon-induced interaction.

The equation of motion for the displacement vectors $\boldsymbol{u}$ are determined by the usual methods developed in phonon physics. Within the harmonic approximation all contributions in the displacement vector $\boldsymbol{u}$ up to second order are kept in the Hamiltonian Eq. (6.1), and one finds that the equation of motion may be represented as an eigenvalue problem. Using the lattice periodicity the eigenvalue problem may be represented in the reciprocal $\boldsymbol{q}$-space, and the displacement vectors are then expressed in terms of the corresponding $\boldsymbol{q}$-space eigenvectors and eigenvalues. As a second step u_α is expressed in terms of the so-called phonon operators which obey the usual Bose-statistics. In this way, we can describe the nucleus Hamiltonian by a sum of non-interacting harmonic oscillators (HO), and written in $\boldsymbol{q}$-space we find

$$H_{\mathrm{HO}} \;=\; \sum_{j\boldsymbol{q}} \hbar\omega_j(\boldsymbol{q}) \left(b^\dagger_{j,\boldsymbol{q}}\, b_{j,\boldsymbol{q}} + \frac{1}{2} \right).$$

Here we have introduced the Bose operators b and $b^\dagger$ with the usual harmonic time dependency $b_{j,\boldsymbol{q}}(t) = b_{j,\boldsymbol{q}} \exp(-i\omega_j(\boldsymbol{q})t)$. The sum over the index j represents different phonon-branches, i.e., LO, TO, LA, TA etc.

According to Schäfer et al. [6.1, 6.2], we may write the phonon-induced interaction in the long-wavelength limit ($\boldsymbol{q} \to 0$) and within the harmonic

and adiabatic approximation as [1]

$$\begin{aligned} W_{\rm ph}(\underline{1},\underline{2}) &= \iint \mathrm{d}\underline{3}\,\mathrm{d}\underline{4}\, W(\underline{1},\underline{3})\, D(\underline{3},\underline{4})\, W(\underline{4},\underline{2}) \\ &= \sum_{\boldsymbol{q}} \sum_{j} e^{-i\boldsymbol{q}(\boldsymbol{r}_1-\boldsymbol{r}_2)}\, M_j^2(\boldsymbol{q})\; D_j(\boldsymbol{q},\underline{t}_1,\underline{t}_2) \\ &= \sum_{\boldsymbol{q}} e^{-i\boldsymbol{q}(\boldsymbol{r}_1-\boldsymbol{r}_2)}\, W_{\rm ph}(\boldsymbol{q},\underline{t}_1,\underline{t}_2), \end{aligned} \tag{6.16}$$

where the phonon Green's function

$$D_j(\boldsymbol{q},\underline{t}_1,\underline{t}_2) = -i\,b_2 \left\langle T_c \left(b_{j,\,\boldsymbol{q}}(\underline{t}_1)\, b^{\dagger}_{j,\,\boldsymbol{q}}(\underline{t}_2) \;+\; b^{\dagger}_{j,-\boldsymbol{q}}(\underline{t}_1)\, b_{j,-\boldsymbol{q}}(\underline{t}_2) \right) \right\rangle , \tag{6.17}$$

is defined in terms of the phonon operators. The phonon Green's function $D_j(\boldsymbol{q},\underline{t}_1,\underline{t}_2)$ is the only part of the density-density correlation function $D(\underline{1},\underline{2})$ which operates in the phonon subspace. All other quantities, including the (instantaneous) screened Coulomb potentials W have been lumped into one big pre-factor $M_j^2(\boldsymbol{q})$.

Using the free harmonic time dependency of the bosonic phonon operators, the free phonon Green's functions read

$$\begin{aligned} D_{0j}^{++}(\boldsymbol{q},t_1t_2) &= -i\left(2N_{0j}(\boldsymbol{q})\cos[\omega_j(\boldsymbol{q})(t_1-t_2)] + e^{-i\,\omega_j(\boldsymbol{q})|t_1-t_2|}\right), \\ D_{0j}^{+-}(\boldsymbol{q},t_1t_2) &= \;\;i\left(2N_{0j}(\boldsymbol{q})\cos[\omega_j(\boldsymbol{q})(t_1-t_2)] + e^{i\,\omega_j(\boldsymbol{q})(t_1-t_2)}\;\right), \\ D_{0j}^{-+}(\boldsymbol{q},t_1t_2) &= -i\left(2N_{0j}(\boldsymbol{q})\cos[\omega_j(\boldsymbol{q})(t_1-t_2)] + e^{-i\,\omega_j(\boldsymbol{q})(t_1-t_2)}\right), \\ D_{0j}^{--}(\boldsymbol{q},t_1t_2) &= \;\;i\left(2N_{0j}(\boldsymbol{q})\cos[\omega_j(\boldsymbol{q})(t_1-t_2)] + e^{i\,\omega_j(\boldsymbol{q})|t_1-t_2|}\;\right), \end{aligned}$$

where

$$N_{0j}(\boldsymbol{q}) \;=\; \left\langle b_j^{\dagger}(\boldsymbol{q}) b_j(\boldsymbol{q}) \right\rangle \;=\; \frac{1}{e^{\beta\hbar\omega_j(\boldsymbol{q})}-1}\,,$$

is the free phonon distribution in equilibrium at the lattice temperature $\beta = 1/k_BT$ given by the usual Bose distribution. Here we have basically assumed that we can describe the vibrational modes of the system as a phonon-bath in thermal equilibrium. It is of course only the zeroth order description of the phonon dynamics, but should nevertheless be a good model to describe the dissipative process of transferring energy between the carrier system and the vibrational modes of the semiconductor. In this approximation we do not care about, nor do we model the kinetics of the phonon-reservoir. So to say, there will always be enough phonons available, and they will not be driven away from equilibrium by the carriers.

[1] Assuming instantaneous screening $W(t_1,t_2) = W(t_1,t_2)\delta(t_1,t_2)$.

6.3 Equation of Motion

From Eq. (6.13) we see that the electron-phonon interaction can be evaluated by the methods developed over the previous last three chapters. Given the potential $W_{\rm ph}(\underline{1},\underline{2})$, all we need to evaluate is the corresponding self-energy $\Sigma_{\rm ph}(\underline{1},\underline{2})$, which subsequently may be used in the kinetic equations. Following the procedure of Chap. 5 the Green's functions and the self-energy are expanded in a given appropriate basis and finally we end up with the equations of motion expressed in this basis. Formally there is no difference from those of Sec. 5.2, but let us just rewrite them once more here.

For simplicity we consider in the following only the carrier-phonon interaction, i.e., $W_{\rm eff}(\underline{1},\underline{2}) = W_{\rm ph}(\underline{1},\underline{2})$, since the pure Coulomb interaction was treated in previous chapters. For the retarded Green's function we then obtain

$$\begin{aligned}
&i\hbar\left[\frac{\partial}{\partial t_1} \mp \frac{\partial}{\partial t_2}\right] G^r_{\nu_1\,\nu_2}(t_1,t_2) \\
&- \sum_{\nu_3}\Big(h^0_{\nu_1\,\nu_3}(t_1)G^r_{\nu_3\,\nu_2}(t_1,t_2) \pm G^r_{\nu_1\,\nu_3}(t_1,t_2)h^0_{\nu_3\,\nu_2}(t_2)\Big) \\
&= (1\pm 1)\,\delta_{\nu_1\nu_2}\,\delta(t_1,t_2) \\
&+ \sum_{\nu_3}\int_{t_2}^{t_1} {\rm d}t_3\,\Big\{\Sigma^r_{\nu_1\,\nu_3}(t_1,t_3)G^r_{\nu_3\,\nu_2}(t_3,t_2) \pm G^r_{\nu_1\,\nu_3}(t_1,t_3)\Sigma^r_{\nu_3\,\nu_2}(t_3,t_2)\Big\},
\end{aligned} \tag{6.18}$$

while for the lesser Green's function we had

$$\begin{aligned}
&i\hbar\left[\frac{\partial}{\partial t_1} \mp \frac{\partial}{\partial t_2}\right] G^<_{\nu_1\,\nu_2}(t_1,t_2) \\
&- \sum_{\nu_3}\Big(h^0_{\nu_1\,\nu_3}(t_1)G^<_{\nu_3\,\nu_2}(t_1,t_2) \pm G^<_{\nu_1\,\nu_3}(t_1,t_2)h^0_{\nu_3\,\nu_2}(t_2)\Big) \\
&= \sum_{\nu_3}\int_{-\infty}^{t_1} {\rm d}t_3\,\Big\{\Sigma^>_{\nu_1\,\nu_3}(t_1,t_3)G^<_{\nu_3\,\nu_2}(t_3,t_2) - \Sigma^<_{\nu_1\,\nu_3}(t_1,t_3)G^>_{\nu_3\,\nu_2}(t_3,t_2) \\
&\qquad\qquad \pm \left[G^>_{\nu_1\,\nu_3}(t_1,t_3)\Sigma^<_{\nu_3\,\nu_2}(t_3,t_2) - G^<_{\nu_1\,\nu_3}(t_1,t_3)\Sigma^>_{\nu_3\,\nu_2}(t_3,t_2)\right]\Big\},
\end{aligned} \tag{6.19}$$

see Eq.(5.5). Since we only consider the carrier-phonon interaction in this chapter we have disregarded the dipole interaction and the Hartree-Fock terms of the single-particle Hamiltonian $\hat{h}$, and are left with the free single-particle contribution h^0 in the equations above. (If needed, they can at any time be included, by the procedure shown in Sec. 5.2.) The subscript "ph" have been dropped on the phonon self-energy to avoid cumbersome notation.

The phonon self-energy has no instantaneous part as compared to the Coulomb self-energy, i.e., $\Sigma^\delta_{\rm ph} = 0$. This is seen from the equation $W_{\rm ph} =$

WDW, which tells us that even if we use the instantaneous bare Coulomb potential instead of the screened Coulomb potential, the phonon-induced potential will at least depend upon the phonon propagator times.

Written in the form above the coupling of the equations of motion for the retarded and lesser Green's functions is not explicitly clear, but is implicit linked through the self-energy. This is however just a different way of writing the coupled kinetic equation, compare e.g. to Eqs. (4.22) and (4.23), and following they should therefore be solved simultaneously.

6.4 Random Phase Approximation

The self-energy for the carrier-phonon interaction is determined by the phonon-induced potential, the Green's function, and the vertex function, see Eq. (6.9). The vertex function depends on the self-energy and the Green's function, and if possible one should solve the equations self-consistently. This is a complicated task and in general one therefore relies on some approximation scheme. The simplest approximation to the vertex function is the random phase approximation (RPA) where all vertex corrections are neglected. Through out this work we use for the carrier-phonon interaction the lowest order approximation to the vertex function, the RPA

$$\Gamma^{\mathrm{RPA}}(\underline{1},\underline{2},\underline{3}) = -e\delta(\underline{1}-\underline{2})\,\delta(\underline{1}-\underline{3}), \tag{6.20}$$

which gives the self-energy

$$\Sigma_{\mathrm{ph}}(\underline{1},\underline{2}) \;=\; i\hbar e^2 b_1 W_{\mathrm{ph}}(\underline{2},\underline{1})G(\underline{1},\underline{2}), \tag{6.21}$$

as we already have encountered for the carrier-carrier Coulomb self-energy, see Eq. (5.27). The RPA self-energy is linear in the phonon-induced interaction and is sometimes refereed to as the one-phonon self-energy [6.1], but should not be confused with perturbation theory, since by the Dyson equation the RPA self-energy is repeated an arbitrary high number of times. The phonon self-energy is diagrammatically depicted in Fig. 6.2.

We can now project the self-energy onto states ν_1 and ν_2 of the eigenfunction expansion of the Green's function which gives

$$\Sigma^{\mathrm{ph}}_{\nu_1\,\nu_2}(\underline{t}_1,\underline{t}_2) \;=\; i\hbar e^2 b_1 \sum_{\nu_3\nu_4} W^{\mathrm{ph}}_{\nu_4\nu_1\nu_3\nu_2}(\underline{t}_2,\underline{t}_1)\, G_{\nu_3\,\nu_4}(\underline{t}_1,\underline{t}_2),$$

where

$$W^{\mathrm{ph}}_{\nu_4\nu_1\nu_3\nu_2}(\underline{t}_2,\underline{t}_1) \;=\; \iint \mathrm{d}\boldsymbol{r}_1\,\mathrm{d}\boldsymbol{r}_2\,\varphi^*_{\nu_4}(\boldsymbol{r}_2)\,\varphi^*_{\nu_1}(\boldsymbol{r}_1) W_{\mathrm{ph}}(\underline{2},\underline{1})\varphi_{\nu_3}(\boldsymbol{r}_1)\,\varphi_{\nu_2}(\boldsymbol{r}_2), \tag{6.22}$$

is the matrix-element for phonon-induced interaction.

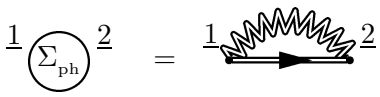

Figure 6.2: Diagrammatic representation of the RPA self-energy for the carrier-phonon interaction.

6.5 Simplifying Approximations

As for the carrier Coulomb interaction, the kinetic equation for changes of the carrier occupation probabilities in time has the structure

$$i\hbar\frac{\partial}{\partial t}f_{\nu_1}(t) \;=\; i\hbar\frac{\partial}{\partial t}f_{\nu_1}(t)\bigg|_{\rm HF} \;+\; i\hbar S_{\nu_1\,\nu_1}(tt), \tag{6.23}$$

where the first term on the right hand side corresponds to changes due to the effective Hartree-Fock one-particle Hamiltonian.

In this section we investigate the scattering term $i\hbar S_{\nu_1\,\nu_1}(tt)$, and study here changes in the carrier population due to carrier-phonon scattering. At first we derive the kinetic-equation describing these scattering processes, and in a second step we derive the corresponding Boltzmann scattering integrals. Our results form the starting point of the discussion of the carrier-phonon scattering in Chap. 8.

The Fröhlich Interaction

A frequently used and successful model for describing the carrier interaction with the longitudinal-optical (LO) phonons is known in semiconductor physics as the Fröhlich interaction. As such it has been applied for decades and can be found in many textbooks, see e.g. Refs. [6.3, 6.7]. Our focus is on the quantum-dot wetting-layer system, and specifically for quantum-dots it has been shown that only phonons with small momenta can efficiently couple to the confined carriers [6.8]. Then interaction with longitudinal-acoustic phonons does not contribute for large transition energies and only quasi-monochromatic LO phonons need to be considered.

Throughout the work presented here we consider only the carrier interaction with the bulk LO phonons, since using the unmodified bulk phonons modes instead of the the confined modes provide reasonable results [6.9, 6.10]. According to Schäfer et al. [6.1, 6.2] the coupling constant for the Fröhlich

interaction $M_j^2(\boldsymbol{q})$ of Eq. (6.16) is then given by

$$\begin{aligned} M^2_{\rm LO}(\boldsymbol{q}) &= V(\boldsymbol{q})\frac{\omega_{\rm LO}}{2\varepsilon^*}, \\ V(\boldsymbol{q}) &= \frac{1}{\varepsilon_0}\frac{1}{q^2}, \end{aligned}$$

where $V(\boldsymbol{q})$ is the 3-dimensional Fourier transform of the bare Coulomb potential $1/(4\pi\varepsilon_0|\boldsymbol{r}|)$ and $\frac{1}{\varepsilon^*} = (\frac{1}{\varepsilon_\infty} - \frac{1}{\varepsilon})$. Here ε_∞ and ε are the high-frequency and static dielectric constants, respectively.

The LO-phonon dispersion relation is almost $\boldsymbol{q}$ independent and becomes constant in the long-wavelength limit ($\boldsymbol{q} \to 0$), following not only that the energy of the LO-phonon mode becomes constant, but also that the phonon propagator D becomes $\boldsymbol{q}$ independent. We have

$$\begin{aligned} \omega_{\rm LO}(\boldsymbol{q}) &= \omega_{\rm LO}, \\ D_{\rm LO}(\boldsymbol{q}, \underline{t}_1, \underline{t}_2) &= D^0_{\rm LO}(\omega_{\boldsymbol{q}}, \underline{t}_1, \underline{t}_2) \\ &= D(\omega_{\rm LO}, \underline{t}_1, \underline{t}_2), \end{aligned}$$

where in the last line we have dropped the indices on $D^0_{\rm LO}$ which was to remind us that we use a bath of LO-phonons in thermal equilibrium.

We can now express the matrix-elements of $W_{\rm ph}$ in terms of the bare Coulomb matrix-elements. Using the simplifications from above, we find for the Fröhlich interaction the relation

$$\begin{aligned} W^{\rm ph}_{\alpha\beta\gamma\delta}(\underline{t}_1, \underline{t}_2) &= \iint {\rm d}\boldsymbol{r}_1 {\rm d}\boldsymbol{r}_2 \\ &\times \left\{ \varphi^*_\alpha(\boldsymbol{r}_1)\, \varphi^*_\beta(\boldsymbol{r}_2) \sum_{\boldsymbol{q}} \frac{\omega_{LO}}{2\varepsilon^*} \frac{1}{\varepsilon_0 q^2} D(\omega_{LO}, \underline{t}_1, \underline{t}_2) e^{-i\boldsymbol{q}(\boldsymbol{r}_1 - \boldsymbol{r}_2)} \varphi^*_\gamma(\boldsymbol{r}_1)\, \varphi^*_\delta(\boldsymbol{r}_2) \right\} \\ &= \frac{\omega_{LO}}{2\varepsilon^*/\varepsilon}\, V_{\alpha\beta\gamma\delta}\, D(\omega_{LO}, \underline{t}_1, \underline{t}_2), \end{aligned} \tag{6.24}$$

where by the first equality we have used the definition of the matrix element and inserted the Fourier transform of the potential $W_{\rm ph}(\underline{1}, \underline{2})$. In going to the third line we have Fourier transformed back the $\boldsymbol{q}$-space Coulomb potential and rewritten the result in terms of the bare Coulomb matrix element $V_{\alpha\beta\gamma\delta}$.

Thus the Fröhlich interaction corresponds to using the bare Coulomb potential in equation for the electron-phonon induced potential $W_{\rm ph}(\underline{1}, \underline{2})$.

Generalized Kadannof-Baym Ansatz

In the following we consider only changes of the carrier occupation probabilities due to single particle carrier-phonon scattering. Thus, following the same procedure as in Sec. 5.4, we should only use the diagonal part of

the eigenfunction expansion of the lesser Green's function within the quantum kinetic equation (6.19). More precisely, for the Green's functions we have $G^{\gtrless}_{\nu_1\,\nu_2} = G^{\gtrless}_{\nu_1\,\nu_1}\delta_{\nu_1\nu_2}$ which by Eq. (5.7) is related to the carrier occupation probabilities by $i\hbar G^{<}_{\nu_1\,\nu_1}(tt) = f_{\nu_1}(t)$. Furthermore, in order to map the two-time lesser Green's function back onto the time-diagonal, we will also apply the generalized Kadanoff-Baym ansatz (GKBA). Within these approximations we obtain

$$\begin{aligned}
\frac{\partial}{\partial t} f_{\nu_1}(t) = i\,\hbar\, e^2 \int \mathrm{d}t_3 \sum_{\nu_3} \Big\{ & \\
& b_- W^{\mathrm{ph}+-}_{\nu_3\nu_1\nu_3\nu_1}(t_3,t)\Big(G^r_{\nu_3\,\nu_3}(t,t_3)\,[1-f_{\nu_3}(t_3)]\Big)\Big(-G^a_{\nu_1\,\nu_1}(t_3,t) f_{\nu_1}(t_3)\Big) \\
- & b_+ W^{\mathrm{ph}-+}_{\nu_3\nu_1\nu_3\nu_1}(t_3,t)\Big(G^r_{\nu_3\,\nu_3}(t,t_3) f_{\nu_3}(t_3)\Big)\Big(-G^a_{\nu_1\,\nu_1}(t_3,t)\,[1-f_{\nu_1}(t_3)]\Big) \\
- & b_+ W^{\mathrm{ph}-+}_{\nu_3\nu_1\nu_3\nu_1}(t,t_3)\Big(G^r_{\nu_1\,\nu_1}(t,t_3)\,[1-f_{\nu_1}(t_3)]\Big)\Big(-G^a_{\nu_3\,\nu_3}(t_3,t) f_{\nu_3}(t_3)\Big) \\
+ & b_- W^{\mathrm{ph}+-}_{\nu_3\nu_1\nu_3\nu_1}(t,t_3)\Big(G^r_{\nu_1\,\nu_1}(t,t_3) f_{\nu_1}(t_3)\Big)\Big(-G^a_{\nu_3\,\nu_3}(t_3,t)\,[1-f_{\nu_3}(t_3)]\Big)\Big\}.
\end{aligned} \tag{6.25}$$

For the Fröhlich interaction the matrix elements of the phonon-induced interaction are expressed in terms of the bare Coulomb matrix elements and the phonon propagator as shown in Eq. (6.24). By introducing the abbreviation

$$\begin{aligned}
\Delta^{\lessgtr}(t_1,t_2) &= i\,D^{\pm\mp}(t_1,t_2)\,b_{\mp} \\
&= \Big[(N_0+1)e^{\pm i\,\omega_{LO}(t_1-t_2)} + N_0 e^{\mp i\,\omega_{LO}(t_1-t_2)}\Big],
\end{aligned} \tag{6.26}$$

we then finally arrive at the quantum kinetic equation for the time changes of the carrier occupation probabilities due to carrier-phonon scattering

$$\begin{aligned}
\frac{\partial}{\partial t} f_{\nu_1}(t) &= 2\mathrm{Re}\sum_{\nu_3}\int \mathrm{d}t_3\,\frac{\hbar\omega_{LO}}{2\varepsilon^*/\varepsilon} V_{\nu_3\nu_1\nu_3\nu_1} \\
&\quad \times G^r_{\nu_3\,\nu_3}(t,t_3)(-G^a_{\nu_1\,\nu_1}(t_3,t)) \\
&\quad \Big\{[1-f_{\nu_3}(t_3)]\,f_{\nu_1}(t_3)\;\Delta^{<}(t_3,t) \\
&\quad -f_{\nu_3}(t_3)\,[1-f_{\nu_1}(t_3)]\;\Delta^{>}(t,t_3)\Big\}.
\end{aligned} \tag{6.27}$$

In deriving this result, we have used that for the Fröhlich interaction line five (four) equals the complex conjugated of line two (three) in Eq. (6.25).

The remaining challenge of solving the equation is to provide a useful spectral function. As in the the case of the carrier-carrier scattering we proceed first with the simple assumption of using the free retarded/advanced Green's functions. An improvement is done in a second step, where we provide a scheme for an approximate solution of the spectral kinetic equation.

Free Spectral Functions and the Markov Approximation

Using the retarded/advanced Green's functions of the free carriers and performing the Markov approximation as in Chap. 5 the above quantum kinetic result is significantly simplified. First, we have assume the non-interacting spectral properties for the system, and following we do not need to solve an additional equation for the retarded/advanced Green's function. Secondly, by the the Markov approximation the time integral can be performed analytic, and we are left with a sum over different scattering channels.

Thus by the procedure outlined in Chap. 5 we find by using the free spectral functions and performing the Markov approximation the Boltzmann limit for the carrier-phonon scattering. The changes of the carrier occupation probability f_ν is then given by

$$\begin{aligned}\frac{\partial}{\partial t} f_{\nu_1} =& \frac{2\pi}{\hbar} \frac{\hbar\omega_{\mathrm{LO}}}{2\varepsilon^*/\varepsilon} \sum_{\nu_3} V_{\nu_3\nu_1\nu_3\nu_1} \\ &\times \Big\{ (1-f_{\nu_1}) f_{\nu_3} \big[\;\; (1+N_0)\, \delta(\varepsilon_{\nu_1} - \varepsilon_{\nu_3} + \hbar\omega_{LO}) \\ &\qquad\qquad + N_0 \;\; \delta(\varepsilon_{\nu_1} - \varepsilon_{\nu_3} - \hbar\omega_{LO}) \big] \\ &- f_{\nu_1}(1-f_{\nu_3}) \big[\qquad N_0 \;\; \delta(\varepsilon_{\nu_1} - \varepsilon_{\nu_3} + \hbar\omega_{LO}) \\ &\qquad\qquad + (1+N_0)\, \delta(\varepsilon_{\nu_1} - \varepsilon_{\nu_3} - \hbar\omega_{LO}) \big] \Big\}. \end{aligned} \tag{6.28}$$

The various terms of the equation above describe the scattering of carriers from states ν_1 into ν_3 under the emission and absorption of an LO-phonon as well as the reverse processes. Thus, under the above assumptions, carrier-phonon scattering between states is only possible when the LO-phonon energy matches the level spacing - known as the phonon bottleneck in the literature.

Spectral Functions II

Using the free spectral functions is only the first step towards a full-fledged quantum-kinetic description of the carrier-phonon interaction. Energy renormalization of the involved states due to the carrier-phonon interaction can in strong polar material systems lead to substantial shifts and broadening, as is know from studies of quantum-well and bulk semiconductors. These effects of the renormalization are mirrored in the spectral functions. The aim of this work is to investigate the spectral properties of the quantum-dot wetting-layer system. In principle all we have to do is to solve the coupled two-time kinetic equations (6.18) and (6.19), but even with todays supercomputers this approach is very challenging.

Things get simpler in an empty semiconductor, i.e. when no electrons in the conduction band and no holes in the valance band are present. This limit corresponds to the low carrier-density regime. We shall show that

in the kinetic equation (6.18) all reference to the lesser Green's function, which is hidden in the self-energy, can be eliminated and, following that, the equation may be solved separately.

Decoupling Scheme

As shown in Chap. 4 the retarded Green's function and self-energy are given by

$$G^r(12) = \Theta(t_1,t_2)\left[G^>(12)+G^<(12)\right], \tag{6.29}$$
$$\Sigma^r(12) = \Theta(t_1,t_2)\left[\Sigma^>(12)+\Sigma^<(12)\right], \tag{6.30}$$

where we have used that the phonon self-energy has no instantaneous contribution, i.e., $\Sigma^\delta_{\rm ph}=0$.

Thus within the RPA we find

$$\begin{aligned}\Sigma^r(12) &= \Theta(t_1,t_2)\, i\hbar e^2 \left[b_1\, W^<_{\rm ph}(21)G^>(12) + b_1\, W^>_{\rm ph}(21)G^<(12)\right]\\ &= i\hbar e^2 b_1\, W^<_{\rm ph}(21)G^r(12).\end{aligned} \tag{6.31}$$

In going from first to second line we have used that the lesser electron/hole Green's function is zero for the empty crystal. As we see from the kinetic equation for the retarded Green's function Eq. (6.18), this is of great importance, since now the equation becomes closed. All reference to the greater or lesser Green's functions have been eliminated, and the equation of motion for the retarded Green's function may be solved alone. This is by no means a coincidence. The empty system is in equilibrium and the equilibrium theory is known [6.7, 6.11] to be described by a single Green's function, the chronological one, which in this (empty) case coincides with the retarded one.

Equilibrium

In equilibrium, such as e.g. the empty semiconductor, the system depends only on the relative time $t_r = t_1 - t_2$ due to time translation invariance and it is sufficient to solve only the $1^{\rm st}$ Kadanoff-Baym equation for the retarded Green's function instead of the symmetrized form of the kinetic equations (6.18). That is, from Eq. (6.18) we solve only the part which is related to the derivative with respect to t_1, since the second part which comes with the $\pm$ sign and is related to the derivative with respect to t_2 can be shown to yield the same solution in equilibrium. See App. 6.A below for details.

Furthermore, as a first approximation we use only the diagonal elements in the eigenfunction expansion of the Green's function and self-energy. The h^0 Hamiltonian is diagonal in all indices, whereas the carrier-phonon interaction is diagonal in the band indices, so that the Green's function is only

diagonal in the band indices. Nevertheless, using the diagonal approximation for the Green's function turns out to be a reasonable approximation. See Chap. 8 for further discussion. Finally using that in equilibrium the retarded Green's function and the self-energy depend only on the relative time, we find by introducing $t_r = t_1 - t_2$ and $\tau = t_3 - t_2$ the differential equation with respect to the relative time t_r for the retarded Green's function

$$\left[i\hbar\frac{\partial}{\partial t_r} - h^0_{\nu_1\,\nu_1}\right] G^r_{\nu_1\,\nu_1}(t_r) = \delta(t_r) + \int_0^{t_r} \mathrm{d}\tau \;\; \Sigma^r_{\nu_1\,\nu_1}(t_r - \tau) G^r_{\nu_1\,\nu_1}(\tau). \quad (6.32)$$

The solution of this equation will be used in the kinetic equation Eq. (6.27), i.e. $G^r(t_1, t_2) = G^r(t_1 - t_2)$ is implied as discussed above for the low carrier-density regime.

In Chap. 8 we present numerical studies for the carrier LO-phonon interaction, discussing the spectral properties, the solution of the kinetic equation as well as studying the scattering rates at the Boltzmann level. The combined solution of Eqs. (6.27) and (6.32) causes substantial computational numerical overhead compared to the Boltzmann scattering integrals of Eq. (6.28). This difference is due to the fact the spectral properties now also have to be determined as well as the memory dependence, expressed through the time integrals which have to be included. Furthermore on a technical level, the Boltzmann scattering integrals rely on a strict energy conservation allowing the sum in Eq. (6.28) to be performed exact by integrating out the delta function. Comparing to the carrier-carrier scattering at the Boltzmann level discussed in Chap. 7 the non-Markovian carrier-phonon problem is numerically more demanding. On the other hand, the carrier-phonon scattering at the Boltzmann level is much simpler than the corresponding carrier-carrier scattering since fewer scattering channels need to be considered. For the carrier-carrier scattering, the screened Coulomb matrix elements must also be evaluated for each new carrier density in the system, while for the carrier-phonon interaction we could recast the interaction matrix elements in terms of the bare Coulomb matrix elements. Once renormalization effects are included in the Coulomb problem, more computation time is also required here.

6.A Equilibrium Spectral Functions

In equilibrium, where the Green's function and the self-energy only depend on the relative time the 1st Kadanoff-Baym equation reads

$$\left[i\hbar\frac{\partial}{\partial t_r} - h^0_{\nu_1\,\nu_2}\right] G^r_{\nu_1\,\nu_2}(t_r) = \delta_{\nu_1\,\nu_2}\,\delta(t_r) + \sum_{\nu_3}\int_0^{t_r} \mathrm{d}\tau\ \ \Sigma^r_{\nu_1\,\nu_3}(t_r-\tau)G^r_{\nu_3\,\nu_2}(\tau). \quad (6.A.33)$$

where we have introduced the relative times $t_r = t_1 - t_2$ and $\tau = t_3 - t_2$. A Fourier transform of the relative time t_r to the frequency domain ω yields

$$\left[\hbar\omega - h^0_{\nu_1\,\nu_2}\right] G^r_{\nu_1\,\nu_2}(\omega) = \delta_{\nu_1\,\nu_2} + \sum_{\nu_3}\ \Sigma^r_{\nu_1\,\nu_3}(\omega)G^r_{\nu_3\,\nu_2}(\omega), \quad (6.A.34)$$

where ω actually lies in the upper complex half-plane,i.e. $\omega \to \omega + i\eta$ with $\eta > 0$, due to the Heaviside step-function in the definition of the retarded Green's function. From this equation we obtain the general expression for the inverse retarded Green's function given by

$$[G^r]^{-1}(\nu_1,\nu_2;\omega) \;=\; (\hbar\omega - h^0_{\nu_1\,\nu_2})\delta_{\nu_1\,\nu_2} - \Sigma^r_{\nu_1\,\nu_2}(\omega). \quad (6.A.35)$$

Starting with the t_2 equation and following the same procedure one obtains the same expression for the inverse retarded Green's function. Hence in equilibrium it is sufficient to start with either the t_1 or the t_2 equation.

The retarded and advanced Green's functions are related to the spectral properties of the system. To illustrate this, let us just consider a homogeneous system like e.g. the bulk semiconductor where the wavevector $\boldsymbol{k}$ is a good quantum number and the Green's function and the self-energy are diagonal in this representation. For a detailed introduction the reader is urged consult to the references.

We introduce the *spectral function* A defined as

$$A(\boldsymbol{k},\omega) \;=\; i\hbar\left[G^r(\boldsymbol{k},\omega) - G^a(\boldsymbol{k},\omega)\right] \quad (6.A.36)$$

$$\;=\; -2\hbar\ \mathrm{Im}\ G^r(\boldsymbol{k},\omega), \quad (6.A.37)$$

which obeys the following identity, see e.g. Ref. [6.11],

$$\int \mathrm{d}\omega\ \frac{1}{2\pi}\,A(\boldsymbol{k},\omega) \;=\; 1. \quad (6.A.38)$$

Since A is positive definite [6.4, 6.7] it can, on the basis of this identity, be interpreted as a probability distribution. It is the probability of finding an electron of momentum $\boldsymbol{k}$ with energy $\hbar\omega$.

For the non-interacting system the retarded Green's function reads

$$G^r(\boldsymbol{k},\omega) \quad = \quad \frac{1}{\hbar\omega - h^0_{\boldsymbol{k}} + i\eta},$$

where $\eta \to 0_+$ is introduced to ensure the right causality of the Green's function upon Fourier transforming back to the time domain, remember that $\Theta(\tau) = \frac{1}{2\pi i}\int d\omega e^{i\omega\tau}/(\omega - i\eta)$. Following, the spectral function reads $A(\boldsymbol{k},\omega) = 2\pi\hbar\delta(\hbar\omega - h^0_{\boldsymbol{k}})$ shows that the non-interacting system has in the frequency plane a pole at the free energy $h^0_{\boldsymbol{k}}$. Hence, there exist a one-to-one correspondence between the free energies $h^0_{\boldsymbol{k}}$ of an electron with momentum $\boldsymbol{k}$ and the poles of the Green's function.

For the interacting system the retarded Green's function reads

$$G^r(\boldsymbol{k},\omega) \quad = \quad \frac{1}{\hbar\omega - h^0_{\boldsymbol{k}} - \Sigma^r(\boldsymbol{k},\omega)}.$$

If the self-energy shows only a weak dependency on $\boldsymbol{k}$ and ω around the previous pole $\hbar\omega = h^0_{\boldsymbol{k}}$ we can as a first attempt approximate it with a complex number, i.e. $\Sigma^r(\boldsymbol{k},\omega) \simeq \Sigma^r(\boldsymbol{k}, \frac{1}{\hbar}h^0_{\boldsymbol{k}}) = \Delta_{\boldsymbol{k}} - i\Gamma_{\boldsymbol{k}}$ where $\Delta_{\boldsymbol{k}} \in \mathbb{R}$ and $\Gamma_{\boldsymbol{k}} \in \mathbb{R}_+$ due to causality. Thus the spectral function A reads

$$A(\boldsymbol{k},\omega) \quad = \quad 2\hbar\frac{\Gamma_{\boldsymbol{k}}}{(\hbar\omega - h^0_{\boldsymbol{k}} - \Delta_{\boldsymbol{k}})^2 + \Gamma^2_{\boldsymbol{k}}},$$

which in the limit of $\Gamma_{\boldsymbol{k}} \to 0_+$ is the delta function representation of $2\pi\hbar\delta(\hbar\omega - h^0_{\boldsymbol{k}} - \Delta_{\boldsymbol{k}})$. Compared to the non-interacting system we say that due to the interaction the free energy $h^0_{\boldsymbol{k}}$ have been shifted by the amount $\Delta_{\boldsymbol{k}}$ and has now a finite lifetime $\Gamma_{\boldsymbol{k}}$. In this picture the energy of state $\boldsymbol{k}$ is no longer peaked a the non-interacting energy but spread out over the energy axis, centered at $h^0_{\boldsymbol{k}} - \Delta_{\boldsymbol{k}}$ and with a spread of $\Gamma_{\boldsymbol{k}}$. In the general case the self-energy $\Sigma^r(\boldsymbol{k},\omega)$ is not independent of $\boldsymbol{k}$ and ω and a complicated pole structure of $G^r(\boldsymbol{k},\omega)$ and following of the spectral function $A(\boldsymbol{k},\omega)$ is to be expected.

For a detailed study of spectral properties for QD-WL system presented in this thesis the reader is urged to consult Ref. [6.5].

References

[6.1] W. Schäfer and M. Wegner, in *Semiconductor Optics and Transport Phenomena* (Springer, Berlin Heidelberg, 2002), Chap. 11.

[6.2] W. Schäfer, P. Gartner, and F. Jahnke, in *Progress in Nonequilibrium Green's Functions*, edited by M. Bonitz and D. Semkat (World Scientific, Singapore, 2003), pp. 274–290.

[6.3] G. Czycholl, *Theoretische Festkörperphysik* (Vieweg Verlag, Braunschweig/Wiesbaden, 2000).

[6.4] P. Gartner, Many-Body Theory Vol. I & II, 2002, lecture notes.

[6.5] J. Seebeck, Quantenkinetische Beschreibung von Polaronen in Halbleiter-Quantenpunkten, Diplomarbeit, 2004, Universität Bremen, Fachberich Physik.

[6.6] R. van Leeuwen, Phys. Rev. B **69**, 115110 (2004).

[6.7] G. Mahan, *Many-Particle Physics* (Plenum, New York, 1990).

[6.8] T. Inoshita and H. Sakaki, Phys. Rev. B **56**, 4355 (1997).

[6.9] H. Rücker, E. Molinari, and P. Lugli, Phys. Rev. B **45**, 6747 (1992).

[6.10] U. Bockelmann and G. Bastard, Phys. Rev. B **42**, 8947 (1990).

[6.11] H. Haug and A.-P. Jauho, *Quantum Kinetics in Transport and Optics of Semiconductors* (Springer, Berlin Heidelberg, 1996).

Part III

Results

Chapter 7

Evaluation of Carrier-Carrier Scattering in QD Systems

A microscopic description of the Coulomb interaction among carriers have proven successful and necessary for modeling the carrier dynamics in bulk and quantum-well semiconductor laser-devices [7.1]. In general any creation of carriers in such systems, either by electrical or optical pumping, will lead to a nonequilibrium situation which is thermalized due to carrier-carrier and carrier-phonon scattering. At high densities carrier-carrier scattering leads to a fast relaxation of the carrier distribution function towards a quasi-equilibrium Fermi-Dirac distribution. Many-body effect such as screening and Pauli blocking play a vital role and must be taken into account.

The aim of this chapter is to study the carrier-carrier scattering, by the general theoretical tools developed in Part II of this thesis, for the quantum-dot (QD) wetting-layer (WL) system introduced in Chap. 2. Thus we consider an ensemble of self-assembled QDs grown on a quasi-two-dimensional WL. Correspondingly, the relevant electronic structure consists of two parts. The localized QD states with discrete energies due to the three-dimensional QD confinement potential are energetically below a quasi-continuum of two-dimensional delocalized WL states.

Such a quantitative description of various electronic scattering processes is necessary to optimize the design of QD based laser devices [7.2, 7.3] as well as to provide a detailed understanding of steady-state and dynamical emission properties in these devices [7.4, 7.5]. While the localized QD states are used for the laser transition, the pump process initially generates carriers in the WL. Hence the carrier dynamics in QD based laser devices critically depends on the capture of carriers from the WL into the QDs as well as on the relaxation of carriers between the discrete QD states. An important question is to what extent these processes limit the laser operation in comparison to the extensively studied quantum-well lasers [7.1].

Experimental evidence for fast capture and relaxation processes is given

by the strong QD ground-state photoluminescence following an excitation of the WL or barrier states. From the rise time of the QD photoluminescence [7.6, 7.7] and the ratio of the QD and WL emission [7.8] the efficiency of capture and relaxation at low temperatures has been studied. Also it has been pointed out that it is not the two-dimensional nature of the WL but the availability of a quasi-continuum of states that facilitates the scattering processes [7.9].

The chapter is organized as follows. In Sec. 7.1 we summarize the main ingredients of our theory which include the kinetic equations, the classification of the scattering processes and the InGaAs model system. Details regarding the WL states and screening effects are given in appendices. In Sec. 7.2 the numerical results for scattering rates are presented.

7.1 Theory for Coulomb Scattering

7.1.1 Boltzmann's Equation

The carrier dynamics under the influence of various scattering processes can be described by kinetic equations. In this section we consider Coulomb-interaction processes up to quadratic order in the screened Coulomb potential (second-order Born approximation) and restrict ourselves to time-scales where the Markov approximation is valid. On this level, the changes of the carrier population f_ν in the state with energy ε_ν due to carrier-carrier scattering are given by, see Sec. 5.4 and Eq. (5.53),

$$\begin{aligned}\frac{\partial}{\partial t} f_\nu \;=\; & \frac{2\pi}{\hbar} \sum_{\nu_1,\nu_2,\nu_3} W_{\nu\nu_2\nu_3\nu_1}[W^*_{\nu\nu_2\nu_3\nu_1} - W^*_{\nu\nu_2\nu_1\nu_3}] \\ & \times\big\{(1-f_\nu)f_{\nu_1}(1-f_{\nu_2})f_{\nu_3} \\ & \quad -f_\nu(1-f_{\nu_1})f_{\nu_2}(1-f_{\nu_3})\big\} \\ & \times\delta(\varepsilon_\nu - \varepsilon_{\nu_1} + \varepsilon_{\nu_2} - \varepsilon_{\nu_3}). \end{aligned} \tag{7.1}$$

Two carriers are scattered out of states ν_1 and ν_3 into states ν and ν_2 and vice versa. Scattering into a state ν is proportional to the nonoccupation of that state $(1-f_\nu)$ while scattering out of this state depends on the population f_ν. Accordingly, the second and third line of Eq. (7.1) determine the availability of scattering partners. Since the scattering involves identical fermions, the scattering cross section is determined by screened Coulomb matrix elements for the direct and exchange interaction, $|W_{\nu\nu_2\nu_3\nu_1}|^2$ and $W_{\nu\nu_2\nu_3\nu_1}W^*_{\nu\nu_2\nu_1\nu_3}$, respectively. The total rate involves the sum over all possible scattering states ν_1, ν_2, ν_3. The delta-function in the last line of Eq. (7.1) ensures energy conservation.

7.1.2 Wave Functions and Coulomb Matrix Elements

The interaction matrix elements of the bare Coulomb potential $v(\mathbf{r}-\mathbf{r}')$,

$$V_{\nu\nu_2\nu_3\nu_1} = \int d^3r\, d^3r' \Phi^*_\nu(\mathbf{r})\Phi^*_{\nu_2}(\mathbf{r}')v(\mathbf{r}-\mathbf{r}')\Phi_{\nu_3}(\mathbf{r}')\Phi_{\nu_1}(\mathbf{r}), \tag{7.2}$$

contain the single-particle wave functions $\Phi_\nu(\mathbf{r})$ of electrons and holes in the confinement potential of the combined QD-WL system. It is a complicated task on its own and beyond the scope of this chapter to compute these single-particle states for a given confinement situation that depends on the QD geometry, the strain profile and possible composition variations within the QD.

As a simple model for the QD confinement, the wave functions within a three-dimensional box with infinitely high walls have been used in Ref. [7.10] to compute the Coulomb interaction matrix elements. Wojs et al. [7.11] have shown that for lens-shaped QDs on a WL with a QD height small in comparison to the QD diameter the in-plane component of the QD wave functions resembles in good approximation that of a two-dimensional harmonic oscillator. In the following we adopt this model for the (weak) in-plane confinement while for the (strong) confinement in the direction perpendicular to the WL a finite-height potential barrier will be used. To account for a finite energetic height of the QD confinement potential only localized states within a given energy range are considered.

In a WL devoid of QDs the states would be described by plane waves for the in-plane part, multiplied by the state corresponding to the finite-height barrier confinement for the perpendicular direction. In the presence of the QDs this picture still holds as a good approximation far away from the dots. Close to the QDs however strong perturbations are expected, mainly due to the orthogonality requirement which brings in additional oscillations. Commonly [7.10, 7.12] this situation is described by using the orthogonalized plane wave (OPW) scheme, summarized in Appendix A.

We consider an ensemble of identical QDs and assume that the states of different QDs are non-overlapping. This is true for low QD densities where the mean QD spacing is much larger than the confinement length of the oscillator states. Another instance of interaction between QDs is provided by the Coulomb matrix elements. As shown below some scattering channels may, in principle, involve localized states belonging to different QDs. Nevertheless, these processes are limited to QDs less than a screening length apart. Considering a regime where the screening length is much smaller than the mean QD distance (sufficientlly high carrier densities and/or sufficiently dilute QDs) no such interaction takes place. The theory can of course be extended beyond this regime of parameters, but this will not be done here.

The advantage of the discussed approximation scheme is that for all possible combinations of QD and WL states the Coulomb matrix elements can be determined to a large extent analytically. For a WL extending in the x-y-plane the separation of the wave function into in-plane and z-components takes the form

$$\Phi_\nu(\mathbf{r}) = \varphi_l^b(\boldsymbol{\varrho})\ \xi_\sigma^b(z)\ u_b(\mathbf{r}) \tag{7.3}$$

where $u_b(\mathbf{r})$ are Bloch functions. The quantum numbers for the in-plane and z-components of the wave functions, l and σ, respectively, as well as the band index $b = e, h$ for electrons and holes are combined in ν. With the help of the Fourier transform of the Coulomb potential, this factorization of the wave functions can be used to introduce in-plane Coulomb matrix elements with the two-dimensional momentum $\mathbf{q}$,

$$\begin{aligned} V^{b,b'}_{\sigma\sigma_2\sigma_3\sigma_1}(\mathbf{q}) = \frac{e^2}{2\varepsilon_0 q} \int dz\ dz' \\ \xi^b_\sigma(z)^* \xi^{b'}_{\sigma_2}(z')^* e^{-q|z-z'|} \xi^{b'}_{\sigma_3}(z') \xi^b_{\sigma_1}(z) \end{aligned} \tag{7.4}$$

and Eq. (7.2) can be cast into the form

$$\begin{aligned} V_{\nu\nu_2\nu_3\nu_1} \quad = \quad & \frac{1}{A} \sum_{\mathbf{q}} V^{b,b_2}_{\sigma\sigma_2\sigma_3\sigma_1}(\mathbf{q})\, \delta_{b,b_1} \delta_{b_2,b_3} \\ & \times \int d^2\varrho\ \varphi^b_l(\boldsymbol{\varrho})^* \varphi^{b_1}_{l_1}(\boldsymbol{\varrho})\ e^{-i\mathbf{q}\cdot\boldsymbol{\varrho}} \\ & \times \int d^2\varrho'\ \varphi^{b_2}_{l_2}(\boldsymbol{\varrho}')^* \varphi^{b_3}_{l_3}(\boldsymbol{\varrho}')\ e^{i\mathbf{q}\cdot\boldsymbol{\varrho}'}. \end{aligned} \tag{7.5}$$

It is seen that the in-plane space integrals over $\boldsymbol{\varrho}$ and $\boldsymbol{\varrho}'$ get separated, one involving the pair formed by the first and the last state, the other the pair formed by the second and the third state of the Coulomb matrix element. In the envelope function approximation, only pairs having the same band index ($b = b_1$ and $b_2 = b_3$) contribute.

While the above discussion is given for matrix elements of the bare Coulomb potential $V_{\nu\nu_2\nu_3\nu_1}$, the kinetic equation (7.1) contains screened Coulomb matrix elements $W_{\nu\nu_2\nu_3\nu_1}$. Within the approximations outlined in Appendix 7.C screening due to WL carriers is included by multiplying Eq. (7.4) with a generalized quasi-two-dimensional inverse longitudinal dielectric function.

For the discrete QD states, the in-plane quantum numbers are $l = (n, m)$ where $n = 0, 1, 2, ...$ determines the energy (s,p,d,... shell). In case of a two-dimensional harmonic confinement we have $E^b_n = (n+1)E^b_{QD}$ for the QD energies where E^b_{QD} is the constant energy spacing between the shells. The second quantum number $m = -n, -n+2, ..., n-2, n$ characterizes the two-dimensional angular momentum. For QDs with confined s and p shell, these states are schematically shown in Fig. 7.1. For the quasi-continuum of

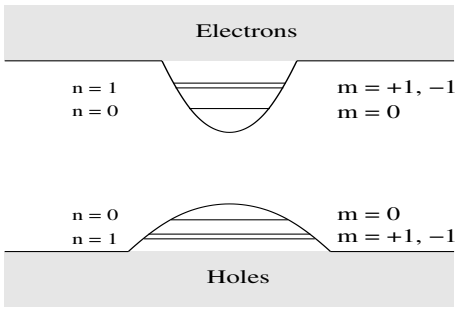

Figure 7.1: Schematic drawing of energy levels in the quantum-dot (QD) on wetting-layer (WL) system. The quasi-continuum of WL states (grey area) has larger interband transition energies than the discrete QD states labeled with the shell index n and the two-dimensional angular momentum m. The energetically degenerate states $m = \pm 1$ are visualized by two separated lines.

WL states, the two-dimensional carrier momentum will be used as in-plane quantum numbers.

7.1.3 Classification of Scattering Processes

The physical content of Eq. (7.1) will be more transparent if we decompose the summation over all quantum numbers ν_1, ν_2, ν_3 into subclasses. This grouping will depend upon whether a given state in the summation belongs to the extended WL or localized QD states. To indicate the particular choice, ν will be replaced for QD states by the quantum number m (n is redundant as long as only s- and p-shells are considered) and the WL states are labeled by the in-plane momentum $\boldsymbol{k}$. The band indices of population functions f and energies ε will be explicitly given, all other quantum numbers are suppressed for notational simplicity.

For the three quantum numbers ν_1, ν_2, ν_3 in the kinetic equation (7.1) we find eight combinations between WL and QD states. In the following we discuss the changes of the QD population in the state $\nu = m$.

When extended WL states are used for the quantum numbers $(\nu_1, \nu_2, \nu_3) = (\boldsymbol{k}_1, \boldsymbol{k}_2, \boldsymbol{k}_3)$, the corresponding scattering rate of the kinetic equation describes carrier transitions between the WL and the QD state by means of other carriers scattered within the WL. Figures 7.2 (a) and (b) show examples for the capture of electrons from the WL to the first excited QD state by means of scattering another electron or hole within the WL. The summation of all processes of this type which contribute to the RHS of Eq. (7.1)

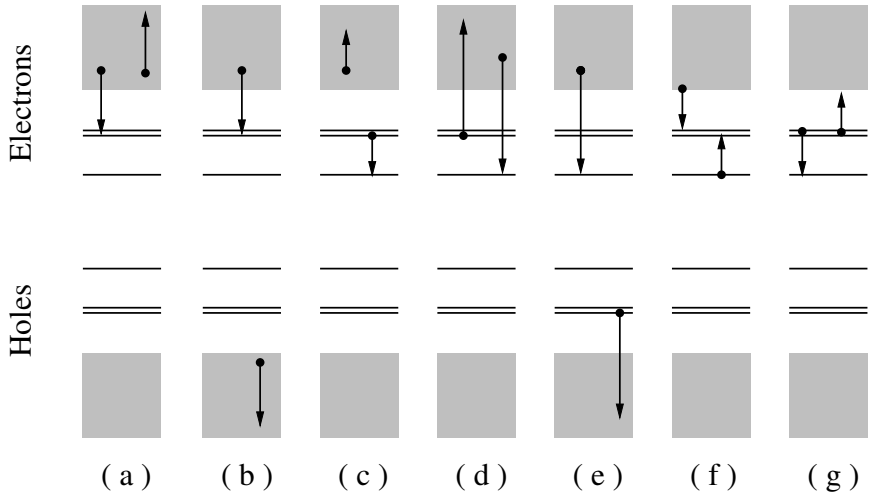

Figure 7.2: Examples of scattering processes: (a) and (b) capture of electrons. (c) relaxation process $S^{(1)}$ for electrons. (d) relaxation process $S^{(2)}$ for electrons. (e) mixed relaxation processes. (f) capture and (g) relaxation process $S^{(3)}$ assisted by QD carriers. The grey areas schematically show the energetic continua for delocalized states of electrons or holes while the three lines correspond to localized states.

is given by

$$\begin{aligned} S^{cap}_{b,m} &= \frac{2\pi}{\hbar} \sum_{\boldsymbol{k}_1,\boldsymbol{k}_2,\boldsymbol{k}_3,b'} \delta(\varepsilon^b_m - \varepsilon^b_{\boldsymbol{k}_1} + \varepsilon^{b'}_{\boldsymbol{k}_2} - \varepsilon^{b'}_{\boldsymbol{k}_3}) \\ &\times W_{m\boldsymbol{k}_2\boldsymbol{k}_3\boldsymbol{k}_1} \left[2\, W^*_{m\boldsymbol{k}_2\boldsymbol{k}_3\boldsymbol{k}_1} - \delta_{b,b'} W^*_{m\boldsymbol{k}_2\boldsymbol{k}_1\boldsymbol{k}_3}\right] \\ &\times \left\{ (1-f^b_m) f^b_{\boldsymbol{k}_1} (1-f^{b'}_{\boldsymbol{k}_2}) f^{b'}_{\boldsymbol{k}_3} - (f \to 1-f) \right\}. \end{aligned} \tag{7.6}$$

The first term in the third line of Eq. (7.6) accounts for the scattering out of states $\boldsymbol{k}_1$ and $\boldsymbol{k}_3$ into m and $\boldsymbol{k}_2$ which increases the QD population. These processes are balanced with the reverse scattering events described by the second term in the third line of Eq. (7.6). Hence the net change of the QD population depends on the filling factors in both subsystems. In the following, we refer to this class of scattering events as *capture* processes.

Assuming that the WL population is independent of the carrier spin, the spin summation leads to a factor of two in the direct scattering term in the second line of Eq. (7.6). Note that the exchange term does not contribute for electron-hole scattering.

The summation over the scattering processes in Eq. (7.1) containing the matrix elements $W_{m\boldsymbol{k}_1\boldsymbol{k}_2m_3}$ and $W_{m\boldsymbol{k}_1m_2\boldsymbol{k}_3}$ can be decomposed into four separate groups of which three correspond to a redistribution of carriers between different QD levels (in the following called QD *relaxation*) by means

of other WL carriers as shown in Fig. 7.2 (c) and (d). The last group represents *mixed* scattering processes where, e.g., a hole is scattered out of a QD state into the WL while an electron is scattered from the WL into the QD, see Fig. 7.2 (e).

The relaxation processes can be grouped in the following way: $S_\nu^{relax} = S_{b,m}^{1D} + S_{b,m}^{2D} - S_{b,m}^{12X}$. Here

$$\begin{aligned} S_{b,m}^{1D} &= \frac{2\pi}{\hbar} \sum_{m_1,\boldsymbol{k}_2,\boldsymbol{k}_3,b'} 2\,|W_{m\boldsymbol{k}_2\boldsymbol{k}_3 m_1}|^2 \\ &\quad \times\{\ (1-f_m^b) f_{m_1}^b (1-f_{\boldsymbol{k}_2}^{b'}) f_{\boldsymbol{k}_3}^{b'} - (f \to 1-f)\ \} \\ &\quad \times \delta(\varepsilon_m^b - \varepsilon_{m_1}^b + \varepsilon_{\boldsymbol{k}_2}^{b'} - \varepsilon_{\boldsymbol{k}_3}^{b'}) \end{aligned} \tag{7.7}$$

contains the direct Coulomb interaction for scattering of QD carriers between levels m and m_1 by means of scattering either electrons or holes within the WL between states $\boldsymbol{k}_2$ and $\boldsymbol{k}_3$.

A redistribution of carries within the QD also takes place when a carrier from the QD scatters to the WL while another carrier from a different WL state scatters back to a different QD level. Such a process is for electrons depicted in Fig. 7.2 (d). The summation of all processes of this type due to direct Coulomb interaction is given by

$$\begin{aligned} S_{b,m}^{2D} &= \frac{2\pi}{\hbar} \sum_{m_1,\boldsymbol{k}_2,\boldsymbol{k}_3} 2\,|W_{m\boldsymbol{k}_2 m_1 \boldsymbol{k}_3}|^2 \\ &\quad \times\{\ (1-f_m^b) f_{\boldsymbol{k}_3}^b (1-f_{\boldsymbol{k}_2}^b) f_{m_1}^b - (f \to 1-f)\ \} \\ &\quad \times \delta(\varepsilon_m^b - \varepsilon_{\boldsymbol{k}_3}^b + \varepsilon_{\boldsymbol{k}_2}^b - \varepsilon_{m_1}^b). \end{aligned} \tag{7.8}$$

The Coulomb exchange contributions to the scattering processes described in Eqs. (7.7) and (7.8) can be combined to

$$\begin{aligned} S_{b,m}^{12X} &= \frac{2\pi}{\hbar} \sum_{m_1,\boldsymbol{k}_2,\boldsymbol{k}_3} 2\,\mathrm{Re}\left[W_{m\boldsymbol{k}_2\boldsymbol{k}_3 m_1} W^*_{m\boldsymbol{k}_2 m_1 \boldsymbol{k}_3}\right] \\ &\quad \times\{\ (1-f_m^b) f_{m_1}^b (1-f_{\boldsymbol{k}_2}^b) f_{\boldsymbol{k}_3}^b - (f \to 1-f)\ \} \\ &\quad \times \delta(\varepsilon_m^b - \varepsilon_{m_1}^b + \varepsilon_{\boldsymbol{k}_2}^b - \varepsilon_{\boldsymbol{k}_3}^b). \end{aligned} \tag{7.9}$$

Finally we have so-called mixed scattering processes where, e.g., an electron is captured from the WL into a QD state by means of a hole which is scattered from a QD into the WL. Since the capture is typically faster for holes as will be discussed below, this process can be important to increase the electron capture with the help of already captured holes. The scattering

rate is given by

$$\begin{aligned} S^{mixed}_{e,m} &= \frac{2\pi}{\hbar} \sum_{m_1,\boldsymbol{k}_2,\nu_1,\boldsymbol{k}_3} 2\,|W_{m\boldsymbol{k}_2 m_1 \boldsymbol{k}_3}|^2 \\ &\quad \times \big\{\, (1-f^e_m) f^e_{\boldsymbol{k}_3} (1-f^h_{\boldsymbol{k}_2}) f^h_{m_1} - (f \to 1-f) \,\big\} \\ &\quad \times \delta(\varepsilon^e_m - \varepsilon^e_{\boldsymbol{k}_3} + \varepsilon^h_{\boldsymbol{k}_2} - \varepsilon^h_{m_1}) \end{aligned} \tag{7.10}$$

and similarly for the holes with $(e \leftrightarrow h)$.

The scattering processes discussed so far describe capture and relaxation *assisted by WL carriers*. Another class involves transitions of carriers *assisted by QD carriers*. Requirements for these processes are more restrictive since i) the scattering partners provide only discrete energies which limits the range of possible transitions, and ii) populated initial and (sufficiently) unpopulated final states in the QD have to be available. As shown in the next section, efficient capture and relaxation processes can be provided even under quasi-equilibrium conditions for intermediate carrier densities.

Capture processes assisted by QD carriers are described by

$$\begin{aligned} S^{cap'}_{b,m} &= \frac{2\pi}{\hbar} \sum_{\boldsymbol{k}_1,m_2,m_3,b'} \delta(\varepsilon^b_m - \varepsilon^b_{\boldsymbol{k}_1} + \varepsilon^{b'}_{m_2} - \varepsilon^{b'}_{m_3}) \\ &\times \; W_{mm_2m_3\boldsymbol{k}_1} \left[2\, W^*_{mm_2m_3\boldsymbol{k}_1} - \delta_{b,b'} W^*_{mm_2\boldsymbol{k}_1 m_3} \right] \\ &\times \; \big\{\, (1-f^b_m) f^b_{\boldsymbol{k}_1} (1-f^{b'}_{m_2}) f^{b'}_{m_3} - (f \to 1-f) \,\big\}. \end{aligned} \tag{7.11}$$

The first term in the third line accounts for the scattering out of states $\boldsymbol{k}_1$ into the state m assisted by carriers scattered from states m_3 into m_2 which increases the QD population, see Fig. 7.2 (f). Again balancing occurs with the reverse processes described by the second term of the third line. For processes involving solely electrons (or holes), energy conservation allows only capture from the WL to the excited QD states.

Relaxation processes assisted by QD carriers can be obtained from

$$\begin{aligned} S^{3DX}_{b,m} &= \frac{2\pi}{\hbar} \sum_{m_1,\boldsymbol{k}_2,m_3,b'} \delta(\varepsilon^b_m - \varepsilon^b_{m_1} + \varepsilon^{b'}_{\boldsymbol{k}_2} - \varepsilon^{b'}_{m_3}) \\ &\times \; W_{m\boldsymbol{k}_2 m_3 m_1} \left[2\, W^*_{m\boldsymbol{k}_2 m_3 m_1} - \delta_{b,b'} W^*_{m\boldsymbol{k}_2 m_1 m_3} \right] \\ &\times \; \big\{\, (1-f^b_m) f^b_{m_1} (1-f^{b'}_{\boldsymbol{k}_2}) f^{b'}_{m_3} - (f \to 1-f) \,\big\}. \end{aligned} \tag{7.12}$$

Assuming that m and m_1 label energetically lower and higher QD energies, respectively, carrier relaxation between these states takes place by means of another QD carrier m_3 scattered into the WL state $\boldsymbol{k}_2$, see Fig. 7.2 (g). In a situation where carrier capture is more efficient for excited QD states, this process is espected to contribute to the carrier relaxation within the QD.

There is yet another combination of QD and WL states contributing to QD-assisted processes,

$$\begin{aligned} S^{4DX}_{b,m} &= \frac{2\pi}{\hbar} \sum_{m_1,m_2,\boldsymbol{k}_3,b'} \delta(\varepsilon^{b}_{m} - \varepsilon^{b}_{m_1} + \varepsilon^{b'}_{m_2} - \varepsilon^{b'}_{\boldsymbol{k}_3}) \\ &\times W_{mm_2\boldsymbol{k}_3m_1} \left[2\, W^{*}_{mm_2\boldsymbol{k}_3m_1} - \delta_{b,b'} W^{*}_{mm_2m_1\boldsymbol{k}_3} \right] \\ &\times \left\{ (1-f^{b}_{m}) f^{b}_{m_1} (1-f^{b'}_{m_2}) f^{b'}_{\boldsymbol{k}_3} - (f \to 1-f) \right\}, \end{aligned} \tag{7.13}$$

which describes, e.g., the carrier depletion of the excited QD states in connection with the relaxation processes of Eq. (7.12) or a transition into an excited QD state due to the assisting scattering partner for a capture processes of Eq. (7.11). It should be noted that the out-scattering events of Eqs. (7.11) and (7.13) are directly related to the in-scattering processes of Eq. (7.12) and vice versa. However, the rates contain summations over different states and different filling factors contribute to the scattering times introduced below.

In the notation of Eqs. (7.11)-(7.13) we assume that for the processes $b{=}b'{=}e,h$ only $\boldsymbol{k}=0$ WL states contribute (see below). Then non-vanishing Coulomb matrix elements are only obtained for different angular-momentum states of the two involved p-shell carriers. In this case both spin combinations of the assisting carriers are allowed which leads to the factor of two in the direct Coulomb terms. When other WL states are involved and two p-shell carriers in the same angular-momentum states contribute, this factor and the exchange term need to be removed.

Scattering contributions involving the following Coulomb matrix elements are left out: $W_{m\,m_1\,m_2\,m_3}$ corresponds to internal QD scattering and energy conserving processes do not change the population while terms containing $W_{m\,m_1\,\boldsymbol{k}_2\,\boldsymbol{k}_3}$ cannot fulfill the energy conservation given by the delta function.

For the single-particle energies entering the scattering integrals, renormalization due to Coulomb interaction has been neglected. Energy shifts of several meV have been calculated for the (bare) Coulomb interaction of few carriers in a QD. The aim of this chapter is, however, the description of the laser regime with a large carrier density in the WL. Efficient screening of WL carriers is expected to reduce the Coulomb shifts. One could argue that for nearby carriers (confined to the same QD) screening due to WL carriers is less efficient, but this has to be put in relation to the high WL carrier density we aim at. Simple Hartree-Fock energy renormalizations are known to strongly overestimate the energy shifts under high excitation conditions. Calculations beyond this level are an area of ongoing research in the field of quantum kinetics and beyond the scope this chapter.

7.1.4 Model System

For the numerical results presented in this chapter we consider an InGaAs QD-WL system. Parabolic dispersion are assumed for conduction and valence bands with effective masses $m_e = 0.067m_0$ and $m_h = 0.15m_0$, respectively, and the dielectric constant $\varepsilon = 12.5$. Unless otherwise noted, a 2.2 nm WL thickness and 2.1 nm additional QD height are used. The finite height of the confinement potential for electrons and holes is taken to be 350 meV and 170 meV, respectively, such that equal z-confinement wave functions $\xi^b_\sigma(z)$ for electrons and holes can be adopted.

For a small WL thickness and QD height the energy spacing of the subbands and sub-levels due to confinement in z-direction is large and only the lowest quantum number σ will be considered.

Furthermore, we assume that the harmonic confinement potential leads to equal QD in-plane wave functions for electrons and holes. Different electron and hole masses then result in different level energies. We investigate QDs where the (double degenerate) ground state and the (four-fold degenerate) first excited state are confined. The energies of the ground state for electrons (holes) are 80meV (30meV) and for the first excited state 40 meV (15meV) below the continuum of the WL. A density of QDs $n_{dot} = 10^{10}$ cm^{-2} entering the OPW procedure discussed in Appendices 7.A and 7.B will be used. Then, for the combined QD-WL system in thermodynamic equilibrium at 300 K, inversion of the lowest QD state as a precondition for optical gain is realized when the WL carrier density exceeds 1.3×10^{11} cm^{-2}.

7.2 Results for Coulomb Scattering

7.2.1 Equilibrium Scattering Rates

As a general property, for any initial carrier distribution function the combined action of the discussed scattering processes will evolve the distribution functions of electrons and holes towards Fermi-Dirac functions where the QD and WL electrons and correspondingly the holes will have the same chemical potential μ_e and μ_h, respectively.

During such a time evolution towards equilibrium the relative importance of various scattering processes is expected to change via their dependence on the (nonequilibrium) carrier distribution functions for WL and QD states. To uniquely compare the influence of various processes, we assume that an equilibrium situation (at 300 K) has been reached and study the dependence of the scattering processes on the WL carrier density.

Equation (7.1) can be cast into the form

$$\frac{\partial}{\partial t} f_\nu \;=\; (1 - f_\nu) S^{in}_\nu - f_\nu S^{out}_\nu, \tag{7.14}$$

and based on the above classification we analyze in detail the in- and out-scattering rates, S_ν^{in} and S_ν^{out}, for capture, relaxation, and mixed processes.

In Fig. 7.3 the scattering rates for the electron and hole capture processes are shown. First we discuss results for the capture assisted by WL carriers. In-scattering becomes more efficient for increasing WL carrier density. The same applies to out-scattering up to intermediate WL carrier densities. In both cases the scattering rate increases due to the larger population of available scattering partners. When the population of the energetically lower WL states approaches unity, Pauli blocking starts to reduce the out-scattering, i.e., the reverse of the processes schematically depicted in Figs. 7.2 (a) and (b), due to the reduction of available final states. The population factors might still allow WL carriers at higher energies to assist the QD-WL scattering. Their contribution is, however, strongly reduced due to the Gaussian decay of the Coulomb interaction matrix elements with the WL carrier momenta.

Processes assisted by QD carriers are only important in an intermediate density range and are typically weaker than the processes assisted by WL carriers. For low carrier densities the initial states of the assisting scattering partners are not populated and for higher carrier densities Pauli blocking prevents scattering into possible final QD states. (Note that we assume a quasi-equilibrium situation for the coupled QD-WL system.) For the used level spacing, energy conservation does not allow electron capture to the s-shell by means of QD electrons or holes while capture of holes to the s-shell is possible by means of QD electrons.

Generally, the processes related to the QD ground states are slower than those for the first excited QD states since the larger energy difference requires WL carriers with larger momenta which again leads to smaller Coulomb interaction matrix elements. For the same reason, the corresponding scattering rates for holes are larger than for electrons. In earlier references, exchange contributions to the scattering rates are often omitted. For processes assisted by WL carriers curves without exchange interaction exhibit a similar shape but results are overestimated by about 20% (10%) for the p(s)-shell, respectively. For processes assisted by QD carriers direct and (possible) exchange Coulomb matrix elements are equal. Hence, contributing exchange terms reduce the scattering rates for these channels by 50%.

The scattering rates for various relaxation processes are shown in Fig. 7.4. In- and out-scattering refer to the QD ground states. When the relaxation processes involve only two (degenerate) confined levels, the corresponding out-scattering rate for the ground state equals the in-scattering rate due to relaxation for the excited state and vice versa.

Processes assisted by WL and QD carriers will be discussed separately. Regarding the first class, the qualitative behavior of the WL carrier density dependence for in- and out-scattering is similar to the capture processes for the reasons discussed above. In all cases S^{1D} provides the dominant

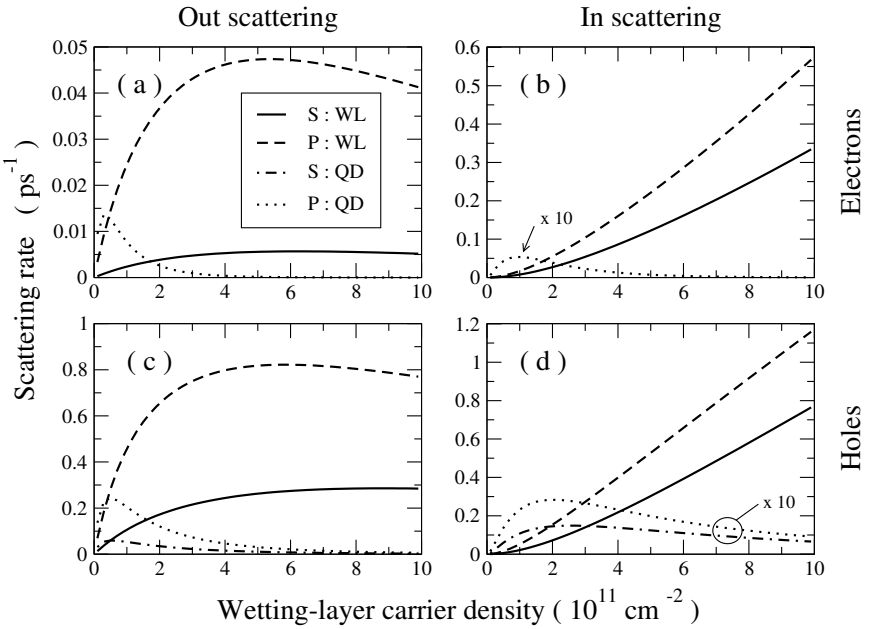

Figure 7.3: Scattering rates for capture processes to QD ground states (solid and dashed-dotted lines: assisted by WL and QD carriers, respectively) and to first excited states (dashed and dotted lines: assisted by WL and QD carriers, respectively) for electrons (a,b) and holes (c,d) as a function of the carrier density in the WL at 300 K. In-scattering rates for processes assisted by QD carriers are scaled up for better visibility.

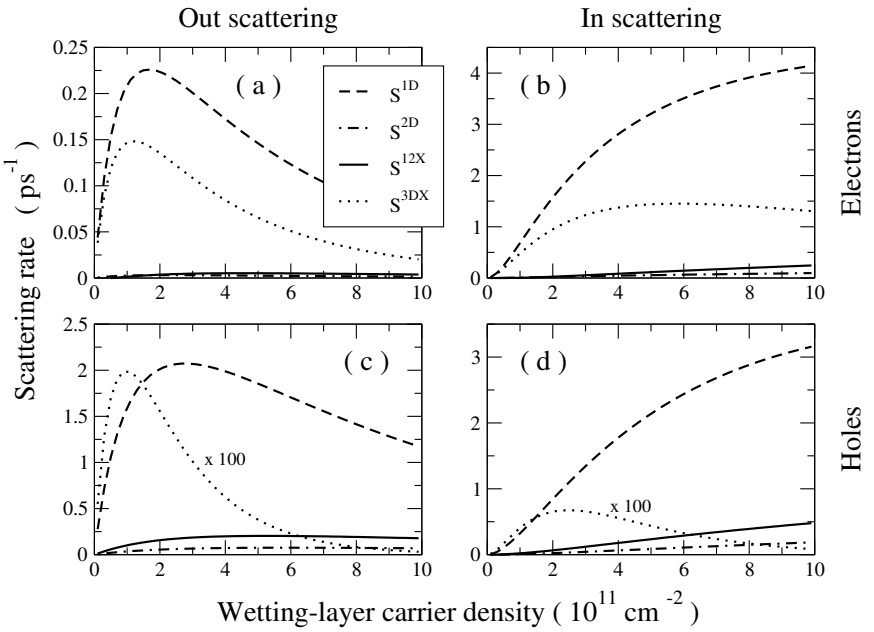

Figure 7.4: Scattering rates for QD carrier relaxation processes according to Eqs. (7.7)-(7.9) and (7.12). (a) and (c) represent scattering out of the QD ground state into the QD excited states while (b) and (d) show results for the reverse processes.

contribution while S^{2D} and S^{12X} are much smaller. Since S^{2D} and S^{12X} contribute with opposite sign, they partly compensate each other. The S^{1D} relaxation rates dominate mainly because the Coulomb interaction matrix elements make it more favorable to scatter between two QD carriers assisted by a transition between two WL carriers, in comparison to two coupled transitions between QD and WL carriers. Furthermore, S^{1D} also contains electron-hole scattering which does not contribute to S^{2D} and S^{12X}.

For the comparison of scattering rates of electrons and holes, two counteracting contributions need to be considered. The energy spacing between QD states is smaller for holes which increases their scattering rates. The smaller population of holes due to their larger effective mass, on the other hand, decreases their in-scattering rate and increases their out-scattering rate. As a result, the in-scattering rates of electrons and holes are comparable while the out-scattering rates are larger for holes.

The relaxation processes assisted by QD carriers require a rather detailed discussion. The rates depend more strongly on the QD energy spacing in comparison to the energetic distance of the excited QD states from the WL continuum. For the used example, relaxation of electrons assisted by QD electrons (ditto for holes) according to Eq. (7.12) involves only the $\boldsymbol{k} = 0$ WL

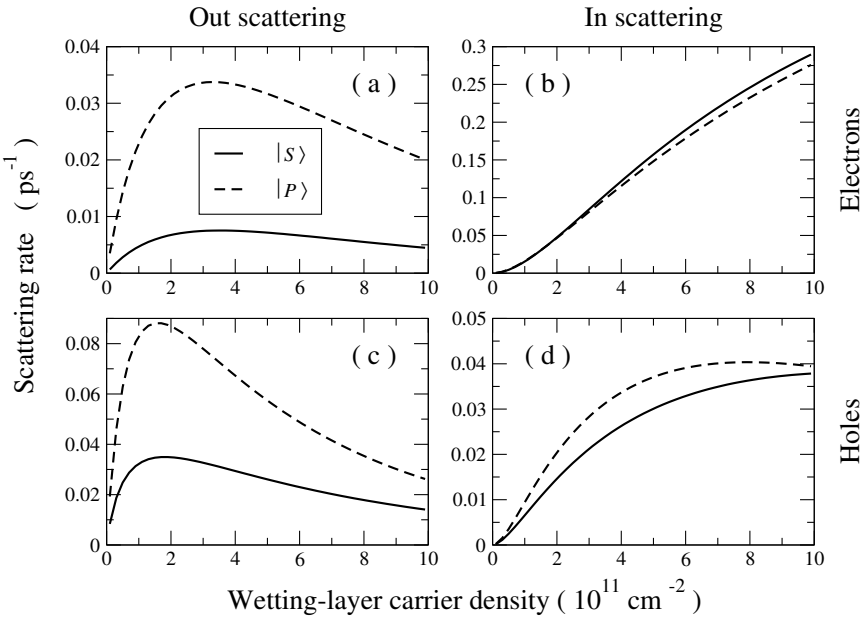

Figure 7.5: Rates for mixed scattering processes. (a) and (b) show electron in- and out-scattering while (c) and (d) are hole in- and out-scattering, respectively.

state. This requires p-shell carriers in opposite angular-momentum states for m_1 and m_3 to obtain nonvanishing Coulomb matrix elements. On the other hand, electron relaxation assisted by holes allows $\boldsymbol{k} \neq 0$ and also the same angular-momentum states for m_1 and m_3 contribute. The corresponding Coulomb matrix elements can be up to an order of magnitude larger (in comparison to the $\boldsymbol{k} = 0$ matrix elements) depending on the involved WL momentum. Hence, the large rate S^{3DX} for electrons is due to efficient e-h scattering while energy conservation does not allow h-e contributions to the hole relaxation and the h-h process involving $\boldsymbol{k} = 0$ is weak. While this situation clearly changes with different spacing of the excited QD states from the WL continuum, the obtained relaxation rates for electrons and holes can be considered as limiting cases (other choices for the QD energy levels are typically in between these extremes).

In Fig. 7.5 the mixed scattering rates are shown in the same notation used in Fig. 7.4. Finding the same WL carrier-density dependence as above, we notice however that in-scattering processes are faster for electrons than for holes. Scattering an electron from the bottom of the WL into the QD ground-state, as schematically shown in Fig. 7.2 (e), puts a QD hole far up in the valence band WL (where the final state population is small) due to the larger QD confinement energy for electrons. The probability for the reverse

process (hole in-scattering) is strongly reduced due to the small initial-state population for holes and large final-state population for electrons.

7.2.2 Equilibrium Capture and Relaxation Times

In- or out-scattering rates alone determine the population changes of the considered QD states when these states are completely empty or completely populated, respectively, as can be seen from Eq. (7.14). On the other hand, when all QD and WL states are in thermodynamic equilibrium with Fermi-Dirac distribution functions F_ν, characteristic scattering times τ_ν can be introduced in response to small perturbations δf_ν. Solving the kinetic equation (7.14) for a carrier distribution function $f_\nu = F_\nu + \delta f_\nu$ we assume that the influence of δf_ν on the scattering rates S_ν^{in} and S_ν^{out} can be neglected:

$$\frac{\partial}{\partial t} f_\nu = -\frac{f_\nu - F_\nu}{\tau_\nu}, \qquad \frac{1}{\tau_\nu} = \left(S_\nu^{\text{in}} + S_\nu^{\text{out}}\right)\Big|_{F_\nu}. \tag{7.15}$$

(For example, when f_ν and F_ν correspond to the same total carrier density, δf_ν is a symmetric perturbation which tends to averages out in the scattering integrals.) Then the inverse of the scattering time τ_ν is given by the sum of in- and out-scattering rates calculated with the RHS of Eq. (7.1) using Fermi-Dirac functions, i.e., the scattering rates discussed in the previous subsection. The scattering time τ_ν determines the evolution back to equilibrium.

In Fig. 7.6 (a) capture times calculated from the in- and out-scattering rates of Eq. (7.6) are shown, Fig. 7.6 (b) contains the relaxation times according to Eqs. (7.7)-(7.9). The decreasing scattering times for increasing WL carrier density and the relative magnitude of the displayed capture and relaxation processes can be directly traced back to the above given detailed discussion of the scattering rates. The nearly constant hole relaxation time for WL carrier densities between 4×10^{11} and 10^{12} cm^{-2} is a result of the interplay of filling factors leading to a decreasing out-scattering rate and increasing in-scattering rate shown in Fig. 7.4.

As a function of carrier density the capture processes assisted by QD carriers, Fig. 7.7 (a), initially dominate in comparison to the WL assisted ones in a range where both types of processes are slow. For intermediate to high carrier densities processes assisted by WL carriers provide the main capture channels. Results in Fig. 7.7 (b) show only slightly smaller efficiency for the electron relaxation assisted by QD carriers in comparison to WL assisted processes. However, the values in Fig. 7.7 (b) depend on the QD-QD vs. QD-WL energy spacing. For other parameters, relaxation of holes can be as fast as for electrons but times are typically larger than for relaxation assisted by WL carriers.

The computed scattering times suggest the following dynamical scenario for the chosen material system. WL carriers are dominantly captured to

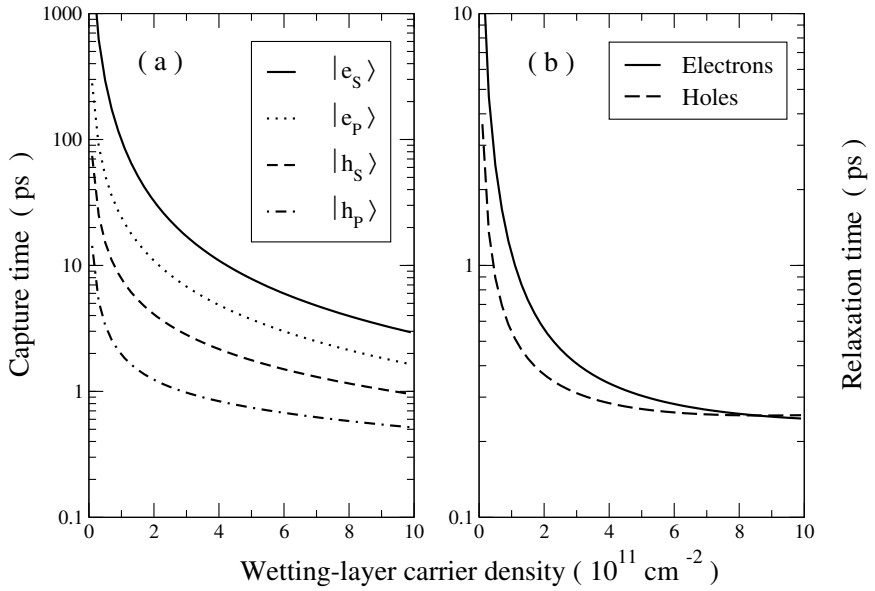

Figure 7.6: Scattering times for processes assisted by WL carriers. (a) Capture times for WL carriers to the QD ground states $|e_S\rangle$ and first excited states $|e_P\rangle$ for electrons and correspondingly for holes. (b) Relaxation times for carrier scattering from first excited states to ground states. The temperature is 300 K. Different axis scaling for capture and relaxation times should be noted.

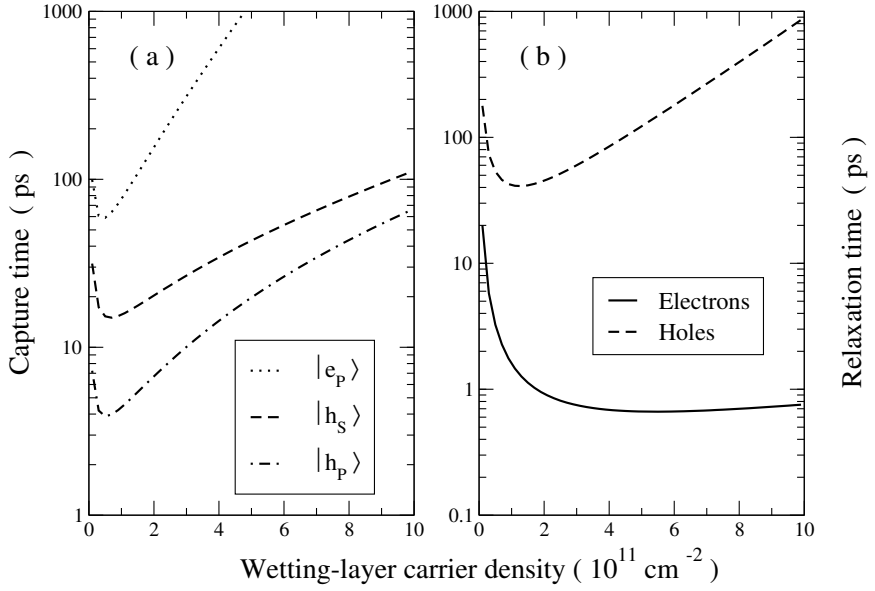

Figure 7.7: Same as Fig. 7.6 but for processes assisted by QD carriers.

the excited states. Filling of the QD ground states occures on almost the same time scale due to fast relaxation of carriers within the QD. Electronic capture processes are an order of magnitude slower than the corresponding processes for holes. Direct capture to the hole QD ground states also weakly contributes while direct capture to the electron QD ground state can be neglected for the considered large energy difference between the electron QD ground state and the WL.

7.3 Conclusion

We have discussed in- and out-scattering rates as well as scattering times for capture and relaxation processes in the QD-WL system. In general, in- and out-scattering rates enter in a kinetic equation (7.14) from which the population dynamics for a given initial situation can be determined. The in-scattering rates solely describe the population changes as long as the final-state population can be neglected. This situation is closely connected to calculations based on Fermi's golden rule where fully populated initial states and empty final states are assumed. In an intermediate situation with existing final-state population, capture and relaxation processes will be less efficient due to Pauli blocking as well as out-scattering contributions. For completely filled states, the discussed out scattering rates solely determine the population losses.

On the other hand, the given scattering times characterize relaxation and capture processes under the assumption that *all* states are populated according to Fermi-Dirac statistics. The carriers in a laser operating under cw-conditions are typically near a quasi-equilibrium distribution. If, for example, the stimulated recombination depletes the lower QD states then the QD relaxation time determines the refilling of this state with carriers from the exited QD states and the capture times determine the refilling from the WL.

For the processes due to Coulomb interaction, relaxation within the QD is typically on a faster timescale than the carrier capture from the WL into the QD. Processes involving holes are typically faster than the corresponding processes involving electrons and capture to the excited states is faster than capture to the ground states. Hence in a dynamical scenario, first the holes are captured to the excited QD states and immediately scattered via relaxation to the QD ground states. Capture of electrons is somewhat slower, the subsequent relaxation for electrons is only slightly slower than for holes.

Depending on the density of QDs the capture and relaxation processes in turn will change the WL carrier distribution. Together with the different timescales of the discussed processes involving QD carriers, a nontrivial interplay in dynamical situations is expected.

One of the goals of the chapter is to study the influence of terms often neglected previously. In addition to the above summarized interplay of in- and out-scattering and scattering times it is shown that the Coulomb vertex contributions typically cannot be neglected in comparison to the direct Coulomb interaction. Scattering processes assisted by QD-carriers contribute especially at lower carrier densities and can add to the relaxation at higher densities. The use of WL wave functions properly orthogonalized to the QD states is found to be important for the evaluation of scattering rates. The relative contribution of OPW corrections depends on how the density of QDs enters. In the discussed Coulomb matrix elements for carrier capture and for relaxation (except in S^{1D}) the orthogonalization even contributes if one would have a single QD in an infinite system, i.e., for zero QD density. Results for these processes based on plane wave WL states can strongly deviate from OPW calculations. On the other hand, screening due to WL carriers is somewhat less influenced by OPW corrections since the derived generalized Lindhard formula for OPW states contains the PW result plus corrections starting in first power of the QD density. Essentially, screening is a "global" effect less influenced by a small number of QDs whereas processes in the QD depend on the "local" features of the wave function. Here the orthogonalization is more important, because it changes the wave function exactly in the region of the QD where the transitions take place.

7.A Orthogonalization Procedure

Our starting point for the constuction of wave functions are WL states in the absence of QDs, which are considered as plane-waves $\varphi^0_{\mathbf{k}}(\boldsymbol{\varrho}) = \frac{1}{\sqrt{A}} e^{i\mathbf{k}\cdot\boldsymbol{\varrho}}$ with two-dimensional carrier momentum $\mathbf{k}$. To describe the combined system we use plane waves orthogonalized to the QD states (OPW) [7.10, 7.12]

$$|\varphi_{\mathbf{k}}\rangle = \frac{1}{N_{\mathbf{k}}} \left(|\varphi^0_{\mathbf{k}}\rangle - \sum_{\alpha} |\varphi_\alpha\rangle\langle\varphi_\alpha\, |\varphi^0_{\mathbf{k}}\rangle \right) \tag{7.A.16}$$

where $N_{\mathbf{k}}$ is the normalization constant. The sum includes all localized states. In the following we assume an ensemble of identical, independent QDs with non-overlapping wave functions. Then $\alpha = (m, \boldsymbol{R})$ contains various QD states m at different QD positions $\boldsymbol{R}$. The QD states are thus mutually orthogonal $\langle\varphi_\alpha|\varphi_{\alpha'}\rangle = \delta_{\alpha,\alpha'}$.

By construction the OPW states for the WL are orthogonal to the QD states, $\langle\varphi_\alpha|\varphi_{\mathbf{k}}\rangle = 0$. To study the orthogonality of OPW states, we use

$$\begin{aligned}\langle\varphi_{\mathbf{k}}|\varphi_{\mathbf{k}'}\rangle = &\frac{1}{N_{\mathbf{k}} N_{\mathbf{k}'}} \Big(\langle\varphi^0_{\mathbf{k}}|\varphi^0_{\mathbf{k}'}\rangle \\ &- \sum_{\alpha} \langle\varphi^0_{\mathbf{k}}|\varphi_\alpha\rangle\langle\varphi_\alpha|\varphi^0_{\mathbf{k}'}\rangle \Big).\end{aligned} \tag{7.A.17}$$

As the plane wave overlap integrals with the QD states at different positions differ only by a phase factor, $\langle\varphi_\alpha\,|\varphi^0_{\mathbf{k}}\rangle = \int d^2\varrho\;\varphi_m(\boldsymbol{\varrho}-\boldsymbol{R})\;\varphi^0_{\mathbf{k}}(\boldsymbol{\varrho}) = \int d^2\varrho\;\varphi_m(\boldsymbol{\varrho})\;\varphi^0_{\mathbf{k}}(\boldsymbol{\varrho}+\boldsymbol{R}) \equiv \langle\varphi_m\,|\varphi^0_{\mathbf{k}}\rangle e^{i\mathbf{k}\cdot\boldsymbol{R}}$, we have

$$\langle\varphi_{\mathbf{k}}|\varphi_{\mathbf{k}'}\rangle = \frac{1}{N_{\mathbf{k}}N_{\mathbf{k}'}}\Big(\delta_{\mathbf{k},\mathbf{k}'} - \sum_{m,\boldsymbol{R}}\langle\varphi^0_{\mathbf{k}}|\varphi_m\rangle \times \langle\varphi_m|\varphi^0_{\mathbf{k}'}\rangle e^{i(\mathbf{k}'-\mathbf{k})\cdot\boldsymbol{R}}\Big). \tag{7.A.18}$$

The sum over $\boldsymbol{R}$ involves now only the phase factors. For randomly distributed QDs these phase factors will average to zero except for $\mathbf{k} = \mathbf{k}'$. More precisely, in the large area limit ($A \to \infty$ with the number of QDs $N \to \infty$ such that the QD density $n_{dot} = N/A$ remains constant) one has

$$\frac{1}{N}\sum_{\boldsymbol{R}} e^{i(\mathbf{k}'-\mathbf{k})\cdot\boldsymbol{R}} = \delta_{\mathbf{k},\mathbf{k}'}. \tag{7.A.19}$$

Hence, "on average", different OPW states are also orthogonal with the normalization

$$N_{\mathbf{k}} = \sqrt{1 - N\sum_m |\langle\varphi^0_{\mathbf{k}}|\varphi_m\rangle|^2}. \tag{7.A.20}$$

Using the normalization area A of the plane waves, the prefactor of the sum over the QD states is accordingly given by the QD density n_{dot}.

7.B Coulomb Matrix Elements

When the first and last or the second and third arguments of the Coulomb matrix elements belong to OPW states, the corresponding in-plane integrals in Eq. (7.5) can be explicitly calculated using Eq. (7.A.16):

$$\begin{aligned}\langle\varphi_{\mathbf{k}}|e^{i\mathbf{q}\cdot\boldsymbol{\varrho}}|\varphi_{\mathbf{k}'}\rangle = \frac{1}{N_{\mathbf{k}}N_{\mathbf{k}'}}\Big(&\langle\varphi^0_{\mathbf{k}}|e^{i\mathbf{q}\cdot\boldsymbol{\varrho}}|\varphi^0_{\mathbf{k}'}\rangle \\ &+ \sum_{\alpha,\alpha'}\langle\varphi^0_{\mathbf{k}}|\varphi_\alpha\rangle\langle\varphi_\alpha|e^{i\mathbf{q}\cdot\boldsymbol{\varrho}}|\varphi_{\alpha'}\rangle\langle\varphi_{\alpha'}|\varphi^0_{\mathbf{k}'}\rangle \\ &- \sum_{\alpha}\langle\varphi^0_{\mathbf{k}}|e^{i\mathbf{q}\cdot\boldsymbol{\varrho}}|\varphi_\alpha\rangle\langle\varphi_\alpha|\varphi^0_{\mathbf{k}'}\rangle \\ &- \sum_{\alpha}\langle\varphi^0_{\mathbf{k}}|\varphi_\alpha\rangle\langle\varphi_\alpha|e^{i\mathbf{q}\cdot\boldsymbol{\varrho}}|\varphi^0_{\mathbf{k}'}\rangle\Big).\end{aligned} \tag{7.B.21}$$

Again, in the large area limit the random QD distribution restores the translation invariance (momentum conservation) of the problem, and one obtains

$$\begin{aligned}\langle\varphi_{\mathbf{k}}|e^{i\mathbf{q}\cdot\boldsymbol{\varrho}}|\varphi_{\mathbf{k}'}\rangle &= \delta_{\mathbf{k}-\mathbf{q}-\mathbf{k}'}\ \frac{1}{N_{\mathbf{k}}N_{\mathbf{k}'}}\\ &\times\Big(1-N\sum_m|\langle\varphi^0_{\mathbf{k}}|\varphi_m\rangle|^2\\ &\quad -N\sum_m|\langle\varphi_m|\varphi^0_{\mathbf{k}'}\rangle|^2\\ &\quad +N\sum_{m,m'}\langle\varphi^0_{\mathbf{k}}|\varphi_m\rangle\langle\varphi_m|e^{i\mathbf{q}\cdot\boldsymbol{\varrho}}|\varphi_{m'}\rangle\langle\varphi_{m'}|\varphi^0_{\mathbf{k}'}\rangle\Big)\end{aligned} \tag{7.B.22}$$

where the remaining overlap integrals of localized QD wave functions and plane waves can be calculated analytically for harmonic oscillator states.

In the case when the pairing of the states in the Coulomb matrix elements involves one OPW state and one QD state the in-plane integrals in Eq. (7.5) lead to

$$\begin{aligned}\langle\varphi_\alpha|e^{i\mathbf{q}\cdot\boldsymbol{\varrho}}|\varphi_{\mathbf{k}}\rangle &= \frac{1}{N_{\mathbf{k}}}\Big(\langle\varphi_\alpha|e^{i\mathbf{q}\cdot\boldsymbol{\varrho}}|\varphi^0_{\mathbf{k}}\rangle\\ &\quad -\sum_{\alpha'}\langle\varphi_\alpha|e^{i\mathbf{q}\cdot\boldsymbol{\varrho}}|\varphi_{\alpha'}\rangle\langle\varphi_{\alpha'}|\varphi^0_{\mathbf{k}}\rangle\Big).\end{aligned} \tag{7.B.23}$$

With the above given arguments we find for a QD at position $\boldsymbol{R}$ that $\langle\varphi_\alpha|e^{i\mathbf{q}\cdot\boldsymbol{\varrho}}|\varphi^0_{\mathbf{k}}\rangle = \int d^2\varrho\ \varphi_m(\boldsymbol{\varrho}-\boldsymbol{R})\ e^{i\mathbf{q}\cdot\boldsymbol{\varrho}}\ \varphi^0_{\mathbf{k}}(\boldsymbol{\varrho}) = \langle\varphi_m\,|\varphi^0_{\mathbf{k}+\mathbf{q}}\rangle e^{i(\mathbf{k}+\mathbf{q})\cdot\boldsymbol{R}}$. Since we neglect the wave function overlap of different QDs, this results in

$$\begin{aligned}\langle\varphi_\alpha|e^{i\mathbf{q}\cdot\boldsymbol{\varrho}}|\varphi_{\mathbf{k}}\rangle &= \frac{1}{N_{\mathbf{k}}}\Big(\langle\varphi_m|\varphi^0_{\mathbf{k}+\mathbf{q}}\rangle\\ &\quad -\sum_{m'}\langle\varphi_m|e^{i\mathbf{q}\cdot\boldsymbol{\varrho}}|\varphi_{m'}\rangle\langle\varphi_{m'}|\varphi^0_{\mathbf{k}}\rangle\Big)\ e^{i(\mathbf{k}+\mathbf{q})\cdot\boldsymbol{R}}.\end{aligned} \tag{7.B.24}$$

Hence for QDs at positions $\boldsymbol{R}$, phase factors $e^{i(\mathbf{k}+\mathbf{q})\cdot\boldsymbol{R}}$ enter the Coulomb matrix elements of the discussed structure which contribute in Eqs. (7.6) and (7.8)-(7.10). When the capture of carriers in a particular QD is calculated from Eq. (7.6) these phase factors cancel exactly, i.e., the processes are independent of the QD position. The same applies when carriers are scattered within the same QD according to Eqs. (7.8)-(7.10). It should be noted that the first Coulomb matrix element in Eq. (7.9) requires that the two QD quantum numbers m and m_1 belong to the same QD position as long as the wave function overlap between different QDs vanishes. For the same reason, Eq. (7.7) describes only carrier scattering within the same QD. However, Coulomb interaction can couple carriers in different QDs (even for vanishing overlap of their wave functions) according to processes described in Eqs. (7.8), (7.10) and depicted in Figs. 7.2 (d),(e) where a carrier from

one QD is scattered into the WL while another carrier from the WL is scattered into a different QD. It can be seen by direct inspection of Eq.(7.2) that these matrix elements are controlled by the strength of the Coulomb interaction at the distance between the two QDs involved. Hence the screening length of the Coulomb interaction in comparison to the QD separation limits these processes. In this chapter we assume sufficiently large screening of the Coulomb interaction due to WL carriers in order to neglect these processes. (For a typical WL carrier density of 10^{11} cm^{-2} at 300 K the Debye screening length is 0.76 in units of the 3d exciton Bohr radius.)

Therefore, Eqs.(7.6)-(7.10) describe scattering processes involving each QD separately and taking place identically in all QDs.

7.C Screening of the Coulomb Interaction

While the discussion of interaction matrix elements in Section 7.1.2 refers to the bare Coulomb potential, the effect of screening will be included in the following. The screened Coulomb interaction $w(\mathbf{r}_1, \mathbf{r}_2)$ obeys the integral equation

$$\begin{aligned} w(\mathbf{r}_1, \mathbf{r}_2) &= v(\mathbf{r}_1 - \mathbf{r}_2) \\ &\quad + \int d^3r_3 \, d^3r_4 \, v(\mathbf{r}_1 - \mathbf{r}_3) P(\mathbf{r}_3, \mathbf{r}_4) w(\mathbf{r}_4, \mathbf{r}_2) \end{aligned} \tag{7.C.25}$$

with the bare Coulomb interaction $v(\mathbf{r} - \mathbf{r}')$ and the longitudinal polarization $P(\mathbf{r}, \mathbf{r}')$, see Eq. (5.23). In the equilibrium situation discussed in this chapter, w and P additionally depend on the frequency ω in connection with dynamical screening effects. In a nonstationaly situation treated in Markov approximation, they furthermore depend on the macroscopic time t. For notational simplicity, these arguments are omitted.

The random-phase approximation for the longitudinal polarization leads to the eigenfunction expansion $P(\mathbf{r}, \mathbf{r}') = \sum_{\nu\nu'} \Phi_\nu(\mathbf{r}) \Phi_{\nu'}(\mathbf{r}') P_{\nu\nu'} \Phi^*_\nu(\mathbf{r}') \Phi^*_{\nu'}(\mathbf{r})$, see Eq. (5.33). In the above discussed limit of large WL carrier densities and/or small density of QDs on the WL we consider only screening of the Coulomb interaction due to WL carriers, i.e., ν and ν' are WL states. With the OPW description of the previous appendices, the WL states are "on average" spatially homogeneous and the longitudinal polarization possesses in-plane translational invariance. This can be directly seen from

$$\begin{aligned} &\int d^2\varrho \int d^2\varrho' \, e^{-i\mathbf{q}\cdot\boldsymbol{\varrho}} \, P(\mathbf{r}, \mathbf{r}') \, e^{i\mathbf{q}'\cdot\boldsymbol{\varrho}'} \\ &= \sum_{\mathbf{k},\mathbf{k}'} \langle \varphi_{\mathbf{k}'} | e^{-i\mathbf{q}\cdot\boldsymbol{\varrho}} | \varphi_{\mathbf{k}} \rangle \langle \varphi_{\mathbf{k}} | e^{i\mathbf{q}'\cdot\boldsymbol{\varrho}} | \varphi_{\mathbf{k}'} \rangle \, P_{\mathbf{k},\mathbf{k}'}(z, z') \\ &= \delta_{\mathbf{q},\mathbf{q}'} \sum_{\mathbf{k}} P_{\mathbf{k},\mathbf{k}-\mathbf{q}}(z, z') \, |F_{\mathbf{k},\mathbf{k}-\mathbf{q}}|^2 \end{aligned} \tag{7.C.26}$$

where in the eigenfunction expansion only the in-plane components of the wave functions has been used. For the evaluation of the overlap integrals involving OPW states we have introduced the short notation,

$$\langle\varphi_{\mathbf{k}}|e^{-i\mathbf{q}\cdot\boldsymbol{\varrho}}|\varphi_{\mathbf{k}'}\rangle = \delta_{\mathbf{k}-\mathbf{q}-\mathbf{k}'}\; F_{\mathbf{k},\mathbf{k}'}, \tag{7.C.27}$$

where $F_{\mathbf{k},\mathbf{k}'}$ can be obtained from a comparison with Eq. (7.B.22) and describes the OPW corrections of the plane-wave result.

Already at this point one can conclude (e.g. from an iterative solution of Eq. (7.C.25) with the structure $w = v + vPv + vPvPv + ...$) that since $P(\mathbf{r},\mathbf{r}') = P(\boldsymbol{\varrho}-\boldsymbol{\varrho}', z, z')$, the screened Coulomb interaction depends also only on the difference of the in-plane space arguments. This behavior is to be expected on intuitive grounds since we consider a uniform distribution of QDs that translates into in-plane homogeneity of the screened Coulomb interaction. The property essentially simplifies the following calculation of screened Coulomb matrix elements along the lines demonstrated for the bare Coulomb interaction in Eqs. (7.2)-(7.5).

Our starting point is the Fourier transform of the bare Coulomb potential with respect to the in-plane space dependence,

$$v(\mathbf{r}-\mathbf{r}') = \frac{1}{A}\sum_{\mathbf{q}}\; e^{i\mathbf{q}(\boldsymbol{\varrho}-\boldsymbol{\varrho}')}\; v(\mathbf{q}, z-z'), \tag{7.C.28}$$

as well as the corresponding in-plane Fourier transform of the screened Coulomb interaction,

$$w(\boldsymbol{\varrho}-\boldsymbol{\varrho}', z, z') = \frac{1}{A}\sum_{\mathbf{q}}\; e^{i\mathbf{q}(\boldsymbol{\varrho}-\boldsymbol{\varrho}')}\; w(\mathbf{q}, z, z'). \tag{7.C.29}$$

From Eq. (7.C.25) an integral equation for the Fourier coefficients is readily obtained,

$$\begin{aligned} w(\mathbf{q}, z_1, z_2) &= v(\mathbf{q}, z_1 - z_2) \\ &+ \int dz_3\; dz_4\; v(\mathbf{q}, z_1 - z_3) P(\mathbf{q}, z_3, z_4) w(\mathbf{q}, z_4, z_2). \end{aligned} \tag{7.C.30}$$

The interaction matrix elements for the bare Coulomb potential are given by Eq. (7.2) and similarly for the screened Coulomb potential. The assumed separation of wave functions into in-plane and z-components allows to introduce quasi-two-dimensional matrix elements. For the bare Coulomb interaction, the quasi-two-dimensional matrix elements are given by Eq. (7.4) where $v(\mathbf{q}, z-z') = \frac{e^2}{2\varepsilon_0 q}\; e^{-q|z-z'|}$ has been used. Then the interaction matrix elements follow from Eq. (7.5) or in the short notation

$$\begin{aligned} V_{\nu_1\nu_2\nu_3\nu_4} = \frac{1}{A}\sum_{\mathbf{q}}\; & V_{\sigma_1\sigma_2\sigma_3\sigma_4}(\mathbf{q}) \\ & \times \langle\varphi_{\nu_1}|e^{-i\mathbf{q}\cdot\boldsymbol{\varrho}}|\varphi_{\nu_4}\rangle\langle\varphi_{\nu_2}|e^{i\mathbf{q}\cdot\boldsymbol{\varrho}}|\varphi_{\nu_3}\rangle \end{aligned} \tag{7.C.31}$$

where σ_i are the quantum numbers for the confinement in z-direction and the band indices b are suppressed for notational simplicity. For the screened Coulomb interaction we obtain in complete analogy

$$W_{\nu_1\nu_2\nu_3\nu_4} = \frac{1}{A}\sum_{\mathbf{q}} W_{\sigma_1\sigma_2\sigma_3\sigma_4}(\mathbf{q}) \times \langle\varphi_{\nu_1}|e^{-i\mathbf{q}\cdot\boldsymbol{\varrho}}|\varphi_{\nu_4}\rangle\langle\varphi_{\nu_2}|e^{i\mathbf{q}\cdot\boldsymbol{\varrho}}|\varphi_{\nu_3}\rangle, \tag{7.C.32}$$

where the corresponding in-plane matrix elements are given by

$$W_{\sigma_1\sigma_2\sigma_3\sigma_4}(\mathbf{q}) = \int dz\, dz' \; \xi^*_{\sigma_1}(z)\xi^*_{\sigma_2}(z')\; w(\mathbf{q},z_1,z_2)\; \xi_{\sigma_3}(z')\xi_{\sigma_4}(z). \tag{7.C.33}$$

The in-plane overlap integrals in the second line of Eq. (7.C.32) have been discussed in Appendix 7.B for the required combinations of WL and QD states. The remaining task is the computation of the in-plane matrix elements $W_{\sigma_1\sigma_2\sigma_3\sigma_4}(\mathbf{q})$. Introducing in-plane matrix elements for the longitudinal polarization,

$$P(\mathbf{q},z_3,z_4) = \sum_{\sigma,\sigma'} \xi_{\sigma}(z)\xi_{\sigma'}(z')\; P_{\sigma,\sigma'}(\mathbf{q})\; \xi^*_{\sigma}(z')\xi^*_{\sigma'}(z), \tag{7.C.34}$$

and using Eqs. (7.C.33) as well as the corresponding equation for the bare Coulomb potential, the integral equation (7.C.30) can be reduced to the algebraic set of equations,

$$W_{\sigma_1\sigma_2\sigma_3\sigma_4}(\mathbf{q}) = V_{\sigma_1\sigma_2\sigma_3\sigma_4}(\mathbf{q}) + \sum_{\sigma\sigma'} V_{\sigma_1\sigma'\sigma\sigma_4}(\mathbf{q})\; P_{\sigma\sigma'}(\mathbf{q})\; W_{\sigma\sigma_2\sigma_3\sigma'}(\mathbf{q}). \tag{7.C.35}$$

A simple solution can be given if we assume identical confinement wave functions for the QD states, $\xi^*_Q(z)$, to be distinguished from the z-confinement in the WL, $\xi^*_W(z)$.

Finally we list the results for the Coulomb matrix elements used in Eqs.(7.6)-(7.10) to describe carrier capture and relaxation processes:

$$W_{m_1\boldsymbol{k}_2\boldsymbol{k}_3\boldsymbol{k}_4} = \frac{1}{A}\, W_{QWWW}(\boldsymbol{k}_2-\boldsymbol{k}_3) \times \langle\varphi_{m_1}|e^{-i(\boldsymbol{k}_2-\boldsymbol{k}_3)\cdot\boldsymbol{\varrho}}|\varphi_{\boldsymbol{k}_4}\rangle\; F_{\boldsymbol{k}_2,\boldsymbol{k}_3} \tag{7.C.36}$$

$$W_{m_1\boldsymbol{k}_2\boldsymbol{k}_3 m_4} = \frac{1}{A}\, W_{QWWQ}(\boldsymbol{k}_2-\boldsymbol{k}_3) \times \langle\varphi_{m_1}|e^{-i(\boldsymbol{k}_2-\boldsymbol{k}_3)\cdot\boldsymbol{\varrho}}|\varphi_{m_4}\rangle\; F_{\boldsymbol{k}_2,\boldsymbol{k}_3} \tag{7.C.37}$$

$$W_{m_1\boldsymbol{k}_2 m_3\boldsymbol{k}_4} = \frac{1}{A}\sum_{\mathbf{q}} W_{QWQW}(\boldsymbol{q}) \times \langle\varphi_{m_1}|e^{-i\boldsymbol{q}\cdot\boldsymbol{\varrho}}|\varphi_{\boldsymbol{k}_4}\rangle\,\langle\varphi_{\boldsymbol{k}_2}|e^{i\boldsymbol{q}\cdot\boldsymbol{\varrho}}|\varphi_{m_3}\rangle \tag{7.C.38}$$

The in-plane Coulomb matrix elements are given by

$$W_{QWWW}(\mathbf{q}) = \frac{V_{QWWW}(\mathbf{q})}{1 - V_{WWWW}(\mathbf{q})\,P(\mathbf{q})} \tag{7.C.39}$$

$$W_{QWWQ}(\mathbf{q}) = \frac{V_{QWWQ}(\mathbf{q})}{1 - V_{WWWW}(\mathbf{q})\,P(\mathbf{q})} \tag{7.C.40}$$

$$\begin{aligned} W_{QWQW}(\mathbf{q}) = [&V_{QWQW}(\mathbf{q}) \\ &- V_{QWQW}(\mathbf{q})\,P(\mathbf{q})\,V_{WWWW}(\mathbf{q}) \\ &+ V_{QWWW}(\mathbf{q})\,P(\mathbf{q})\,V_{WWQW}(\mathbf{q})] \\ &/[1 - V_{WWWW}(\mathbf{q})\,P(\mathbf{q})] \end{aligned} \tag{7.C.41}$$

with $P(\mathbf{q}) = P_{WW}(\mathbf{q})$.

For the matrix elements W_{QWWW} and W_{QWWQ} it is directly possible to introduce a longitudinal dielectric function that obeys a generalized Lindhard formula when the longitudinal polarization is computed in random-phase approximation [7.13] for the OPW states,

$$P(\mathbf{q},\omega) = \frac{1}{A}\sum_{b,\mathbf{k}} \frac{f^b_{\boldsymbol{k}-\boldsymbol{q}} - f^b_{\boldsymbol{k}}}{\hbar\omega + \varepsilon^b_{\boldsymbol{k}-\boldsymbol{q}} - \varepsilon^b_{\boldsymbol{k}} + i\delta}\,|F_{\boldsymbol{k},\boldsymbol{k}-\boldsymbol{q}}|^2, \tag{7.C.42}$$

where the frequency-dependence has been added for completeness. The matrix structure of Eq. (7.C.35) in principle prevents the simple structure with a generalized dielectric function for W_{QWQW} but the additional terms containing the polarization in the numerator of Eq. (7.C.41) nearly compensate.

In conclusion, the assumed separation of the wave functions into in-plane and z-components results in quasi-two-dimensional matrix elements of the bare Coulomb interaction, Eq. (7.4). Screening due to WL carriers can be included in this formula (for $W_{m_1\mathbf{k}_2\mathbf{k}_3\mathbf{k}_4}$ and $W_{m_1\mathbf{k}_2\mathbf{k}_3 m_4}$ strictly and for $W_{m_1\mathbf{k}_2 m_3\mathbf{k}_4}$ in good approximation) by dividing with a longitudinal dielectric function $\epsilon(\mathbf{q},\omega) = 1 - V_{WWWW}(\mathbf{q})\,P(\mathbf{q},\omega)$ that contains the in-plane Coulomb interaction between WL states and their longitudinal polarization calculated with OPW corrections. For the presented calculations the generalized Lindhard formula is used in quasi-static approximation.

7.D Role of the Wave Function Model

In this appendix we discuss the influence of various assumptions of the wave-function model on the calculated scattering rates. In lens-shaped QDs on a

WL the spatial height of the z-confinement changes within the QD. In the adiabatic approximation discussed in Ref. [7.11] the wave function contains in-plane and z-confinement parts according to

$$\Phi_\nu(\mathbf{r}) = \varphi_l^b(\boldsymbol{\varrho})\ \xi_\sigma^b(\varrho, z)\ u_b(\mathbf{r}). \tag{7.D.43}$$

For a confinement potential with cylindrical symmetry, the in-plane part can be expressed using $\varphi_l^b(\boldsymbol{\varrho}) = e^{im\phi}/\sqrt{2\pi} f_l(\varrho)$ with the in-plane angle ϕ. For a discretization of the potential into ring-shaped regions of (approximately) constant z-confinement $f_l(\varrho)$ obeys Bessel's differential equation. Boundary conditions determine the matching of wave functions in different regions. This procedure allows to construct piecewise analytically determined wave functions for a given confinement geometry. Nevertheless, using these wave functions in Eq. (7.5) is a challenging task since for an appropriate discretisation of the WL continuum a large number of Coulomb matrix elements is required.

Instead of using this approach we checked on a simpler level, how sensitive the discussed calculations of scattering rates are to the particular choice of confinement wave functions. We consider two limiting cases:

i) Constant height z_{QD} within the QD and smaller height z_{WL} throughout the WL. (For shallow QDs the wave functions average over a weakly changing height).

ii) In the limit of equal z-confinement for QD and WL the QD-confinement would be purely due to composition changes and/or strain in the x-y-plane.

In both cases, Eq. (7.D.43) reduces to Eq. (7.3). In the first case of different confinement functions $\xi_\sigma^b(z)$ for the QD- and WL-states, a three-dimensional OPW scheme according to

$$|\Phi_{\mathbf{k}}\rangle = \frac{1}{N_{\mathbf{k}}} \left(|\Phi_{\mathbf{k}}^0\rangle - \sum_\alpha |\Phi_\alpha\rangle\langle\Phi_\alpha\, |\Phi_{\mathbf{k}}^0\rangle \right) \tag{7.D.44}$$

is necessary. We compared results for the QD relaxation rates S^{1D} based on this scheme (solid line in Fig. 7.8) with a simplified calculation where only the in-plane part of the wave functions $\varphi_l^b(\boldsymbol{\varrho})$ is subject to the OPW scheme according to Eq. (7.A.16) and different z-confinement functions enter in the form factor of the in-plane Coulomb-matrix elements, Eq. (7.4). Both, in- and out-scattering rates of electrons and holes are practically unchanged and differences would not be visible in Fig. 7.8.

The result using plane-waves for the in-plane part of the WL states is shown as short-dashed line in Fig. 7.8. For the relaxation rates S^{1D} the Coulomb interaction matrix elements contain only pairing of WL states or pairing of QD states. Hence the missing orthogonality of plane waves and QD states does not influence the results and OPW corrections are small. The situation is different for the carrier capture rates where Coulomb interaction matrix elements contain pairings of WL- and QD-states. For the

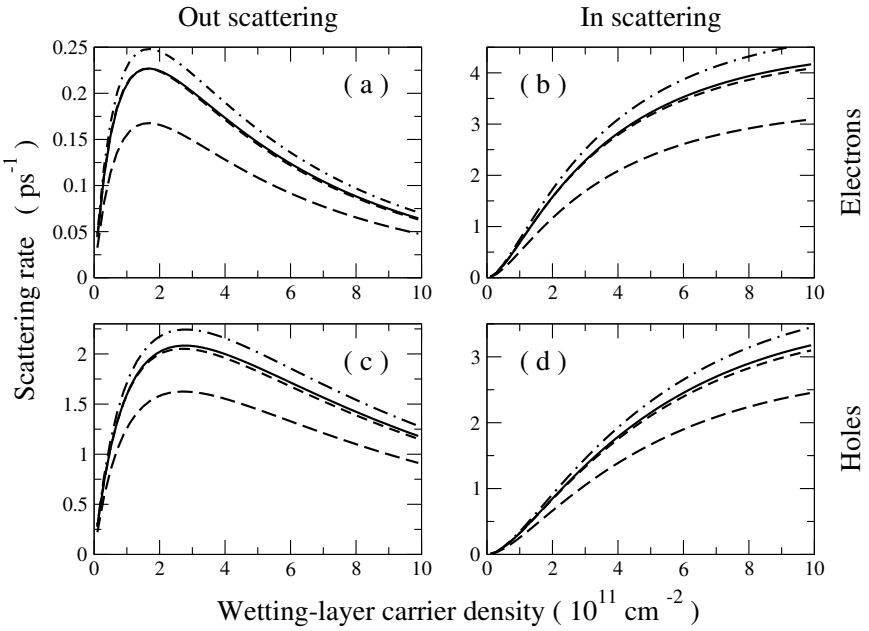

Figure 7.8: Scattering rates for QD carrier relaxation processes S^{1D} similar to Fig. 7.4 but with different approximations for the confinement wave functions. Solid line: OPW calculation, short-dashed line: plane-wave WL states, long-dashed line: larger QD height and smaller WL thickness, dashed-dotted line: equal confinement in growth direction for QD and WL.

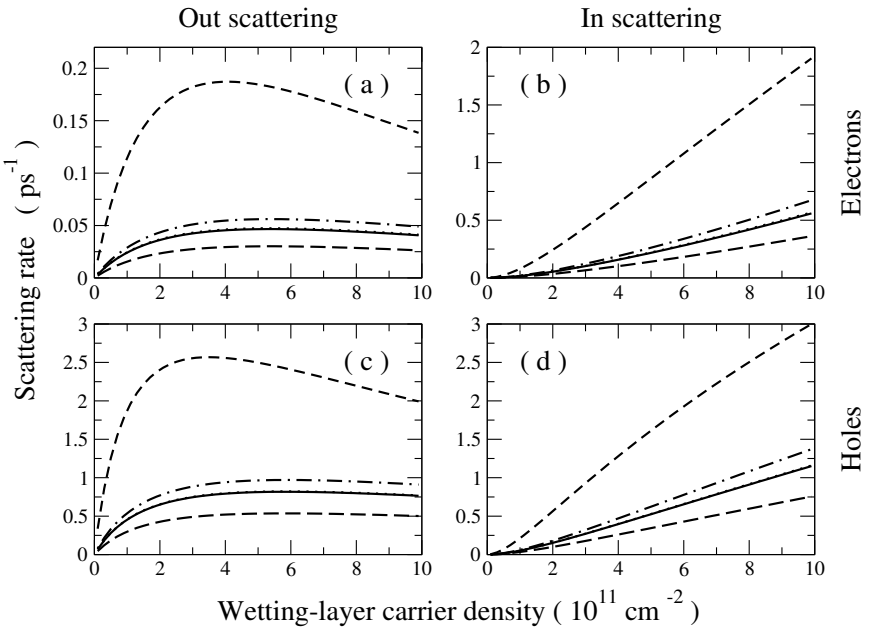

Figure 7.9: Scattering rates for carrier capture from WL to first excited QD states similar to Fig. 7.3 but with different approximations for the confinement wave functions. Solid line: 3d-OPW calculation, dotted line: 2d-OPW model. For other lines, see Fig. 7.8.

capture rates to the first excited states, Fig. 7.9, the plane-wave results (short-dashed lines) strongly depart from the OPW calculations. On the other hand, deviations between 3d-OPW results (solid lines) and the 2d-OPW model (dotted lines) are small. Similar results (not shown) are found for the scattering rates S^{2D}, S^{12X} and S^{mixed}. Since the 2d-OPW model greatly simplifies the calculations, it has been used in Figs. 7.3-7.7

Next we investigate the dependence of the results on the particular choice of parameters for the confimenent potential. While variations of the confinement potential will also affect the QD energies, we are here only interested in the influence of the confinement potential on the Coulomb matrix elements. Hence, we artificially use the same QD energies as before but take different functions $\xi^b_\sigma(z)$. While previous calculations are done for 2.2 nm WL height and additional 2.1 nm QD height, the long-dashed lines in Figs. 7.8 and 7.9 correspond to a 1.6 nm WL height and additional 4.4 nm QD height (using the 2d-OPW model). While this is a rather large change of the confinement situation, the changes of the scattering rates are relatively small. The dashed-dotted lines in Figs. 7.8 and 7.9 show results for the limiting case of equal confinement in z-direction for QW and WL discussed above. Calculations are done for a 4 nm finite-height confinement potential. Due

to the maximized overlap for the z-components of the QD and WL wave functions, the scattering rates are larger than in the previous cases. The capture and relaxation times for this situation using GaAs parameters are given in Ref. [7.14].

References

[7.1] W. W. Chow and S. W. Koch, *Semiconductor - Laser Fundamentals* (Springer, Berlin, 1999).

[7.2] P. Bhattacharya, K. Kamath, J. Singh, D. Klotzkin, J. Phillips, H.-T. Jiang, N. Chervela, T. Norris, T. Sosnowski, J. Laskar, and M. Murty, IEEE Transactions on Electron Devices **46**, 871 (1999).

[7.3] G. Park, O. B. Shchekin, D. L. Huffaker, and D. G. Deppe, Electron. Lett. **36**, 1283 (2000).

[7.4] P. Borri, W. Langbein, J. M. Hvam, F. Heinrichsdorff, M.-H. Mao, and D. Bimberg, IEEE Photonics Technology Letters **12**, 594 (2000).

[7.5] J. Zimmermann, S. T. Cundiff, G. von Plessen, J. Feldmann, M. Arzberger, G. Böhm, M.-C. Amann, and G. Abstreiter, Appl. Phys. Lett. **79**, 18 (2001).

[7.6] B. Ohnesorge, M. Albrecht, J. Oshinowo, A. Forchel, and Y. Arakawa, Phys. Rev. B **54**, 11532 (1996).

[7.7] D. Morris, N. Perret, and S. Fafard, Appl. Phys. Lett. **75**, 3593 (1999).

[7.8] S. Raymond, K. Hinzer, S. Fafard, and J. L. Merz, Phys. Rev. B **61**, R16331 (2000).

[7.9] S. Sanguinetti, K. Watanabe, T. Tateno, M. Wakaki, N. Koguchi, T. Kuroda, F. Minami, and M. Gurioli, Appl. Phys. Lett. **81**, 613 (2002).

[7.10] U. Bockelmann and T. Egeler, Phys. Rev. B **46**, 15574 (1992).

[7.11] A. Wojs, P. Hawrylak, S. Fafrad, and L. Jacak, Phys. Rev. B **54**, 5604 (1996).

[7.12] H. Schneider, F. Jahnke, S. W. Koch, J. Tignon, T. Hasche, and D. Chemla, Phys. Rev. B **63**, 045202 (2001).

[7.13] G. D. Mahan, *Many-Particle Physics*, 2. ed. (Plenum, New York, 1990).

[7.14] T. Nielsen, P. Gartner, and F. Jahnke, phys. stat. sol. (c) **0**, 1532 (2003).

Chapter 8

Evaluation of Carrier-Phonon Scattering in QD Systems

In this chapter we apply the general theoretical tools derived in Chap. 6 to study the carrier-phonon scattering in quantum-dot (QD) wetting-layer (WL) systems using the same InGaAs model parameters as already utilized in the previous chapter for the carrier-carrier scattering.

As in any coupled system, carrier-phonon interaction renormalizes both electronic and vibrational states. However, in bulk semiconductors or quantum wells with weak polar coupling, the net effect can be described by renormalized effective carrier masses, a small polaron shift of the band-edge, and lattice distortions only modify the background dielectric constant for the Coulomb interaction of carriers. The broadening of the transition energies due to carrier-phonon interaction remains weak.

For carriers in QDs, the discrete nature of localized electronic states changes the role of polaronic effects [8.1–8.3]. Restricting the analysis to a single QD state coupled to phonons, polaron effects can be obtained from an exact diagonalization of the Hamiltonian [8.4]. While an extension to several discrete levels has been presented [8.5], the influence of the energetically nearby continuum of WL states, typical for self-assembled QDs, has not been included. Furthermore, only quasiparticle properties have been discussed which provide no direct information about the scattering efficiency for various processes. Calculations of carrier transition rates based on the polaron picture are missing.

Experimentally, the role of the carrier-phonon scattering is still controversy. On one side work have been published suggesting a inefficient scattering mechanism (phonon-bottleneck) [8.6–8.8], as well as work indicating a efficient carrier-phonon scattering mechanism [8.9–8.11]. However, systematic investigations including studies of different samples under different excitation conditions must still be performed to clarify the issue.

The chaper is organized as follows. As a first step we evaluate in Sec. 8.1

the carrier transition rates on the basis of a Boltzmann equation. The interaction with longitudinal-optical (LO) phonons can lead to efficient scattering channels provided that the free-carrier energy conservation is fulfilled. As a second step we use in Sec. 8.2 a quantum kinetic treatment for carrier-phonon interaction in the polaron picture. Starting point here is to determine the quasi-particle renormalizations due to the polar interaction for both QD and WL carriers. The WL states exhibit weak LO-phonon satellites. For the QD states, the hybridization of one state with strong satellites of another state leads to a rich multi-peak structure. Finally, based on the spectral properties of QD and WL polarons, quantum kinetic equations for the capture process (carrier transitions from the WL into the QD) and relaxation processes (transitions between QD states) are solved in Sec. 8.3. For situations where, in terms of free-carrier energies, energy conserving scattering processes are not possible, the quantum-kinetic treatment provides efficient scattering rates. Even for the InGaAs material system with weak polar coupling, sub-picosecond scattering times are obtained.

Model System

In this section we shortly recall the main parameters of the model system. For the InGaAs system the weak polar coupling is $\alpha = 0.06$ and the monochromatic LO-phonon energy equals $\hbar\omega_{\mathrm{LO}} = 36$ meV. The effective-mass approximation is assumed to be valid with $m_e = 0.067m_0$ and $m_h = 0.15m_0$ for the conduction band and valance band, respectively. For flat lens-shaped QDs the in-plane wave-functions of an isotropic two-dimensional harmonic potential are used while for the (strong) confinement in the direction perpendicular to the WL a finite-height potential barrier is considered (see Chap. 7 for parameters and further details). To account for a finite energetic height of the QD confinement potential, the calculations only include the (double degenerate) ground state and the (four-fold degenerate) first excited state, in the following called s and p-shell, respectively with s-p spacing and p-WL separation of 40 meV for electrons while for holes the spacing is 15 meV. Using the procedure of Chap. 7 WL states orthogonal to the QD states are constructed for a density of QDs $n_{dot} = 10^{10}$ cm^{-2}.

8.1 Boltzmann's Equation

In Markov-approximation the kinetic equation determining the changes of the carrier population f_α is given by, see Sec. 6.5,

$$\begin{aligned}\frac{\partial}{\partial t} f_\alpha =& \frac{2\pi}{\hbar} \frac{\hbar\omega_{\rm LO}}{2\varepsilon^*/\varepsilon} \sum_\beta V_{\beta\alpha\beta\alpha} \\ &\times \Big\{ (1-f_\alpha) f_\beta \big[\quad (1+n_{\rm LO})\, \delta(\varepsilon_\alpha - \varepsilon_\beta + \hbar\omega_{\rm LO}) \\ &\qquad\qquad + n_{\rm LO} \quad \delta(\varepsilon_\alpha - \varepsilon_\beta - \hbar\omega_{\rm LO}) \big] \\ &- f_\alpha (1-f_\beta) \big[\qquad n_{\rm LO} \quad \delta(\varepsilon_\alpha - \varepsilon_\beta + \hbar\omega_{\rm LO}) \\ &\qquad\qquad + (1+n_{\rm LO})\, \delta(\varepsilon_\alpha - \varepsilon_\beta - \hbar\omega_{\rm LO}) \big] \Big\}. \end{aligned} \tag{8.1}$$

Here α is an arbitrary (QD or WL) electronic state with free-carrier energy ε_α. For the phonon population $n_{\rm LO}$ a Bose-Einstein function at the lattice temperature will be used to describe the crystal lattice in thermodynamic equilibrium, hence $n_{\rm LO} = 1/(e^{\hbar\omega_{\rm LO}/kT} - 1)$. The Fröhlich coupling has been formulated in a general eigenfunction basis with the bare Coulomb matrix elements, Eq. (7.2). Hence, the calculation of the polar-coupling interaction matrix elements for WL and QD states can be done along the lines of Sec. 7.1.2 and App. 7.B. The effective dielectric constant $\frac{1}{\varepsilon^*} = (\frac{1}{\varepsilon_\infty} - \frac{1}{\varepsilon})$ contains the static and high-frequency relative dielectric constants, ε and ε_∞, respectively.

Various terms on the RHS of Eq. (8.1) describe the scattering of carriers from states α into β under the emission or absorption of an LO-phonon as well as the reverse processes from β to α. Under the assumption of strict energy conservation, carrier relaxation between the QD states is only possible when the LO-phonon energy matches the level spacing. Furthermore, contributions to carrier capture are obtained only for an energy difference between the QD states and the WL larger than $\hbar\omega_{\rm LO}$.

For our InGaAs system with $\hbar\omega_{\rm LO}$=36 meV and $\alpha = 0.06$ only hole capture is possible. To uniquely compare the influence of various processes with the result from the carrier-carrier scattering of Chap. 7 we assume that an equilibrium situation (at 300 K) has been reached and study the dependence of the scattering processes on the WL carrier density. According to Fig. 8.1, capture to both p- and s-shells is possible with an in-scattering rate comparable to the hole-capture due to Coulomb scattering in Fig. 7.3 which shows also a similar WL carrier-density dependence. Note that the *capture time* is defined according to Eq. (7.15) as the response time of the system to small perturbations from equilibrium and, hence, contains both in- and out-scattering rates, i.e., $\dot{f}_\alpha = (1-f_\alpha)S_\alpha^{in} - f_\alpha S_\alpha^{out}$ and $\tau_\alpha^{-1} = S_\alpha^{in} + S_\alpha^{out}$. Since the out-scattering rate only weakly depends on the WL carrier-density, the same holds for the capture time. In addition to the results obtained with OPW wave functions for the WL states (solid and dotted lines) also

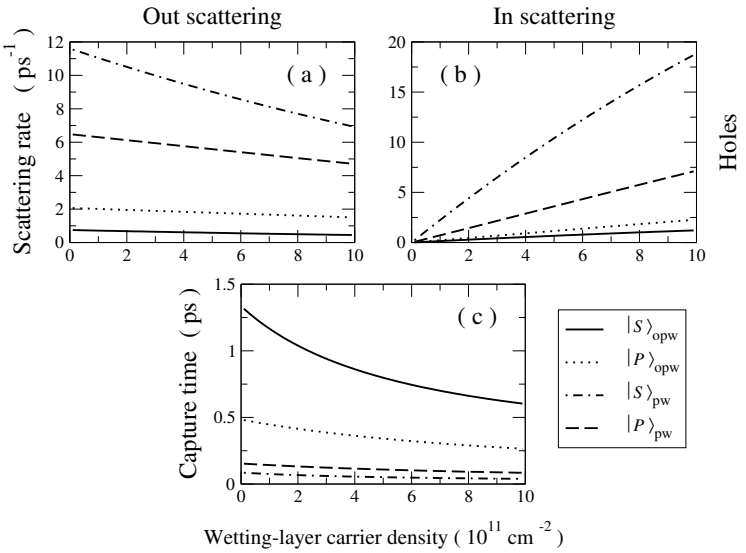

Figure 8.1: (a) and (b) Scattering rates for hole capture from the WL to the QD ground states (solid line: OPW, dashed-dotted line: PW) and to first excited states (dotted line: OPW, dashed line: PW) and corresponding capture times (c) at 300 K.

the plane-wave (PW) results are given (dashed and dashed-dotted lines). In this case the rates are strongly overestimated which emphasizes again the importance of the OPW scheme discussed in Appendices 7.A and 7.B.

In Refs. [8.12, 8.13] also two-phonon processes have been studied based on Fermi's golden rule. For weak polar coupling, their efficiency is clearly reduced in comparison to one-phonon processes. Furthermore, in a perturbational treatment state filling effects of the intermediate states is neglected, which further reduces the scattering efficiency.

8.2 Quantum-Dot Polarons

The Boltzmann equation is based on strict energy conservation between the involved scattering states, which lead to inefficient scattering channels for the QD electrons. Let us relax the exact energy requirement and formulate the problem in a quantum kinetic approach in terms of the polaron picture, the quasi-particle picture generated by the carrier-phonon interaction. In the polaron picture, we shall show that both relaxation and capture become efficient for the QD electrons.

The single-particle properties of carriers under the influence of lattice distortions are determined by the retarded Green's function (GF), G^r_α, which

obeys the Dyson equation, see Sec. 6.5,

$$\left[i\hbar\frac{\partial}{\partial t_1} - \varepsilon_\alpha\right] G^r_\alpha(t_1,t_2) = \delta(t_1-t_2) + \int dt_3 \;\; \Sigma^r_\alpha(t_1,t_3)\; G^r_\alpha(t_3,t_2). \quad (8.2)$$

In the polaron theory one usually considers all possible virtual transitions from state α due to emission or absorption of phonons. This corresponds to a self-energy Σ^r_α for the carrier-phonon interaction where the population of the involved carrier states is neglected (electron vacuum). The corresponding retarded self-energy in random-phase approximation (RPA) is given by

$$\Sigma^r_\alpha(t_1,t_2) = i\hbar \sum_\beta \; G^r_\beta(t_1,t_2)\; D^<_{\beta\alpha}(t_2-t_1). \quad (8.3)$$

In general, Green's functions and self-energies depend on two quantum numbers α, β. For the situation described in this chapter, off-diagonal contributions can be neglected, which has been verified numerically by J. Seebeck [8.14]; see also Ref. [8.1, 8.2]. Assuming that the phonon system is in thermal equilibrium, the phonon propagator combined with the interaction matrix elements is given by, see Eqs. (6.24) and (6.26),

$$\begin{aligned} i\hbar\; D^<_{\beta\alpha}(\tau) &= \frac{\hbar\omega_{\rm LO}}{2\varepsilon^*/\varepsilon}\, V_{\alpha\beta\alpha\beta}\; \Delta^<(\tau) \\ &= \sum_{\boldsymbol{q}} \; |M_{\beta\alpha}(\boldsymbol{q})|^2 \Big[n_{\rm LO}\; e^{-i\omega_{\rm LO}\tau} \;+\; (1+n_{\rm LO})\; e^{i\omega_{\rm LO}\tau}\Big], \end{aligned} \quad (8.4)$$

where the prefactor and the bare Coulomb matrix element have been rewritten in terms of the more familiar for the polaron theory Fröhlich interaction matrix element

$$M_{\beta\alpha}(\boldsymbol{q}) = \frac{M_{\rm LO}}{q}\; \langle\beta|e^{i\boldsymbol{q}\boldsymbol{r}}|\alpha\rangle, \quad (8.5)$$

which contains the overlap between the electronic states and the phonon mode. For localized electronic states this acts as a form factor. The prefactor $M^2_{\rm LO} = 4\pi\alpha\frac{\hbar}{\sqrt{2m}}(\hbar\omega_{\rm LO})^{3/2}$ includes the polar coupling strength α and the reduced electron-hole-mass m. The dimensionless coupling constant reads $\alpha = \frac{e^2}{4\pi\varepsilon_0\hbar}\sqrt{\frac{m}{2\hbar\omega_{LO}}}\,(\frac{1}{\varepsilon_\infty}-\frac{1}{\varepsilon})$. As a result of the above assumptions, the retarded GF itself depends only on the difference of time arguments and its Fourier transform can be directly related to the quasi-particle properties.

Due to energetic separation between the discrete QD states and the WL continuum, polaronic effects in QDs are often computed by neglecting the presence of the WL [8.1–8.3, 8.5]. For a single discrete level this amounts to the exactly solvable independent Boson model [8.4] and for several discrete levels it was shown to be nearly exactly solvable [8.5]. In both cases, even for non-zero temperatures, the spectral function contains a series of sharp delta-like peaks. In real QDs, however, the interaction with the WL continuum (which might require multi-phonon processes) leads to a broadening of

these peaks. The RPA accounts for this broadening effect while it retains a hybridization effect (see below) characteristic for the full solution. Therefore the RPA is expected to provide an adequate description *in the presence of the continuum*. Comparison with an alternative method supports this statement: the first term of a cumulant expansion, which is known to be exact for the independent Boson model [8.4], agrees well with the RPA for quasi-continuous electronic states. An additional source of broadening is the finite LO-phonon lifetime due to anharmonic interaction between phonons.

The Fourier transform of the electron spectral function, -2 Im $G^r_\alpha(\omega)$ (see App. 6.A and e.g. Ref. [8.15]), is shown in Fig. 8.2 for the $k = 0$ WL state and for the QD p- and s-shell (from top to bottom). In the absence of polar coupling to lattice distortions, the spectral functions are delta functions at the free-particle energies indicated by the vertical lines. The dotted line in Fig. 8.2(a) is the result for the $k = 0$ WL state without coupling to the QD states, indicating that their influence on the WL polarons is weak. The WL spectral function is broadened, the central peak exhibits a small polaron shift, and multiple sidebands due to LO-phonon emission (absorption) appear to the right (left). The polaron broadening is a result of the irreversible decay in the continuous WL density of states.

The LO-phonon sidebands of the localized QD states in Fig. 8.2(b) and (c) are more pronounced and the hybridization of peaks from one shell with the energetically close sidebands of the other shell can be observed. This effect stems from the discrete nature of the localized states and requires that the coupling strength, which is modified by the form factors in Eq. (8.5), exceeds the polaron damping. The hybridization is analogous to the coupling of a coherent light field to a two-level system [8.1]. The asymmetry is due to the energetic difference between level spacing (40 meV) and LO-phonon energy (36 meV). A finite LO-phonon lifetime of 5 ps due to anharmonic interaction between phonons has been included in the calculations.

8.3 Carrier Kinetics of Relaxation and Capture Processes

In this section we study consequences of the renormalized quasi-particle properties on the scattering processes. Fermi's golden rule, which has been frequently used in the past, describes only transition rates from fully populated initial into empty final states. Proper balancing between in- and out-scattering events, weighted with the population f of the initial states and the blocking $1 - f$ of the final states, leads to the kinetic equation Eq. (8.1). Quasiparticle and Markov approximation can also be applied to renormalized polaronic states which results in a rate-equation description for the population of these states [8.16].

A quantum-kinetic approach extends Eq. (8.1) in the sense that the

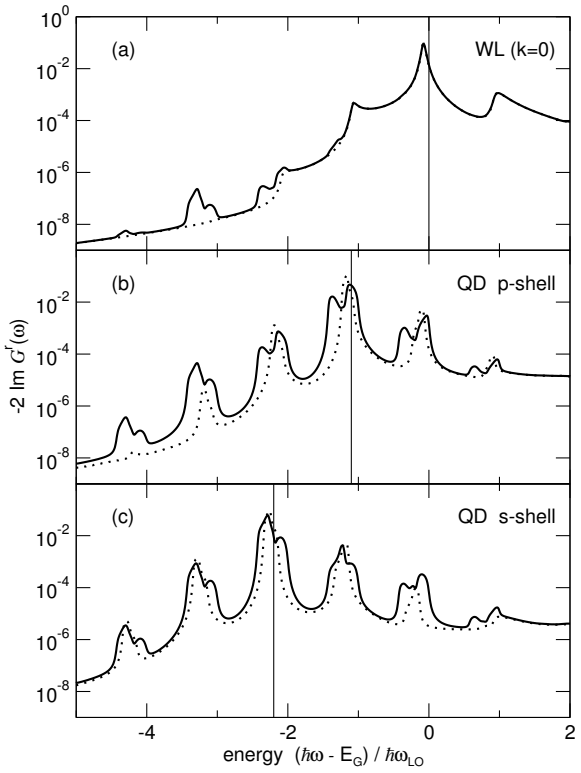

Figure 8.2: (a) Spectral function of electrons for the lowest WL state at $k = 0$ under the influence of polar coupling in the combined QD-WL system (solid line) and without coupling to the QD states (dotted line). For electrons in the QD p-shell (b) and s-shell (c) full coupling between all states (solid line) is compared to the case without coupling to other QD states (dotted line). Vertical lines show the corresponding free-carrier energies. Energies are given relative to the continuum edge E_G in units of the phonon energy $\hbar\omega_{LO}$. The temperature is 300 K.

delta-functions with free-carrier energies are replaced by time-integrals over polaronic retarded GFs. Furthermore, the population factors are no longer instantaneous but explicitly depend on the time evolution. This is the time-domain picture for the inclusion of renormalized quasi-particle properties (beyond a quasi-particle approximation and beyond Markov approximation). Using the generalized Kadanoff-Baym ansatz (GKBA) [8.15], the quantum-kinetic equation has the form, see Sec. 6.5,

$$\frac{\partial}{\partial t_1} f_\alpha(t_1) = 2\mathrm{Re} \sum_\beta \int_{-\infty}^{t_1} dt_2 \;\; G^r_\beta(t_1 - t_2) \; \left[G^r_\alpha(t_1 - t_2)\right]^* \times \Big\{ \big[1 - f_\alpha(t_2)\big] f_\beta(t_2) \; i\hbar D^<_{\alpha\beta}(t_2 - t_1) - f_\alpha(t_2) \big[1 - f_\beta(t_2)\big] \; i\hbar D^>_{\alpha\beta}(t_2 - t_1) \Big\}. \quad (8.6)$$

The phonon propagator $D^>$ follows from Eq. (8.4) by replacing $\tau \to -\tau$. A Markov approximation *in the renormalized quasi-particle picture* corresponds to the assumption of a slow time-dependence of the population $f_\alpha(t_2)$ in comparison to the retarded GFs such that the population can be taken at the external time t_1. The Boltzmann scattering integral of Eq. (8.1) follows if one additionally neglects quasi-particle renormalizations and uses free-carrier retarded GFs. The quantum-kinetic equation provides energy-conserving scattering processes only in the long-time limit. The corresponding spectral function in Fig. 8.2 is obtained from a complete Fourier transform whereas on a short timescale the peaks shown there are only partially emerged (since only a finite-time contribution of the retarded GF enters in the quantum-kinetic equation at a given time.).

To demonstrate the influence of quantum-kinetic effects due to QD-polarons, we first study the relaxation of electrons from p-shell to s-shell for the above discussed situation where the level spacing does not match the LO-phonon energy such that both, Fermi's golden rule and the kinetic equation (8.1) predict the absence of transitions. A direct time-domain calculation of the polaron GFs from Eq. (8.2)-(8.5) together with Eq. (8.6) is used. We assume an initial population $f_s(t_0) = 0$, $f_p(t_0) = 0.3$ and start the calculation at time t_0. While this example addresses the relaxation process itself, more advanced calculations would also include the carrier generation via optical excitation or carrier capture discussed below. Then ambiguities due to initial conditions can be avoided since the population vanishes prior to the pump process which naturally provides the lower limit of the time integral in Eq. (8.6). In practice, we find that within the GKBA results weakly depend on the details of the initial conditions.

The evaluation of the quantum-kinetic theory (solid lines in Fig. 8.3) yields a fast population increase of the initially empty QD s-shell accompanied by oscillations which reflect in the time-domain the hybridization of

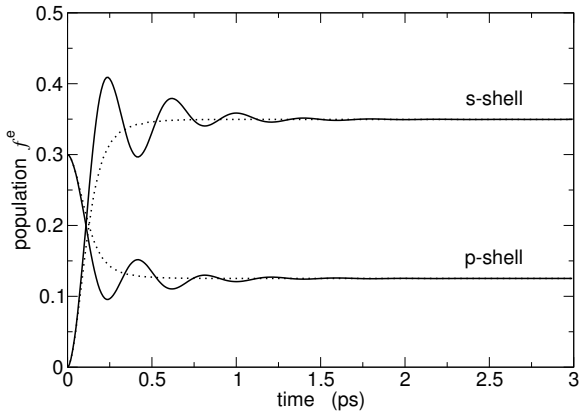

Figure 8.3: Temporal evolution of the electron QD population due to carrier-phonon scattering between p-shell and s-shell for an energy spacing larger than the LO-phonon energy. The solid lines correspond to a quantum-kinetic calculation whereas for the dotted line the Markov approximation is used together with polaronic spectral functions.

coupled carrier and phonon states. If one uses the Markov approximation together with polaronic retarded GFs in Eq. (8.6), such that quasi-particle renormalizations are still included, these transient oscillations disappear. In both cases the same steady-state solution is obtained which corresponds to a thermal population at the renormalized energies. Note that particle number conservation is obeyed in Fig. 8.3 since the degeneracy of the p-shell is twice that of the s-shell. The equilibrium solution can be obtained from the polaron spectral function using the Kubo-Martin-Schwinger (KMS) relation, $f_\alpha = -\int \frac{d\hbar\omega}{\pi}\ f(\omega)\,\mathrm{Im}G^r_\alpha(\omega)$ where $f(\omega)$ is a Fermi function with the lattice temperature [8.15].

Another important process is the capture of carriers from the delocalized WL states into the localized QD states, see Fig. 8.4. For the used QD parameters, where the spacing between the electron p-shell and the lowest WL state (40 meV) exceeds the LO-Phonon energy, again Fermi's golden rule and Eq. (8.1) predict the absence of electronic transitions. For the numerical solution of Eq. (8.6) we use now as initial condition empty QD states and a thermal population of carriers in the polaronic WL states (obtained from the KMS relation) corresponding to a carrier density 10^{11} cm^{-2} and temperature 300 K. For small carrier densities, we use the polaron GF for the electron vacuum since it is weakly influenced by population effects, see Ref. [8.17]. Also in this situation the quantum-kinetic theory predicts a fast population of the initially empty p-shell while direct capture to the s-shell is somewhat slower. Since the WL states form a quasi-continuum, beating at early times is strongly suppressed.

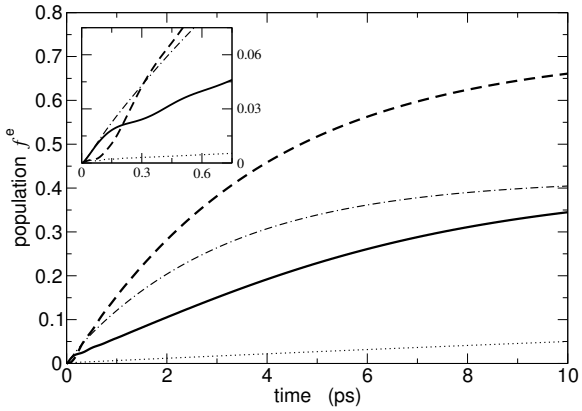

Figure 8.4: Time-evolution of the QD p-shell (solid line) and s-shell (dashed line) electron population due to carrier capture from the WL including the effect of carrier relaxation between QD shells. If only direct capture processes are considered, the dashed-dotted and dotted lines are obtained for p-shell and s-shell, respectively. The temperature is 300 K.

Quantum Kinetic Equation vs. Boltzmann's Equation

Following the same approach as outlined above for the study of the quantum kinetics of the electrons, J. Seebeck [8.14] has also investigated the polaron dynamics for the holes. Using the same parameters as given in this chapter the author found by solving simultaneously Eq. (8.2) and Eq. (8.6) capture times on the same order of magnitude as derived by using the Boltzmann equation (8.1), see table 8.1 below. The good agreement between the two methods is related to the fact the capture processes are allowed even at the Boltzmann level with strict energy requirements, and to the fact that we are in the weak polar coupling regime.

WL-density [10^{11} cm^{-2}]	0.1	1.0	4.0	7.0	10.0
BE: τ_p [ps]	0.47	0.44	0.36	0.30	0.26
QK: τ_p [ps]	0.44	0.38	0.27	0.23	0.19
BE: τ_s [ps]	1.32	1.17	0.86	0.70	0.60
QK: τ_s [ps]	1.13	0.94	0.64	0.51	0.41

Table 8.1: Comparaison of hole capture times τ_p and τ_s to p-shell and s-shell, respectively, based on the Boltzmann Equation (BE) (8.1) and the Quantum Kinetic equation (QK) (8.6) from Ref. [8.14].

8.4 Conclusion

In summary, when capture processes due to emission of LO-phonons are possible at the Boltzmann level, their efficiency is comparable to Coulomb scattering at elevated WL carrier densities, while at low WL carrier densities LO-phonon capture times are faster than those provided by Coulomb scattering. The quantum-kinetic treatment of carrier-phonon interaction explains the absence of a phonon bottleneck in terms of scattering between renormalized quasi-particle states. A quasi-equilibrium situation is reached on a ps-timescale at elevated temperatures even in materials with weak polar coupling.

References

[8.1] T. Inoshita and H. Sakaki, Phys. Rev. B **56**, 4355 (1997).

[8.2] K. Kral and Z. Khas, Phys. Rev. B **57**, 2061 (1998).

[8.3] O. Verzelen, R. Ferreira, G. Bastard, T. Inoshita, and H. Sakaki, phys. stat. sol. (a) **190**, 213 (2002).

[8.4] G. Mahan, *Many-Particle Physics* (Plenum, New York, 1990).

[8.5] T. Stauber, R. Zimmermann, and H. Castella, Phys. Rev. B **62**, 7336 (2000).

[8.6] J. Urayama, T. B. Norris, J. Singh, and P. Bhattacharya, Phys. Rev. Lett. **86**, 4930 (2001).

[8.7] A. W. E. Minnaert, A. Y. Silov, W. van der Vleuten, J. E. M. Haverkort, and J. H. Wolter, Phys. Rev. B **63**, 075303 (2001).

[8.8] S. Xu, A. A. Mikhailovsky, J. A. Hollingsworth, and V. I. Klimov, Phys. Rev. B **65**, 045319 (2002).

[8.9] E. Tsitsishvili, R. v. Baltz, and H. Kalt, Phys. Rev. B **66**, 161405 (2002).

[8.10] E. Peronne, F. Fossard, F. H. Julien, J. Brault, M. Gendry, B. Salem, G. Bremond, and A. Alexandrou, Phys. Rev. B **67**, 205329 (2003).

[8.11] F. Quochi, M. Dinu, L. N. Pfeiffer, K. W. West, C. Kerbage, R. S. Windeler, and B. J. Eggleton, Phys. Rev. B **67**, 235323 (2003).

[8.12] T. Inoshita and H. Sakaki, Phys. Rev. B **46**, 7260 (1992).

[8.13] H. Jiang and J. Singh, IEEE J. Quantum Electron **34**, 1188 (1998).

[8.14] J. Seebeck, Quantenkinetische Beschreibung von Polaronen in Halbleiter-Quantenpunkten, Diplomarbeit, 2004, Universität Bremen, Fachberich Physik.

[8.15] For a review see: H. Haug and P. Jauho, *Quantum Kinetics in Transport & Optics of Semiconductors*, Springer-Verlag, Berlin, 1996.

[8.16] O. Verzelen, R. Ferreira, and G. Bastard, Phys. Rev. B **62**, 4809 (2000).

[8.17] P. Gartner, L. Bányai, and H. Haug, Phys. Rev. B **60**, 14234 (1999).

Chapter 9

Evaluation of Coulomb Scattering in Nitride QD systems

Group-III nitrides have as new material system attracted much attention within the last decade due to their extended range of emission frequencies from red up to ultraviolet as well as their potential for high-power/high-temperature electronic devices [9.1, 9.2]. While the nonradiative loss of carriers due to trapping at threading dislocations lowers the efficiency of group-III nitride quantum-well light emitters, this effect is reduced by the three-dimensional confinement in quantum dots (QDs) [9.3]. Studies of the photoluminescence spectra [9.4] and dynamics [9.5, 9.6] are used to demonstrate and analyze efficient recombination processes from the localized QD states.

Extensive work has been done to study the electronic states in group-III nitrides [9.7]. The valence-band structure has a strongly non-parabolic dispersion and a pronounced mass anisotropy [9.8]. Nitride-based heterostructures with a wurtzite crystal structure are known to have strong built-in electrostatic fields due to the spontaneous polarization and piezoelectric effects which have been analyzed in ab-initio electronic structure calculations [9.9, 9.10] and in comparison with photoluminescence experiment [9.11]. Tight-binding calculations of QD states have been used to study free-carrier optical transitions [9.12].

While the aforementioned theoretical investigations are devoted to the single-particle states and transitions, it is known from GaAs-based QD systems, that the emission properties are strongly influenced by many-body effects. Self-organized QD systems, grown in the Stranski-Krastanow mode, exhibit a single-particle energy spectrum with discrete energies for localized states as well as a quasi-continuum of delocalized wetting layer (WL) states at higher energies. The carrier-carrier Coulomb interaction provides

efficient scattering processes from the delocalized into the localized states (carrier capture) as well as fast transitions between localized states (carrier relaxation), which can be assisted by carriers in bound (QD) or extended (WL) states. The dependence of the scattering efficiency on the excitation conditions has been calculated for GaAs-based QDs on various levels of refinement [9.13–9.17]. The scattering rates are of central importance for the photoluminescence as well as for the laser efficiency and dynamics. The same interaction processes also lead to a renormalization of the electronic states (resulting in line shifts for the optical transitions) as well as to dephasing (line broadening) effects, which directly determine absorption and gain spectra [9.18].

With the current attention on nitride-based QDs the question raises, to which extent previous results are modified by the peculiarities of this material system. Specifically, we study how the strong electrostatic fields and the corresponding changes of the single-particle wave functions and energies influence the carrier-carrier scattering processes. For this purpose, we have to analyze the competing influence of the internal fields and of the many-body renormalizations. Since previous investigations of carrier-carrier scattering in semiconductor QDs have been performed for free-carrier energies entering the scattering integrals, an independent second purpose of this chapter is the inclusion of self-consistently renormalized energies.

Renormalizations of the single-particle energies are due to direct electrostatic (Hartree) Coulomb interaction, exchange interaction, and screening. While these effects generally contribute due to possible charging of the QDs, in the considered wurtzite structure they are additionally modified by the presence of the built-in fields. In this chapter we show that the discussed changes of the single-particle energies have a much stronger impact on the carrier scattering processes than modifications of the single-particle wave functions.

Many-body effects were also considered for the case of few excited carriers restricted to localized states of GaN-QD [9.19]. In this regime, the emission properties reflect the multi-exciton states. In our chapter, we are interested in kinetic processes for the opposite limit of high densities of carriers populating both QD and WL states (as typical for QD lasers).

The work presented in this chapter is based on the general theoretical tools developed in Part II as well as on the studies presented in Chap. 7. For the evaluation of scattering processes, we use kinetic equations for the carrier occupation probabilities which include direct and exchange Coulomb interaction under the influence of carrier screening as well as population effects (Pauli-blocking) of the involved electronic states. Based on the single particle states and Coulomb interaction matrix elements, scattering processes are evaluated on the level of second-order Born approximation.

The chapter is organized as follows. In Sec. 9.1 we summarize the main ingredients of our theory which include the kinetic equations, the single-

particle states and their renormalization as well as the interaction matrix elements. Details regarding the WL states and screening effects are given in appendices. In Sec. 9.2 the QD model is described and the numerical results for energy renormalization and scattering times are presented.

9.1 Theory for carrier-carrier Coulomb scattering

To analyze the role of carrier-carrier scattering in nitride-based QD systems, we use a kinetic equation with Boltzmann scattering integral, see Eq. (5.53) of Sec. 5.4. The dynamics of the carrier population $f_\nu(t)$ in an arbitrary state ν is determined by in-scattering processes, weighted with the nonoccupation of this state, and by out-scattering processes, weighted with the occupation according to

$$\frac{\partial}{\partial t} f_\nu \;=\; (1-f_\nu) S_\nu^{\rm in} - f_\nu S_\nu^{\rm out}. \tag{9.1}$$

The in-scattering rate is given by

$$\begin{aligned} S_\nu^{\rm in} = \frac{2\pi}{\hbar} \sum_{\nu_1,\nu_2,\nu_3} & W_{\nu\nu_2\nu_3\nu_1} [W^*_{\nu\nu_2\nu_3\nu_1} - W^*_{\nu\nu_2\nu_1\nu_3}] \\ & \times \left\{ f_{\nu_1}(1-f_{\nu_2}) f_{\nu_3} \delta(\widetilde{\varepsilon}_\nu - \widetilde{\varepsilon}_{\nu_1} + \widetilde{\varepsilon}_{\nu_2} - \widetilde{\varepsilon}_{\nu_3}) \right\}, \end{aligned} \tag{9.2}$$

where the first and second term in the square brackets correspond to direct and exchange Coulomb scattering, respectively. The matrix elements of the screened Coulomb interaction, $W_{\nu\nu_2\nu_3\nu_1}$, are calculated in Section 9.1.2. The delta-function describes energy conservation in the Markov limit. Single-particle energies $\widetilde{\varepsilon}_\nu$ of state ν are renormalized by the Coulomb interaction as discussed in Sections 9.1.4 and 9.1.5. A similar expression for the out-scattering rate $S_\nu^{\rm out}$ is obtained by replacing $f \to 1-f$.

Scattering processes described by Eqs. (9.1) and (9.2) conserve the total energy and separately the electron and hole numbers. As a result, the combined action of the discussed scattering processes will evolve the distribution functions of electrons and holes towards Fermi-Dirac functions with common temperature where the QD and WL electrons (holes) will have the same chemical potential μ_e (μ_h). During such a time evolution towards quasi-equilibrium the relative importance of various scattering processes is expected to change via their dependence on the (non-equilibrium) carrier distribution functions for WL and QD states. A direct measure for the efficiency of various scattering processes can be given in the relaxation-time approximation introduced in Sec. 7.2, where one calculates the characteristic time on which a small perturbation of the system from thermal equilibrium is obliterated. We use this method to investigate the influence of the built-in electrostatic field in nitride-based QDs on the carrier-density dependent scattering efficiency.

9.1.1 Quantum-dot model system

Recent progress in tight-binding and $\boldsymbol{k}\cdot\boldsymbol{p}$ models has been made in calculating QD electronic single-particle states including the confinement geometry, strain and built-in electrostatic field effects. The special features of the wurtzite QD structures have been addressed in Refs. [9.12, 9.20–9.22], while zinc-blende QD structures have been studied in Refs. [9.21–9.26]. Our goals differ from these investigations in the respect that, for given single-particle states and energies, we need to determine Coulomb interaction matrix elements in order to calculate many-body energy renormalizations and scattering processes. For this purpose we choose a simple representation of wave functions for lens-shaped quantum dots [9.27] which allows to separate the in-plane motion (with weak confinement for the states localized at the QD position and without confinement for the states delocalized over the WL plane) from the motion in growth direction with strong confinement. This leads to the ansatz

$$\Phi_\nu(\mathbf{r}) = \varphi_l^b(\boldsymbol{\varrho})\ \xi_\sigma^b(z)\ u_b(\mathbf{r}) \tag{9.3}$$

where the WL extends in the plane described by $\boldsymbol{\varrho} = (x, y)$. φ and ξ are the envelope functions in this plane and in the perpendicular growth direction, respectively, and u are Bloch functions. ν represents a set of quantum numbers with l for the in-plane component (including the spin), σ for the z-direction, and b is the band index. In the following we consider an ensemble of randomly distributed identical QDs with non-overlapping localized states. The total number of QDs, N, leads in the large area limit to a constant QD density $n_{\mathrm{QD}} = \lim_{A\to\infty} N/A$.

9.1.2 Coulomb matrix elements

The interaction matrix elements of the bare Coulomb potential $v(\mathbf{r}-\mathbf{r}') = e^2/(4\pi\varepsilon_0\epsilon|\mathbf{r}-\mathbf{r}'|)$ with the background dielectric function ϵ are given by

$$V_{\nu\nu_2\nu_3\nu_1} = \int d^3r\ d^3r'\ \Phi_\nu^*(\mathbf{r})\Phi_{\nu_2}^*(\mathbf{r}')v(\mathbf{r}-\mathbf{r}')\Phi_{\nu_3}(\mathbf{r}')\Phi_{\nu_1}(\mathbf{r}). \tag{9.4}$$

This expression is further specified with the help of Eq. (9.3), the Fourier transform of the Coulomb potential, and by introducing the in-plane Coulomb matrix elements with the two-dimensional momentum $\mathbf{q}$,

$$V^{b,b'}_{\sigma\sigma_2\sigma_3\sigma_1}(\mathbf{q}) = \frac{e^2}{2\varepsilon_0\epsilon\, q}\int dz\ dz'\ \xi_\sigma^b(z)^*\xi_{\sigma_2}^{b'}(z')^* e^{-q|z-z'|}\xi_{\sigma_3}^{b'}(z')\xi_{\sigma_1}^b(z). \tag{9.5}$$

Limiting the calculations to the first bound state of the strong confinement problem (in z-direction), all the σ indices above take only one value and will be dropped in what follows. Also, the band indices associated with ν_1 and

ν_3 are the same as those of ν and ν_2, respectively, so that only two of them have to be specified. Therefore Eq. (9.4) reads

$$\begin{aligned} V^{b,b_2}_{l,l_2,l_3,l_1} &= \frac{1}{A}\sum_{\mathbf{q}} V^{b,b_2}(\mathbf{q}) \\ &\quad\times \int d^2\varrho\, \varphi^b_l(\boldsymbol{\varrho})^*\varphi^b_{l_1}(\boldsymbol{\varrho})\, e^{-i\mathbf{q}\cdot\boldsymbol{\varrho}} \\ &\quad\times \int d^2\varrho'\, \varphi^{b_2}_{l_2}(\boldsymbol{\varrho}')^*\varphi^{b_2}_{l_3}(\boldsymbol{\varrho}')\, e^{i\mathbf{q}\cdot\boldsymbol{\varrho}'}. \end{aligned} \tag{9.6}$$

The obtained separation of integrals over in-plane and z-components greatly simplifies the computational effort. For practical calculations we use solutions of a two-dimensional harmonic potential for the in-plane wave functions of the localized states and OPW solutions, discussed in Appendix 9.A, for the in-plane components of the delocalized states. Then the in-plane integrals in Eq. (9.6) can be determined to a large extent analytically for all possible combinations of QD and WL states. The calculation of the wave functions in growth direction, which is used to evaluate the in-plane Coulomb matrix elements, Eq. (9.5), is outlined in the next section. Screened Coulomb matrix elements are obtained from Eqs. (9.5) and (9.6) according to the procedure described in detail in Sec. 7.C.

9.1.3 Quantum-confined Stark effect

To account for the built-in electrostatic fields of the wurtzite structure in the growth-direction, which gives rise to the quantum-confined Stark effect, we solve the one-dimensional Schrödinger equation [9.28, 9.29]

$$\left[-\frac{\hbar^2}{2m_b}\frac{\partial^2}{\partial z^2} + U^b(z)\right]\xi^b(z) = E_b(z)\xi^b(z), \tag{9.7}$$

where the potential

$$U^b(z) = U^b_0(z) + U^b_{\mathrm{p}}(z) + U^b_{\mathrm{scr}}(z), \tag{9.8}$$

consists of the bare confinement potential in z-direction, $U^b_0(z)$, as well as the intrinsic electrical and screening fields, $U^b_{\mathrm{p}}(z)$ and $U^b_{\mathrm{scr}}(z)$, respectively. The latter is the electrostatic field due to the separation of electron and hole wave functions by the built-in field. Following Ref. [9.29] we calculate the corresponding screening potential from a solution of the Poisson equation for a set of uniformly charged sheets according to

$$U^{e,h}_{\mathrm{scr}}(z) = \frac{\mp e^2 N_{\mathrm{sys}}}{2\varepsilon_0\epsilon}\int \mathrm{d}z' \left[|\xi^e(z')|^2 - |\xi^h(z')|^2\right]|z-z'|. \tag{9.9}$$

Equations (9.7)-(9.9) have to be evaluated selfconsistently for a given total (QD plus WL) carrier density N_{sys} in the system.

9.1.4 Hartree-Fock energy renormalization

The Hartree-Fock (HF) contribution to the energy renormalization of an arbitrary state ν (QD or WL) is given by

$$\widetilde{\varepsilon}_\nu \;=\; \varepsilon_\nu + \Delta_\nu^{\mathrm{HF}}, \tag{9.10}$$

where ε_ν is the free-carrier energy and the HF shift follows from

$$\begin{aligned} \Delta_\nu^{\mathrm{HF}} &= \Delta_\nu^{\mathrm{H}} + \Delta_\nu^{\mathrm{F}} \\ &= \sum_{\nu'} \left[V_{\nu\nu'\nu'\nu} - V_{\nu\nu'\nu\nu'} \right] f_{\nu'}. \end{aligned} \tag{9.11}$$

The first part corresponds to the Hartree (direct) term and the second part is the Fock (exchange) contribution. The equation is written in a general basis. For a system with local charge neutrality, like bulk semiconductors or quantum wells, the Hartree term vanishes while the Fock term leads to an energy reduction as used, e.g., in the semiconductor Bloch equations [9.30].

For the QD and OPW-WL states discussed in this chapter, the absence of local charge neutrality leads to Hartree terms which are evaluated in Appendix 9.B. Regarding the quantum numbers, introduced in Section 9.1.1, we further specify the following notation: For the in-plane envelopes we use the two-dimensional momentum $\boldsymbol{k}$ for the delocalized WL states and $\alpha = (m, \boldsymbol{R})$ for the localized QD states, where $\boldsymbol{R}$ is the QD position and the discrete quantum numbers for a particular QD are collected in m. The spin index is tacitly included in either m or $\boldsymbol{k}$.

Following Appendix 9.B, we find that the Hartree shifts of the WL states vanish due to compensating contributions from QD and WL carriers,

$$\Delta_{b,\boldsymbol{k}}^{\mathrm{H}} \;=\; 0. \tag{9.12}$$

For a random distribution of QDs this is related to the spatial homogeneity restored on a global length scale and to the global charge neutrality of the system. For the same reason, the Hartree shift of a localized QD state is only provided by states from the same QD while Hartree shifts due to carriers in other QD and WL states compensate each other,

$$\Delta_{b,m}^{\mathrm{H}} \;=\; \sum_{b',m'} V_{mm'm'm}^{b,b'}\, f_{m'}^{b'}\,. \tag{9.13}$$

From electrostatics one expects the same result, provided that the WL is modeled as a constant area charge of opposite sign to the QD total charge. Then the constant part of the Fourier expansion of the Coulomb matrix elements in Eq. (9.6), i.e. the $\boldsymbol{q} = 0$ contribution, for the QDs balances the constant area charge from the WL.

On the other hand, since $\Delta_{b,m}^{\mathrm{H}}$ probes the local charge density at the site of the QD due to the contributions of QD and WL carriers, one expects

an influence of the WL on the QD Hartree energy shift. Locally on the QD length scale, the WL states are not homogeneous as a result of the QD presence. This causes a departure from the picture where the WL states contribute only in an averaged manner (via the $\boldsymbol{q} = 0$ term). Intuitively, one would expect that an increasing amount of carriers in the WL will start to screen the Coulomb interaction between the QD carriers. Following this picture we therefore replace the bare Coulomb potential with the screened one in Eq. (9.13), i.e., $\Delta^{\mathrm{H}}_{b,m} \to \Delta^{\mathrm{SH}}_{b,m}$. In Appendices 9.B and 9.C more support is given to this argumentation.

In the exchange terms, the summation over the QD positions can be performed directly, since the associated QD phase factors disappear for the Coulomb matrix elements $V_{mm'mm'}$ and $V_{\alpha\boldsymbol{k}\alpha\boldsymbol{k}}$ as seen from Eq. (9.A.20) and Eq. (9.A.21), respectively. The resulting exchange energy shifts contain the QD and WL contributions,

$$\Delta^{\mathrm{F}}_{b,m} = - \sum_{m'} V^{b,b}_{mm'mm'} f^{b}_{m'} - \sum_{\boldsymbol{k}'} V^{b,b}_{m\boldsymbol{k}'m\boldsymbol{k}'} f^{b}_{\boldsymbol{k}'}, \tag{9.14}$$

$$\Delta^{\mathrm{F}}_{b,\boldsymbol{k}} = -N \cdot \sum_{m'} V^{b,b}_{\boldsymbol{k}m'\boldsymbol{k}m'} f^{b}_{m'} - \sum_{\boldsymbol{k}'} V^{b,b}_{\boldsymbol{k}\boldsymbol{k}'\boldsymbol{k}\boldsymbol{k}'} f^{b}_{\boldsymbol{k}'}. \tag{9.15}$$

Since there is an area associated with the Coulomb matrix element $V_{\boldsymbol{k}m'\boldsymbol{k}m'}$, the QD density $n_{\mathrm{QD}} = N/A$ enters in Eq. (9.15).

9.1.5 Screened exchange and Coulomb hole

The HF Coulomb interaction provides only the first approximation for energy renormalizations; correlation contributions can lead to important corrections. A frequently used extension of the HF energy shifts for high-density plasma excitation is the screened-exchange and Coulomb-hole approximation [9.30]. On this level, the combined contributions of Coulomb exchange interaction and Coulomb correlations beyond HF to the energy renormalizations are approximated with the screened exchange term (where the bare Coulomb potential in the Fock term is replaced by a screened one) plus an energy shift denoted as Coulomb-hole contribution. The Coulomb hole self-energy reads [9.30]

$$\Sigma^{\mathrm{CH}}(\boldsymbol{r}_1, \boldsymbol{r}_2, t_1, t_2) = \frac{1}{2}\delta(\boldsymbol{r}_1 - \boldsymbol{r}_2)\delta(t_1 - t_2) \times \left[W(\boldsymbol{r}_1, \boldsymbol{r}_2, t_1) - V(\boldsymbol{r}_1 - \boldsymbol{r}_2)\right], \tag{9.16}$$

with the statically screened Coulomb potential W. In a general eigenfunction basis, this leads to the Coulomb-hole energy shift

$$\Delta^{\mathrm{CH}}_{\nu}(t) = \frac{1}{2}\sum_{\nu'} \left[W_{\nu\nu'\nu\nu'}(t) - V_{\nu\nu'\nu\nu'}\right]. \tag{9.17}$$

In Eqs. (9.14) and (9.15) we therefore replace the bare Coulomb potential with the screened one and substitute the Fock energy shift with the screened exchange plus the Coulomb hole, $\Delta_\nu^{\mathrm{F}} \to \Delta_\nu^{\mathrm{SX}} + \Delta_\nu^{\mathrm{CH}}$. In the limit of low carrier densities, the screened Coulomb potential reduces to the bare one, the Coulomb hole vanishes, and we recover the HF result.

9.2 Results

We start this Section by describing the model we use and the material parameters employed for calculating the one-particle states. These correspond to the unexcited system. The next step is to renormalize these states in a self-consistent way to include the influence of the carrier population and the presence of the built-in field, as described in Section 9.1. These single-particle properties enter the scattering integrals, Eq. (9.2).

For the discussion of the numerical results one should bear in mind the two main consequences of the built-in field. On the one hand, the self-consistent energies entering the Fermi functions and the energy-conservation are sensitive to the electron-hole separation induced by the built-in electrostatic field. On the other hand, the Coulomb matrix elements are changed due to modifications in the wave-function shapes and overlapping.

9.2.1 The model and its parameters

In the following examples we consider an InGaN/GaN QD-WL system using typical InGaN parameters [9.7] listed in Table 9.1. For the alloy, we have interpolated linearly the dielectric constant ϵ, the isotropic electron mass m_e, the hole mass parameters A_i and the spin-orbit splitting Δ_{so}.

A specific feature of the wurtzite structure nitrides is the strong mass anisotropy of the holes. The mass of the heavy hole (HH) in the z-direction, is given by $m_z^* = m_0/|A_1 + A_3|$ with the free electron mass m_0 and the mass parameters A_1 and A_3 [9.8]. For the in-plane motion, a strong hybridization between the HH and the light-hole (LH) subband leads to nonparabolic bands. This is due to the fact that the small HH-LH splitting, induced by the spin-orbit interaction, is enhanced by neither the strain nor the z-confinement. To include the hybridization effect we use a nonparabolic HH dispersion [9.8],

$$\varepsilon_{\boldsymbol{k}}^h = -\alpha(A_2 + A_4)\boldsymbol{k}^2 - \sqrt{\Delta_2^2 + \alpha^2 A_5^2 \boldsymbol{k}^4}, \tag{9.18}$$

where $\alpha = \hbar^2/2m_0$ and $\Delta_2 = \Delta_{\mathrm{so}}/3$. For the motion of the electrons, isotropic effective mass and parabolic dispersion are considered. Conduction (ΔE_e) and valence (ΔE_h) band offsets for InGaN grown on GaN have been estimated by splitting the gap energy difference between bulk GaN and the

Table 9.1: Material parameters used in the calculations.

Parameters	GaN	InN	$In_{0.2}Ga_{0.8}N$
E_g[300 K] (eV)	3.438	0.756	2.677
ΔE_e (eV)			0.457
ΔE_h (eV)			0.304
ϵ	8.9 [a]	15.3 [a]	10.2
m_e (m_0)	0.2	0.07	0.174
A_1	-7.21	-8.21	-7.41
A_2	-0.44	-0.68	-0.488
A_3	6.68	7.57	6.858
A_4	-3.46	-5.23	-3.814
A_5	-3.40	-5.11	-3.742
Δ_{so} (eV)	0.017	0.005	0.0146
Quantum well (nm)			3.0
$F_{\text{QD-WL}}$ (MV/cm)			1.5
F_{barrier} (MV/cm)			0.75

[a] From:Ref. [9.31]

alloy with a band offset ratio 60:40 for electrons and holes, according to Refs. [9.32, 9.33].

Compared to usual zinc-blende structure, the wurtzite structure is characterized by large built-in electric fields. The strength of the fields is related to the spontaneous polarization discontinuity at the heterojunction interfaces and the piezoelectric polarization [9.9, 9.10]. Internal fields in InGaN/GaN heterojunctions of a few MV/cm have been reported [9.33, 9.34], typically in a sawtooth profile, where the field in the QD-WL system has a different magnitude and opposite direction to the field of the barrier (reflecting a set of capacitors with non-equal surface charges). For the field inside the QD-WL region and in the barrier, we consider $F_{\text{QD-WL}} = 1.5$ MV/cm and $F_{\text{barrier}} = 0.75$ MV/cm, respectively.

As the estimated effective hole masses [9.8] are larger than the electron mass, we expect the QD's to confine more states for holes than for electrons. On the same basis, the level spacing which scales inversely with the mass, is larger for electrons than for holes. The in-plane QD confinement is modeled with a 2D parabolic potential, capable of binding two energy shells (s and p) for electrons and three (s,p,d) for holes. The degeneracies of these shells (apart from spin) are $1, 2$ and 3 for s,p and d, respectively. For electrons we assume a level spacing of 90 meV with the p-shell 70 meV below the WL continuum edge, while for holes we assume a level spacing of 30 meV with

Table 9.2: QD parameters used in the calculations.

Parameter	Electrons	Holes	
Shells	s, p	s, p, d	
Level spacing (meV)	90.0	30.0	
$\varepsilon_{\rm s}$ (meV)	-160.0	-80.0	
$\varepsilon_{\rm p}$ (meV)	-70.0	-50.0	
$\varepsilon_{\rm d}$ (meV)		-20.0	
QD density ($\rm cm^{-2}$)			10^{10}

the d-shell 20 meV below the WL continuum edge. Thus the $e_s - h_s$ QD transition is close to the range given in Ref. [9.6, 9.35]. The QD parameters are summarized in Table 9.2. Finally, we assume z-direction confinement wave functions which are band dependent but equal for QD and WL states.

The harmonic oscillator (HO) inverse localization length β is deduced from the level spacing via $\hbar\omega_{\rm HO} = \hbar^2\beta^2/m^*$. For electrons the effective mass of Table 9.1 is taken. For holes we use the mass resulting from Eq. (9.18) in the small k limit, $m_h^* = m_0/|A_2 + A_4|$. This is justified by the typical QD diameters of 100Å - 200Å , which correspond to the region around $k = 0$ where the first term of Eq. (9.18) is dominant.

9.2.2 Schrödinger and Poisson equations

The charge separation of carriers along the growth direction z under the influence of the built-in electrostatic fields, obtained from a self-consistent solution of Eqs. (9.7)-(9.9) is shown in Fig. 9.1 (a) and (b). A clear overlap reduction of the wave functions for electrons and holes is observed. This leads to a decreasing form factor (the double integral in Eq. (9.5) which modifies the 2D Fourier transform of the Coulomb interaction) for the electron-hole interaction while the stronger carrier localization increases the form factors for electron-electron and hole-hole interaction. Thus, the presence of the built-in field leads to an effective reduction of the electron-hole interaction, while the electron-electron and the hole-hole interaction is enhanced. The screening field turns out to be a small correction to the strong built-in field for the range of densities considered.

9.2.3 Renormalized energies

For a total carrier density $N_{\rm sys}$, the corresponding carrier distributions f_ν in thermal equilibrium are used to determine the renormalized energies from the self-consistent solution of the equation $\widetilde{\varepsilon}_\nu = \varepsilon_\nu + \Delta_\nu^{\rm SH} + \Delta_\nu^{\rm SX} + \Delta_\nu^{\rm CH}$, for

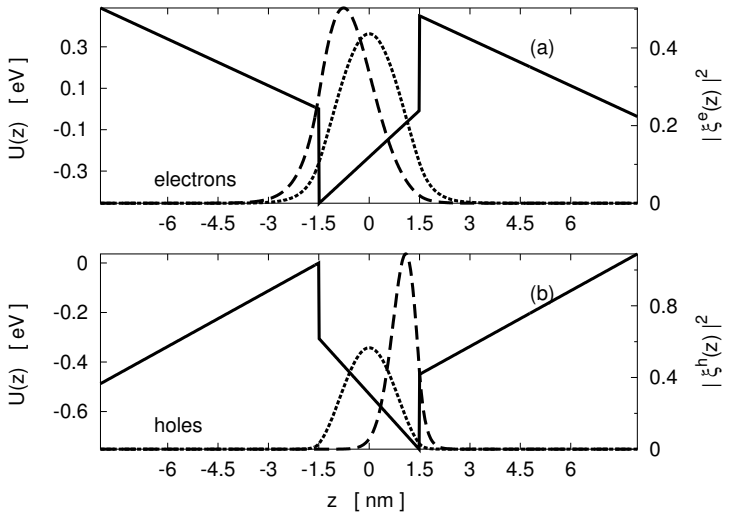

Figure 9.1: Total confinement potential $U(z)$ (solid line) and particle distribution $|\xi(z)|^2$ (dashed line) along the growth direction z for electrons (a) and holes (b) in the presence of the built-in field at a total carrier density $N_{\rm sys} = 10^{10}$ cm^{-2}. The dotted lines are the particle distribution for zero field.

the QD and WL states. For ε_ν we use the energies listed in Table 9.2 for the QD bound states and the dispersion law of Eq. (9.18) for the WL hole states.

The density dependence of the renormalized electron and hole energies is shown in Fig. 9.2 (a) and (c), respectively, in the presence of the built-in field. The corresponding results without the built-in field are given in Fig. 9.2 (b) and (d) for comparison. The renormalized d-shell is split into two degenerate $\mathrm{d}_\pm$ states and a d_0 state, with a separation of a few meV.

Quantitatively, the QD levels experience a smaller energy shift for the built-in field compared to the zero field case. The origin of this difference lies in the Hartree term, which reflects the electrostatic interaction of a given carrier with all the others. The field-induced change of the z-confinement functions tends to separate the electrons from the holes and, as a consequence for both, the repulsive part of the Hartree term is increased and the attractive part is decreased. This effect is illustrated explicitly in Fig. 9.3 for the p-shell where the four different contributions to the renormalized energies are shown. For electrons the Hartree shift is repulsive both in the presence and in the absence of the built-in field, but more so in the former case. For holes, the built-in field makes the Hartree term less attractive. In both cases the net result is a set of shallower bound states. For the sake of completeness we mention that the different sign of the Hartree field for elec-

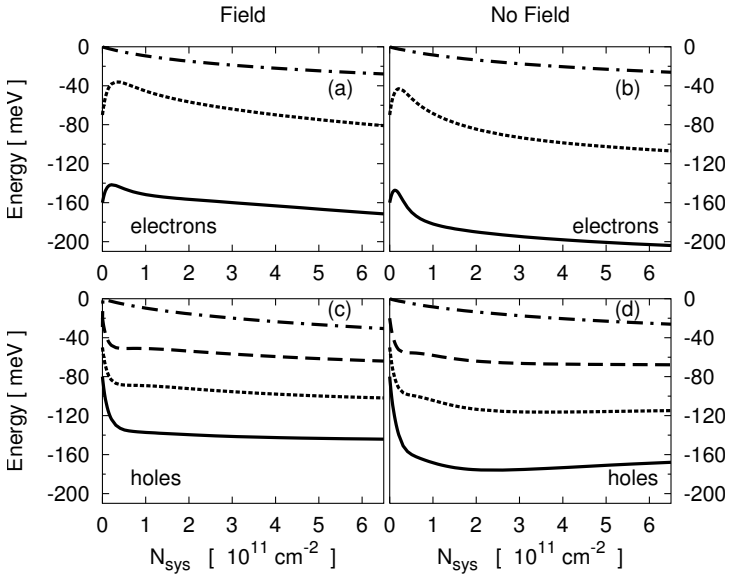

Figure 9.2: Renormalized energies as a function of the total carrier density in system $N_{\rm sys}$ for s-shell (solid lines), p-shell (dotted lines), $d_{\pm}$-shell (dashed lines), and WL $\boldsymbol{k} = 0$ (dashed-dotted lines). Calculation with (a),(c) and without (b),(d) electrostatic field are shown for electrons (a),(b) and holes (c),(d). The temperature is 300 K.

trons and holes comes from the difference in the QD population of electrons and holes and from the band dependence of the Coulomb matrix elements.

The screened exchange and Coulomb hole terms are not significantly different for with and without built-in field. As the extended WL states are only renormalized by the screened exchange and Coulomb hole term, we find an overall negative energy shift, lowering the free spectrum by an almost $\boldsymbol{k}$-independent shift (not shown).

9.2.4 Capture and relaxation times

To quantify the importance of the different scattering processes, we study their dependence on the total carrier density in thermal equilibrium. Using the relaxation time approximation of Sec. 7.2 one can introduce a scattering time τ_ν for a given process according to

$$\tau_\nu \;=\; \left[S_\nu^{\rm in} + S_\nu^{\rm out}\right]^{-1}, \tag{9.19}$$

which gives a characteristic time on which the system will return to its thermal equilibrium distribution if exposed to a small perturbation. More precisely, for the carrier population we have $\delta \dot{f}_\nu = -\delta f_\nu/\tau_\nu$, with δf_ν being the deviation from thermal equilibrium f_ν.

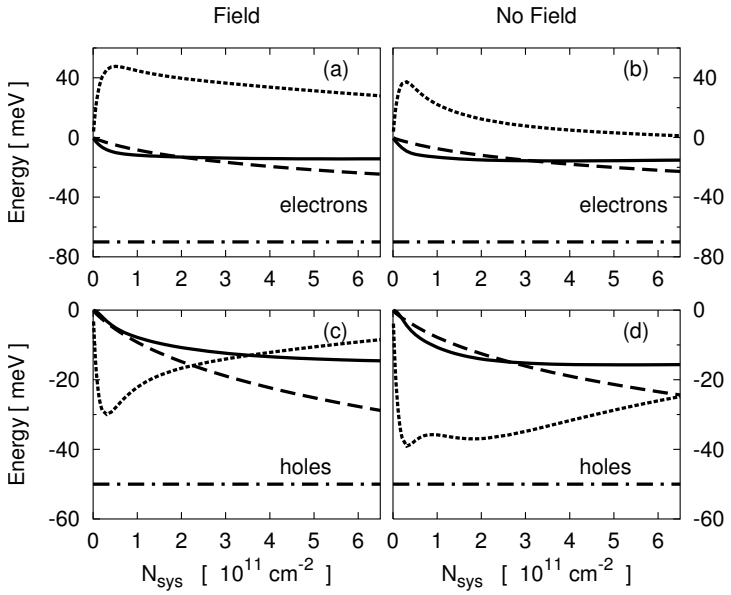

Figure 9.3: Same as Fig. 9.2 for different contributions to the renormalized p-shell energy $\widetilde{\varepsilon}_{\mathrm{p}}$ which are the free energy ε_{p} (dashed dotted line), screened Hartree shift $\Delta_{\mathrm{p}}^{\mathrm{SH}}$ (dotted line), screened exchange shift $\Delta_{\mathrm{p}}^{\mathrm{SX}}$ (solid line), and Coulomb hole shift $\Delta_{\mathrm{p}}^{\mathrm{CH}}$ (dashed line).

The scattering times are changed by the built-in field through different competing mechanisms. On the one hand the matrix elements are modified (see Section 9.2.2), on the other hand the QD energies are pushed closer to the WL continuum (Section 9.2.3).

For illustrative purposes, we first study the influence of the built-in field on the scattering times by using the free (unrenormalized) energies within the scattering integrals. This reveals the field effect solely on the Coulomb matrix elements via the wave-function changes. As an example we consider a capture process, where an electron or hole from the WL is scattered into the QD while another WL carrier (electron or hole) is scattered to an energetically higher WL state, as well as the reverse process. (Both contribute to the scattering time according to the relaxation-time approximation.) Thus the outer index in Eq. (9.1) is a QD state while the three summation indices in Eq. (9.2) belong to the WL states for this example shown in Figure 9.4.

First we discuss the density dependence. The capture time decreases with increasing carrier density, as more scattering partners become available. Furthermore, capture times for electrons are slower than for holes, because the QD electron levels are placed energetically deeper below the WL continuum edge. For energy-conserving scattering processes, the excess energy of a WL electron which is captured to the QD must be transferred to

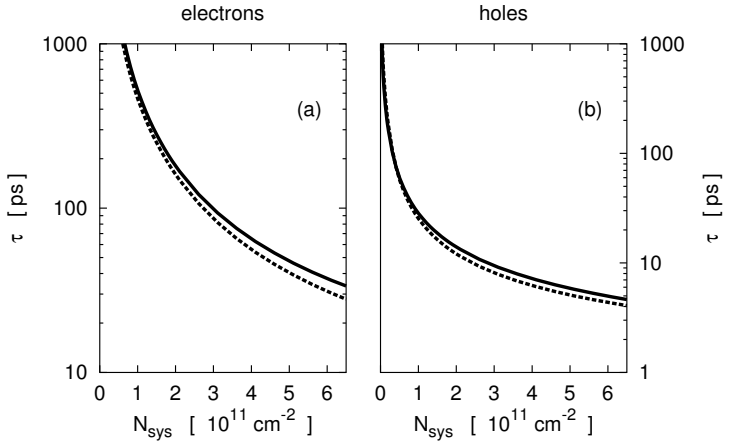

Figure 9.4: Capture times for the p-shell as a function of the total carrier density in the system $N_{\rm sys}$ using the free (unrenormalized energies), with (solid lines) and without (dotted lines) built-in electrostatic field.

another carrier from the WL in the present example. In this way a capture to an energetically deep lying QD state is associated with large momentum transfer for the WL carriers. As the matrix elements have a Gaussian dependence on the in-plane momentum, scattering to WL states with high momentum is suppressed.

The changes in the capture times produced by the field in the case of unrenormalized energies are minimal. This proves that the competing trends described in Section 9.2.2 are nearly compensating each other, with a slight dominance of the effect of electron-hole scattering reduction.

For the calculation of the capture times in Fig. 9.5, based on various possible capture processes dicussed in Sec. 7.2, the renormalized energies are included in the scattering integrals $S_\nu^{\rm in,out}$. Now the capture times become substantially shorter in the presence of the built-in field compared to the zero field case. Thus, the energy separation of the QD levels from the WL edge plays now the dominant role in the scattering times. Even though for the built-in field, the capture processes are somewhat slowed down by the reduction of the electron-hole interaction, they are still faster compared to the zero field case, where due to the electron-hole interaction the QD levels are energetically deeper in the QD.

Figure 9.6 shows the WL assisted QD relaxation times for processes where a QD electron (hole) scatters to a different QD electron (hole) state by means of a WL carrier. Alternatively, a QD carrier performs a transition to the WL while another WL carrier scatters into a different QD state; see Sec. 7.2 to recall dicussion of different scattering processes. Thus the outer index in Eq. (9.1) belongs to a QD state while two of the summation indices

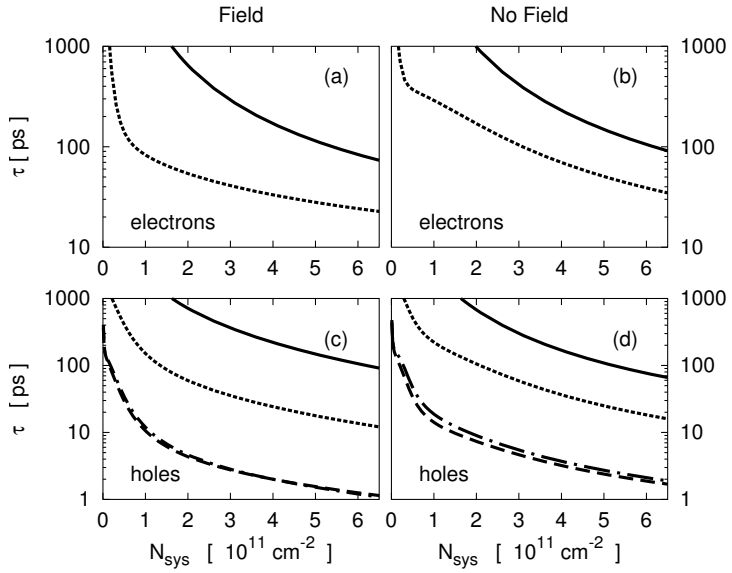

Figure 9.5: Capture times as a function of the total carrier density in the system N_{sys} for s-shell (solid lines), p-shell (dotted lines), d_0-shell (dashed-dotted lines), and $d_{\pm}$-shell (dashed lines).

in Eq. (9.2) correspond to WL states and one label to a QD state. Mixed QD relaxation processes, where e.g. a QD electron scatters out to the WL while another hole from the WL scatters down to the QD hole state play only a minor role due to the charge separation of the electrons and holes caused by the built-in field.

Generally, the relaxation times for holes are one or two orders of magnitude shorter than for electrons, since the QD energy level spacing is larger for the latter. With built-in field the relaxation times become shorter compared to the zero field case, where the QD energy level spacing is larger (with the exception of a slightly slower relaxation of the s-shell electrons). Relaxation times for scattering between QD states are in general more than one order of magnitude shorter than capture. For the p-shell electron relaxation, a saturation effect due to Pauli blocking is observed at higher densities, which leads to comparable capture and relaxation times.

9.3 Conclusion

The presence of the built-in electrostatic field in wurtzite heterostructures causes a charge separation of electrons and holes along the growth direction, which in turn reduces the electron-hole interaction and increases the electron-electron and hole-hole interaction.

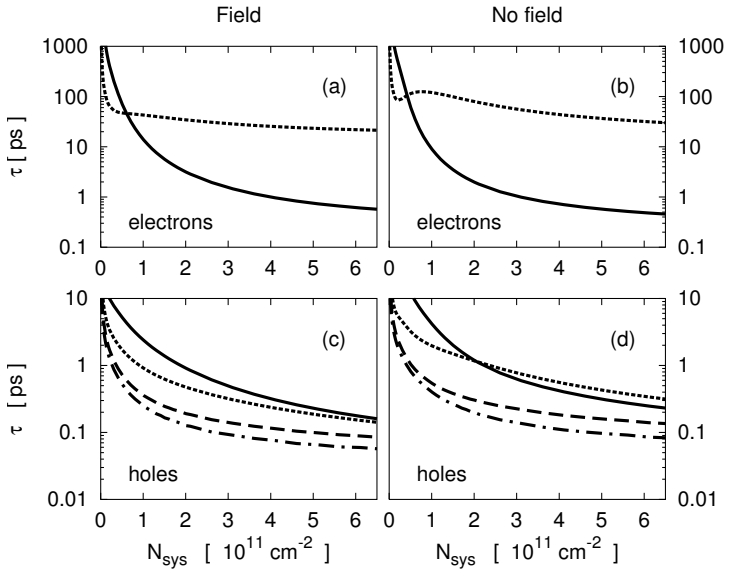

Figure 9.6: Relaxation times as a function of the total carrier density in the system N_{sys} with labeling as in Fig. 9.5.

Our results show that the usually discussed importance of this effect on the interaction matrix elements only weakly influences the scattering rates. It turns out that the change of the self-consistently renormalized energies due to charge separation leads to a much stronger modification of the scattering rates. Specifically, for the influence on the interaction matrix elements, the reduction of electron-hole scattering is partly compensated by the increase of electron-electron and hole-hole scattering. In contrast, for the energy renormalization, the charge separation leads to increased repulsion and decreased attraction in the Hartree terms, both effects working in the same direction of shallower confined levels. This in turn causes an enhancement of the scattering efficiency.

As expected for the QD-WL system, the rates for carrier capture and relaxation strongly depend on the density of excited carriers in the localized and delocalized states. For intermediate densities, the scattering efficiency increases with carrier density. For large densities, Pauli-blocking and screening of the interaction matrix elements slow down a further increase of the scattering rates. For typical InGaN QD parameters, a QD density of 10^{10} cm^{-2} and a carrier density of 10^{11} cm^{-2} at room temperature, direct capture of electrons (holes) to excited QD states results in scattering times on the order of 100 (10) ps. Relaxation times for scattering between the QD hole states are more than one order of magnitude shorter than capture, while at elevated densities the electron p-shell relaxation is of the same order of magnitude as capture.

9.A OPW states and interaction matrix elements

The basic idea of the following scheme is to construct an approximate single-particle basis for the combined QD-WL system which provides a feasible way to compute the interaction matrix elements, Eq. (9.4). We start from localized QD states φ_α, as introduced in Sections 9.1.1 and 9.1.4 with $\alpha = (m, \boldsymbol{R})$, and WL states in the absence of QDs, which are assumed to have plane-wave envelope functions $\varphi^0_{\mathbf{k}}(\boldsymbol{\varrho}) = 1/\sqrt{A}\, e^{i\mathbf{k}\cdot\boldsymbol{\varrho}}$ in the WL plane with the two-dimensional carrier momentum $\boldsymbol{k}$. Quantum numbers for spin, band index, and confinement in z-direction are not explicitly written for notational simplicity. In the presence of the QDs the orthogonality condition of the basis is imposed by projecting the plane waves on the subspace orthogonal to the QD states (OPW), as outlined in Sec. 7.A. The WL states are therefore given by the OPW functions $|\varphi_{\mathbf{k}}\rangle = \frac{1}{N_{\mathbf{k}}}(|\varphi^0_{\mathbf{k}}\rangle - \sum_\alpha |\varphi_\alpha\rangle\langle\varphi_\alpha|\varphi^0_{\mathbf{k}}\rangle)$. Assuming QDs with nonoverlapping wave functions, the sum over $\alpha = (m, \boldsymbol{R})$ counts various QD states m at different QD positions $\boldsymbol{R}$. For randomly distributed identical QDs, the normalization is given by $N^2_{\mathbf{k}} = 1 - N\sum_m |\langle\varphi_m|\varphi^0_{\mathbf{k}}\rangle|^2$.

This scheme allows us to evaluate the in-plane integrals $\langle\nu|e^{i\boldsymbol{q}\cdot\boldsymbol{\varrho}}|\nu'\rangle = \int \mathrm{d}^2\varrho\ \varphi^*_\nu(\boldsymbol{\varrho}) e^{i\boldsymbol{q}\cdot\boldsymbol{\varrho}}\varphi_{\nu'}(\boldsymbol{\varrho})$ which appear in the Coulomb matrix elements, see Eq. (9.6), for various combinations of QD and WL states. When ν and ν' are two QD states, one obtains

$$\left\langle\ \alpha\ |e^{i\boldsymbol{q}\cdot\boldsymbol{\varrho}}|\ \alpha'\ \right\rangle = \left\langle\ m\ |e^{i\boldsymbol{q}\cdot\boldsymbol{\varrho}}|\ m'\ \right\rangle\ e^{i\boldsymbol{q}\cdot\boldsymbol{R}}\,\delta_{\boldsymbol{R},\boldsymbol{R}'}\,, \tag{9.A.20}$$

with the QD positions $\boldsymbol{R}$ and $\boldsymbol{R}'$. For combinations of QD and WL states, one finds

$$\left\langle\ \alpha\ |e^{i\boldsymbol{q}\cdot\boldsymbol{\varrho}}|\ \varphi_{\mathbf{k}'}\ \right\rangle = \left\langle\ m\ |e^{i\boldsymbol{q}\cdot\boldsymbol{\varrho}}|\ \varphi_{\mathbf{k}'}\ \right\rangle\ e^{i(\boldsymbol{k}'+\boldsymbol{q})\cdot\boldsymbol{R}}\,, \tag{9.A.21}$$

and for two WL states

$$\left\langle\ \varphi_{\mathbf{k}}\ |e^{i\boldsymbol{q}\cdot\boldsymbol{\varrho}}|\ \varphi_{\mathbf{k}'}\ \right\rangle = \delta_{\boldsymbol{k},\,\boldsymbol{q}+\boldsymbol{k}'}\ D_{\mathrm{OPW}}(\boldsymbol{k},\boldsymbol{k}',\boldsymbol{q})\,, \tag{9.A.22}$$

follows with

$$\begin{aligned} D_{\mathrm{OPW}}(\boldsymbol{k},\boldsymbol{k}',\boldsymbol{q}) = {} & \frac{1}{N_{\boldsymbol{k}}N_{\boldsymbol{k}'}} \\ & \times[1 - N\sum_m |\langle\varphi^0_{\mathbf{k}}|\varphi_m\rangle|^2 - N\sum_m |\langle\varphi_m|\varphi^0_{\mathbf{k}'}\rangle|^2 \\ & + N\sum_{m,m'}\langle\varphi^0_{\mathbf{k}}|\varphi_m\rangle\langle\varphi_m|e^{i\mathbf{q}\cdot\boldsymbol{\varrho}}|\varphi_{m'}\rangle\langle\varphi_{m'}|\varphi^0_{\mathbf{k}'}\rangle]. \end{aligned} \tag{9.A.23}$$

The orthogonality requirement of the wave functions is directly reflected in the interaction vertices $\langle\nu_1|e^{+i\boldsymbol{q}\cdot\boldsymbol{\varrho}}|\nu_2\rangle = \delta_{\nu_1,\nu_2}$ for $\boldsymbol{q} = 0$. Meaningful results for the interaction matrix elements can be expected only when the approximate model shows the same behavior. Since we start from orthogonal

QD states at a given QD position and assume nonoverlapping wave functions for different QDs, Eq. (9.A.20) reduces to a Kronecker delta for $\boldsymbol{q} = 0$. QD and OPW-WL states are orthogonal by construction, i.e., the requirement is also fulfilled for Eq. (9.A.21). As described in Sec. 7.A, it is the assumption of randomly distributed QDs which, in the large-area limit restores - on average - translational invariance and provides mutually orthogonal OPW states such that the above requirement is also obeyed by Eq. (9.A.22). Note that $D_{\mathrm{OPW}}(\boldsymbol{k}, \boldsymbol{k}, 0) = 1$.

9.B Hartree energy renormalization

Starting from Eq. (9.11), the Hartree energy shift of the QD states has contributions form the QD and from the WL carriers,

$$\begin{aligned}\Delta^{\mathrm{H}}_{b,\alpha} &= \sum_{b',\alpha'} V^{b,b'}_{\alpha\alpha'\alpha'\alpha}\, f^{b'}_{\alpha'} + \sum_{b',\boldsymbol{k}'} V^{b,b'}_{\alpha\boldsymbol{k}'\boldsymbol{k}'\alpha}\, f^{b'}_{\boldsymbol{k}'} \\ &= \Delta^{\mathrm{H,QD}}_{b,\alpha} + \Delta^{\mathrm{H,WL}}_{b,\alpha}\,. \end{aligned} \tag{9.B.24}$$

The QD contribution can be specified further using the notation introduced above and Eq. (9.6),

$$\begin{aligned}\Delta^{\mathrm{H,QD}}_{b,\alpha} = \sum_{\boldsymbol{R}'} \sum_{b',m'} \frac{1}{A} \sum_{\boldsymbol{q}} V^{b,b'}(\boldsymbol{q})\, f^{b'}_{m'} \\ \times \langle m|e^{-i\boldsymbol{q}\cdot\boldsymbol{\varrho}}|m\rangle\langle m'|e^{+i\boldsymbol{q}\cdot\boldsymbol{\varrho}}|m'\rangle \\ \times e^{-i\boldsymbol{q}\cdot(\boldsymbol{R}-\boldsymbol{R}')}. \end{aligned} \tag{9.B.25}$$

The result depends on the QD positions through the phase factor arising from the interaction vertices as given by Eqs. (9.A.20)-(9.A.22). In the large area limit one obtains, by the law of large numbers, that the distribution of these quantities is sharply peaked around their configurational averaged value. Therefore we may replace the QD contribution in Eq. (9.B.24) by

$$\begin{aligned}\Delta^{\mathrm{H,QD}}_{b,m} = \frac{1}{N} \sum_{\boldsymbol{R},\boldsymbol{R}'} \sum_{b',m'} \frac{1}{A} \sum_{\boldsymbol{q}} V^{b,b'}(\boldsymbol{q})\, f^{b'}_{m'} \\ \times \langle m|e^{-i\boldsymbol{q}\cdot\boldsymbol{\varrho}}|m\rangle\langle m'|e^{+i\boldsymbol{q}\cdot\boldsymbol{\varrho}}|m'\rangle \\ \times e^{-i\boldsymbol{q}\cdot(\boldsymbol{R}-\boldsymbol{R}')}. \end{aligned} \tag{9.B.26}$$

Note that the resulting Hartree shift does not depend on the QD position any more. The summation over the random positions $\boldsymbol{R}, \boldsymbol{R}'$ is evaluated as in the disordered system theory (see e.g. Ref. [9.36]):

$$\begin{aligned}\sum_{\boldsymbol{R},\boldsymbol{R}'} f(\boldsymbol{R}) g(\boldsymbol{R}') &= \sum_{\boldsymbol{R}\neq\boldsymbol{R}'} f(\boldsymbol{R}) g(\boldsymbol{R}') + \sum_{\boldsymbol{R}} f(\boldsymbol{R}) g(\boldsymbol{R}) \\ &= N^2 \langle\langle f \rangle\rangle \cdot \langle\langle g \rangle\rangle + N \langle\langle fg \rangle\rangle\,, \end{aligned} \tag{9.B.27}$$

where $\langle\langle F\rangle\rangle = 1/A \int d^2R\, F(\boldsymbol{R})$ denotes the configuration average. The first term is the uncorrelated average of the two random variables, while the second takes into account that for the same point they are correlated.

In our case $f(\boldsymbol{R}) = e^{-i\boldsymbol{q}\cdot\boldsymbol{R}}, g(\boldsymbol{R'}) = e^{i\boldsymbol{q}\cdot\boldsymbol{R'}}$, $\langle\langle f\rangle\rangle = \langle\langle g\rangle\rangle = \delta_{\boldsymbol{q},0}$ and $\langle\langle fg\rangle\rangle = 1$, so that one may write:

$$\Delta^{\mathrm{H,QD}}_{b,m} \;=\; n_{\mathrm{QD}} \sum_{b',m'} V^{b,b'}(\boldsymbol{q}=0) f^{b'}_{m'} \;+\; \sum_{b',m'} V^{b,b'}_{mm'm'm}\, f^{b'}_{m'}. \qquad \text{(9.B.28)}$$

The first term, arising from the Coulomb interaction between different QDs is proportional to the total QD charge density, while the second one describes the Hartree interaction inside a given dot.

The WL contribution to the QD Hartree energy shift can be evaluated similarly,

$$\begin{aligned}
\Delta^{\mathrm{H,WL}}_{b,\alpha} &= \sum_{b',\boldsymbol{k'}} \frac{1}{A} \sum_{\boldsymbol{q}} V^{b,b'}(\boldsymbol{q})\; f^{b'}_{\boldsymbol{k'}} \\
&\times \;\langle m|e^{-i\boldsymbol{q}\cdot\boldsymbol{\varrho}}|m\rangle e^{-i\boldsymbol{q}\cdot\boldsymbol{R}} \\
&\times \;\delta_{\boldsymbol{k'},\boldsymbol{k'}+\boldsymbol{q}} D_{\mathrm{opw}}(\boldsymbol{k},\boldsymbol{k'},\boldsymbol{q}) \\
&= \frac{1}{A} \sum_{b',\boldsymbol{k'}} V^{b,b'}(\boldsymbol{q}=0) f^{b'}_{\boldsymbol{k'}}. \qquad \text{(9.B.29)}
\end{aligned}$$

The result has the same structure as the first term of Eq. (9.B.28) and adds the WL charge density to the QD contribution. By charge neutrality these terms cancel each other and, as expected, the Coulomb singularity at $\boldsymbol{q} = 0$ is removed. One is left with the second term of Eq. (9.B.28), which gives Eq. (9.13).

Following the same steps as above we find for the WL Hartree energy shift

$$\begin{aligned}
\Delta^{\mathrm{H}}_{b,\boldsymbol{k}} &= \sum_{b',\alpha'} V^{b,b'}_{\boldsymbol{k}\alpha'\alpha'\boldsymbol{k}}\; f^{b'}_{\alpha'} + \sum_{b',\boldsymbol{k'}} V^{b,b'}_{\boldsymbol{k}\boldsymbol{k'}\boldsymbol{k'}\boldsymbol{k}} f^{b'}_{\boldsymbol{k'}} \\
&= V^{b,b'}(\boldsymbol{q}=0)\Big\{ n_{\mathrm{QD}} \sum_{b',m'} f^{b'}_{m'} + \frac{1}{A} \sum_{b',\boldsymbol{k'}} f^{b'}_{\boldsymbol{k'}} \Big\} \\
&= 0, \qquad \text{(9.B.30)}
\end{aligned}$$

which vanishes due to global charge neutrality.

9.C WL screening contributions to the QD Hartree interaction

In our description of the QD-WL system, the summation over randomly distributed QDs restores, in the large area limit, the in-plane translational

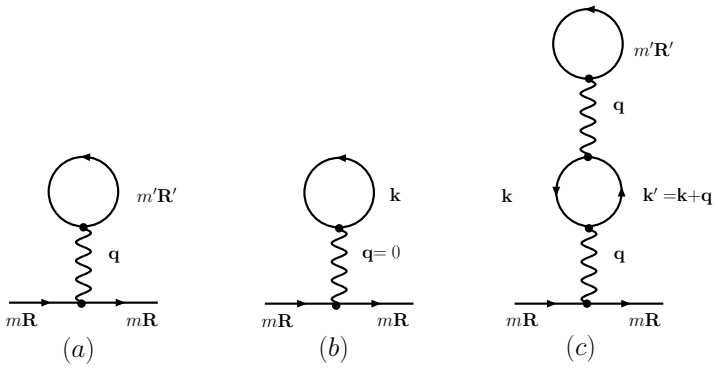

Figure 9.7: Feynman diagrams for the Hartree Coulomb interaction.

invariance of the OPW-WL states. On this level, only the averaged QD properties enter - a picture which is consistent with the expectation that in a system with a macroscopic number of QDs, like a QD-laser, only the averaged properties of the QD ensemble should be important. On a local scale at a QD position, however, the WL states do not obey translational invariance since perturbations of the WL states due to the QD appear. In truly homogeneous systems one has a $\boldsymbol{q} = 0$ Coulomb singularity which is canceled out by the global charge neutrality and no other Hartree contribution is present. Here one expects that a similar singularity is produced by the configuration averaging and is removed by global neutrality arguments, but local Hartree fields are still felt by the carriers in the QD.

The phenomenon is illustrated, using the Green's function (GF) formalism [9.36], by the diagrams in Fig. 9.7, describing terms of the Hartree contribution to the QD energies. Since the QDs are identical, the QD propagators are position independent, but the interaction vertices contain phase factors related to the position and to the adjoining momenta, as given by Eqs. (9.A.20)-(9.A.22). The procedure described in the previous Appendix amounts to the averaging of the Hartree self-energies. For instance, the self-energies in diagrams (a) and (b) correspond to the terms $\Delta_{b,\alpha}^{\mathrm{H,QD}}$, $\Delta_{b,\alpha}^{\mathrm{H,WL}}$ discussed in Appendix 9.B.

The phase factors in diagram (c) are the same as in diagram (a). Again, applying Eq. (9.B.27) to diagram (c) gives rise to two terms. The first one, corresponding to the uncorrelated averaging, produces a $\boldsymbol{q} = 0$ singularity. Since this entails the restriction $\boldsymbol{k} = \boldsymbol{k}'$, the diagram contributes to the renormalization of the WL propagator of index $\boldsymbol{k}$ in diagram (b). Therefore this is already included in a selfconsistent calculation.

More interesting is the second term, arising from the correlated averaging. In this case one has $\boldsymbol{R} = \boldsymbol{R}'$ and the summation over the momentum transfer $\boldsymbol{q}$ remains unrestricted. The structure is similar to the second term

of diagram (a), i.e., it corresponds to the intra-QD Hartree field, but with the additional $\boldsymbol{k}$ and $\boldsymbol{k}'$ WL propagators forming a Lindhard loop. The loop describes the screening by the WL carriers of the intra-QD Hartree field.

The usual procedure in the GF theory is to leave the Hartree interaction unscreened and to include the Lindhard loop in the 'tadpole head' GF of diagram (b). This avoids the double counting of such diagrams. As a result a nondiagonal $(\boldsymbol{k}, \boldsymbol{k}')$ GF appears in the Hartree loop of diagram (b). Alternatively, one can avoid double counting by keeping only momentum-diagonal WL propagators and leave the Lindhard loop for the screening of the Coulomb line. We have chosen this second approach, which also considerably simplifies the formalism.

A fully systematic analysis of all the possible diagrams and the action of the configuration averaging over them is way beyond the scope of this chapter. The approximation proposed here includes the following physically important features. The random phases associated with the QD positions give rise to a $\boldsymbol{q} = 0$ singularity, which is canceled out by the global charge neutrality. On the other hand, the intra-QD fields are not influenced by the phase factors and therefore are not averaged out. The same is true for the local WL charges that respond to these fields and induce their screening.

9.D Renormalization scheme

In this Appendix we compare the screened HF and CH energy renormalization with the usual HF approach based on the bare Coulomb interaction. Figure 9.8 shows the renormalized QD p-shell energy using these two schemes.

First we dicuss the case of zero field. For electrons at high densities, renormalization of the p-shell is overestimated for the bare Coulomb interaction compared to the screened renormalization. The holes are subjected to the same renormalization using either of the two schemes. For the built-in field, the screened renormalization leads to a larger shift for both electrons and hole compared to the bare energy renormalization. The difference is manly due the Coulomb correlations.

In Fig. 9.9 the capture times for the p-shell using the two energy renormalization schemes are plotted. With the built-in field, the capture times for electrons evaluated with the bare HF renormalization scheme are shorter than capture times obtained with the screened procedure. However, the difference between the two schemes is not as big as Fig. 9.8 (a) would indicated, since the WL states are also shifted by the energy renormalization. The screened renormalization shifts the WL states energetically deeper towards the QD levels than for the bare Coulomb renormalization. For the same reasons, the electron capture times for zero field are shorter using the screened renormalization in comparison to the bare renormalization. With the built-

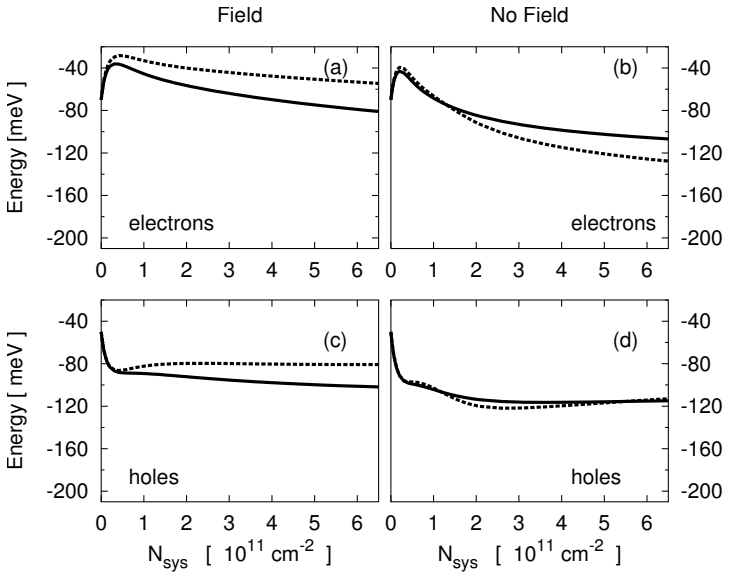

Figure 9.8: Same as Fig. 9.2 for the renormalized p-shell energy $\widetilde{\varepsilon}_{\rm p}$, with screened renormalization scheme $\widetilde{\varepsilon}_{\rm p} = \varepsilon_{\rm p} + \Delta_{\rm p}^{\rm SH} + \Delta_{\rm p}^{\rm SX} + \Delta_{\rm p}^{\rm CH}$ (solid lines) and bare renormalization scheme $\widetilde{\varepsilon}_{\rm p} = \varepsilon_{\rm p} + \Delta_{\rm p}^{\rm H} + \Delta_{\rm p}^{\rm F}$ (dotted lines).

in field the capture times for holes obtained by the screened renormalized scheme are shorter than using the bare renormalization scheme. This is opposite to what Fig. 9.8 (c) would indicate, and is caused by the Coulomb correlations and the stronger z-confinement for holes. The case of zero field can be analyzed along the same lines, giving shorter scattering times for the screened renormalization scheme.

References

[9.1] A. Nakamura, Science **281**, 956 (1998).

[9.2] S. C. Jain, M. Willander, J. Narayan, and R. V. Overstraeten, J. Appl. Phys. **87**, 965 (2000).

[9.3] B. Damilano, N. Grandjean, F. Semond, J. Massies, and M. Leroux, Appl. Phys. Lett. **75**, 962 (1999).

[9.4] S. Kalliakos, T. Bretagnon, P. Lefebvre, T. Taliercio, B. Gil, N. Grandjean, B. Damilano, A. Dussaigne, and J. Massies, J. Appl. Phys. **96**, 180 (2004).

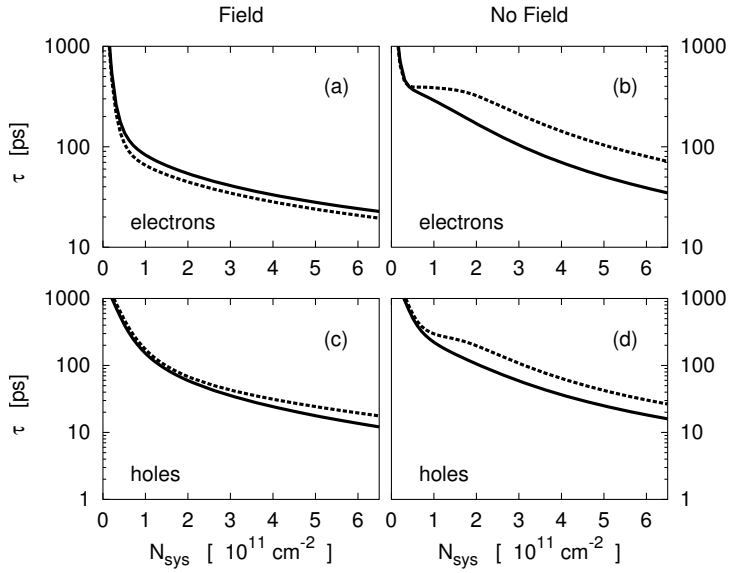

Figure 9.9: Capture times for the p-shell as a function of the total carrier density in the system N_{sys} with labeling as in Fig. 9.8.

[9.5] I. L. Krestnikov, N. N. Ledentsov, A. Hoffmann, D. Bimberg, A. V. Sakharov, W. V. Lundin, A. F. Tsatsul'nikov, A. S. Usikov, and Z. I. Alferov, Phys. Rev. B **66**, 155310 (2002).

[9.6] R. A. Oliver, G. A. D. Briggs, M. J. Kappers, C. J. Humphreys, S. Yasin, J. H. Rice, J. D. Smith, and R. A. Tayler, Appl. Phys. Lett. **83**, 755 (2003).

[9.7] I. Vurgaftman and J. R. Meyer, J. Appl. Phys. **94**, 3675 (2003).

[9.8] S. L. Chuang and C. S. Chang, Phys. Rev. B **54**, 2491 (1996).

[9.9] F. Bernardini, V. Fiorentini, and D. Vanderbilt, Phys. Rev. Lett. **79**, 3958 (1997).

[9.10] F. Bernardini and V. Fiorentini, Phys. Rev. B. **57**, R9427 (1998).

[9.11] R. Cingolani, A. Botchkarev, H. Tang, H. Morko, G. Traetta, G. Coli, M. Lomascolo, A. D. Carlo, F. D. Sala, and P. Lugli, Phys. Rev. B **61**, 2711 (2000).

[9.12] A. Ranjan, G. Allen, C. Priester, and C. Delerue, Phys. Rev. B **68**, 115305 (2003).

[9.13] U. Bockelmann and T. Egeler, Phys. Rev. B **46**, 15574 (1992).

[9.14] I. Vurgaftman, Y. Lam, and J. Singh, Phys. Rev. B **50**, 14309 (1994).

[9.15] M. Brasken, M. Lindberg, M. Sopanen, H. Lipsanen, and J. Tulkki, Phys. Rev. B **58**, R15993 (1998).

[9.16] I. Magnusdottir, S. Bischoff, A. V. Uskov, and J. Mørk, Phys. Rev. B **67**, 205326 (2003).

[9.17] T. R. Nielsen, P. Gartner, and F. Jahnke, Phys. Rev. B **69**, 235314 (2004).

[9.18] H. C. Schneider, W. W. Chow, and S. W. Koch, Phys. Rev. B **70**, 235308 (2004).

[9.19] S. De Rinaldis, I. D'amico, and F. Rossi, Phys Rev. B **69**, 235316 (2004).

[9.20] A. D. Andreev and E. P. O'Reilly, Phys. Rev. B **62**, 15851 (2000).

[9.21] A. Bagga, P. K. Chattopadhyay, and S. Ghosh, Phys. Rev. B **68**, 155331 (2003).

[9.22] V. A. Fonoberov and A. A. Balandin, J. Appl. Phys. **94**, 7178 (2003).

[9.23] W. Sheng, S.-J. Cheng, and P. Hawrylak, Phys. Rev. B **71**, 035316 (2005).

[9.24] A. J. Williamson, L. W. Wang, and A. Zunger, Phys. Rev. B **62**, 12963 (2000).

[9.25] G. Bester and A. Zunger, Phys. Rev. B **71**, 045318 (2005).

[9.26] S. Schulz and G. Czycholl, arXiv:cond-mat/0507052, 2005.

[9.27] A. Wojs, P. Hawrylak, S. Fafrad, and L. Jacak, Phys. Rev. B **54**, 5604 (1996).

[9.28] W. W. Chow, M. Kira, and S. W. Koch, Phys. Rev. B **60**, 1947 (1999).

[9.29] W. W. Chow and S. W. Koch, *Semiconductor - Laser Fundamentals* (Springer, Berlin, 1999).

[9.30] H. Haug and S. W. Koch, *Quantum Theory of the Optical and Electronic Properties of Semiconductors*, 3. ed. (World Scientific Publ., Singapore, 1994).

[9.31] *Properties of Advanced Semiconductor Materials GaN, AlN, InN, BN, SiC, SiGe*, edited by M. R. Levinshtein, S. L. Rumyantsev, and M. S. Shur (John Wiley & Sons, Inc., New York, 2001), GaN: pp 1-30 (V. Bourgrov, et al.); InN: pp 49-66 (A. Zubrilov, et al.).

[9.32] J. Wu and W. Walukiewicz, Superlattices and Microsctrutures **34**, 63 (2003).

[9.33] H. Zang, E. J. Miller, E. T. Yu, C. Poblenz, and J. S. Speck, J. Vac. Sci. Technol. B **22**, 2169 (2004).

[9.34] C. Y. Lai, M. Hus, W.-H. Chang, K.-U. Tseng, C.-M. Lee, C.-C. Chuo, and J.-I. Chyi, J. Appl. Phys. **91**, 531 (2002).

[9.35] Y.-S. Lin, K.-J. Ma, C. Hsu, Y.-Y. Chung, C.-W. Liu, S.-W. Feng, Y.-C. Chang, C. C. Yang, H.-W. Chuang, C.-T. Kuo, J.-S. Tsang, and T. E. Weirich, Appl. Phys. Lett. **80**, 2571 (2002).

[9.36] S. Doniach and E. H. Sondheimer, *Green's functions for solid state physicists* (Imperial College Press, London, 1998).

Part IV

Chapter 10

Conclusion and Outlook

The topic of this thesis is carrier-carrier and carrier-phonon interaction in semiconductor self-assembled quantum dots (QDs). Our focus is on the scattering processes by these interactions leading to carrier capture into and relaxation inside the QDs. Previous studies based on perturbation theory or rate equations fail to incorporate the many-body effects of such QD systems and are often too crude in their descriptions. Instead, the problem is formulated in this thesis within the more general framework of the nonequilibrium Green's function theory. The advantage of this approach is the straightforward inclusion of many-body effects, such as Pauli blocking, screening of the Coulomb interaction, renormalization of the interacting electronic states, as well as being adequate for a description on a pico-second time scale where quantum kinetic effects dominate the evolution.

For the description of carrier-carrier and carrier-phonon scattering in self-assembled QDs new methods are necessary which, compared to the standard bulk or quantum-well semiconductor systems, offer a simultaneous description of the localized QD states and the energetically nearby continuum of extended states of the wetting-layer (WL). The orthogonalized plane waves (OPW) scheme used in this thesis incorporates the main features of WL and QD states being orthogonal, while still allowing for all possible combinations of QD and WL states entering the interaction matrix elements to be determined analytically to a large extent. Furthermore, our studies also stress the importance of describing the QD states in the presence of a continuum, giving attention not only to the localized but also to the extended states.

Using the OPW scheme, carrier-carrier scattering is investigated within the second order Born approximation. In general the population dynamics for a given initial situation is determined through a kinetic equation governed by in- and out-scattering rates. Using the relaxation time approximation we can contrast different scattering processes, under quasi-equilibrium conditions. The corresponding scattering time has by the structure of the

kinetic equation contributions from both the in- and an out-scattering rates. Our results for the InGaAs system show that, not only the direct Coulomb scattering but also the exchange scattering is important. For the former both electron-electron and electron-hole scattering are important, the same being true for the hole-hole and hole-electron scattering. Furthermore it is compulsory that all scattering channels must be addressed simultaneously. Direct capture from the WL to the QD is slower than relaxation inside the QD, since the involved interaction matrix elements for the capture processes are smaller. In general, scattering times for electrons are longer than for holes since by the larger electron QD level spacing the Coulomb matrix elements for the involved states in an energy conserving scattering process are smaller. This is a general trend, showing that scattering processes for deep levels are slower than for the shallower ones. Finally the scattering times show a strong dependence on the carrier density in the system due to the influence of the Paul blocking and screening effects.

The studies of carrier-carrier scattering in InGaAs QDs are performed by using the free un-renormalized energies within the energy conserving delta functions entering the Boltzmann scattering integrals. The question rises to which extent these results are influenced by charging effects of the QDs. The answer is given by studying the carrier-carrier scattering in InGaN QD systems. The presence of a built-in electrostatic field in wurtzite nitride heterostructures causes a charge separation of electrons and holes and from electrostatic considerations alone one is lead to consider the Hartree (electrostatic) energy shift for the states involved in the scattering processes. Our results show that the usually discussed importance of the charge separation on the Coulomb matrix elements only weakly influences the scattering rates. It turns out that the effects of the charge seperation on the self-consistently renormalized energies leads to a much stronger modification of the scattering rates. Specifically, for the influence on the interaction matrix elements, the reduction of electron-hole scattering is partly compensated by the increase of electron-electron and hole-hole scattering. In contrast, for the energy renormalization, the charge separation leads to increased repulsion and decreased attraction in the Hartree terms, both effects working in the same direction of shallower confined levels. This in turn causes an important enhancement of the scattering efficiency.

The above described studies of carrier-carrier scattering drives any given carrier distribution towards a quasi-equilibrium distribution. To bring the carrier system to the lattice temperature a dissipative mechanism is needed to cool it. This is done by the carrier-phonon scattering. Furthermore, at low carrier densities the carrier scattering is dominated by the interaction with phonons. The carrier-phonon scattering is investigated within the random phase approximation for the InGaAs model system. As for the carrier Coulomb interaction the population dynamics for a given initial situ-

ation is determined through a kinetic equation containing both in- and out-scattering rates. When capture processes due to emission of longitudinal-optical (LO) phonons are possible at the Boltzmann level, their efficiency is comparable to Coulomb scattering at elevated carrier densities, while at low carrier densities LO-phonon capture times are shorter than those provided by Coulomb scattering. However, the interaction of carriers with LO phonons at the Boltzmann level predicts inefficient scattering (phonon bottleneck) when the transition energies of the quantum dot states do not match the LO-phonon energy. Nonetheless, for situations where in terms of free-carrier energies energy conserving scattering processes are not possible, we demonstrate that a quantum kinetic description of the carrier-phonon interaction supports experimentally observed fast scattering processes. A key ingredient in this description is the polaron picture, where the electronic states are dressed by the interaction with phonons. Carrier-phonon scattering is then formulated in terms of the new renormalized states, which allow for efficient scattering channels.

The theoretical investigations presented in this thesis on the carrier Coulomb and carrier phonon interaction may serve as foundation for further studies of ultra-fast carrier dynamics in self-assembled QDs. As a first step the incoherent limit of the carrier-carrier scattering for the population dynamics of a nonequilibrium carrier distribution can be investigated. In a follow-up study, the coherent limit should be considered, i.e., when carriers are excited with an optical pulse the polarization dynamics also have to be included. Within this framework pump-probe experiments, like e.g. differential transmission spectra, can be modeled. On a more general level, one could combine the theoretical tools developed in this thesis to describe the carrier Coulomb interaction and the carrier-phonon interaction, with elaborated methods like tight-binding or $\boldsymbol{k} \cdot \boldsymbol{p}$ for evaluating the corresponding interaction matrix elements.

Appendix A

Material-Parameters

A.1 3D Exciton Units

$$\epsilon = \epsilon_0 \epsilon_r \qquad \text{Dielectric constant} \qquad (A.1)$$

$$\frac{1}{m_r} = \frac{1}{m_e} + \frac{1}{m_h} \qquad \text{Inverse reduced mass} \qquad (A.2)$$

$$m_r = \widetilde{m}_r m_0 \qquad \text{Reduced mass} \qquad (A.3)$$

$$a_0 = \frac{\hbar^2 \epsilon}{\frac{e^2}{4\pi} m_r} \qquad \text{Exciton Bohr radius} \qquad (A.4)$$

$$E_0 = \frac{\hbar^2}{2 m_r a_0^2} \qquad \text{Exciton binding energy} \qquad (A.5)$$

$$E_0 = 13.605 \, \frac{\widetilde{m}_r}{\epsilon_r^2} \, [\text{eV}] \qquad (A.6)$$

$$a_0 = 0.5290 \, \frac{\epsilon_r}{\widetilde{m}_r} \, \cdot 10^{-10} [\text{m}] \qquad (A.7)$$

A.2 InGaAs

Parameters			
Bandgap (GaAs 300K)	E_{G}	1.42	[eV]
Electron mass	m_{e}	0.067 [a]	[m_0]
Hole mass	m_{h}	0.150 [b]	[m_0]
Static dielectric constant	ϵ_r	12.5 [a]	[ε_0]
Heigh-frequency dielectric constant	ϵ_∞	10.9	[ε_0]
Exciton Bohr radius (3D)	a_0	142.77	[Å]
Exciton binding energy (3D)	E_{B}	4.036	[meV]
Phonon energy	$\hbar\omega_{\mathrm{LO}}$	36 [c]	[meV]
Electron-phonon coupling	α	0.06 [c]	
Life-time LO phonon	τ_{LO}	5 [d]	[ps]
Semiconductor Structure			
Height quantum dot	L_{QD}	4.3	[nm]
Height wetting-layer	L_{WL}	2.2	[nm]
Quantum-dot density	n_{QD}	10^{10}	[cm^{-2}]
Quantum-Dot Energies			
Electron s-shell	ε_{s}	-80 [e]	[meV]
Electron p-shell	ε_{p}	-40 [e]	[meV]
Electron band-offset	U_0	350 [a]	[meV]
Hole s-shell	ε_{s}	-30 [e]	[meV]
Hole p-shell	ε_{p}	-15 [e]	[meV]
Hole band-offset	U_0	170 [a]	[meV]

Table A.1: Material parameters used in Chap. 7 and 8.

[a] From: A. Wojs, P. Hawrylak, S. Fafard, and L. Jack, Phys. Rev. B **54**, 5604 (1996)

[b] From: Th. Wimbauer and K. Oettinger et al., Phys. Rev. B **50**, 8889 (1994); N. Baer, Diplomarbeit, Universität Bremen (2003)

[c] From: Landolt-Börnstein

[d] From: S. Sauvage et al., Phys. Rev. Lett. **88**, 177402 (2002)

[e] From: H. C. Schneider, W. W. Chow, and S. W. Koch, Phys. Rev. B **64**, 115315 (2001)

A.3 InGaN

Table A.2: Material parameters* used in Chap. 9.

Parameters	GaN	InN	$In_{0.2}Ga_{0.8}N$
E_g[300 K] (eV)	3.438	0.756	2.677
ΔE_e (eV)			0.457
ΔE_h (eV)			0.304
ϵ_r	8.9 [a]	15.3 [a]	10.2
m_e (m_0)	0.2	0.07	0.174
A_1	-7.21	-8.21	-7.41
A_2	-0.44	-0.68	-0.488
A_3	6.68	7.57	6.858
A_4	-3.46	-5.23	-3.814
A_5	-3.40	-5.11	-3.742
Δ_{so} (eV)	0.017	0.005	0.0146
Quantum well (nm)			3.0
$F_{\text{QD-WL}}$ (MV/cm)			1.5
F_{barrier} (MV/cm)			0.75

Table A.3: QD parameters used in Chap. 9.

Parameters	Electrons	Holes	
Shells	s, p	s, p, d	
Level spacing (meV)	90	30	
ε_s (meV)	-160	-80	
ε_p (meV)	-70	-50	
ε_d (meV)		-20	
QD density (cm^{-2})			10^{10}

* From: I. Vurgaftman and J. R. Meyer, J. Appl. Phys. **94**, 3675 (2003)

[a] From: Levinshtein et al., *Properties of Advanced Semiconductor Materials GaN, AlN, InN, BN, SiC, SiGe*, John Wiley & Sons, New York, 2001.

Appendix B

Matrix Elements

Assuming a separation of the wave function into in-plane and z-component is valid, $\Phi_\nu(\mathbf{r}) = \varphi_l^b(\boldsymbol{\varrho})\ \xi_\sigma^b(z)\ u_b(\mathbf{r})$ where $u_b(\mathbf{r})$ are Bloch functions, the Coulomb matrix elements

$$V_{\nu\nu_2\nu_3\nu_1} = \int d^3r\ d^3r'\ \Phi_\nu^*(\mathbf{r})\Phi_{\nu_2}^*(\mathbf{r}')v(\mathbf{r}-\mathbf{r}')\Phi_{\nu_3}(\mathbf{r}')\Phi_{\nu_1}(\mathbf{r}),$$

can be cast into the form

$$\begin{aligned} V_{\nu\nu_2\nu_3\nu_1} =& \frac{1}{A}\sum_{\mathbf{q}} V_{\sigma\sigma_2\sigma_3\sigma_1}^{b,b_2}(\mathbf{q})\,\delta_{b,b_1}\delta_{b_2,b_3} \\ & \times \int d^2\varrho\ \varphi_l^b(\boldsymbol{\varrho})^*\varphi_{l_1}^{b_1}(\boldsymbol{\varrho})\,e^{-i\mathbf{q}\cdot\boldsymbol{\varrho}}\ \times \int d^2\varrho'\ \varphi_{l_2}^{b_2}(\boldsymbol{\varrho}')^*\varphi_{l_3}^{b_3}(\boldsymbol{\varrho}')\,e^{i\mathbf{q}\cdot\boldsymbol{\varrho}'}, \end{aligned}$$

with

$$V_{\sigma\sigma_2\sigma_3\sigma_1}^{b,b'}(\mathbf{q}) = \frac{e^2}{2\varepsilon_0 q}\int dz\ dz'\ \xi_\sigma^b(z)^*\xi_{\sigma_2}^{b'}(z')^*e^{-q|z-z'|}\xi_{\sigma_3}^{b'}(z')\xi_{\sigma_1}^{b}(z),$$

where the combined index ν contains all quantum numbers for the in-plane and z-components of the wave functions, l and σ, respectively, as well as the band index $b = e, h$ for electrons and holes.

In Secs. B.1 and B.2 we list the in-plane wave functions for the quantum dots (QDs) and wetting-layer (WL) states, respectively. The corresponding in-plane overlap integrals, needed to evaluate the Coulomb matrix elements, are listed in Secs. B.3 and B.4.

B.1 Single particle states of the two-dimensional harmonic oscillator

The single particle energies $E_{n,m}$ and states $\varphi_{n,m}$ of a particle with mass m^* confined in a two-dimensional harmonic potential[1] are labeled by the

[1] From: C. Cohen-Tannoudji, B. Diu and F. Laloë., *Quantum Mechanics Vol. I*, p. 734, John Wiley & Sons, 1977.

quantum numbers $l = (n, m)$. The first quantum number $n = 0, 1, 2, ...$ determines the energy (s,p,d,... shell). The second quantum number $m = -n, -n+2, ..., n-2, n$ characterizes the two-dimensional angular momentum. The corresponding energies and first few eigenfunctions using polar coordinates are listed below

$$E_{n,m} = \hbar\omega_{\mathrm{HO}}\,(n+1)\,, \tag{B.1}$$

$$\hbar\omega_{\mathrm{HO}} = \frac{\hbar^2\beta^2}{m^*}, \tag{B.2}$$

$$\varphi_{0,0}(\boldsymbol{\varrho}) = \frac{\beta}{\sqrt{\pi}}\,\exp\left\{-\frac{\beta^2\varrho^2}{2}\right\}, \tag{B.3}$$

$$\varphi_{1,+1}(\boldsymbol{\varrho}) = \frac{\beta}{\sqrt{\pi}}\,\beta\varrho\,\exp\left\{-\frac{\beta^2\varrho^2}{2}\right\}\,\exp\{+i\phi\}\,, \tag{B.4}$$

$$\varphi_{1,-1}(\boldsymbol{\varrho}) = \frac{\beta}{\sqrt{\pi}}\,\beta\varrho\,\exp\left\{-\frac{\beta^2\varrho^2}{2}\right\}\,\exp\{-i\phi\}\,, \tag{B.5}$$

$$\varphi_{2,-2}(\boldsymbol{\varrho}) = \frac{\beta}{\sqrt{2\pi}}\,(\beta\varrho)^2\exp\left\{-\frac{\beta^2\varrho^2}{2}\right\}\,\exp\{-i2\phi\} \tag{B.6}$$

$$\varphi_{2,+2}(\boldsymbol{\varrho}) = \frac{\beta}{\sqrt{2\pi}}\,(\beta\varrho)^2\exp\left\{-\frac{\beta^2\varrho^2}{2}\right\}\,\exp\{+i2\phi\}\,, \tag{B.7}$$

$$\varphi_{2,0}(\boldsymbol{\varrho}) = \frac{\beta}{\sqrt{\pi}}\,\left[(\beta\varrho)^2-1\right]\exp\left\{-\frac{\beta^2\varrho^2}{2}\right\}. \tag{B.8}$$

B.2 Orthogonalized Plane Waves

Starting point for the construction of the delocalized wave functions are WL states in the absence of QDs, which are considered as plane-waves (PW)

$$\varphi^0_{\boldsymbol{k}}(\boldsymbol{\varrho}) = \frac{1}{\sqrt{A}}\,e^{+i\boldsymbol{k}\cdot\boldsymbol{\varrho}}, \tag{B.9}$$

with two-dimensional carrier momentum $\mathbf{k}$. The delocalized WL states are constructed according to the orthogonalized plane waves (OPW) scheme given in Chap. 7,

$$|\,\varphi_{\boldsymbol{k}}\,\rangle = \frac{1}{N_{\boldsymbol{k}}}\left(|\,\varphi^0_{\boldsymbol{k}}\,\rangle - \sum_{\alpha}\,|\,\varphi_\alpha\,\rangle\cdot\langle\,\varphi_\alpha\,|\,\varphi^0_{\boldsymbol{k}}\,\rangle\right), \tag{B.10}$$

$$N^2_{\boldsymbol{k}} = 1 - N_{\mathrm{dot}}\sum_{l}\,|\,\langle\,\varphi^0_{\boldsymbol{k}}\,|\,\varphi_l\,\rangle\,|^2, \tag{B.11}$$

with $\alpha = \{\boldsymbol{R}, l\}$ giving the position $\boldsymbol{R}$ and l all other quantum numbers needed to specify the specific QD state and N_{dot} giving the QD density.

B.3 OPW Overlap Integrals

The Coulomb matrix elements for localized and delocalized states contain overlap integrals of the type

$$\langle \varphi_{\alpha'} \,|e^{-i\boldsymbol{q}\boldsymbol{\varrho}}|\, \varphi_{\boldsymbol{k}} \rangle \;=\; \frac{1}{N_{\boldsymbol{k}}} \Bigg[\langle \varphi_{\alpha'} \,|e^{-i\boldsymbol{q}\boldsymbol{\varrho}}|\, \varphi^0_{\boldsymbol{k}} \rangle - \sum_{\alpha} \langle \varphi_{\alpha'} \,|e^{-i\boldsymbol{q}\boldsymbol{\varrho}}|\, \varphi_{\alpha} \rangle \cdot \langle \varphi_{\alpha} \,|\, \varphi^0_{\boldsymbol{k}} \rangle \Bigg]. \tag{B.12}$$

For our model system, we have at the most three shells (s, p, d) confined at the QDs. Thus, we have to evaluate the following QD-OPW overlap integrals

$$\begin{aligned} \langle\, \varphi_{n,m} \,|e^{-i\boldsymbol{q}\boldsymbol{\varrho}}|\, \varphi_{\boldsymbol{k}} \,\rangle \;=\; \frac{1}{N_{\boldsymbol{k}}} \Bigg[& \langle\, \varphi_{n,m} \,|\, e^{-i\boldsymbol{q}\boldsymbol{\varrho}} \,|\, \varphi^0_{\boldsymbol{k}} \,\rangle \\ & - \Bigg(\quad \langle\, \varphi_{0,0} \,|\, \varphi^0_{\boldsymbol{k}} \,\rangle \cdot \langle\, \varphi_{n,m} \,|\, e^{-i\boldsymbol{q}\boldsymbol{\varrho}} \,|\, \varphi_{0,0} \,\rangle \\ & \quad + \langle\, \varphi_{1,+1} \,|\, \varphi^0_{\boldsymbol{k}} \,\rangle \cdot \langle\, \varphi_{n,m} \,|\, e^{-i\boldsymbol{q}\boldsymbol{\varrho}} \,|\, \varphi_{1,+1} \,\rangle \\ & \quad + \langle\, \varphi_{1,-1} \,|\, \varphi^0_{\boldsymbol{k}} \,\rangle \cdot \langle\, \varphi_{n,m} \,|\, e^{-i\boldsymbol{q}\boldsymbol{\varrho}} \,|\, \varphi_{1,-1} \,\rangle \\ & \quad + \langle\, \varphi_{2,0} \,|\, \varphi^0_{\boldsymbol{k}} \,\rangle \cdot \langle\, \varphi_{n,m} \,|\, e^{-i\boldsymbol{q}\boldsymbol{\varrho}} \,|\, \varphi_{2,0} \,\rangle \\ & \quad + \langle\, \varphi_{2,+2} \,|\, \varphi^0_{\boldsymbol{k}} \,\rangle \cdot \langle\, \varphi_{n,m} \,|\, e^{-i\boldsymbol{q}\boldsymbol{\varrho}} \,|\, \varphi_{2,+2} \,\rangle \\ & \quad + \langle\, \varphi_{2,-2} \,|\, \varphi^0_{\boldsymbol{k}} \,\rangle \cdot \langle\, \varphi_{n,m} \,|\, e^{-i\boldsymbol{q}\boldsymbol{\varrho}} \,|\, \varphi_{2,-2} \,\rangle \Bigg)_{\text{OPW corr.}} \\ & \Bigg]. \end{aligned} \tag{B.13}$$

For the WL states we have according to Chap. 7

$$\langle\, \varphi_{\mathbf{k}} \,|e^{i\boldsymbol{q}\cdot\boldsymbol{\varrho}}|\, \varphi_{\mathbf{k}'} \,\rangle = \delta_{\boldsymbol{k},\,\boldsymbol{q}+\boldsymbol{k}'}\; D_{\mathrm{OPW}}(\boldsymbol{k},\boldsymbol{k}',\boldsymbol{q})\,, \tag{B.14}$$

with

$$D_{\mathrm{OPW}}(\boldsymbol{k},\boldsymbol{k}',\boldsymbol{q}) = \frac{1}{N_{\boldsymbol{k}}N_{\boldsymbol{k}'}} \times\big[1 - N\sum_{l}|\langle\varphi^0_{\mathbf{k}}|\varphi_l\rangle|^2 - N\sum_{l}|\langle\varphi_l|\varphi^0_{\mathbf{k}'}\rangle|^2 + N\sum_{l,l'}\langle\varphi^0_{\mathbf{k}}|\varphi_l\rangle\langle\varphi_l|e^{i\mathbf{q}\cdot\boldsymbol{\varrho}}|\varphi_{l'}\rangle\langle\varphi_{l'}|\varphi^0_{\mathbf{k}'}\rangle\big]. \tag{B.15}$$

QD-PW Overlap Integrals

To evaluate the QD-OPW overlap integral the following integrals are needed,

$$\langle\,\varphi_{0,0}\,|\,\varphi^0_{\boldsymbol{k}}\,\rangle = \frac{2\sqrt{\pi}}{\beta\sqrt{A}}\exp\left\{-\frac{k^2}{2\beta^2}\right\}, \tag{B.16}$$

$$\langle\,\varphi_{1,\pm1}\,|\,\varphi^0_{\boldsymbol{k}}\,\rangle = +i\frac{2\sqrt{\pi}}{\beta\sqrt{A}}\,\frac{k}{\beta}\exp\left\{-\frac{k^2}{2\beta^2}\right\}\exp\{\mp i\phi_{\boldsymbol{k}}\}, \tag{B.17}$$

$$\langle\,\varphi_{2,0}\,|\,\varphi^0_{\boldsymbol{k}}\,\rangle = \frac{2\sqrt{\pi}}{\beta\sqrt{A}}\exp\left\{-\frac{k^2}{2\beta^2}\right\}\left[1-\frac{k^2}{\beta^2}\right], \tag{B.18}$$

$$\langle\,\varphi_{2,\pm2}\,|\,\varphi^0_{\boldsymbol{k}}\,\rangle = -\frac{\sqrt{2\pi}}{\beta\sqrt{A}}\,\frac{k^2}{\beta^2}\exp\left\{-\frac{k^2}{2\beta^2}\right\}\exp\{\mp i2\phi_{\boldsymbol{k}}\}. \tag{B.19}$$

Normalization Constant

Given the QD-PW overlap integrals, the normalization constant for the delocalized WL states is

$$N^2_{\boldsymbol{k}} = 1 - N_{\mathrm{dot}}\frac{4\pi}{\beta^2 A}\exp\left\{-\frac{k^2}{\beta^2}\right\} \times\left[\begin{array}{ll} 1 & \text{for s-shell}\\ +2\dfrac{k^2}{\beta^2} & \text{for p-shell}\\ +\left(1-\dfrac{k^2}{\beta^2}\right)^2+\dfrac{k^4}{\beta^4} & \text{for d-shell}\end{array}\right]. \tag{B.20}$$

B.4 QD-QD Overlap Integrals

For the evaluation of Coulomb matrix elements involving at least two localized states, as well as for determining the OPW states the following QD-QD overlap integrals must be computed

$$\langle \varphi_{n,m} \,|\, e^{\pm i\boldsymbol{q}\boldsymbol{\varrho}} \,|\, \varphi_{n',m'} \rangle = \int \mathrm{d}^2\varrho \; \varphi^*_{n,m}(\boldsymbol{\varrho}) \; e^{\pm i\boldsymbol{q}\boldsymbol{\varrho}} \; \varphi_{n',m'}(\boldsymbol{\varrho}) \tag{B.21}$$

$$\equiv (n,m|n',m'), \tag{B.22}$$

$$\pm 1_{\boldsymbol{q}} = \begin{cases} +1 & \text{for} \quad e^{+i\boldsymbol{q}\boldsymbol{\varrho}} \\ -1 & \text{for} \quad e^{-i\boldsymbol{q}\boldsymbol{\varrho}} \end{cases} \tag{B.23}$$

where we have introduced a compact notation for the overlap integrals in order to present the results in a short an transparent way.

We find,

$$(0,0\,|\,0,0) \;=\; \exp\left\{-\frac{q^2}{4\,\beta^2}\right\}, \tag{B.24}$$

$$(0,0\,|\,1,1) \;=\; \pm 1_{\boldsymbol{q}}\, i\,\frac{q}{2\,\beta}\,\exp\left\{-\frac{q^2}{4\,\beta^2}\right\}\exp\{+i\Theta_{\boldsymbol{q}}\}, \tag{B.25}$$

$$(0,0\,|\,1,-1) \;=\; \pm 1_{\boldsymbol{q}} i\,\frac{q}{2\,\beta}\,\exp\left\{-\frac{q^2}{4\,\beta^2}\right\}\exp\{-i\Theta_{\boldsymbol{q}}\}, \tag{B.26}$$

$$(1,1\,|\,1,-1) \;=\; -\frac{q^2}{4\,\beta^2}\,\exp\left\{-\frac{q^2}{4\,\beta^2}\right\}\exp\{-i2\Theta_{\boldsymbol{q}}\}, \tag{B.27}$$

$$(1,-1\,|\,1,1) \;=\; -\frac{q^2}{4\,\beta^2}\,\exp\left\{-\frac{q^2}{4\,\beta^2}\right\}\exp\{+i2\Theta_{\boldsymbol{q}}\}, \tag{B.28}$$

$$(1,+1\,|\,1,+1) \;=\; \left(1-\frac{q^2}{4\,\beta^2}\right)\,\exp\left\{-\frac{q^2}{4\,\beta^2}\right\}, \tag{B.29}$$

$$(1,-1\,|\,1,-1) \;=\; (1,+1\,|\,1,+1), \tag{B.30}$$

$$(1,1\,|\,0,0) \;=\; (0,0\,|\,1,-1), \tag{B.31}$$

$$(1,-1\,|\,0,0) \;=\; (0,0\,|\,1,1), \tag{B.32}$$

$$(2,\quad 0\,|\,0,\quad 0) = -\left[\frac{q^2}{4\beta^2}\right]\exp\left\{-\frac{q^2}{4\beta^2}\right\}, \tag{B.33}$$

$$(2,\quad 0\,|\,1,+1) = \quad i(\pm 1_{\boldsymbol{q}})\exp\{+i\Theta_{\boldsymbol{q}}\}\left[\frac{q}{2\beta}-\frac{q^3}{8\beta^3}\right]\exp\left\{-\frac{q^2}{4\beta^2}\right\}, \tag{B.34}$$

$$(2,\quad 0\,|\,1,-1) = \quad i(\pm 1_{\boldsymbol{q}})\exp\{-i\Theta_{\boldsymbol{q}}\}\left[\frac{q}{2\beta}-\frac{q^3}{8\beta^3}\right]\exp\left\{-\frac{q^2}{4\beta^2}\right\}, \tag{B.35}$$

$$(2,\quad 0\,|\,2,\quad 0) = \quad \left[1-\frac{q^2}{4\beta^2}\right]^2\exp\left\{-\frac{q^2}{4\beta^2}\right\}, \tag{B.36}$$

$$(2,\quad 0\,|\,2,+2) = \qquad (2,-2\,|\,2,\quad 0), \tag{B.37}$$

$$(2,\quad 0\,|\,2,-2) = \qquad (2,+2\,|\,2,\quad 0), \tag{B.38}$$

$$(2,+2\,|\,0,\quad 0) = \quad \frac{i^2}{\sqrt{2}}\exp\{-i2\Theta_{\boldsymbol{q}}\}\left[\frac{q^2}{4\beta^2}\right]\exp\left\{-\frac{q^2}{4\beta^2}\right\}, \tag{B.39}$$

$$(2,-2\,|\,0,\quad 0) = \quad \frac{i^2}{\sqrt{2}}\exp\{+i2\Theta_{\boldsymbol{q}}\}\left[\frac{q^2}{4\beta^2}\right]\exp\left\{-\frac{q^2}{4\beta^2}\right\}, \tag{B.40}$$

$$(2,+2\,|\,1,+1) = \quad \frac{i}{\sqrt{2}}(\pm 1_{\boldsymbol{q}})\exp\{-i\Theta_{\boldsymbol{q}}\}\left[\frac{q}{\beta}-\frac{q^3}{8\beta^3}\right]\exp\left\{-\frac{q^2}{4\beta^2}\right\}, \tag{B.41}$$

$$(2,-2\,|\,1,+1) = -\frac{i}{\sqrt{2}}(\pm 1_{\boldsymbol{q}})\exp\{+i3\Theta_{\boldsymbol{q}}\}\left[\frac{q^3}{8\beta^3}\right]\exp\left\{-\frac{q^2}{4\beta^2}\right\}, \tag{B.42}$$

$$(2,+2\,|\,1,-1) = -\frac{i}{\sqrt{2}}(\pm 1_{\boldsymbol{q}})\exp\{-i3\Theta_{\boldsymbol{q}}\}\left[\frac{q^3}{8\beta^3}\right]\exp\left\{-\frac{q^2}{4\beta^2}\right\}, \tag{B.43}$$

$$(2,-2\,|\,1,-1) = \quad \frac{i}{\sqrt{2}}(\pm 1_{\boldsymbol{q}})\exp\{+i\Theta_{\boldsymbol{q}}\}\left[\frac{q}{\beta}-\frac{q^3}{8\beta^3}\right]\exp\left\{-\frac{q^2}{4\beta^2}\right\}, \tag{B.44}$$

$$(2,+2\,|\,2,\quad 0) = -\frac{1}{2^{3/2}}\exp\{-i2\Theta_{\boldsymbol{q}}\}\left[\frac{q^2}{\beta^2}-\frac{q^4}{8\beta^4}\right]\exp\left\{-\frac{q^2}{4\beta^2}\right\}, \tag{B.45}$$

$$(2,-2\,|\,2,\quad 0) = -\frac{1}{2^{3/2}}\exp\{+i2\Theta_{\boldsymbol{q}}\}\left[\frac{q^2}{\beta^2}-\frac{q^4}{8\beta^4}\right]\exp\left\{-\frac{q^2}{4\beta^2}\right\}, \tag{B.46}$$

$$(2,+2\,|\,2,+2) = \quad \frac{1}{2}\left[2-\frac{q^2}{\beta^2}+\frac{q^4}{16\beta^4}\right]\exp\left\{-\frac{q^2}{4\beta^2}\right\}, \tag{B.47}$$

$$(2,-2\,|\,2,+2) = \quad \frac{1}{2^5}\exp\{+i4\Theta_{\boldsymbol{q}}\}\left[\frac{q^4}{\beta^4}\right]\exp\left\{-\frac{q^2}{4\beta^2}\right\}, \tag{B.48}$$

$$(2,+2\,|\,2,-2) = \quad \frac{1}{2^5}\exp\{-i4\Theta_{\boldsymbol{q}}\}\left[\frac{q^4}{\beta^4}\right[\exp\left\{-\frac{q^2}{4\beta^2}\right\}, \tag{B.49}$$

$$(2,-2\,|\,2,-2) = \quad \frac{1}{2}\left[2-\frac{q^2}{\beta^2}+\frac{q^4}{16\beta^4}\right]\exp\left\{-\frac{q^2}{4\beta^2}\right\}. \tag{B.50}$$

Acknowledgments

I am grateful for the support I have received from my advisor Prof. Frank Jahnke. In the first place for inviting me to Bremen to join the Semiconductor Theory Group, and in second place for providing a pleasant and very inspiring atmosphere in the group both on a personal as well as on scientific research level.

My thanks also go to Dr. Paul Gartner, for many helpful discussions; always ready to answer any question, at any time and anywhere. Furthermore for stories and tales about Romania, Vikings in Greenland, and mysterious paintings in Schwerin.

My office colleagues Michael Buck, Jan Seebeck and Michael Lorke I thank for discussions and a good-humored milieu. Norman Baer for always being willing to calculate QD single-particle states.

For proofreading this thesis, my special tanks go to Paul Gartner, Jan Seebeck, and Michael Lorke.

Finally, my thanks go to the other people in our institute: Prof. Gerd Czycholl's group for good company, as well as to our secretary Carmen Niemeyer-Zander and the technicians, Klaus Bowe and Andreas Beuthner for always being willing to help on practical matters.